Investigation of Biomimetic and Engineered Surface Textures for Biofouling Reduction and Prevention on Environmental Sensing Platforms.

By

Timothy Sullivan B.Sc. (Hons.)

A thesis submitted to Dublin City University in partial fulfilment of the requirements for the award of

Doctor of Philosophy

Marine and Environmental Sensing Technology Hub (MESTECH),
School of Chemical Sciences,
Dublin City University, Dublin,
April 2012.

Academic Supervisor: Prof. Fiona Regan

Head of School: Prof. Conor Long

I hereby certify that this material, which I now submit for assessment on the programme of study leading to the award of PhD is entirely my own work, that I have exercised reasonable care to ensure that the work is original, and does not to the best of my knowledge breach any law of copyright, and has not been taken from the work of others save and to the extent that such work has been cited and acknowledged within the text of my work.

Signed: _____ (Candidate)

ID No.: _____

Date: _____

Table of Contents

List of Abbreviations

Notation	Meaning
AF	Antifouling
AFM	Atomic force microscopy
AO	Acridine Orange
BSE	Backscattered electron
CA	Contact angle
CLSM	Confocal laser scanning microscopy
dH_2O	Distilled water
DVLO	Derjaguin, Landau, Verwey and Overbeek theory of colloidal stability
ED	Engineered design
EDS	Energy dispersive spectroscopy
EPS	Exopolymeric substances
LHMR	Lough Hyne marine reserve
NSW	Natural filtered seawater
PDMSe	Poly(dimethylsiloxane) elastomer
QS	Quorum sensing
SE	Secondary electron
SEM	Scanning electron microscopy
TBT	Tributyltin
vdW	van der Waals forces
NAP	National Access Programme
ODO	Optical Dissolved Oxygen
ANOVA	Analysis of Variance
Chl a	Chlorophyll A
NTU	Nephelometric Turbidity Units

FRC	Foul Release Coating
CAD	Computer Automated Drawing
CFD	Computational Fluid Dynamics
SAM	Self-Assembled Monolayer
SHCs	Superhydrophobic Surfaces
SIMPLE	Semi-Implicit Method for Pressure-Linked Equations

Abstract

Biofouling – the undesirable growth of organisms at interfaces is of great importance in a wide range of industrial and environmental fields. Such are the problems caused by biofouling, that strategies and materials are required to prevent such growth. Measures and methods directed at preventing biofouling are known broadly as antifouling (AF). At present, there is a lack of environmentally sustainable and effective AF materials, surfaces and coatings.

The rate and nature of biofouling on a material surface is known to be dependent upon the surface characteristics of the material in question. The physical parameters of surface topography, roughness, and texture are important in this regard, and it has been reported that propagules and cells of most biofouling organisms are influenced by topographic cues when choosing a potential site for permanent adhesion. Additional considerations include the fact that surface topography may alter the hydrodynamic conditions and chemical environment experienced by a settling biofouling organism at the surface.

This thesis examines the influence of surface texture on biological adhesion with the goal of developing novel non-toxic AF surfaces. Natural surfaces such as sharkskin and the crustacean carapace have been characterised to determine the role of surface topography in reducing or preventing the settlement of marine biofouling organisms. Reproduction of these topographically complex surfaces in artificial materials has been completed and tested against biological adhesion in laboratory and field experiments. Both positive and negative settlement interactions between common marine organisms and surface topography have been recorded. Further work has fabricated of a series of engineered textured surfaces in artificial materials to examine the influence of surface textures on recruitment of biofouling diatom species to a surface. Production and testing of surface texture based on the typical cell dimensions of a small biraphid diatom species, *Amphora coffeaeformis*, have shown that topographically textured surfaces can selectively influence the immigration, settlement and proliferation rates of these organisms. This has important implications for the optimisation and development of future AF coatings and materials.

Acknowledgments

I would firstly like to acknowledge the funding and support provided by the Beaufort Marine Research Awards grant-aided by the Irish Government under the National Development Plan 2007-2013 (NDP). A heartfelt expression of gratitude is due to my academic supervisor, Prof. Fiona Regan, without whom this thesis simply would not have been possible.

I wish to extend my gratitude to all the researchers and technicians alike in School of Chemistry at DCU who have provided invaluable assistance throughout this project. Huge thanks are due to those who are currently part of, or who have previously been part of the research group – I would name you all here but the list would run to several pages – suffice to say that I remember you all and thank you. Thanks to those in the engineering and biology departments who have helped out when necessary with technical discussions, modelling and access to equipment. Thanks are also due to all in the School of BEES at University College Cork and the Tyndall Institute who have helped with access to Lough Hyne, provided boats, equipment and help where necessary.

On a very personal note, I would like to thank all my friends in Dublin; their monumental help and encouragement has made this endeavour possible. Special thanks to my parents for all their help and support, especially my dad for his technical expertise, boating and help with research at Lough Hyne, and my brother who has ensured that things are never taken too seriously. Finally, last but certainly not least, I would like to thanks Lorena for her love and support, her patience, and her understanding throughout this whole project.

List of Publications

T. Sullivan and F. Regan, *The characterization, replication and testing of dermal denticles of Scyliorhinus canicula for physical mechanisms of biofouling prevention*. Bioinspiration and Biomimetics, 2011, **6**, 1-11.

T. Sullivan and F Regan, *Biomimetic design for the development of novel sustainable antifouling methods for ocean monitoring technology*. Journal of Ocean Technology, 2011, **6**, 41-54.

C. Briciu-Burghina, J. Chapman, **T. Sullivan**, A. Lawlor, L. Jones and F. Regan, *How Continuous Monitoring of a Complex Estuarine System Can Inform Sampling*. Manuscript in preparation.

T. Sullivan, S. Brozeit, K. P. A. O' Sullivan, R. McAllen, J. Davenport and F. Regan. *High resolution monitoring of episodic stratification events in an enclosed marine system*. Manuscript in preparation.

Books and Book Chapters

T. Sullivan, J. Chapman and F. Regan, in *Nano-antimicrobials: Progress and Prospects*. Eds. N. Cioffi and M. Rai, Springer Verlag, Heidelberg, 2012, p. 181-208.

J. Chapman, **T. Sullivan**, and F. Regan, *Nanoparticles in Anti-Microbial Materials: Use and Characterisation*, In Press, RSC Nanoscience & Nanotechnology, (Release date 2012).

Conference Proceedings

T. Sullivan and F Regan, *Novel materials for Mitigation of Diatom Biofouling on Marine Sensors*, Fourth international workshop on marine technology, MARTECH 2011, 22-23rd September 2011, Cadiz, Spain.

Oral Presentations

T. Sullivan and F. Regan, *Continuous monitoring to detect short-term variability and long-term change in Irish marine waters: local and global benefits*. ICES Oceans of Change, 23rd–27th April 2012, Calvià, Majorca, Spain.

T. Sullivan and F. Regan, *Monitoring Ireland's only marine reserve: a natural laboratory to support coastal management.* ENVIRON 2012, Irish Environmental Researchers Colloquium, 7-9th March 2012, University College Dublin.

T. Sullivan, R. McAllen, J. Davenport and F. Regan, *Continuous aquatic monitoring of Ireland's only marine reserve: current status and future needs.* Monitoring the Aquatic Environment Using Sensor Technologies, Royal Society of Chemistry, 19th October 2012, Burlington House, London.

T. Sullivan and F. Regan; *Benthic diatoms of Lough Hyne*, Lough Hyne Marine Reserve @ 30, 03rd-04th June 2011, University College Cork.

T. Sullivan and F. Regan; *Applying biomimetic design to the development of sustainable antifouling for environmental monitoring technology*, ENVIRON 2011 Colloquium, April 6th- Friday April 8th, 2011, University College Cork.

T. Sullivan and F. Regan, *The role of diatoms in biofouling and antifouling*, The 2010 British & Irish Diatom Meeting, 22-24th October 2010, Glencree Reconciliation Centre, Co. Wicklow.

T. Sullivan and F. Regan; *Novel materials for Mitigation of Diatom Biofouling on Marine Sensors*, Fourth International Workshop on Marine Technology, MARTECH 2011, Cadiz, Spain.

Poster Presentations

T. Sullivan and F. Regan, *The Role of surface texture and microtopographic patterning on biofilm development on natural marine surfaces*, 5th Annual Biofilms Conference, American Society for Microbiology, 14th- 20th November 2009, Cancun, Mexico.

T. Sullivan and F. Regan, *Characterisation of diatom biofilm growth, succession, and development on natural marine surfaces using multidisciplinary imaging and analysis approaches*, Biofilms 4 International Conference, 1-3rd September 2010, Winchester, UK.

1 Introduction

1.1 **Biofouling and antifouling**

The adhesion and growth of microorganisms at an interface between any non-sterile medium and a solid surface is a pervasive occurrence in most environments on Earth. This process occurs on almost all natural and synthetic materials, including those immersed in marine and freshwaters, industrial pipelines and countless other locations. Furthermore this process is frequently undesirable on synthetic materials and surfaces from a technological, health or economic perspective. Hence, undesirable biological attachment and growth on synthetic surfaces has been termed biofouling [1-3].

Since biofouling presents technical obstacles and often results in large financial costs, a range of methods designed to prevent or reduce microbial growth have been developed and applied to surfaces. Methods of preventing biofouling are widely known as antifouling (AF) mechanisms or strategies [4-7]. Initially, the term antifouling referred primarily to marine coatings designed to prevent biofouling through the use of biocides, but now the term covers a wide range of materials and strategies designed to kill, reduce or prevent the settlement of organisms through other non-biocidal mechanisms, or to remove organisms once attached to a surface.

Biofouling is regarded as ubiquitous in aquatic environments and, although the species colonising an immersed surface (often referred to as a substratum once colonised) may vary widely with latitude, season and the physiochemical properties of the surface and surrounding medium, the initial stages of biofouling appear to have some universal mechanisms in common. This is the predominant reason for the broad definition of biofouling presented above, since different research groups encountering biofouling in different environments and contexts, have introduced varying definitions of biofouling. For example, Flemming defines biofouling as the unwanted deposition and growth of biofilms [8], while the shipping industry frequently regards biofouling as the visible growth and development of macroorganisms such as algae or invertebrates on surfaces.

The term biofilm, first introduced in 1978 [9], refers to multispecies microbial communities encased in self-excreted exopolymeric substances attached to a surface [10, 11]. Research into the nature and mechanisms of biofilm formation has grown rapidly in the last two decades resulting in the understanding that microbial life preferentially exists in biofilms rather than as loosely associated individual cells as was previously believed [10]. It has now been established that such microbial communities are capable of

complex behaviour and communication, and that biofilm formation results in disparate responses to antimicrobial compounds compared to that of single or planktonic cells.

1.2 **Microbial biofilms and biofouling**

Microbial attachment to and subsequent colonisation of solid surfaces are fundamental aspects of biofouling [12]. Much of the pioneering research and advances in understanding biofilm formation have been achieved by microbiologists primarily concerned with pathogenic biofilms. These studies have produced detailed models of biofilm formation and the biological adhesion process. However, much remains to be understood about the fundamental aspects of biofilm development and the chemical and physical processes occurring within biofilms in general. Understanding the fundamental drivers of microbial adhesion to surfaces is vital to understanding biofilms, especially if new avenues to the development of novel AF materials are to be discovered and exploited.

1.2.1 *The process of biofilm formation*

It has been known since the early work of Claude ZoBell and contemporaries that aquatic life is concentrated at interfaces [13-15]. The observations of ZoBell and co-workers were remarkable for early insights gained into the mechanisms of microbial attachment at surfaces using the microscopy techniques available at the time. Indeed the work of these early pioneers has led to the present understanding of biofilm formation and the processes that occur upon immersion of a "new" surface into an aqueous environment.

It is now understood that the process of biofilm formation can be divided up into a number of distinct stages [12]. These stages are governed by the length of time that a surface has been exposed to the environment, nutrient availability and other environmental conditions such as temperature and pH. However, in general the process can be divided into a number of phases that occur in sequence after initial immersion of a "new and clean" surface in an aquatic environment. The first chemical changes occur as the surface adsorbs dissolved molecules and ions from the surrounding medium [16, 17]. This process is known as the formation of a conditioning layer and represents the foundational for subsequent microbial adhesion to the surface. An abstract view of microbial biofilm formation and dispersal subsequent to adsorption of a conditioning film is shown in Figure 1-1.

Figure 1-1: A cartoon representation of the stages of biofilm growth and dispersal, beginning with initial colonisation of the surface by single planktonic cells (1) which then adhere and develop microcolonies on the surface. These colonies continue to grow and form a biofilm in which cells are protected and capable of intercellular communication (2) until dispersal of cells occurs in order that further surfaces can be colonised (3) (Figure with permission from the Centre for Biofilm Engineering, MSU-Bozeman, Montana).

As shown in Figure 1-1, early colonising microorganisms must make the transition from planktonic (free-swimming) organisms to cells that are part of a complex, surface-attached community [18]. If environmental conditions are suitable, and they often are, initial colonising cells will adhere to the surface and begin to divide until cell microcolonies are formed (Panel 1, Figure 1-1). These microcolonies develop and divide, simultaneously producing exopolymeric substances (EPS). The function of EPS is to bind cells together forming large (often mushroom-shaped) colonies on the surface, facilitating intercellular communication and other complex microbial behaviour (Panel 2, Figure 1-1). Eventually, some combination of environmental conditions, hydrodynamic shear forces or chemical cues will trigger release of cells or colonies from the surface so that the process will begin anew on another surface (Panel 3, Figure 1-1). Although the fundamental aspects of microbial biofilm formation can be represented simplistically as in the above description, the mechanisms by which each step occurs is variable, and is highly dependent on local physiochemical conditions encountered by microbial cells and the subsequent biofilm [19].

1.2.2 *The conditioning layer*

The general model of biofilm formation presented in Figure 1-1 is reported to be valid in a wide range of physiochemical conditions. However, the process of biofilm formation does not begin with microbial attachment, but rather with the surface adsorption of ions and dissolved substances such as sugars, amino acids, and proteins from the surrounding medium. Such surface conditioning or conditioning film formation is thought to occur immediately upon environmental exposure of a "clean" surface in an aquatic environment [4, 16]. Formation of a conditioning film on surfaces is also thought to have an important role in microbial adhesion and is certainly known to affect the physiochemical properties of the surface which microorganisms eventually contact, including the overall strength of adhesion of the biofilm [17]. Measurable parameters such as interfacial free energy, wettability, surface chemistry and surface roughness are altered from those of the initial surface by a conditioning film [20, 21]. Initial adsorption of proteins and carbohydrate polymers is reported to be especially important and is thought of as having a significant effect on subsequent microbial adhesion to a surface [22].

Jain and co-workers recently analysed conditioning films on glass panels immersed in the marine environment for total carbohydrates, total proteins and total uronic acids [16]. Uronic acids were reported as the most abundant component of conditioning film examined, the presence of which significantly affected adhesion of three bacterial strains tested. However, the study also concluded that significant seasonal variation in conditioning film composition occurred; indicating that composition of the conditioning film may be unstable with variation in composition due to localised conditions. Seasonal variability in the conditioning film has also been examined on exposed stainless steel surfaces immersed in seawater, where successive adsorptions of two different compound types were found to occur; nitrogen-containing species in the first stage and carbohydrates in the second [23]. The latter study also concluded that the original surface properties might still play a role in initial bacterial adhesion, as a continuous conditioning film was not present on the examined stainless steel surfaces after 24 h immersion.

The predominance of proteins in the conditioning layer was first noted by Baier [24], and proteins are widely regarded as the significant component of conditioning films in most environments. Thus, prevention of initial protein absorption to a surface presents an

opportunity to influence the adhesion strength or even attachment of subsequent biofouling organisms. Indeed, prevention of non-specific protein adsorption to a surface and reduction of subsequent microbial settlement has been exploited in a number of AF materials. Cheng and co-workers have recently reported the ability of long-chain zwitterionic poly(sulfobetaine methacrylate) (pSBMA) surfaces grafted via Atom Transfer Radical Polymerization (ATRP) to prevent biofouling [25]. These researchers concluded that such zwitterionic surfaces had significant AF potential, related to the ability of such surfaces to resist non-specific protein adsorption. Zwitterionic molecules are molecules with an overall neutral charge but with both a positive and a negative electrical charge at different locations within a single molecule. It is thought that both a steric exclusion effect and hydration are crucial to impart protein resistance to a surface [26]; however, a successful commercial AF coating has not yet emerged based on this system and few data are available on the performance of coatings based on this principle in field trials.

1.2.3 *Microbial adhesion to surfaces*

Contact with and subsequent adhesion of microbial cells to a surface is generally considered as occurring after absorption of a conditioning layer. Prior to adhesion, a cell must be brought into contact or close proximity to the surface in question. This can either occur by passive mechanisms, i.e. the cell does not actively expend energy in transportation to the surface or by active mechanisms. Mechanisms such as mass transport (current and water movement in marine and freshwater environments) often result in initial cell contact with a surface. Active transport mechanisms also have a role if settling organisms are motile and cell motility (or the lack of) may profoundly affect subsequent biofilm architecture [27]. Many marine bacterial strains and propagules of macroorganisms possess flagella and are motile, and furthermore have been demonstrated to exhibit both positive and negative chemotaxis towards a surface, a factor in determining the composition of the subsequent biofilm [28].

The process of microbial adhesion to a surface is a series of complex physiochemical and biological interactions. Claude ZoBell appears to have been the first to propose that microbial adhesion to a surface immersed in seawater consisted of two distinct phases, an initial reversible adhesion, and a secondary, irreversible adhesion [15]. Reversible adhesion is described as spontaneous attraction of bacteria to a surface such that cells

are weakly held near the surface. Cells are still able to exhibit Brownian motion and are readily removed from the surface by washing. Irreversibly adsorbed cells no longer exhibit Brownian motion and are not removed by gentle washing. It was not until 1971 that Marshall and co-workers provided conclusive proof of the existence of both stages of attachment in bacterial cells using a motile *Pseudomonas* species and a non-motile *Achromobacter* species [29]. The *Achromobacter* species was used as very low electrolyte concentrations do not cause cell lysis in this species. Thus by altering the electrolyte concentration, reversible sorption of the non-motile *Achromobacter sp.* decreased to zero with increasing electrolyte concentration. Meanwhile, it was also demonstrated that irreversible sorption of *Pseudomonas* was affected by divalent cations and without Ca^{2+} and Mg^{2+}, the production of exopolymeric substances was not detected and irreversible sorption did not occur.

For bacterial cells, the initial reversible adhesion phase appears to be almost completely controlled by physical mechanisms and relies on the random collision of a cell with the surface. The rate of contact and successful adhesion of cells depends upon the concentration of bacteria in the surrounding water body and the number of previously adhered bacteria, as demonstrated by Fletcher and co-workers [30, 31]. Initial adhesion is controlled by electrostatic and dispersive forces and it has been demonstrated that models developed to describe adhesion of colloidal particles are valid for bacterial cells, or at least for those that have a general approximation to the behaviour of colloidal particles. Thus, the forces acting on a bacterial cell can be widely explained by the classical Derjaguin–Landau–Verwey–Overbeek (DLVO) theory formulated to describe lyophobic colloid stability [32-34].

DLVO theory relates the force between charged surfaces interacting through a liquid medium, specifically the van der Waals (vdW) attractive forces, and the electrostatic repulsive forces due to the electrical double layer (between the cell and the substratum in the case of biological adhesion). The validity and limitations of the DLVO theory to describe both qualitative and quantitative bacterial adhesion has been extensively examined [35] and was recently comprehensively reviewed [36]. Microbial cells are generally negatively charged and may exhibit varying degrees of hydrophobicity leading to repulsive electrostatic interactions between the cell and the surface. Thus, a resulting plot of the interaction between a bacterial cell and a hard surface demonstrates that two energy minimums occur, referred to as the primary and secondary energy

minimums. This is illustrated in Figure 1-2 where the two energy minimums are shown as a function of the electrostatic forces acting on cells.

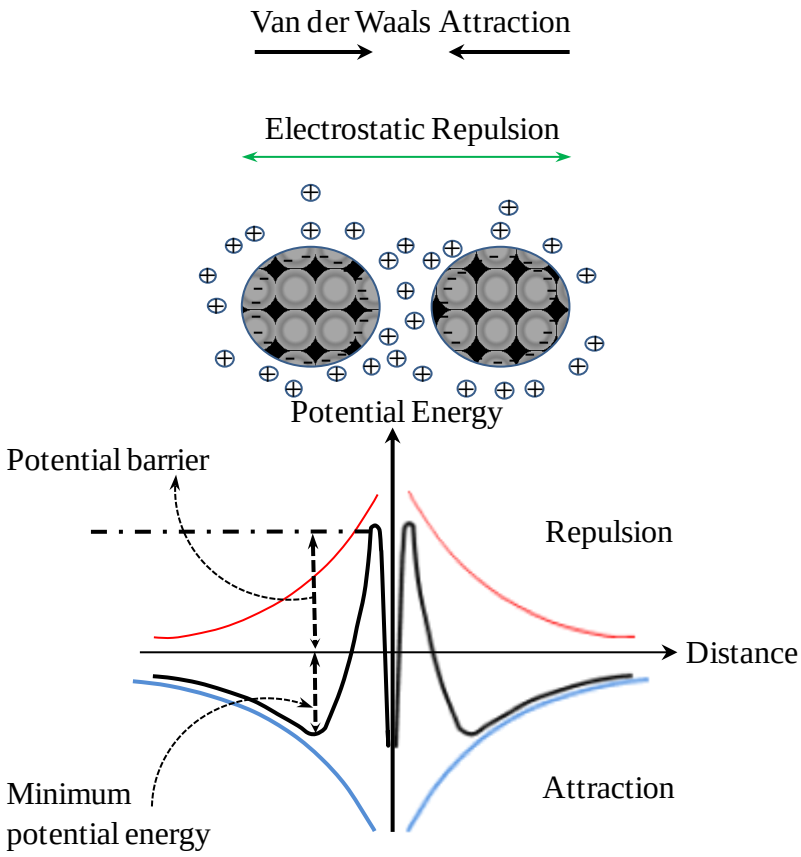

Figure 1-2: An illustration of the forces acting between individual cells with respect to interaction distance in suspension as described by the DLVO theory of colloidal stability.

In order for adhesion to occur, a bacterial cell must be positioned at the distances corresponding to either the primary or secondary energy minima. This has been approximated as 10-15 nm for the secondary and 0.5-1 nm for the primary energy minimum [3]. This has been demonstrated to be valid for many experimental scenarios and is capable of predicting the effects of changing ionic strength on relative bacteria adhesion particularly well. An increase in electrolyte concentration or the magnitude of the cation charge results in a reduction in the threshold of repulsion and thus greater bacterial adhesion. As elegantly explained by Zita and Hermansson in their study of the effects of ionic strength on bacterial adhesion and stability in wastewater flocs [37], three different situations are possible, depending on the electrolyte concentration. (i) The net interaction is repulsive at all separation distances, and the two surfaces may not come into contact. This happens at low electrolyte concentrations, when the double layers are extensive. (ii) At an intermediate electrolyte concentration, a shallow secondary

minimum may be formed at some separation distance (typically 5 to 15 nm), where the cell may be attached in a reversible manner.(iii) At high electrolyte concentrations, the net interaction is attractive at all separation distances and results in a strong, irreversible adhesion.

This role of solution chemistry on bacterial adhesion has recently been thoroughly investigated for the groundwater bacterium, *Burkholderia cepacia*, and a marine bacterium, *Halomonas pacifica* using a Radial Stagnation Point Flow (RSPF) system combined with an experimental microscopy system [38]. Using carefully controlled hydrodynamic and solution chemistry conditions, the influence of a range of ionic strength and valence (KCl vs $CaCl_2$) were demonstrated, simulating groundwater and marine environments on bacterial adhesion behaviour. The deposition rates of the two bacteria species in both KCl and $CaCl_2$ solutions increased with ionic strength in accordance with DLVO theory, however, bacterial deposition behaviour also deviated from DLVO predictions on occasion, leading the authors to propose that bacterial adhesion is determined by a combination of factors including DLVO interactions, electrosteric interactions associated with solution chemistry, and the hydrodynamics of the deposition system.

Viable bacteria are not inert colloidal particles and thus the DLVO theory has certain limitations when applied to the description of the behaviour of bacterial cells. In order to increase the validity of the DLVO model to bacterial adhesion, a number of extensions to the theory have been proposed. Hoek and Agarwal recently examined DLVO and extended the theory to account for interactions between spherical particles and surface roughness [39]. These authors reported that in all cases, the magnitude of the average interaction energy profile is reduced, but that reduction of energy also depends on particle size, surface roughness, and density of surface features. They also reported that in limited cases a surface that is on average unfavourable for deposition (repulsive) may possess locally favourable (attractive) sites solely due to nanoscale surface roughness. However, in general the influence of EPS and the role of flagella or other protrusions from the cell or surface on the rate and strength of adhesion is largely unclear for many situations.

1.2.4 *Irreversible microbial adhesion*

The adhesive bond between an organism and a surface strengthens in a time dependent manner through contact with that surface. This essentially permanent adhesion has been termed irreversible adhesion, such that the cell can no longer be released from the surface with minimal hydrodynamic shear forces [40]. Irreversible attachment involves molecularly mediated binding between specific adhesins and the surface mechanisms and active expenditure of energy on the part of the bacterium. Excretion of adhesive exopolymeric substances (EPS) to bind the cell to the surface often mediates permanent attachment. Figure 1-3 illustrates early colonisation of glass and silicon surfaces by bacterial cells.

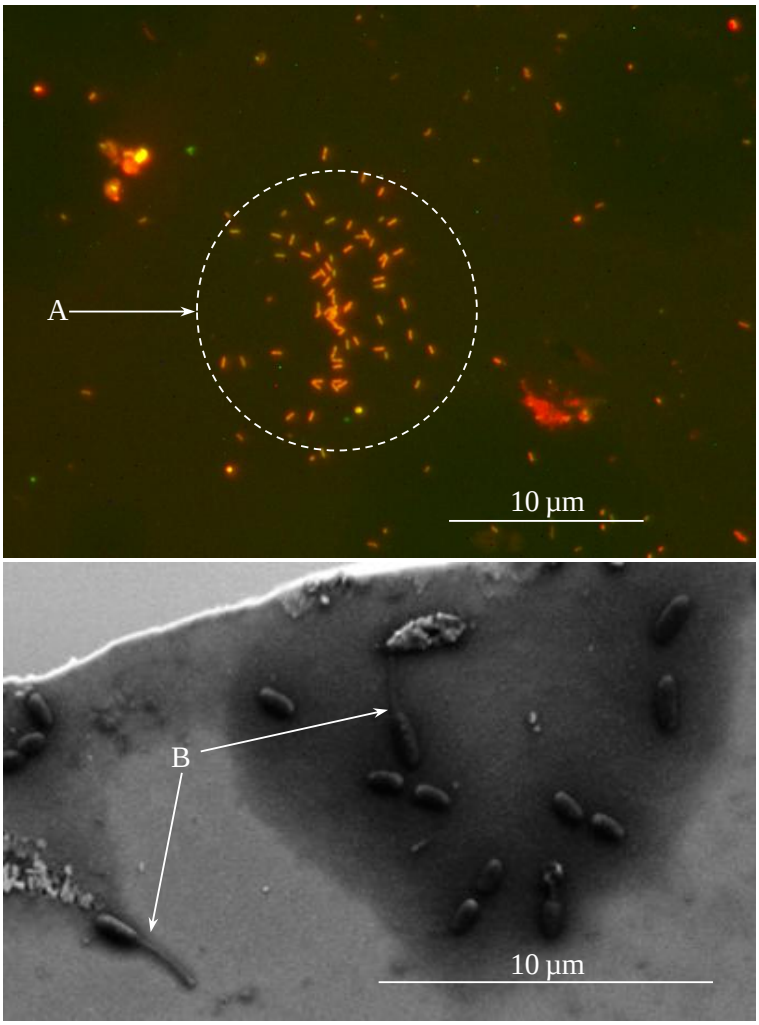

Figure 1-3: (A) an epifluorescence micrograph of a bacterial microcolony (circled) attached to a glass surface and (B) a scanning electron micrograph of a stalked bacterial species (arrowed) belonging to the Caulobacter genus attached to a silicon wafer surface.

Cells such as those in Figure 1-3 have been transported to the surfaces, perhaps by passive transport mechanisms, however once contact with the surface has occurred the cells rapidly adhere and once permanent adhesion has occurred, and cells have begun to multiply on the surfaces. A number of adhesion strategies are evident, particularly in stalked bacterial species such as *Caulobacter* where cells have an adhesive holdfast material, with which the stalked cell can adhere to surfaces. The adhesive force of *C. crescentus* has recently been measured on borosilicate materials with a novel configuration [41]. Adhesion of this species was reported as averaging 0.59 ± 0.62 μN (based on 14 measured cells), the strongest adhesive strength yet measured for microbial cells and biological adhesives.

Secondary, irreversible adhesion appears to be intricately to the production of exopolymeric substances (EPS) by microbial cells. Production of EPS is generally one of the most important aspects of biofilm development, providing a cohesive, three-dimensional biopolymer structure within which biofilm cells exist as well as having a role in initial biofilm adhesion. The specific influences of EPS on microbial adhesion have been investigated by Tsuneda and co-workers who examined the influence of extracellular polymeric substances (EPS) on bacterial cell adhesion to solid surfaces using 27 heterotrophic bacterial strains isolated from a wastewater treatment reactor [42]. They concluded that the effect of EPS on bacterial adhesion depends on the amount of EPS produced by a cell. Cell adhesion to solid surfaces is inhibited by electrostatic interaction when small amounts of EPS are produced and enhanced by polymeric interaction when large amounts are produced.

EPS can comprise between 50-90% of the total organic matter present in a biofilm [12]. The role of the biofilm matrix and EPS production has recently been reviewed by Flemming and Wingender who provide a comprehensive account of EPS functions and the influence of EPS on the architecture of microbial biofilms [43]. EPS is generally described as having two forms distinguishable by physical structure: capsule exopolymers, which closely surround cells, and exopolymers, which are loosely associated with cells [44]. Outside of a role in adhesion and cell protection, EPS are an important component of many environmental processes and biological food webs, having multiple roles including stabilisation of sediments and forming a major part of most dissolved organic matter (DOM). The extensive nature of microbial EPS in a mature biofilm is illustrated in Figure 1-4 where the intercellular binding that occurs through excretion of EPS is visible.

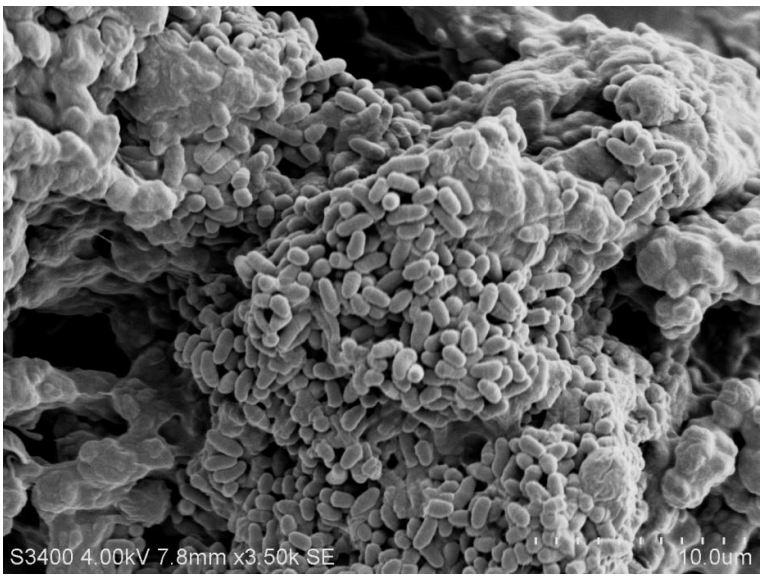

Figure 1-4: Scanning electron micrograph of a mature microbial biofilm primarily composed of bacterial and fungal species. Individual cells are encased in exopolymeric substances (EPS) and cells are both bound together into a cohesive community and bound to the surface using EPS.

The importance of EPS in biofilm processes and the microbial adhesion process have only recently been understood, and much research effort is currently being expended in determining the spatial and temporal heterogeneity of biofilm EPS. The widespread availability of advanced microscopy modalities such as Confocal Laser Scanning Microscopy (CLSM), allowing visualisation of fully hydrated specimens has provided advanced means of understanding the role and composition of EPS other than those provided by biochemical approaches [45].

Extra-cellular polysaccharides, thought to be the primary component of EPS after water, are high molecular weight carbohydrate polymers. The biofilm matrix is also highly hydrated and water may comprise up to 97 % of EPS [46]. Other components frequently include extracellular proteins nucleic acids, lipids and humic substances [47]. Variation in EPS composition and charge is also though to occur in bacteria, depending on the cell wall composition. In Gram-negative bacteria, some of the polysaccharides are neutral or polyanionic while the EPS of Gram-positive bacteria may be different due to the cationic nature of the cell wall. Therefore, the increased anionic properties of EPS may increase the binding force in a mature Gram-negative biofilm by allowing the association of divalent cations such as calcium and magnesium [47].

The exact role of EPS in biofilm formation appears to vary significantly with nutritional and physical conditions; however, it is known that EPS aids bacteria in surviving

adverse conditions, and in growth be the formation of micro-colonies and attachment [48]. Interestingly, Allison and Sutherland in their study of the role of exopolysaccaride in the adhesion of freshwater bacteria determined that EPS was not involved in the attachment process *per se*, but in the formation of microcolonies and thus in the synthesis of a microbial surface film [49].

1.2.5 *Multispecies microbial communities*

Although theoretical models such as DLVO theory can approximate the experimental results obtained from qualitative and quantitative assessment of bacterial cells, marine and most natural aquatic biofilms contain a high diversity of microorganisms other than bacteria. The process illustrated in Figure 1-1 represents a very simplified view of the process of natural biofilm formation. Bacteria are rarely sole colonisers of a surface exposed in a natural environment. Instead, a diverse group of planktonic propagules from larger organisms (e.g. serpulids, cirripeds, macroalgae) compete for space on the surface using a variety of adhesion strategies. These propagules are referred to as larvae for invertebrates and spores for algae.

Microalgae and diatoms (Bacillariophyceae, Ochrophyta) are common in benthic zones of aquatic ecosystems. Thus, diatoms often form a substantial if not dominant, component of microfouling on illuminated surfaces [50-52]. Diatoms are unicellular protists with a unique protective outer structure known as a frustule primarily composed of silica and, although such organisms are frequently described as arriving at a surface after the first colonising bacteria, it is likely that simultaneous colonisation of a surface occurs. Figure 1-5 demonstrates the presence of diatom cells on an epoxy substrate and the remains of silica cell walls (frustules) in which this group of biofouling organisms are encased. Diatom species are present in both marine and freshwaters and are frequent colonisers of immersed artificial surfaces alongside bacteria in these environments.

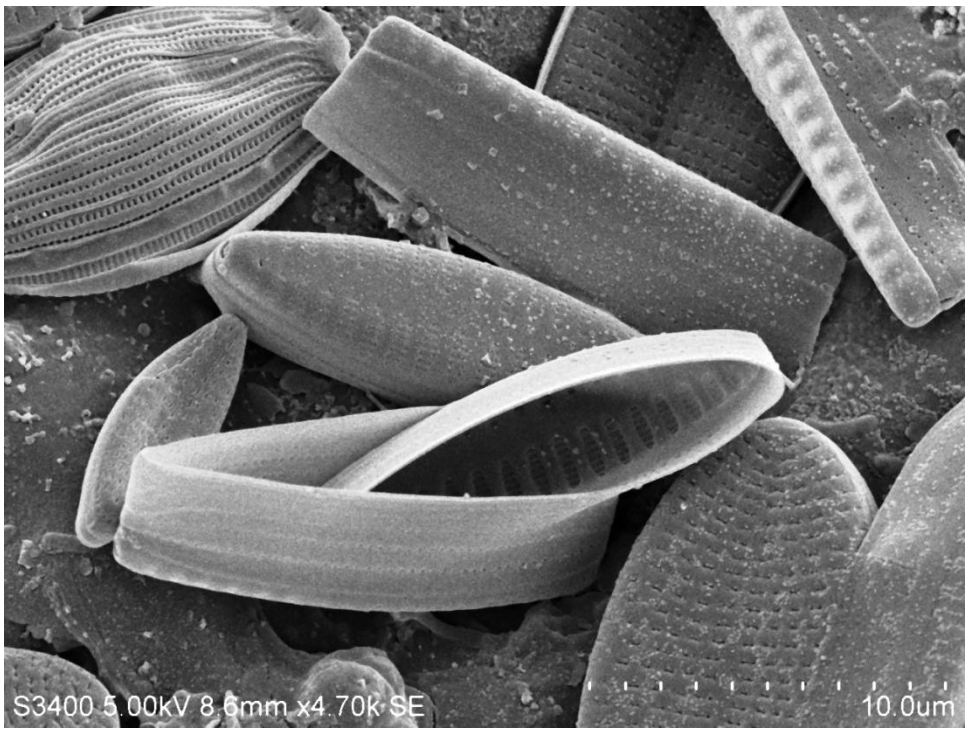

Figure 1-5: Scanning electron micrograph of diatom frustules on an epoxy substrate after 14 d immersion in the marine environment.

Although it is estimated that greater than 10,000 diatom species exist, only species from about 8–10 genera, typically from the genera *Amphora*, *Craspedostauros*, *Toxarium*, *Licmophora*, *Navicula*, *Nitzschia*, *Cocconeis* and *Achnanthes* are commonly reported as significant proportions of biofouling formed on modern AF coatings [52]. Of these, species such as *Amphora coffeaeformis* or *Achnanthes longipes* are ubiquitous on surfaces immersed in the marine environment globally. These organisms have been widely utilised as representative biofouling organisms for laboratory studies of diatom adhesion and as general assays for single-species based laboratory efficacy tests on potential AF materials [53, 54]. The tenacious adhesion of these species as representative biofouling raphid diatoms, rapid and facile culture conditions and comparatively well-studied biochemistry make them suitable for such assays.

Despite the widespread use of diatom species in AF assays, some aspects of the diatom life cycle including adhesion and motility on surfaces, and the role of diatom EPS in these processes are not well understood. It has been demonstrated that diatoms, lacking an active means of propulsion, are not actively motile in the planktonic stage and contact a surface through passive mechanisms [55]. Although the exact mechanisms of transport and adhesion are poorly studied, colloidal theory is not able to provide a valid description of the adhesion process among these organisms as cells are 10-100 times

larger or more than bacteria. Instead, adhesion and motility require extensive expenditure of metabolic energy associated with protein and glycoprotein synthesis.

Diatoms display much greater motility on a surface than bacteria, and cells are capable of active exploration once contact with the surface has occurred. This may be related to seeking out areas of the surface which provide the highest strength adhesive bond [50, 52, 54], optimal photosynthesis conditions or be related intra- and interspecies competition or the presence of simple sugars (D-glucose, D-mannose) [56]. Motility is achieved through the extrusion of EPS from an elongated opening on the frustule, known as a raphe and diatoms possessing such capability are known as raphid diatoms [57].

EPS production is thus crucial to both motility and adhesion in raphid diatoms, and both processes are closely linked in these organisms. Secretion of EPS through the raphe is believed to be involved in both motility and the initial adhesion process through what has been termed the adhesion complex (AC). The AC has been described as being composed of a polarised continuum of connector molecules coupled with associated intracellular proteins that extend from actin filaments through transmembrane connections to extracellular adhesive strands that are attached to the substratum [52]. This model remains a hypothesis as specific components and processes remain unknown or poorly described, although the use of specific inhibitors to target key components of the process and new techniques to study viscoelastic properties such as the Quartz Crystal Microbalance (QCM) has recently strengthened the model considerably [58]. An illustration of the cell constituents involved in operation of the AC in a diatom cell is shown in Figure 1-6.

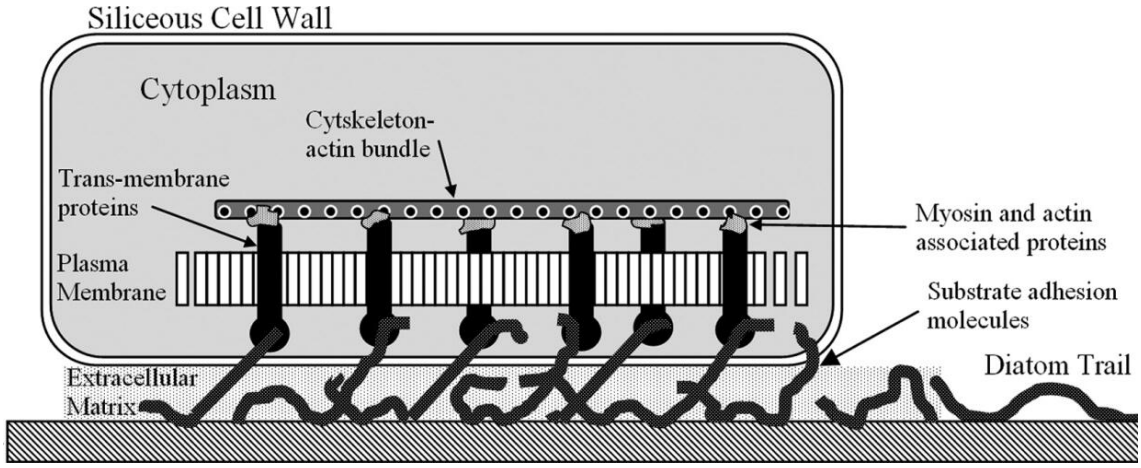

Figure 1-6: Schematic of the proposed structure of the adhesion complex (AC) in a raphid diatom such as Amphora coffeaeformis. (Image adapted from [52]).

Motility is mediated by viscous polymer mucopolysaccharides, synthesised in the Golgi apparatus [59]. These polymer mucopolysaccharides are extruded at high velocity from the anterior or posterior ends of the raphe opening, resulting in the cell sliding in the opposite direction to extrusion. A high extrusion rate, combined with hydration prior to extrusion, increase both the volume and pressure of the polymer leaving the cell and serve to provide substantial force capable of propelling the cell over the surface at velocities of up to 35 μm s^{-1} on certain surfaces [60]. It has also been established that Ca^{2+} and other ions are essential to adhesion and mobility in many diatom species, and certainly in the diatom *Amphora coffeaeformis*, the species studied in most detail [61-63].

The siliceous frustule of diatoms is also covered by an organic envelope of EPS composed of polysaccharides, proteins, and glycoproteins. Evidence exists that the composition of this EPS is different to that of EPS used in motility. Adhesion to hard surfaces is mediated by this EPS, as is the production of a number of secondary adhesive structures such as stalks, mucilage pads or fibrils for attachment. The development of high-resolution material characterisation techniques such as Atomic Force Microscopy (AFM) have facilitated analysis of diatom adhesion and the role of diatom EPS in detail ([64] and references therein). AFM allows examination of fully hydrated EPS at nanometre resolution with minimal sample preparation, and a number of different modalities allow determination of the adhesive force, viscosity, elasticity and other mechanical properties of the EPS. Landoulsi and co-workers recently reviewed knowledge of both biofouling and biocorrosion of stainless steel surfaces by diatoms, in which the advantages of AFM for analysis of such aspects were outlined in detail [65].

1.3 **The requirement for AF materials**

Thus far, this chapter has examined the fundamental stages of the process of biofilm formation and biofouling. However, the difficulties caused by biofouling in many marine and industrial situations are due to the establishment of a mature macrofouling community. Establishment of a mature microbial biofilm and the germination and growth of propagules of larger biofouling organisms such as barnacles and macro-algae eventually results in macrofouling. This stage represents the final stage in an ecological succession model of biofouling and is evident on most surfaces immersed for greater than a few weeks in marine waters. Macrofouling often represents the most visible aspect of biofouling and is associated with the greatest technical problems and high financial costs for many industries. Biomass accumulation associated with macrofouling is largely responsible for the increased drag and higher fuel consumption of shipping, while stationary objects become less buoyant. Loading of anchoring and mooring structures and will result from increased drag often ending in loss of technical instruments and other deployed structures unless biofouling is removed. Structures with large surface areas such as grates, nets and heat exchangers are particularly affected by macrofouling, and complete blocking of pipes and cooling mechanisms often result from macrofouling.

The technical problems and financial costs associated with biofouling are often underappreciated by those who do not have firsthand experience of the extent of biofouling in the marine and industrial environment. Although the cost of biofouling is difficult to quantify as indirect costs can often go unrecorded, many organisations spend a large proportion of their annual budget on biofouling research, mitigation and maintenance programmes. According to Callow and Callow [66] the US Navy has estimated their annual costs attributable to biofouling in 2002 as being in the region of $1 billion USD per annum. Schultz and co-workers recently reassessed the impact of biofouling on a naval surface ship (Arleigh Burke-class destroyer DDG-51) in detail, concluding that increased fuel consumption was the main cost, rather than hull cleaning and painting, associated with biofouling. They also estimated that the overall cost associated with hull fouling for the US Navy's present coating, cleaning, and fouling level is currently $56 million USD per annum, for the entire DDG-51 class or approximately $1 billion USD over 15 years.

Although comparably few detailed analyses are available in other industries, it is certain that marine biofouling increases the cost of ownership of any underwater installations in other sectors in a similar way. Commercial shipping vessels include the cost of routine maintenance, dry dock time, increased passage times and fuel consumption as the hydrodynamic drag resulting from biofouling increases with immersion period [67, 68]. Aside from these costs, there may also be high indirect and unaccounted costs associated with biofouling of commercial vessels, including the fact that such vessels may act as vectors for transport of invasive species [69, 70].

Other technology that must be protected from biofouling includes semi-submersible oilrigs [71], energy platforms [72] and environmental sensing technology [73-75] and almost any other immersed or periodically immersed surface. Static environmental sensors are prone to biofouling and it is often the case that sensors developed in the laboratory do not meet expectations or produce valid data when deployed in field studies because of biofouling. With the possible exceptions of telemetry and power supply limitations, biofouling currently represents the greatest obstacle to widespread long-term development and deployment of autonomous environmental sensors in aquatic environments [73, 74, 76, 77]. Micro-fluidic and micro-mechanical sensors have been developed that function satisfactorily in the laboratory but are not sufficiently robust to collect data when subjected to biofouling in field trials. A number of examples of macrofouling and the visible presence of biofouling are shown in Figure 1-7.

Figure 1-7: Examples of macrofouling including a freshwater optical sensor window (A), the concrete piling of a pier in an estuarine environment (B), commercial AF coating applied to a fibreglass yacht hull (C) and the sensors of an environmental sensing sonde(D).

Environmental sensors and other submersed scientific instrumentation present a unique AF challenge. Sensors are generally constructed of a variety of materials and it is often necessary to apply different AF strategies, dictated by both material and function. Obviously, the AF strategy must not interfere with the operation of the sensor or alter the value of the measurements recorded. An additional restriction involves the limitations imposed by power consumption that must also be considered when designing mechanical AF strategies for autonomous sensors, although many of the current instrument manufacturers have opted for low-powered mechanical AF systems such as wipers and shutter systems.

Macrofouling is also associated with increased corrosion rates and mechanical damage as macrofouling organisms adhere to and compromise anticorrosion coatings and damage even steel and stainless steel structures. The sharp edges of highly calcified organisms such as barnacles are primarily responsible for such damage and even removal of such organisms often results in further damage. Figure 1-8 illustrates the tenacious adhesion of barnacles to a steel navigation infrastructure immersed in the Irish Sea for approximately 6 years. The infrastructure is periodically removed for maintenance involving industrial cleaning of components and replacement of the protective anti-corrosion coatings. The necessity of maintenance is largely due to

biofouling, where even after industrial high pressure washing, biofouling can remain on surfaces, affecting later coatings.

Figure 1-8: Digital images of basal pads of adult barnacles on a commercial paint protecting a steel navigation buoy after > 6 yr deployment at sea, demonstrating (left) the remains of a large barnacle shell (A). Despite high-pressure washing, the basal plate often remains intact on the surface, damaging the coating (B) (Coin diameter = 25 mm)

Microfouling of surfaces is also undesirable in many situations. In addition to presenting a technical obstacle to flawless operation of devices and technology, biofilms composed of pathogenic organisms can have serious health consequences in clinical and medical contexts. Recent research has implicated biofilms in many persistent infections [78], particularly those associated with medical implants and devices [79], but also on living tissue such as in the case of endocarditic infections. It has been demonstrated that biofilm formation provides additional protection for microorganisms encased in the biofilm against both antibiotics and immune system responses [80], although a complete understanding of how biofilm formation provides this protection remains elusive. Thus, an understanding of biofouling and biofilm formation with the ultimate aim of producing non-fouling surfaces or AF materials is also required for medical applications and the knowledge gained through the study of clinical biofilms has proven useful to AF research in general.

1.4 **AF Strategies**

Acknowledgment and description of the biofouling in the marine environment is not a recent phenomenon as biofouling has likely been a problem in this environment since the first sailing vessels were launched. It is thought that the Phoenicians were aware of the difficulties caused by biofouling and were among the first to attempt a practical solution to the problem, including the first attempts at using copper and tar as coatings to prevent biofouling ([5] and references therein). Many of the early naval powers would have been acutely aware of loss of speed and manoeuvrability when the hulls of sailing vessels became heavily colonised by biofouling organisms, particularly as these ships had wooden hulls and thus were susceptible to damage by biofouling organisms such as shipworm. Thus, naval research has led the development of novel large-scale solutions to biofouling.

Of the early solutions, copper, a potent natural biocide was the most effective and was used extensively on wooden ships where fastening of rolled copper sheets to the hull could be easily accomplished. Indeed this solution is still in use today on many of the historic wooden ships afloat. The application of coatings to immersed surfaces specifically formulated for biofouling protection occurred in the 18th century with the advent of iron hulls, where copper sheeting could not be easily applied. Copper oxide, arsenic, and mercury oxide were incorporated into early AF coatings and were applied using various matrices formulated from rosin or varnish with appropriate solvents [5]. However, the majority of these formulations, in addition to being noxious and damaging to health, were ineffective or had impractically short lifetimes as AF coatings. Development continued apace until the end of the Second World War when synthetic petroleum-based resins were introduced. Mechanically stability and general suitability for flexible application in the marine environment meant that coatings containing these compounds had significant advantages over previously developed coatings.

First reports of the AF possibilities of the broad-spectrum high-toxicity tributyltin-containing compounds were made in the mid 1950s by Van de Kerk and co-workers [81]. The tributyltin (TBT) moiety was commercialised in the 1960s and coatings containing TBT quickly became market leaders with the introduction of TBT self-polishing copolymer (TBT-SPC) technology, patented by Milne and Hails in 1974 [82].

From the early 1970s onwards, TBT-based AF coatings dominated the market and were widely used in many applications requiring effective, durable AF protection. However, it soon became apparent that TBT was harmful and persistent in the marine environment, starting in the late 1970s and early 1980s when oyster crops (primarily *Crassostrea gigas*) began to fail in Arcachon Bay, France. Investigation of the causes indicated that TBT was responsible and demonstrated that the compound was an endocrine disruptor effecting sensitive species such as the gastropod species *Nucella lapillus* [83, 84]. Subsequent to these findings, many local bans on the application of TBT were introduced; however, legislation to ban TBT globally was not agreed until the 43rd meeting of the Marine Environmental Protection Committee (International Maritime Organisation, London) in 1999. The last date for the application of organotin paints on vessels was set as the 1st January 2003 with a complete ban on organotin AF coatings by 1st January 2008.

This has resulted in the current situation where the market-leading AF system has been legislatively controlled, yet no viable novel alternatives to the problem of biofouling have been developed. Thus, an intensive research effort is required to both understand the fundamental aspects of biofouling and microbial adhesion to surfaces, and to utilise this knowledge to develop AF strategies and materials that do not retain the undesirable characteristics of previous attempts.

1.5 **The ideal AF surface**

According to the International Maritime Organisation (IMO) a good biocide for incorporation into a commercial AF system should possess:

- Broad spectrum activity;
- Low mammalian toxicity;
- Low water solubility;
- No bioaccumulation in the food chain;
- No persistence in the environment.

Additionally the biocide should be compatible with paint raw materials and have favourable price and performance. Performance metrics are often related to the anticipated end use of the AF coating or material and vary depending on the end user. For example, shipping applications frequently require > 5 year effective coating lifetime while effective coatings for >1 year would better those solutions currently available for environmental sensors. However, while producing materials with these performance characteristics is certainly possible, the ideal physiochemical characteristics of an ideal AF surface are still a matter of debate; and no definite consensus has yet been reached on many aspects of material properties known to influence biofouling. Promising marine natural products as novel antifoulants, are controlled under the Biocidal Products Directive (98/8/EC), resulting in the necessity for through testing prior to market authorisation [85]. This process can be prohibitively expensive and has resulted in exploration of non-chemical based methods of AF such as control of surface topography.

It is highly desirable that the ideal AF surface should optimise many elements of material design to reduce biological adhesion. For instance, surface texture combined with surface chemistry to produce surfaces with a hydrophobic contact angle can be combined with a suitable biocide in order to produce a complete AF solution. However in practise this is difficult to achieve and it is particularly difficult to assess the individual contribution of each surface parameter to any measurable AF effect [86]. Thus, it is unknown as to which elements of an AF surface provide the greatest effect – which in turn is further complicated by the necessity to treat each individual parameter in isolation. For instance, much research effort has been expended in examining the influence of surface free energy on adhesion of many biofouling organisms; however,

this measurement is likely to be influenced by adsorption of the conditioning film and subsequent microbial adhesion once immersed. Therefore, it is relatively unknown as to which are the true values of surface free energy encountered by a settling organism at the surface after immersion.

1.6 **New approaches to AF development**

Greater research funding is now available since the legislative ban imposed on the application of TBT compounds in AF materials. It was envisioned that a gradual ban on the application of such compounds would allow sufficient time for the discovery and development of effective alternatives, however, to date few materials have proven to be wholly satisfactory, and many of those that have demonstrated potential as replacements to TBT are also toxic [87]. In the interim, many industries have resorted to the use of traditional AF materials such as copper in various applications with questionable environmental toxicity [88]. Approximately 18 different organic herbicides such as Irgarol 1051, diuron, chlorothalonil, dichlorofuanid and zineb are also in use [89]. Unfortunately, research into the eventual environmental fate and lasting toxicity of these so-called "booster" biocides and the respective metabolites has been limited, and the long-term effects of such compounds are largely unknown [90].

Despite the fact that a definite replacement to TBT has not yet been developed, a relatively low number of novel coatings and materials have shown promise as possible replacements to TBT-SPC systems. The most promising of these include silicone-based or fluoropolymer-based foul-release coatings (FRCs). These coatings have received widespread attention have been effectively commercialised by Sigma Paints (Amsterdam, The Netherlands) and Akzo Nobel (Gateshead, UK) among others for over a decade [91, 92].

FRCs function as AF materials by reducing the strength of adhesion between biofouling organisms and the surface, resulting in removal of biofouling by hydrodynamic shear forces. Reduction in the strength of the adhesive bond between a biofouling organism and the surface is achieved by utilising coatings and materials possessing a low critical surface tension, a surface parameter considered essential for foul releasing ability [93]. Both silicones and fluoropolymers have been explored as fouling release surfaces as both exhibit the required surface tensions, critical surface free energy (22–24 mN m^{-1}) and low elastic modulus to facilitate the failure of the adhesive joint between most hard macrofouling organisms and the surface [94]. The relationship between surface free energy and bioadhesion is not linear and the values for FRCs developed to date fall within those predicted by in early work by Baier for minimal adhesion ([95] and references therein). This relationship between critical surface tension and bioadhesion, subsequently known as the Baier curve, is shown in Figure 1-9.

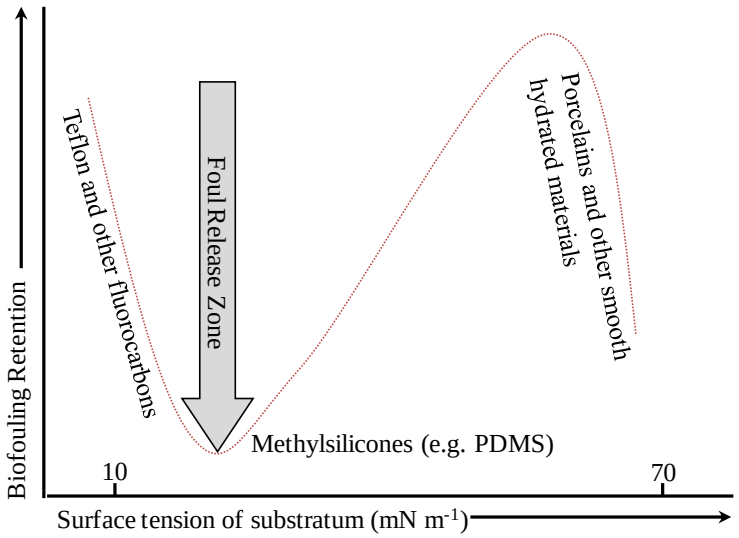

Figure 1-9: Graph of the relationship between surface tension or surface free energy of a substratum (mN m^{-1}) and the strength of adhesion of biofouling organisms to that substratum. This relationship generates the Baier curve (dashed red line) showing the adhesion strength of organisms such as barnacles at a minimum between 20-30 mN m^{-1}. This corresponds to the surface free energy values of commercial silicone foul-release coatings. (Figure redrawn from [95]).

Although further improvement of FRCs promises to provide a broad-spectrum AF material without biodegradation problems, or fees necessary to register an active AF compound, there are a number of drawbacks to the use of such systems at present. Firstly, shear forces are required to remove biofouling, typically only provided by a minimum speed of 10–20 knots by a dynamic surface. While this is achievable with commercial vessels, extensive biofouling occurs if the vessel is stationary for extended periods or the coatings are applied to static installations. Secondly, provided the required shear forces are achieved, FRCs are only effective for macrofouling and even then largely only for hard calcareous organisms such as barnacles. Microfouling, and particularly diatoms, demonstrate an affinity for such coatings and are capable of adhering tenaciously to the surface, providing a suitable substrate for further biofouling to attach [50, 54]. Lastly, in their current form, FRCs are fragile and susceptible to mechanical damage, reducing the lifetime and effectiveness of coatings dramatically, and precluding the widespread application of such coatings in important sectors such as yacht and pleasure boat industry. Despite the unsuitability of FRCs for many AF applications, these coatings represent the most successful alternatives to biocide-based coatings developed to date.

1.7 **Biomimetic AF approaches**

One of the most promising approaches to developing novel materials is to borrow ideas and concepts from nature in order to provide elegant technological solutions. Several million species exist worldwide, all of which have survived and adapted under high evolutionary pressure to thrive in specific ecological niches [96]. Many of these species have evolved specific novel chemical and physical attributes that allow survival in harsh environments. This is of interest in AF research where species have developed chemical and physical mechanisms of preventing the growth and attachment of other organisms on their outer surfaces. These natural solutions are potential sources of novel effective AF compounds and strategies [6]. Sessile organisms like macro-algae are reported to have developed chemical defences against extensive epibiont microbial growth. This would seem likely, as extensive epibiont growth results in reduced photosynthetic efficiency, increased fluid drag and parasitism, resulting in increased mortality and reduced evolutionary fitness [4, 97]. The biomimetic approach has recently gained momentum and a number of reviews have been published concerning biomimetics and AF [98-100].

1.7.1 *Natural chemical defences*

Biomimetic AF solutions have been examined from a number of perspectives. These include natural products and chemical compounds (secondary metabolites) associated with chemical defences of marine organisms, surface topography, physical surface properties and mechanical methods of marine organisms such as sharks, marine mammals and corals among other groups. Biomimicry of chemical defences against epibiosis for AF purposes offers a promising avenue to novel AF mechanisms and a number of research groups have examined organic extracts from natural organisms [101-104]. The defences of the red alga, *Delisea pulchra*, which produces halogenated furanones at the surface of the thallus has been studied in detail [105-107]. Extracts of sessile marine species such as soft corals, sponges, algae and ascidians, and tunicates have also been extensively examined among many others [103, 108]. Such compounds are attractive for incorporation into AF materials with the potential to provide a potent anti-settlement cue or deterrent to microorganisms or propagules.

Hellio and co-workers have examined chemical extracts of marine macroalgae from the Brittany coast for inhibitory activity against a wide range of bacterial isolates [101, 102, 109]. Of 90 extracts tested from 30 macroalgae against some 35 potential biofouling bacterial

strains, 18 extracts showed antibacterial activity [109]. Further examination of the effects of seasonality on activity indicated that antimicrobial activity of the extracts from *Bifurcaria bifurcata*, against two marine bacteria, *Cobetia marina* and *Pseudoalteromonas haloplanktis* and cyprids of *Balanus amphitrite* were subject to seasonal variation, with highest activity recorded from extracts between April and September [101]. This seasonality corresponds to the period of highest productivity and highest epibiosis rates along the Brittany coastline and thus would indicate that macroalgae only produce secondary metabolites for epibiosis reduction or prevention when required, although further effort to investigate the structure and mechanisms of activity of active compounds is required. The final objective of such research would be to isolate a compound or class of compounds that would offer protection from biofouling without the possibility of associated negative environmental impact of synthetic biocides.

1.7.2 *Wettability and AF materials*

The wettability of a surface refers to the ability of a liquid to spread over that surface, and is intimately related to both chemical composition and the physical topography of the surface in question [110, 111]. Control of surface wettability is important in AF materials as this surface property influences bioadhesion and the ability of biological adhesives to spread on surfaces. As pointed out by Marmur [112], two distinct approaches are possible when designing AF surfaces for reduced bioadhesion: one approach is to design a solid surface that 'prefers to be' in contact with water rather than with biological matter, or alternatively minimisation of water contact with the solid surface may also be an effective tool in preventing biofouling. Separating the influence of both of these material characteristics on wettability is however difficult for most materials.

Surface wettability can be easily visualised using the forces acting on a liquid droplet spreading on a surface by the contact angle (θ) of a liquid drop positioned on the surface. This measurement is related to the interfacial energies acting between the solid-liquid (γ_{SL}), solid-vapor (γ_{SV}) and liquid-vapor (γ_{LV}) interfaces by Young's Equation:

$$\gamma_{LV}\cos(\theta) = \gamma_{SV-}\gamma_{SL} \qquad \text{(Equation 1-1)}$$

Young's Equation as presented is a simplification of a real surface and the equation is only valid for chemically homogenous, atomically smooth surfaces. Surfaces exhibiting

surface texture will be described by one of two other wettability models: Wenzel wetting [113] or Cassie-Baxter wetting [114]. Under the Wenzel regime, the test liquid will completely wet the surface but the contact angle measured (θ*) will differ from the "true" contact angle (θ) by a factor that will depend on the ratio (R) of the true surface area (resulting from surface roughness) to the apparent surface area. This is expressed in the Wenzel equation as:

$$\cos(\theta^*) = R \cdot \cos(\theta) \qquad \text{(Equation 1-2)}$$

As pointed out by Genzer and Efimenko, according to the above wettability equation, roughness can promote either wettability (θ < 90°) or non-wettability (θ > 90°) depending on the surface chemistry [110]. If complete wetting of the surface does not occur and the surface texture is a sufficient size and dimensions such that air bubbles are trapped under the deposited liquid, then the wetting regime shifts to a Cassie-Baxter wettability model [114]. The contact angle formed between the liquid and the surface now depends on the fraction of the surface in contact with air and that in contact with the liquid. This is described by the Cassie-Baxter equation:

$$\cos(\theta^*) = -1 + \emptyset_s\,[\cos(\theta) + 1] \qquad \text{(Equation 1-3)}$$

The term $\emptyset_s$ is the fraction of the surface that is in contact with the liquid while the remaining fraction $(1 - \emptyset_s)$ is in contact with air. Equation 1-3 only applies if the liquid used just touches the top of the surface features present and does not penetrate into surface, if this does occur then calculating the wettability regime becomes further complicated [110].

Another important consideration for AF surfaces based on wettability is that any real surface exhibits two contact angles, the advancing (γ_{ADV}) and receding (γ_{REC}) contact angle. The difference between these two measurements is commonly referred to as the contact angle hysteresis (CAH), a factor that is intimately linked with adhesion of materials to a surface [110, 115]. Depending on the value of the contact angle, measured using pure water, so-called hydrophilic (θ < 90°) surfaces can be distinguished from hydrophobic (θ > 90°) surface. Surfaces that exhibit extreme low wettability, to the extent that they are almost non-wettable (typically taken as θ > 150°) are known as superhydrophobic surfaces. Surface and materials exhibiting superhydrophobicity have been extensively examined for AF ability, since such surfaces should offer minimal contact for adhering aquatic organisms. The relationship between the wettability of a

typical surface and that of a superhydrophobic surface as indicated by contact angle is shown diagrammatically in Figure 1-10.

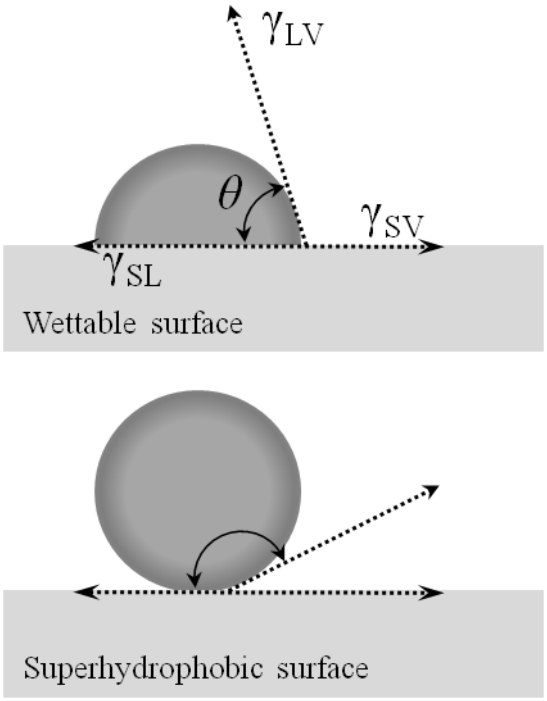

Figure 1-10: An illustration of a normal surface and superhydrophobic surface as characterised by measurement of the contact angle (θ) of a liquid drop resting on the surface. Superhydrophobic surfaces demonstrate much greater contact angles approaching 180°, thus reducing the wettability of the surface and hence the ability of some biofouling organisms to approach the surface.

Scardino and co-workers recently generated and tested a series of superhydrophobic coatings (SHCs) with water contact angles (θ) >150° and concomitant low hysteresis (<10°) for AF ability [116]. The authors detected the presence of air incursions or nanobubbles at the interface of the SHCs when immersed using small angle X-ray scattering, a technique sensitive to local changes in electron density contrast resulting from partial or complete wetting of a rough interface. It was demonstrated that factors other than superhydrophobicity such as large advancing contact angle and low contact angle hysteresis were important in surface selection by the organisms tested.

1.8 **Surface texture and AF**

The influence of physical parameters such as surface texture on microbial adhesion has been examined in a number of studies [117-119]. Surface texture influences a number of key aspects of biofilm formation and biofouling, particularly corrosion processes, hydrodynamic flow and micromixing at the surface, initial protein adsorption and cellular adhesion to a substrate [1]. Nanoscale and microscale topographic surface features are frequently referred to as surface topography, a term that includes surface patterning and texture, dimensions and directionality of surface features. Surface texture may be formed either during the surface manufacturing process or intentionally engineered onto a surface for a specific function such as increased or decreased microbial adhesion [120]. Both nanoscale and microscale surface features can also affect the bulk properties and overall behaviour of materials. This has been utilised to advantage in many modern engineering materials, where tailored surface texture or roughness is used to perform certain functions or create desirable surface characteristics. Examples of this include antireflective coatings, self-cleaning surfaces, or surfaces designed increased adhesion or grip [120, 121].

Surface roughness is defined as "The irregularities in the surface texture which are inherent in the production process but excluding waviness and errors of form" [122]. Roughness is a measured two-dimensional (2-D) parameter extracted from a random transect across the distributed topographic features of a surface. The capability to obtain 2-D measurements of roughness have been available since the 1930s and are usually achieved using vertical deflection of stylus instruments. Hence a large number of terms (>100) have been applied to describe roughness. The arithmetic surface roughness (*Ra* value), which is defined as the average absolute deviation of the roughness irregularities from the mean line over one sampling length, is the most commonly reported value. The *Ra* value is given by Equation 1-4:

$$Ra = \frac{1}{L}\int_0^L |Y(x)|/dx \qquad \text{(Equation 1-4)}$$

In the above equation, *Ra* = the arithmetic average deviation from the mean line, *L* = the sampling length, *Y* = the ordinate of the profile curve. *Ra* measurements are of limited value when describing a surface profile and it is quite possible for a number of surfaces, indistinguishable by measured *Ra* value, to have very different surface topographies. The difficulties and limitations of the use of *Ra* values as topographical descriptors have

been reviewed by Verran and Boyd [123]. Choosing the correct descriptor of surface topography is important when reporting studies on the performance of a material when exposed to microorganisms, where distinction between texture and orientation of features may be more relevant than general roughness.

Surface topography is important in theoretical modelling of microbial adhesion, affecting both the magnitude and nature of the forces acting on a cell approaching a surface [124, 125]. The DLVO theory of microbial adhesion to surfaces is only valid for perfectly smooth surfaces, which in reality do not exist [36]. Hoek and Agarwal, have recently attempted to extend the DLVO theory to account for surface roughness in predicting microbial interactions [39]. In their model simulation of nanoscale surface roughness on particle–substrate interactions they concluded that the magnitude of extended DLVO potential is reduced on average by surface roughness as the particle–substrate interfacial separation is effectively larger [39]. Hence, rough surfaces are made more favourable for colloid deposition because attractive van der Waals interactions are stronger at long range than either acid–base or electrostatic interactions. Clearly, the texture and topographic profile of a surface influences the fundamental interaction between the surface and the surrounding medium.

This is reflected in the increasing interest in the influence of surface topography on cellular behaviour in the last three decades as it has become clear that both prokaryotic and eukaryotic cell types respond to microtopographic and nanotopographic cues [126-128]. This interaction is considered important for microbial colonisation of artificial surfaces such as hip prostheses where integration of the prosthesis with eukaryotic cells must also be considered. Movement of mammalian cells in response to topographically patterned surfaces (known as contact guidance) has recently been reported for periodontal ligament fibroblasts on nanometre grooves; an important development in the regeneration of periodontal ligaments [129]. Evidence that specific bacterial strains and assemblages also respond to topographic cues has emerged [130]. Opposite responses of eukaryotic and prokaryotic cells to surface topography have been recently reported [131], an exciting possibility for the integration of artificial materials into the body while reducing the possibility of bacterial infection [132]. Emerson and co-workers recently evaluated the effects of surface chemistry and surface texture on the adhesive strength of a strain of *Staphylococcus epidermidis* [133]. Their results suggested that increased surface roughness decreases bacterial adhesion when nano and microscale roughness is considered. This is in contrast to results reported previously in which it was suggested

that small increases in roughness measurements (average roughness values (*Ra*): 0.04–1.24 µm) resulted in a significant increase in bacterial adhesion [134]. Surface features affect orientation of bacteria and can alter the surface area available for adhesion of individual cells [117]. Figure 1-11 shows the effect of 500 nm wide linear grooves (100 nm deep) in a polycarbonate surface on the orientation of individual bacterial cells during initial stages of biofilm formation. Cells can be observed to align along surface features, affecting both strength of adhesion and retention of cells when exposed to shear forces [135, 136].

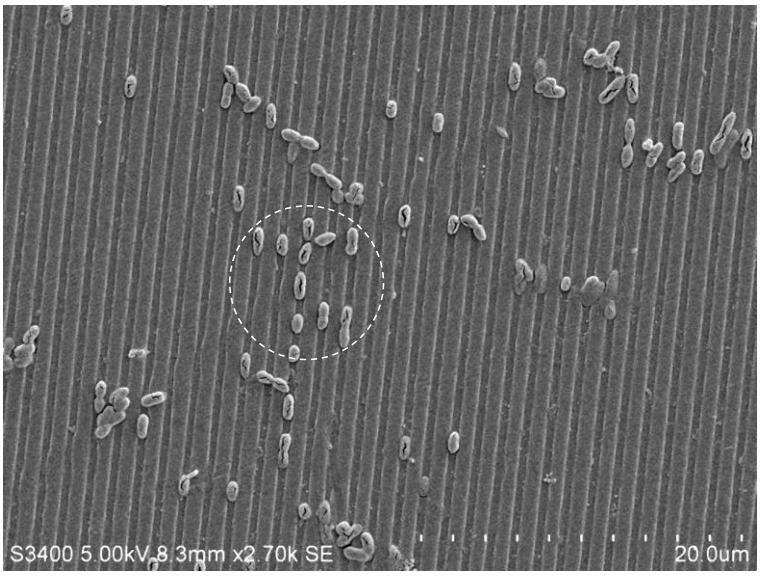

Figure 1-11: Scanning electron micrograph of cell retention of the bacterial strain Pseudomonas putida on a grooved surface. Cells are aligned along grooves to maximise cell-surface contact. The grooves are 500 nm wide and 100 nm in depth, causing alignment of bacterial cells on the surface (circled).

However, topographic feature size is not the sole determinant of bacterial alignment and retention. Edwards and Rutenberg, investigating of the role of microtopographic surface features on bacterial adhesion to sulphide minerals, reported that the depth of a surface feature such as a scratch is less important than its cross-sectional shape [137]. The authors of the latter study also presented theoretical calculations of bacterial adhesion on topographic surface features. Their results suggest that details of the interaction potential, the surface geometry, and bacterial cell shape all affect surface binding of bacteria on rough surfaces. Of particular significance is that modelling of elastic deformation of individual bacterial cells using a finite-element elastic model indicates that elastic effects are unimportant and that the cell behaves like a rigid object. This allows calculation of the binding energies of a bacterium to a range of surface features

without having to account for losses due to elastic offsets. Ultimately, this model predicts the binding strength of a bacterial cell is reduced by small grooves, but increased when the groove width exceeds a critical radius that is close to the bacterial cell size. However, caution should be exercised in broadly applying these results as the authors indicate that the particular species modelled (*Thiobacillus caldus*) does not have an external (capsular) EPS coating. The lack of an EPS coating able to fill voids between the cell and the substratum is likely to affect the binding energy of a cell.

Conflicting reports regarding the influence of surface texture on biofouling and cell adhesion/retention often result from inability to adequately characterise topographic features and describe surface texture/roughness. Surface texture can vary widely with sampling location on a surface, characterisation method used and the conditions in which measurements are taken. Topography, rugosity, roughness, and texture are terms variously used to describe surface features [135]. Additional ambiguity in surface characterisation may be introduced when a particular surface has topographical features of more than one size scale. Smaller surface features often exist among larger features and intriguing these surfaces with different length scales are reported as affecting biological response to the surface [138, 139].

Engineered surface topography, as distinguished from random surface roughness, refers to the deliberate manufacture of surface features with precise texture and dimensions. Surface texture or engineered topography is a three-dimensional parameter and includes complex surfaces such as porous surfaces. Common terms to describe textured or patterned surfaces such as macrotopography, microtopography, and nanotopography are based upon the average size of topographic features on the surface. Measurements based on 3-D surface parameters allow a stronger distinction to be drawn between surfaces as values can be calculated for terms such as waviness or angular direction of features. Table 1-1 summarises the general terms applied to each category of feature size and describes how such surface features arise.

Table 1-1: A summary of surface topographies commonly relevant to the development of AF materials, distinguished in terms of the dominant feature size. Topographies of all scales can exist on any one surface, making attribution of cell-substrate interactions to any one particular feature size difficult. (Table modified from reference [140])

	Size	Description
Macrotopography	R_a > 10 µm	Surface finish from manufacturing, engineered topography
Microtopography	R_a ~ 1 µm	Microscale features, recognised as important in hygienic surfaces
Nanotopography	R_a < 1 µm	Nanoscale features on the surface, nanoparticles, found on all surfaces
Angstrom-scale topography	1 - 10 nm	Functional groups on the surface, brushes and self assembled monolayer (SAMS)
Molecular topography	molecules	Influential in surface charge and cell-surface adhesion

Effects of surface topography on microbial behaviour have been shown for various biofilm forming organisms including bacteria and yeast cells [141], resulting in the identification of surface topography optimisation at various scales as one of the key requirements for novel anti-bacterial or AF surfaces. However, complete understanding of the fundamental interactions between bacteria and biofilms and surface topography is lacking, especially with regard to the effects of feature shape, size, and distance between features. The conventional view of the influence of topography on microbial behaviour has been that the presence of surface features or roughness increases microorganism contact with the surface due to increased surface area provided by surface features. The likelihood of biofilm removal is also reduced on rough surfaces, coupled with decreased cleaning efficiency due to protection from shear forces. This is in direct contrast to ultra-smooth surfaces that reduce the propensity for bacterial adhesion and for subsequent biofilm development [142], while increasing the likelihood of biofilm removal.

Akesso and co-workers reported the manufacture of a number of silicon-oxide-like (SiO_x) surfaces with different surface textures using plasma-assisted chemical vapour deposition (PACVD) [143]. A positive correlation between surface free energy, nanotopography and the rate of removal of the tested organisms was observed, and it was speculated that the sharp topography of surfaces was responsible for the antimicrobial effects observed. The use of specific nanotopographic roughness to create

superhydrophobic surfaces (SHCs) has also been reported as a broad-spectrum AF coating [116].

However, recent re-evaluation of surface roughness has indicated that rather than a function of the purely passive mechanisms, active exploration of suitable surfaces for settlement leads to increased settlement on "preferred" surfaces [144]. This means that the recruitment rate of specific biofouling organisms to a textured surface can be related to triggering of specific settlement cues when the settling organism encounters surface features of some yet unspecified critical dimension. The effects of texture on recruitment and adhesion in this manner have been recently reported for cypris larvae of the barnacle *Balanus amphrite* [145, 146]. The ability of cypris larvae to settle on surfaces with a texture that allows maximum likelihood of an adult barnacle remaining attached permanently to the chosen surface is remarkable. The effect of surface roughness and texture on the exopolymeric substances (EPS) which are functional in adhesion and motility of biofouling organisms must also be considered. Few data are available on the effects of topographic roughness or texture on the production of EPS or on the ability of EPS to spread over such surfaces once produced.

Novel AF strategies involving a biomimetic approach for developing novel surface textures has been attempted and several coatings have been developed based on natural systems [100]. This is particularly true in the design of engineered surface features resembling those found in nature and several studies have examined the effects of biomimetic surface topography on the settlement rate of fouling organisms [116, 147, 148]. Figure 1-12 demonstrates a series of natural surface textures images on various marine organisms. The diversity of feature dimensions, shape and fractal dimension found on natural surfaces is evident.

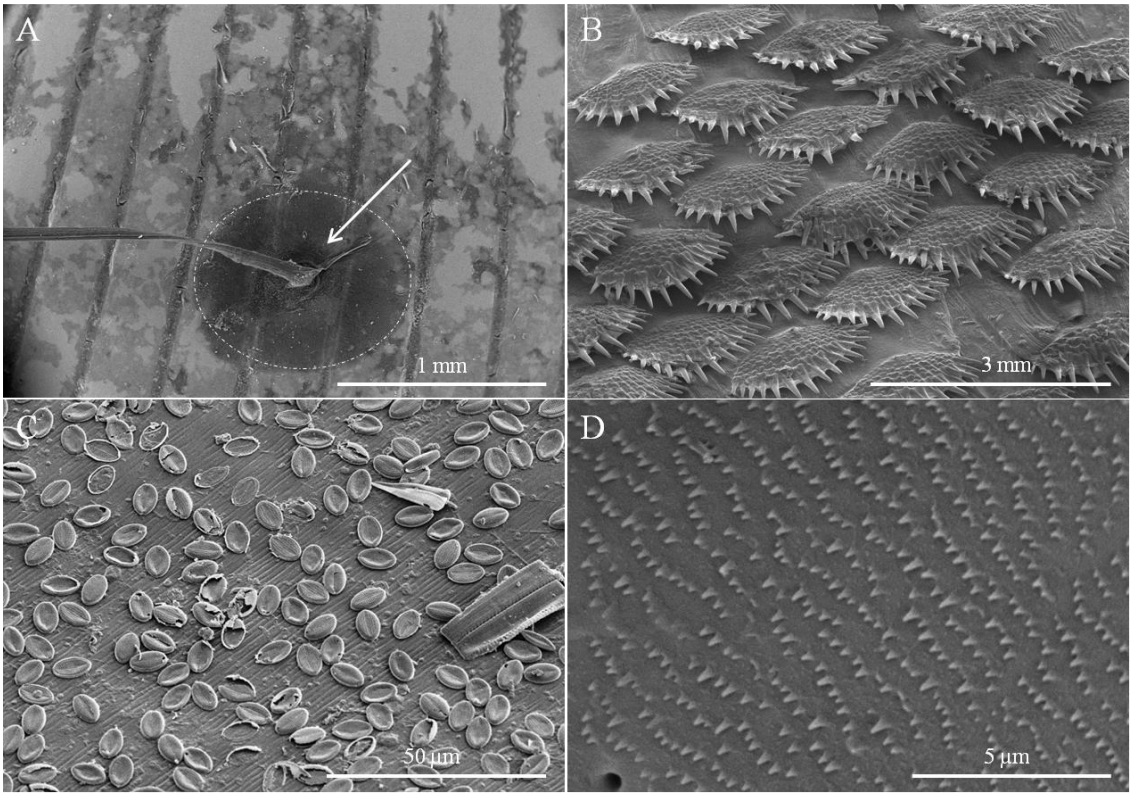

Figure 1-12: A series of scanning electron micrographs illustrating the range of surface textures on the surface of marine organisms. The attachment plaque and byssus thread of Mytilus edulis attached to the linear features of a bivalve mollusc (A,) the macro-textured surface of fish scales (B), cells primarily from the diatom genus Cocconeis attached to the rippled surface of the periostracum of Mytilus edulis (C) and (D) nanometre texturing consisting of microtrichia on the surface of a marine amphipod species.

Reports of biomimetic surface texture and topography for AF purposes have centred on structures such as the shells of bivalve molluscs like the blue mussel (*Mytilus edulis*). Such organisms are easily studied, sessile and inhabit the intertidal zone, the zone of greatest biofouling propagule abundance. The outer coating of bivalve shells, known as a periostracum, reportedly protects the outer surfaces of mytilid shells from shell boring organisms . Chemical extracts of this layer have been tested for inhibition of larval settlement against known biofouling species in which settlement of the benthic diatom *Amphora coffeaeformis* was significantly reduced [149]. Intriguingly, the surface texture of the periostracum is also reported as having significant anti-settlement effects against biofouling organisms [97, 148]. Indeed, a common topographic mechanism of AF may exist among mytilids and considerable research effort has been focused on determining the properties of such surfaces that provide AF ability [148, 150].

Sharklet AF® (Figure 1-13) inspired by the surface texture of sharkskin, albeit with dimensions much reduced compared to that of natural sharkskin is reported as a

successful anti-settlement material against a number of common biofouling organisms [139, 151]. This surface is also under development as a commercial antimicrobial product. The fouling pressure of many organisms, with vastly different size scales and adhesion mechanisms as well as physical processes such as abrasion may mean that the anti-settlement properties that the surface processes may not last indefinitely. However, such surface features may reduce initial fouling rates and it must be considered that surface structures and engineered features may improve the overall AF performance of a surface by improving biofouling removal rates.

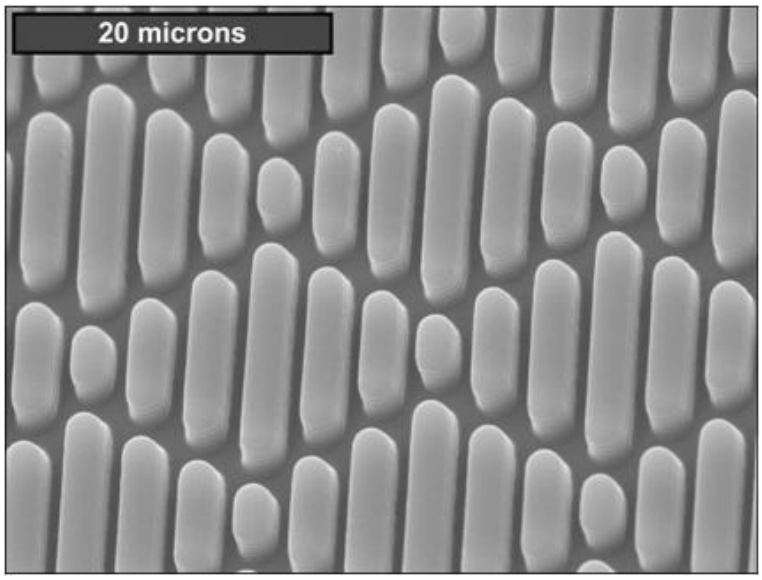

Figure 1-13: Scanning electron micrograph of the commercialised Sharklet AF textured AF surface inspired by the presence of riblets on the dermal denticles of a shark (Image from [152]).

The carapace of crustaceans has also been examined for prevention of biofouling and mechanisms such as ecdysis and grooming have been studied in detail [4, 147], [100]. Although it has been noted surface texture has a role in AF, many of the early reported studies did not attempt to identify the underlying mechanisms responsible for the anti-settlement properties. A number of recent studies have tried to rectify this by providing theoretical models for anti-settlement cues of surface texture, particularly the work of Scardino and co-workers. [153]. It was believed that a universal underlying surface property, linked to evolutionary adaptation to avoid epibiosis, was responsible for the anti-settlement properties of natural surfaces that display AF capability. However, recent research has cast doubt upon this viewpoint [150].

Understanding the underlying mechanisms responsible for AF or anti-settlement properties of the surface is complicated by size variation between and within surfaces

and the difficulties in accurately measuring surface parameters. Confocal microscopy has been used to measure surface parameters over a specified area on a range of mollusc shells, correlated with the degree of fouling on the shells examined [153]. A low fractal dimension has emerged as the most important factor in fouling resistance while a higher mean waviness supported fouling removal on the mollusc shells tested. The authors concede that foul release from mollusc shells may not be the most relevant, as molluscs are generally sedentary organisms. However as yet much research remains to be completed on the ideal surface topography for AF purposes, and the fundamental influence of surface features on microbial adhesion.

1.9 **Conclusions**

Biofouling presents a technical challenge and a source of financial expenditure for many industries. Current AF strategies offer insufficient protection from biofouling for many applications, e.g. environmental sensing technologies, and effective novel methods of AF are urgently required. Non-toxic approaches to AF are an attractive prospect; however, further advancement of effective non-toxic AF materials requires a greater understanding of the interaction between a biofouling organisms and a surface. At present, there is a lack of consensus regarding the fundamental influence of surface parameters such as surface texture on microbial behaviour at an interface.

Surface texture and roughness has been reported to both negatively and positively affect biofouling organism recruitment to a surface. However, it appears that the response can vary with both organism and adhesion mechanisms, and nature of the surface texture. These parameters influence the surface area available to a settling cell, the adhesive strength of a cell to a substrate, and direction of local hydrodynamic forces, the local chemical nature of the substrate and accumulation of organic matter on the surface. Surface topography encountered by a settling organism or propagule is also dynamic and changes with the length of immersion and size and abundance of previously adhered cells.

With this in mind, it is clear that further investigation of the potential to optimise surface texture for reduced biofouling of surfaces is required. A synopsis must be reached on the feasibility of engineering future AF coatings with specific surface topographies in order to reduce biofouling. A recommendation can then be made as to whether surface topography optimisation should be incorporated into the future development of novel non-toxic AF materials.

1.10 **Aims and objectives**

The aim of this thesis is to examine the influence of surface texture on biofouling in both field and laboratory studies. The effectiveness and influence of surface texture as a means of creating novel AF materials and coatings, specifically for application to environmental sensing instrumentation, will be assessed. A number of recent publications have reported that surface topography can have both positive and negative influences on recruitment of specific biofouling species to an exposed surface. Many of the reported surface textures have been derived from or inspired by natural surface textures of marine organisms that appear capable of epibiosis reduction or prevention. Therefore a central objective of this thesis is to evaluate the potential of biomimetic approaches to designing novel AF surface textures. In order to do this, a series of natural and engineered surface topographies will be examined and evaluated for AF potential. It is envisioned that insights into fundamental aspects of the biofouling process will be gained through this research which will contribute to development of novel non-toxic AF strategies.

1.11 **References**

1 W. G. Characklis, *Biotechnol. Bioeng.*, 1981, **23**, 1923-1960.

2 S. Abarzua and S. Jakubowski, *Mar. Ecol. Prog. Ser.*, 1995, **123**, 301-312.

3 A. I. Railkin, *Marine biofouling: colonization processes and defenses*, CRC Press, Boca Raton, Florida, 2004.

4 M. Wahl, *Mar. Ecol. Prog. Ser.*, 1989, **58**, 175-189.

5 D. M. Yebra, S. Kiil and K. Dam-Johansen, *Prog. Org. Coat.*, 2004, **50**, 75-104.

6 L. D. Chambers, K. R. Stokes, F. C. Walsh and R. J. K. Wood, *Surf. Coat. Technol.*, 2006, **201**, 3642-3652.

7 I. Banerjee, R. C. Pangule and R. S. Kane, *Adv. Mater.*, 2011, **23**, 690-718.

8 H. C. Flemming, *Appl. Microbiol. Biotechnol.*, 2002, **59**, 629-640.

9 J. W. Costerton, G. G. Geesey and K. J. Cheng, *Sci. Am.*, 1978, **238**, 86-95.

10 J. W. Costerton, Z. Lewandowski, D. E. Caldwell, D. R. Korber and H. M. Lappin-Scott, *Annu. Rev. Microbiol.*, 1995, **49**, 711-745.

11 G. O'Toole, H. B. Kaplan and R. Kolter, *Annu. Rev. Microbiol.*, 2000, **54**, 49-79.

12 R. M. Donlan, *Emerg. Infect. Dis.*, 2002, **8**, 881-890.

13 C. E. Zobell and E. C. Allen, *J. Bacteriol.*, 1935, **29**, 239-251.

14 C. E. Zobell and S. C. Rittenberg, *J. Bacteriol.*, 1938, **35**, 275-287.

15 C. E. Zobell, *J. Bacteriol.*, 1943, **46**, 39-56.

16 A. Jain and N. B. Bhosle, *Biofouling*, 2009, **25**, 13-19.

17 H. J. Busscher and R. B. H. C. Der Mei, *FEMS Microbiol. Lett.*, 1995, **128**, 229-234.

18 J. W. Costerton, P. S. Stewart and E. P. Greenberg, *Science*, 1999, **284**, 1318-1322.

19 V. Hancock, I. Witsø and P. Klemm, *Int. J. Med. Microbiol.*, 2011, **301**, 570-576.

20 R. E. Baier, in *Adsorption of microorganisms to surfaces*, ed. Bitton, G., Marshall, K.C., Wiley-Interscience, New York, 1980, p. 104-104.

21 D. P. Bakker, H. J. Busscher, J. van Zanten, J. de Vries, J. W. Klijnstra and H. C. van der Mei, *Microbiology*, 2004, **150**, 1779-1784.

22 R. Gubner and I. Beech, *Biofouling*, 2000, **15**, 25-36.

23 C. Compere, M. N. Bellon-Fontaine, P. Bertrand, D. Costa, P. Marcus, C. Poleunis, C. M. Pradier, B. Rondot and M. Walls, *Biofouling*, 2001, **17**, 129-145.

24 R. E. Baier, *Influence of the initial surface condition of materials on bioadhesion, Proc. 3rd Int. Congr. Marine Corrosion and Fouling.*, Northwestern University Press, Evanston, Illinois, 1972.

25 G. Cheng, Z. Zhang, S. Chen, J. D. Bryers and S. Jiang, *Biomaterials*, 2007, **28**, 4192-4199.

26 G. Li, G. Cheng, H. Xue, S. Chen, F. Zhang and S. Jiang, *Biomaterials*, 2008, **29**, 4592-4597.

27 T. K. Wood, A. F. González Barrios, M. Herzberg and J. Lee, *Appl. Microbiol. Biotechnol.*, 2006, **72**, 361-367.

28 G. H. Wadhams and J. P. Armitage, *Nature Rev. Mol. Cell. Biol.*, 2004, **5**, 1024-1037.

29 K. C. Marshall, R. Stout and R. Mitchell, *Microbiology*, 1971, **68**, 337-348.

30 J. H. Pringle and M. Fletcher, *Appl. Environ. Microbiol.*, 1983, **45**, 811-817.

31 S. McEldowney and M. Fletcher, *Arch. Microbiol.*, 1987, **148**, 57-62.

32 N. Churaev and B. Derjaguin, *J. Colloid Interface Sci.*, 1985, **103**, 542-553.

33 E. J. W. Verwey, *J. Phys. Chem.*, 1947, **51**, 631-636.

34 B. V. Derjaguin, *Acta Physicochim.USSR*, 1941, **14**, 633-662.

35 M. C. M. van Loosdrecht, J. Lyklema, W. Norde and A. J. B. Zehnder, *Microb. Ecol.*, 1989, **17**, 1-15.

36 M. Hermansson, *Colloids Surf. , B*, 1999, **14**, 105-119.

37 A. Zita and M. Hermansson, *Appl. Environ. Microbiol.*, 1994, **60**, 3041-3048.

38 G. Chen and S. L. Walker, *Langmuir*, 2007, **23**, 7162-7169.

39 E. Hoek and G. K. Agarwal, *J. Colloid Interface Sci.*, 2006, **298**, 50-58.

40 W. M. Dunne Jr, *Clin. Microbiol. Rev.*, 2002, **15**, 155-166.

41 P. H. Tsang, G. Li, Y. V. Brun, L. B. Freund and J. X. Tang, *PNAS*, 2006, **103**, 5764-5768.

42 S. Tsuneda, H. Aikawa, H. Hayashi, A. Yuasa and A. Hirata, *FEMS Microbiol. Lett.*, 2003, **223**, 287-292.

43 H. C. Flemming and J. Wingender, *Nat. Rev. Microbiol.*, 2010, **8**, 623-633.

44 A. W. Decho, *Oceanogr. Mar. Biol. Annu. Rev.*, 1990, **28**, 73-153.

45 J. R. Lawrence, G. D. W. Swerhone, G. G. Leppard, T. Araki, X. Zhang, M. M. West and A. P. Hitchcock, *Appl. Environ. Microbiol.*, 2003, **69**, 5543-5554.

46 X. Zhang, P. L. Bishop and M. J. Kupferle, *Water Sci. Technol.*, 1998, **37**, 345-348.

47 B. Vu, M. Chen, R. J. Crawford and E. P. Ivanova, *Molecules*, 2009, **14**, 2535-2554.

48 A. M. Romaní, K. Fund, J. Artigas, T. Schwartz, S. Sabater and U. Obst, *Microb. Ecol.*, 2008, **56**, 427-436.

49 D. G. Allison and I. W. Sutherland, *J. Gen. Microbiol.*, 1987, **133**, 1319-1327.

50 P. J. Molino, E. Campbell and R. Wetherbee, *Biofouling*, 2009, **25**, 685-694.

51 C. Totti, M. Poulin, T. Romagnoli, C. Perrone, C. Pennesi and M. De Stefano, *Polar Biol.*, 2009, **32**, 1681-1691.

52 P. J. Molino and R. Wetherbee, *Biofouling*, 2008, **24**, 365-379.

53 J. A. Finlay, M. E. Callow, L. K. Ista, G. P. Lopez and J. A. Callow, *Integr. Comp. Bio*, 2002, **42**, 1116-1122.

54 R. Holland, T. M. Dugdale, R. Wetherbee, A. B. Brennan, J. A. Finlay, J. A. Callow and M. E. Callow, *Biofouling*, 2004, **20**, 323-329.

55 L. A. Edgar and J. D. Pickett-Heaps, *Prog. Phycol. Res.*, 1984, **3**, 47-88.

56 B. Wigglesworth-Cooksey and K. Cooksey, *Biofouling*, 1992, **5**, 227-238.

57 F. E. Round, R. M. Crawford and D. G. Mann, *The diatoms: biology & morphology of the genera*, Cambridge University Press, Cambridge, UK, 1990.

58 P. J. Molino, O. M. Hodson, J. F. Quinn and R. Wetherbee, *Langmuir*, 2008, **24**, 6730-6737.

59 K. E. Cooksey and B. Wigglesworth-Cooksey, *Aquat. Microb. Ecol.*, 1995, **9**, 87-96.

60 S. I. Hay, T. C. Maitland and D. M. Paterson, *Diatom Research*, 1993, **8**, 371-384.

61 G. G. Geesey, B. Wigglesworth-Cooksey and K. E. Cooksey, *Biofouling*, 2000, **15**, 195-205.

62 B. Cooksey and K. E. Cooksey, *Plant Physiol.*, 1980, **65**, 129-131.

63 K. E. Cooksey, *Appl. Environ. Microbiol.*, 1981, **41**, 1378-1382.

64 I. B. Beech, J. A. Sunner and K. Hiraoka, *Int. Microbiol.*, 2005, **8**, 157-168.

65 J. Landoulsi, K. Cooksey and V. Dupres, *Biofouling*, 2011, **27**, 1109-1128.

66 M. E. Callow and J. A. Callow, *Biologist*, 2002, **49**, 1-5.

67 M. P. Schultz, *Biofouling*, 2007, **23**, 331-341.

68 R. L. Townsin, *Biofouling*, 2003, **19**, 9-15.

69 A. D. M. Coutts and M. D. Taylor, *N. Z. J. Mar. Freshwat. Res.*, 2004, **38**, 215-229.

70 I. C. Davidson, C. W. Brown, M. D. Sytsma and G. M. Ruiz, *Biofouling*, 2009, **25**, 645-655.

71 R. M. Wanless, S. Scott, W. H. H. Sauer, T. G. Andrew, J. P. Glass, B. Godfrey, C. Griffiths and E. Yeld, *Biol. Invasions*, 2010, **12**, 2573-2583.

72 O. Langhamer, K. Haikonen and J. Sundberg, *Renew. Sust. Energ. Rev.*, 2010, **14**, 1329-1335.

73 D. V. Manov, G. C. Chang and T. D. Dickey, *J. Atmos. Ocean. Technol.*, 2004, **21**, 958-968.

74 A. Kerr and M. J. Cowling, *Philos. Mag.*, 2003, **83**, 2779-2795.

75 A. Whelan and F. Regan, *J. Environ. Monit.*, 2006, **8**, 880-886.

76 L. Delauney and C. Compère, in *Marine and Industrial Biofouling*, ed. H. C. Flemming, P. S. Murthy and R. Venkatesan, Springer, 2009, p. 119-134.

77 L. Delauney, C. Compère and M. Lehaitre, *Ocean Sci. Discuss*, 2009, **6**, 2993-3018.

78 L. Hall-Stoodley, J. W. Costerton and P. Stoodley, *Nat. Rev. Microbiol.*, 2004, **2**, 95-108.

79 M. Habash and G. Reid, *J. Clin. Pharmacol.*, 1999, **39**, 887-898.

80 P. S. Stewart and J. William Costerton, *The Lancet*, 2001, **358**, 135-138.

81 V. Kerk and G. Der, *J. Appl. Chem*, 1954, **4**, 314-319.

82 A. Milne and G. Hails, , Patent GB 1 457 590, UK, 1977.

83 G. W. Bryan, P. E. Gibbs, G. R. Burt and L. G. Hummerstone, *J. Mar. Biol. Assoc. U. K.*, 1987, **67**, 525-544.

84 G. W. Bryan, P. E. Gibbs, L. G. Hummerstone and G. R. Burt, *J. Mar. Biol. Assoc. U. K.*, 1986, **66**, 611-640.

85 H. C. Flemming and M. Greenhalgh, in *Marine and Industrial Biofouling Vol. 4, XII*, ed. H. C. Flemming, R. Venkatesan, P. Sriyutha Murthy and K. Cooksey, Springer Series on Biofilms, Berlin Heidelberg, 2009, p. 189-199.

86 M. E. Callow and J. Callow, *Biofouling*, 2000, **15**, 49-56.

87 S. M. Evans, A. C. Birchenough and M. S. Brancato, *Mar. Pollut. Bull.*, 2000, **40**, 204-211.

88 M. Srinivasan and G. W. Swain, *Environ. Manage.*, 2007, **39**, 423-441.

89 K. V. Thomas, *Biofouling*, 2001, **17**, 73-86.

90 K. V. Thomas and S. Brooks, *Biofouling*, 2009, **26**, 73-88.

91 J. Stein, K. Truby, C. D. Wood, J. Stein, M. Gardner, G. Swain, C. Kavanagh, B. Kovach, M. Schultz and D. Wiebe, *Biofouling*, 2003, **19**, 71-82.

92 R. F. Brady, *Prog. Org. Coat.*, 2001, **43**, 188-192.

93 E. Lindner, *Biofouling*, 1992, **6**, 193-205.

94 R. F. Brady Jr and I. L. Singer, *Biofouling*, 2000, **15**, 73-81.

95 R. E. Baier, *J. Mater. Sci. Mater. Med.*, 2006, **17**, 1057-1062.

96 R. M. Hassan, R. Scholes and N. Ash, *Ecosystems and human well-being: current state and trends: findings of the Condition and Trends Working Group of the Millennium Ecosystem Assessment*, Island Press, Washington, 2005.

97 M. Wahl, K. Kröger and M. Lenz, *Biofouling*, 1998, **12**, 205-226.

98 M. Salta, J. A. Wharton, P. Stoodley, S. P. Dennington, L. R. Goodes, S. Werwinski, U. Mart, R. J. K. Wood and K. R. Stokes, *Phil. Trans. R. Soc. A.*, 2010, **368**, 4729-4754.

99 A. J. Scardino and R. de Nys, *Biofouling*, 2011, **27**, 73-86.

100 E. Ralston and G. Swain, *Bioinspir. Biomim.*, 2009, **4**, 015007-015011.

101 C. Hellio, H. Thomas-Guyon, G. Culioli, L. Piovettt, N. Bourgougnon and Y. le Gal, *Biofouling*, 2001, **17**, 189-201.

102 C. Hellio, G. Bremer, A. M. Pons, Y. Le Gal and N. Bourgougnon, *Appl. Microbiol. Biotechnol.*, 2000, **54**, 543-549.

103 N. Fusetani, *Nat. Prod. Rep.*, 2004, **21**, 94-104.

104 M. Slattery, J. B. McClintock and J. N. Heine, *J. Exp. Mar. Biol. Ecol.*, 1995, **190**, 61-77.

105 R. De Nys, P. D. Steinberg, P. Willemsen, S. A. Dworjanyn, C. L. Gabelish and R. J. King, *Biofouling*, 1995, **8**, 259-271.

106 S. A. Dworjanyn, R. de Nys and P. D. Steinberg, *Mar. Ecol. Prog. Ser.*, 2006, **318**, 153-163.

107 S. A. Dworjanyn, J. T. Wright, N. A. Paul, R. de Nys and P. D. Steinberg, *Oikos*, 2006, **113**, 13-22.

108 J. W. Blunt, B. R. Copp, W. P. Hu, M. H. G. Munro, P. T. Northcote and M. R. Prinsep, *Nat. Prod. Rep.*, 2009, **26**, 170-244.

109 C. Hellio, J. P. Marechal, B. Veron, G. Bremer, A. S. Clare and Y. Le Gal, *Mar. Biotechnol.*, 2004, **6**, 67-82.

110 J. Genzer and K. Efimenko, *Biofouling*, 2006, **22**, 339-360.

111 L. K. Ista, M. E. Callow, J. A. Finlay, S. E. Coleman, A. C. Nolasco, R. H. Simons, J. A. Callow and G. P. Lopez, *Appl. Environ. Microbiol.*, 2004, **70**, 4151-4157.

112 A. Marmur, *Biofouling*, 2006, **22**, 107-115.

113 R. N. Wenzel, *Ind. Eng. Chem.*, 1936, **28**, 988-994.

114 A. B. D. Cassie and S. Baxter, *Trans. Faraday Soc.*, 1944, **40**, 546-551.

115 L. Gao and T. J. McCarthy, *Langmuir*, 2006, **22**, 6234-6237.

116 A. J. Scardino, H. Zhang, D. J. Cookson, R. N. Lamb and R. d. Nys, *Biofouling*, 2009, **25**, 757-767.

117 E. Medilanski, K. Kaufmann, L. Y. Wick, O. Wanner and H. Harms, *Biofouling*, 2002, **18**, 193-203.

118 W. Teughels, N. Van Assche, I. Sliepen and M. Quirynen, *Clin. Oral Implants Res.*, 2006, **17**, 68-81.

119 P. Roach, D. Farrar and C. C. Perry, *J. Am. Chem. Soc.*, 2006, **128**, 3939-3945.

120 C. J. Evans and J. B. Bryan, *CIRP Ann.*, 1999, **48**, 541-556.

121 H. Assender, V. Bliznyuk and K. Porfyrakis, *Science*, 2001, **297**, 8913-976.

122 Anonymous, *BS1134-1 Assessment of surface texture—Part 1:Methods and Instrumentation.*, British Standards Institute, Milton Keynes, UK, 1972.

123 J. Verran and R. D. Boyd, *Biofouling*, 2001, **17**, 59-71.

124 W. R. Wilkerson, C. A. Seegert, A. W. Feinberg, L. C. Zhao, J. A. Callow, M. E. Callow and A. B. Brennan, *Polym. Prepr.*, 2001, **42**, 147-148.

125 E. T. Den Braber, J. E. De Ruijter, H. T. J. Smits, L. A. Ginsel, A. F. Von Recum and J. A. Jansen, *J. Biomed. Mater. Res.*, 1995, **29**, 511-518.

126 A. Curtis and C. Wilkinson, *Biomaterials*, 1997, **18**, 1573-1583.

127 A. S. G. Curtis, B. Casey, J. O. Gallagher, D. Pasqui, M. A. Wood and C. D. W. Wilkinson, *Biophys. Chem.*, 2001, **94**, 275-283.

128 R. G. Flemming, C. J. Murphy, G. A. Abrams, S. L. Goodman and P. F. Nealey, *Biomaterials*, 1999, **20**, 573-588.

129 D. W. Hamilton, C. J. Oates, A. Hasanzadeh, S. Mittler and C. Egles, *PloS one*, 2010, **5**, 517-532.

130 K. K. Chung, J. F. Schumacher, E. M. Sampson, R. A. Burne, P. J. Antonelli and A. B. Brennan, *Biointerphases*, 2007, **2**, 89-94.

131 L. Ploux, K. Anselme, A. Dirani, A. Ponche, O. Soppera and V. Roucoules, *Langmuir*, 2009, **25**, 8161-8169.

132 Y. H. An and R. J. Friedman, *J. Biomed. Mater. Res. , Part B*, 1998, **43**, 338-348.

133 R. J. Emerson I.V., T. S. Bergstrom, Y. Liu, E. R. Soto, C. A. Brown, W. G. McGimpsey and T. A. Camesano, *Langmuir*, 2006, **22**, 11311-11321.

134 R. L. Taylor, J. Verran, G. C. Lees and A. J. P. WARD, *J. Mater. Sci. Mater. Med.*, 1998, **9**, 17-22.

135 K. A. Whitehead and J. Verran, *Food Bioprod. Process.*, 2006, **84**, 253-259.

136 K. A. Whitehead, J. Colligon and J. Verran, *Int. Biodeterior. Biodegrad.*, 2004, **54**, 143-151.

137 K. J. Edwards and A. D. Rutenberg, *Chem. Geol.*, 2001, **180**, 19-32.

138 K. Efimenko, J. Finlay, M. E. Callow, J. A. Callow and J. Genzer, *ACS Appl. Mater. Interfaces*, 2009, **1**, 1031-1040.

139 J. F. Schumacher, N. Aldred, M. E. Callow, J. A. Finlay, J. A. Callow, A. S. Clare and A. B. Brennan, *Biofouling*, 2007, **23**, 307-317.

140 H. C. Flemming, R. Venkatesan, P. Sriyutha Murthy and K. Cooksey, *Marine and Industrial Biofouling Vol. 4, XII*, Springer Verlag, Berlin, Heidelberg, 2009.

141 J. Verran and C. J. Maryan, *J. Prosthet. Dent.*, 1997, **77**, 535-539.

142 T. R. Scheuerman, A. K. Camper and M. A. Hamilton, *J. Colloid Interface Sci.*, 1998, **208**, 23-33.

143 L. Akesso, M. E. Pettitt, J. A. Callow, M. E. Callow, J. Stallard, D. Teer, C. Liu, S. Wang, Q. Zhao, F. D'Souza, P. R. Willemsen, G. T. Donnelly, C. Donik, A. Kocija, M. Jenko., J. A. Lathe and P. C. Guinaldo, *Biofouling*, 2009, **25**, 55-67.

144 J. Köhler, P. D. Hansen and M. Wahl, *Biofouling*, 1999, **14**, 237-248.

145 N. Aldred, *Biofouling*, 2008, **24**, 351-363.

146 N. Aldred, A. Scardino, A. Cavaco, R. de Nys and A. S. Clare, *Biofouling*, 2010, **26**, 287-299.

147 A. V. Bers and M. Wahl, *Biofouling*, 2004, **20**, 43-51.

148 A. V. Bers, G. S. Prendergast, C. M. Zürn, L. Hansson, R. M. Head and J. C. Thomason, *Biol. Lett.*, 2006, **2**, 88-91.

149 A. V. Bers, F. D'Souza, J. W. Klijnstra, P. R. Willemsen and M. Wahl, *Biofouling*, 2006, **22**, 251-259.

150 A. V. Bers, E. R. Dıaz, B. A. P. da Gama, F. Vieira-Silva, S. Dobretsov, N. Valdivia, M. Thiel, A. J. Scardino, C. D. McQuaid and H. E. Sudgen, *Biofouling*, 2010, **26**, 367-377.

151 J. F. Schumacher, M. L. Carman, T. G. Estes, A. W. Feinberg, L. H. Wilson, M. E. Callow, J. A. Callow, J. A. Finlay and A. B. Brennan, *Biofouling*, 2007, **23**, 55-62.

152 C. J. Long, J. F. Schumacher, P. A. C. Robinson, J. A. Finlay, M. E. Callow, J. A. Callow and A. B. Brennan, *Biofouling*, 2010, **26**, 411-419.

153 A. J. Scardino, D. Hudleston, Z. Peng, N. A. Paul and R. de Nys, *Biofouling*, 2009, **25**, 83-93.

2 Field Assessment of Biofouling on AF Materials and Environmental Sensors

2.1 **Introduction to autonomous environmental sensors**

Sensors have long been deployed in aquatic environments to collect data on a host of ecologically and environmentally important parameters. Those currently deployed are designed to collect data on physical and chemical parameters such as pH, dissolved oxygen (DO), conductivity, temperature and depth (CTD), flow, turbidity or nutrients among others [1, 2]. These instruments are often augmented as required with other instruments such as underwater cameras, lights or hydrophones for acoustic monitoring. Until recently, most sensors were briefly deployed on tethered buoys, moorings or platforms when and where required or as part of routine aquatic monitoring programmes. Collected data were then augmented and validated by retrieving and transporting samples back for laboratory-based analysis of chemical parameters for which deployable sensors lack sufficient accuracy, sensitivity or robustness.

Wireless data transmission and the development of a new generation of micro- and nano-mechanical sensors (MEMS and NEMS) sensors have made it possible to advance autonomous environmental monitoring [3, 4] . Theoretically, it is no longer necessary to visit monitoring sites repeatedly to collect data or samples for analysis as this can be done autonomously by a network of remote sensors, sometimes termed Environmental Sensor Networks (ESN) [5]. When functioning as designed, these networks are capable of communicating on-site in real time and transmitting data directly to a remote data storage and analysis facility. This has multiple advantages for current aquatic monitoring requirements where large surface areas require monitoring, many of which are currently under-sampled or not sampled. Advances in telemetry and power requirements also allow data to be transmitted back to the laboratory for analysis, perhaps completely avoiding taking spot samples and laboratory-based analysis altogether.

2.1.1 *Biofouling and environmental sensors*

Biofouling is recognised as one of the main obstacles to autonomous environmental sensing in aquatic environments [6, 7]. All immersed components of the sensor system, including the operational components (membranes, optical windows, and electrodes), housings (casings), and mooring components are subject to biofouling. Adequate AF of all components is difficult since deployed sensors are frequently constructed of many different materials. Table 2-1 summarises some of these materials and indicates how

each is used. The list of materials presented is not exhaustive and it is highly likely that materials used in future environmental sensors may be quite different from those listed. The diverse array of materials currently used in sensor construction means that each component material must be considered individually in terms of an optimal AF strategy. At present materials are generally chosen based on durability, initial cost and corrosion resistance rather than AF properties.

Table 2-1: Common materials utilised in environmental sensor construction.

Material	Application	Sensor Type
Metals		
Anodised aluminium	Sensor housings	Available in commercial turbidity sensors.
304L Stainless steel	Sensor housings	All, freshwater applications.
316L Stainless steel	Sensor housings	Specifically marine applications and corrosive industrial applications
Stainless steel microscreens	Filtration	Available for particulate matter screening on some sensors e.g. conductivity and temperature.
Titanium	Sensor housings	Replacement for SS housings.
Copper	AF	Most commercial systems
Plastics		
Polyoxymethylene (Acetal, Delrin ®)	Sensor housings	Available on commercial pH, fluorimetry and ORP sensors.
Polyphenylene sulfide (PPS) (Ryton ®)	Sensor housings	Available on some pH and ORP sensors.
FEP Teflon	Membranes	Dissolved oxygen.
Polyurethane	Cabling	Most.
Acrylonitrile butadiene styrene (ABS)	Sensor housings	Some models e.g. OTT Orpheus Mini.
HD polyurethane	Cabling	Most.
Additional Materials		
Epoxy resins	Electronics, housing material	Most.
Silicon	Diaphragms	Water level sensors.
Sapphire	Optical windows	Turbidity.
PVDF membranes	Filtration membranes	Phosphate, combined models.
Glass	Optical windows	Turbidity.

In common with other applications requiring AF strategies, sensors are currently protected using a variety of mechanisms, including mechanical wipers, shutters or chemical means such as the application of coatings containing biocides, local chlorination and sprays for reduction of surface energy. The use of ultra violet (UV) light and electrolysis has also trialled [1]. User-controlled mechanical wipers that rotate periodically (perhaps with each measurement taken) are now one of the most common AF mechanisms on sensors. AF capabilities of mechanical wipers are frequently augmented with copper, for instance adhesive copper tape is applied to the outer casing

of each sensor as an additional AF measure. Copper is also now incorporated into many other components, particularly where algal biofouling is problematic on optical sensors. Mechanical wipers and shutters are now constructed of copper or copper/zinc alloys in order to combine the biocidal effects of copper in order to increase the AF effect [8]. Figure 2-1 illustrates a typical example of current AF measures for environmental sensors from many commercial sensor manufacturers. The sensing components are protected by an array of mechanisms, including copper as a biocide, mechanical wipers and brushes for removal of algal biofouling.

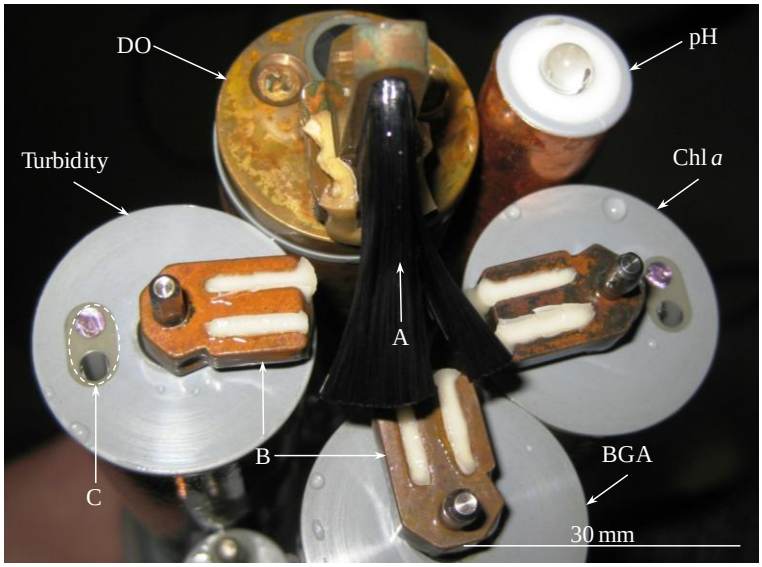

Figure 2-1: Digital image of a commercial multiparameter environmental sensing sonde. Installed sensors are labelled (pH, DO=dissolved oxygen, Turbidity, Chl a = Chlorophyll a, BGA = blue/green algae). AF is provided by mechanical brushes (A) and copper mechanical wipers (B) to protect the optical windows of optical sensors (C).

Aside from mechanical wipers, biofouling strategies are rarely designed specifically for use on environmental sensing technology and thus there is a lack of knowledge regarding optimum sensor design for AF purposes. Investigation of biofouling specifically associated with sensor design is required and recommendations regarding material selection for optimum performance are required.

2.1.2 *Aims and Objectives*

The aim of this chapter is to conduct a spatial and temporal evaluation of biofouling affecting both current sensor platforms and to evaluate current commercial AF materials in use.

The objectives of this work include:

(1) Deployment of environmental sensors in a range of environmental conditions followed by investigation of subsequent biofouling. Possible improvements in sensor design for optimal AF performance will be highlighted.

(2) Design, construction and deployment of test panels to test a range of materials including current AF materials at different locations.

(2) Identification of surface parameters requiring optimisation for AF purposes.

2.2 **Materials and Methods**

2.2.1 *Sensor acquisition and data analysis*

Multiparameter environmental monitoring sondes (YSI 6600 V2) were purchased from YSI Hydrodata (Letchworth, UK). Prior to deployment, each sonde was calibrated as per manufacturer's instructions and set to collect data synchronously. Data were collected at 15 min intervals and either downloaded periodically onsite with a Panasonic CF-29 Toughbook using Windows XP (SP2) and EcoWatch software (YSI Hydrodata, Letchworth, UK version 3.18.00), or transmitted directly to the Internet over available 3G networks using telemetry provided by the manufacturer. Data were analysed using the EcoWatch software, AQUARIUS 360° software (Aquatics Informatics Inc, BC Canada, version 3.0 R2), and SPSS statistics version 17.0.

2.2.2 *Site selection*

Three separate sites were chosen to investigate biofouling on sensors. Sensors were deployed at three locations, one in an estuarine environment and two marine sites listed in Table 2-2. The study sites were chosen based on likely differences in biofouling composition and variability in local environmental conditions. In addition to being of environmental interest, other considered factors of importance before final site selection included availability of access and site security.

Table 2-2: Summary of location and deployment conditions for the sites investigated in this study.

Site Name	GPS co-ordinates	Environment	Deployment depth (m)	Deployment Date and time (d)
Poolbeg Marina	N 53.344158°, W 06.2178°	Estuarine	2.5	01/09/2010 – 01/05/2011 (242 d)
South Basin, Lough Hyne Marine Nature Reserve.	N 51.50061°, W 09.29802°	Marine	10.0	03/05/2011 – 01/07/2011 (59 d)
North Basin, Lough Hyne Marine Nature reserve.	N 51.50286°, W 09.30058°	Marine	10.0	03/05/2011 – 01/07/2011 (59 d)

2.2.3 *Site Description*

Site 1: The Liffey Estuary, Dublin port.

Poolbeg Marina, Dublin Port, is a highly industrialised location in the River Liffey estuary. Sensors and materials were deployed on the 01/09/2010 from a pontoon belonging to the marina at a location as close to the channel centre as possible. The location is shown in Figure 2-2. This site is the lower portion of the River Liffey estuary and the river channel is some 200 m wide at this point. Total depth of water at mean lower low water at this location is 4 m although the channel deepens rapidly towards the centre of the river to allow commercial shipping access.

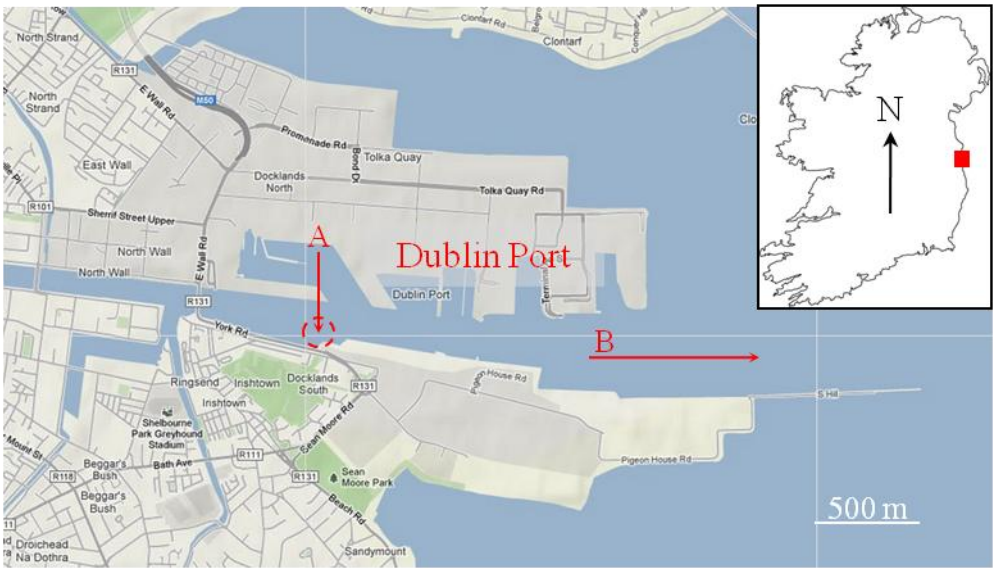

Figure 2-2: Aerial image and location of Poolbeg Marina, Dublin, A = the deployment site, B = River Liffey and flow direction to Dublin Bay.

Site 2: Lough Hyne Marine Nature Reserve

Lough Hyne (= Lough Ine) Marine Nature Reserve is situated on the South Coast of Ireland and is a statutory marine reserve. The hydrodynamics and ecology of Lough Hyne are well-described [9-16] and the site is considered as an important future candidate site for continuous environmental monitoring [17]. A map of Lough Hyne and the two sites chosen for examination of biofouling within Lough Hyne are shown in Figure 2-3.

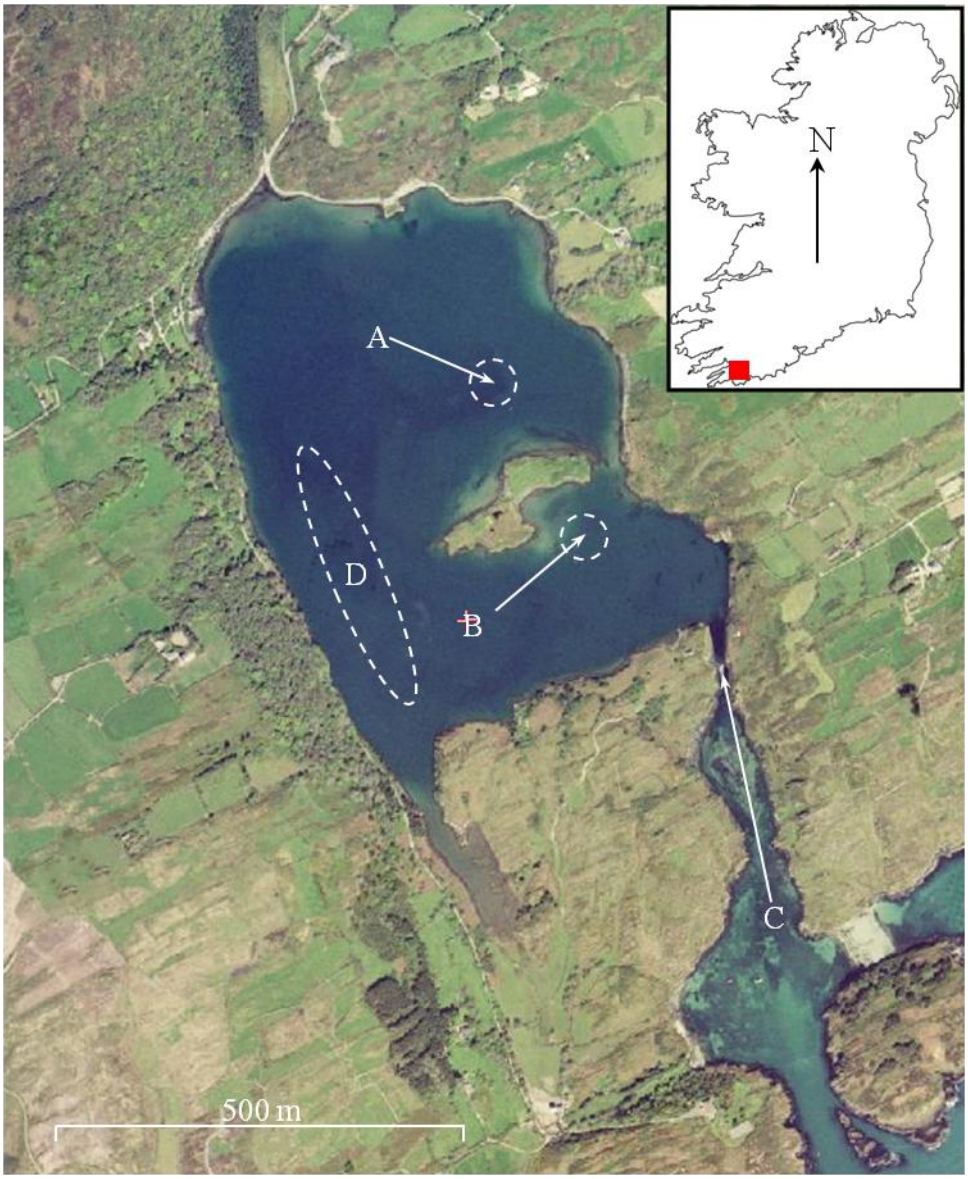

Figure 2-3: Aerial photograph of Lough Hyne Marine Reserve and location (red square), A = the North Basin Site (N51.50286º W009.30058º ± 6 m), B = the South Basin Site (N51.50061º W009.29802º ± 6 m). Other sites indicated include, (C) the exit to the sea ("The Rapids") and D, the Western Trough: the area of greatest depth (> 50 m) within Lough Hyne.

2.2.4 *Environmental sensing parameters*

Measurements were collected on the environmental parameters listed in Table 2-3 at the described test sites.

Table 2-3: Summary of environmental variables measured over the study period.

Measured environmental variable (units)	South Basin, Lough Hyne	North Basin, Lough Hyne	Poolbeg Marina, Dublin
Temperature (ºC)	✔	✔	✔
Conductivity (mS cm^{-1})	✔	✔	✔
Optical dissolved oxygen (reported as % or mg L^{-1})	✔	✔	✔
Turbidity (NTU)	✔	✔	✔
Depth (m)	✔	—	—
pH	✔	—	—
Other reported variables			
Derived salinity (ppt)	✔	✔	✔
Battery (V)	✔	✔	✔
Resistivity (S m^{-1})	✔	✔	✔
Specific conductance (mS cm^{-1})	✔	✔	✔

Experimental test frames incorporating coupons of standard microscope slide dimensions (75 x 25 x 0.96-1.06 mm) (Corning, NY, USA) were specifically designed and constructed to accommodate 12 test coupons for this study. Construction details of this frame are shown in Figure 2-4. This frame was constructed of acetal plastic strips (450 x 20 x 5 mm) with milled slots to secure individual coupons, drilled and secured using Nylon machine screws. The clamping length was 5 mm at each edge of each coupon and gave a surface area of 1625 mm^2 exposed to biofouling. Panels containing coupons were suspended vertically in the water at each test site.

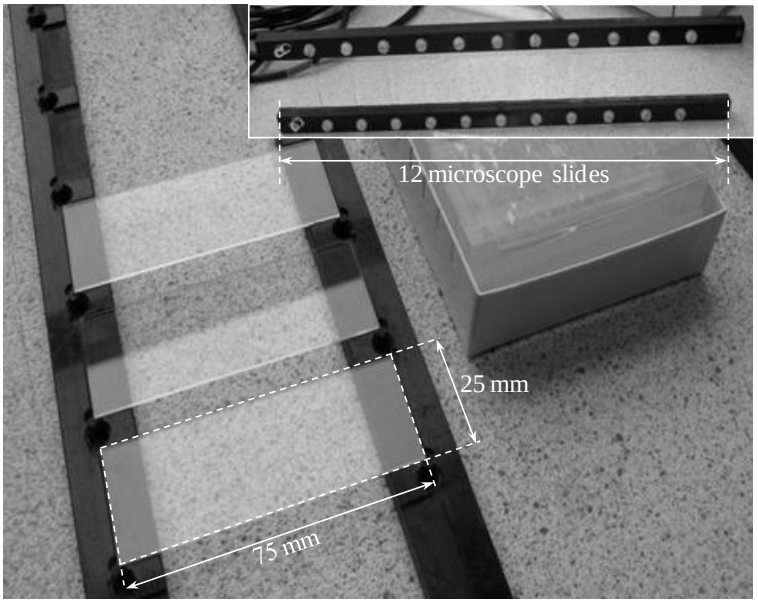

Figure 2-4: Digital image of test panel details designed for deployment of microscope slide-sized coupons. The panel holds 12 individual test coupons with a 5 mm space between each (inset). A hole at each end of the frame allows the panel to be secured to a mooring or other structure using cable ties.

2.2.6 *Mooring design*

Sensors and materials were deployed directly from a pontoon at Poolbeg Marina. However, both sites at Lough Hyne were open water sites and therefore mooring systems were designed and constructed to incorporate both sensors and coupons within close proximity. The details and dimensions of this mooring are shown in Figure 2-5. Mooring systems were constructed using Nylon rope (12 mm) and a weight and buoy system as shown in Figure 2-5. To minimise any possible interaction between AF materials and sensor performance, a minimum distance of 0.5 m was maintained between the test panels and the sensors.

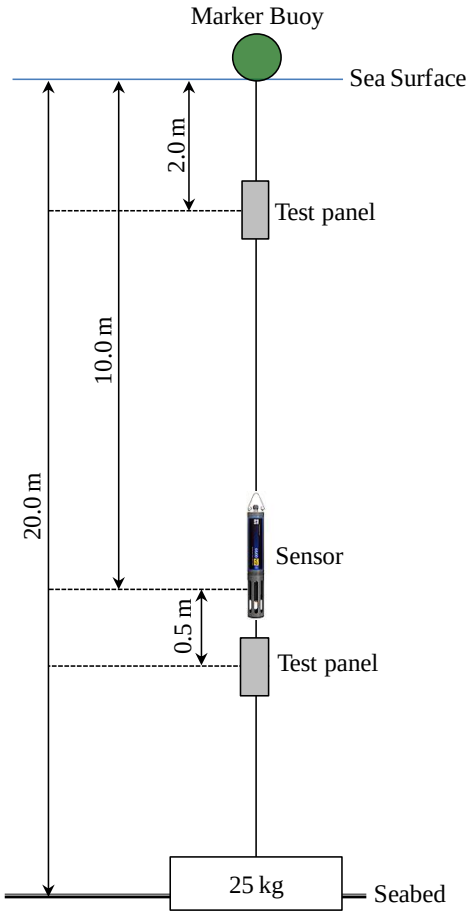

Figure 2-5: Schematic and dimensions of the mooring used for test panels and sensors. Two test panels were deployed at each location, at 2 m depth and at 10.5 m, 0.5 m below the environmental sonde.

2.2.7 *Coating and material preparation*

To examine differences in biofouling due to variation in chemical and physical properties a range of materials and coatings including commercial AF coatings were deployed. The details of each material and coating are given in Table 2-4.

Table 2-4: Summary of deployed materials at each location in this study.

Material/Coating	Poolbeg Marina	Lough Hyne Marine Reserve	AF Mechanism	Material/Coating Thickness (µm)
Control glass slide	✔	✔	None	1000 ± 60
PDMSe-coated glass	✔	✔	Foul-release	48 ± 2
Unpolished SS 316L	✔	✔	None	~ 1000
Abraded SS 316L	✔	_	None	~ 1000
PDMSe + Cu particles	✔	✔	Cu^{+}	variable
Commercial AF				
Waterways AF	✔	_	Biocide	22.5 ± 0.85
Copper plate	✔	✔	Cu^{+}	350
Cruiser Uno AF	✔	✔	Biocide	20 ± 0.2
Trilux	✔	✔	Biocide	30.6 ± 0.9
Micron Extra	✔	✔	Biocide	17.2 ± 0.2
Interspeed Ultra	✔	✔	Biocide, SPC	27.8 ± 3.7

Copper plate (Radionics Ltd., Ireland) and stainless steel plate were guillotined to standard microscope slide dimensions and fitted to the slide holders. Copper powder was obtained from Coppercoat commercial AF (Aquarius Marine Coatings Ltd). Commercial coatings were applied to glass microscope slides with a spin-coater (Model KW4A, Chemat Technologies Inc, Northridge CA). Poly(dimethylsiloxane) elastomer (PDMSe) (Sylgard 184 kit, Dow Corning, Michigan USA) was prepared by mixing base to curing agent in the ratio 10:1 by weight, followed by degassing of thoroughly mixed uncured elastomer in a dessicator. To investigate any improvement in performance of this material by incorporation of a biocide, copper power was added to mixed uncured elastomer (5% w/v). The structure of this elastomer is shown in Figure 2-6.

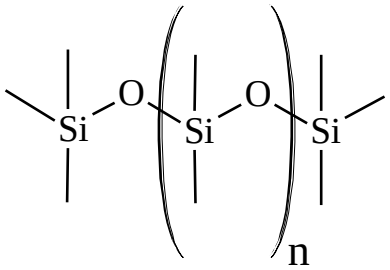

Figure 2-6: The chemical structure of poly(dimethylsiloxane) elastomer used in this study.

Cleaned and degreased slides were coated using the spin-coater operated at 3000 rpm for 30 s. The mixed uncured elastomer or commercial coatings were transferred with a pipette onto the surface of the slide to be coated while held in a purpose built vacuum chuck. Slides coated in this manner were then cured at 50 °C for 24 h in a vacuum oven (Technico, Fistreem International Ltd., UK). Final dry film thickness (DFT) was determined by measurement of the mass and area of the coating. Slides were weighed before and after coating and the thickness calculated using Equation 2-1.

$$T = \frac{m \times 10}{A \times d} \qquad \text{Equation } 2-1$$

Where T is the coating thickness (μm), m is the mass of the coating (mg), A is the area coated (cm^2), and d is the density of material ($g\ cm^{-3}$).

2.2.8 *Roughness measurements*

Material roughness measurements were performed with a TR200 Portable Surface Roughness Tester (Beijing TIME high technology Ltd) and Timesurf Software (Version 1.4). The device setting parameters used in measurements were sampling length, 0.25 mm; traversing speed, $V_t = 0.135\ mm\ s^{-1}$; measuring range, ±40 μm; and resolution 0.01 μm.

2.2.9 *Spectrophotometric measurement*

Spectrophotometric analysis of transparent and semi-transparent coatings (Glass, PDMSe and PDMSe incorporating Cu particles) was conducted with a spectrophotometer (Red Tide, USB-650, Oceanoptics) equipped with a 150 mm diameter integrating sphere assembly (Labsphere) and a HL2000 light source. Measurements were conducted complete exposed and reference slides using a slide holder and spectrophotometer setup as illustrated in Figure 2-7. Prior to analysis slides were stained with AO (Sigma-Aldrich, Tallaght, Dublin) by immersion of slides and attached materials in 10 µg mL^{-1} AO, dissolved in de-ionised H_2O for 120 s at ambient temperature. Slides were then dip-rinsed twice in de-ionised H_2O to remove excess stain. Measurements were conducted on exposed slides and referenced to an unexposed control slide stained in the same manner as exposed slides.

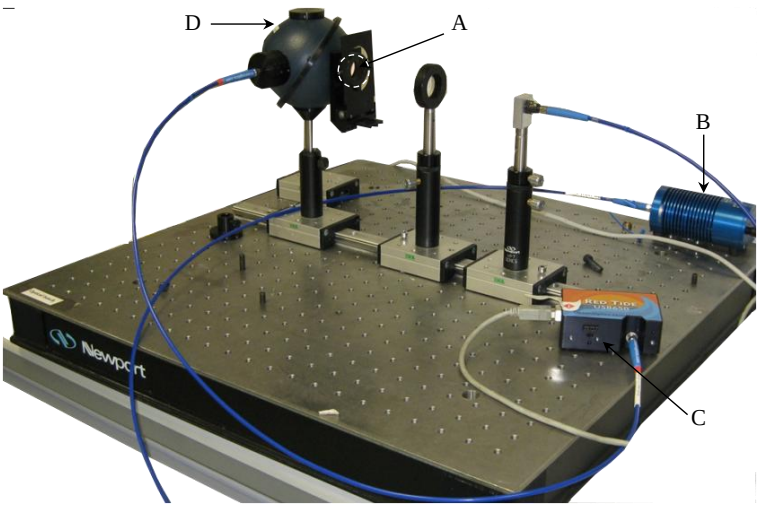

Figure 2-7: Digital image of the experimental setup for spectrophotometric analysis, A=slide holder, B=light source, C=USB 600 spectrometer, D=integrating sphere.

2.2.10 *Wettability measurements*

Wettability of materials was measured before and after deployment with an FTA 200 contact angle analyser (First Ten Angstroms Inc., Portsmouth, VA) using a sessile drop technique. For measurement of control and coated slides, 5 µL of ultra-pure Milli-Q water (resistivity < 18 MΩ cm^{-1}) was placed on the slide surface using a syringe. For contact angle analysis, a single frame movie was taken with a video CCD camera, and the contact angle was measured by fitting a mathematical expression to the shape of the

drop and then calculating the slope of the tangent to the drop at the liquid-solid-vapour interface line.

2.2.11 *Preservation of microbial biofilms*

Attached microbial biofilms on deployed slides were chemically fixed by placing the slides with attached biofilms into 50 mL centrifuge tubes (Sarstedt, Ireland) containing 2.5% (v/v) gluteraldehyde (Sigma-Aldrich, Tallaght, Dublin) in 0.45 µm filtered seawater, desalted by rinsing in 50:50 seawater distilled water, followed by distilled water and dried before analysis.

2.2.12 *Microbial biomass calculations*

Coated slides and materials were weighed before deployment with a scientific balance (Model BP211D, Sartorius, Germany). Increases in the mass of deployed materials after immersion was calculated upon removal and used as an indication of biomass growth. Complete slides with attached material were dried in a glassware oven (LEEC Ltd., UK) at 40 °C until no change in mass had occurred for 24 h. Slides were then weighed and the percentage change in mass calculated prior and post deployment.

2.2.13 *Scanning electron microscopy (SEM)*

Attached biofouling was visually analysed with a thermionic emission variable-pressure SEM (Hitachi, VP-SEM S-3400N) equipped with an Everhardt Thornley secondary electron (SE) detector, high sensitivity semiconductor backscattered electron (BSE) detector and Oxford Energy Dispersive X-ray Spectrometry (EDS/EDX) detector. Biofilm samples from fixed and dehydrated microscope slides were divided into subsamples approximately 1 cm^2 using a ceramic glasscutter. Samples were sputter-coated with either gold (Edwards 150B sputter-coater) or carbon coated (Agar Auto, Agar scientific, Stansted, UK). Samples were mounted on 15 mm diameter aluminium stubs using double-sided adhesion carbon tabs (Agar scientific, Stansted, UK). Samples were imaged in both SE and BSE mode where stated.

2.2.14 *Epifluorescence microscopy*

Attached biofilms were stained with acridine orange (AO) (Sigma-Aldrich, Tallaght, Dublin) and epifluorescence microscopy was used to enumerate attached cells on transparent substrates. The chemical structure and excitation and emission wavelengths of AO are shown in Figure 2-8.

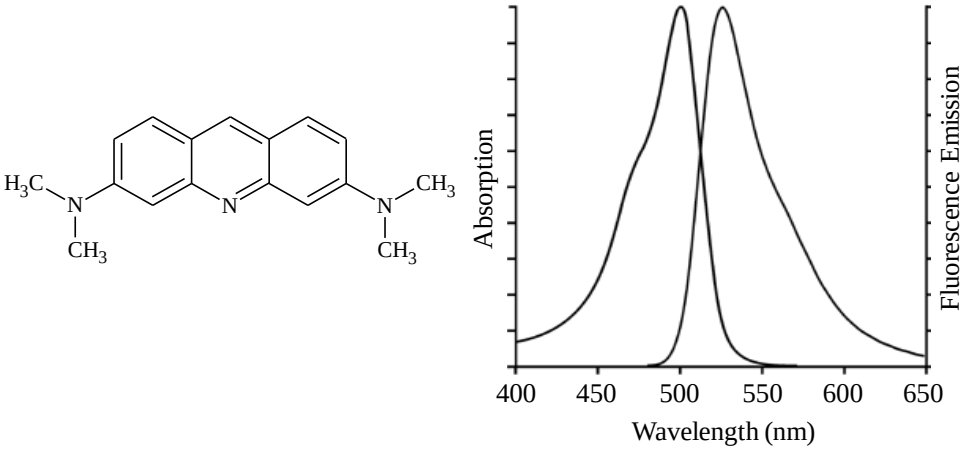

Figure 2-8: Chemical structure (left) and graph of both absorption and emission spectra of AO bound to DNA (right). DNA intercalated AO fluoresces green (525 nm) while RNA electrostatically bound AO fluoresces red (>630 nm) (Spectrum from Molecular Probes®, www.invitrogen.com)

Samples were stained by immersion of slides and attached materials in 10 µg mL^{-1} AO, dissolved in de-ionised H_2O for 120 s at room temperature. Slides were then dip-rinsed twice in de-ionised H_2O to remove excess stain. Epifluorescence microscopy was conducted with a Leica epifluorescence microscope equipped with a DFC 500 high-resolution digital camera system (Leica Microsystems Ltd., Switzerland, software version 2.7.1 R1 Build 1384) and a 100-W mercury vapour lamp using 20x/0.40 and 40x lenses giving a magnification of 200/400 x. Epifluorescence imaging was conducted with both a Leica I3 and N2.1 filter cube providing excitation wavelengths in the range 450-490 nm (LP515) and 515-560 nm (LP590) respectively.

2.2.15 *Enumeration and identification of diatom frustules*

Biofouling of materials was analysed for diatom settlement with ImageJ image analysis software [18]. Images acquired from 15 random fields of view (FOV) per slide at magnifications of ×400 (0.66 mm^2) and used to enumerate intact diatom cells. Diatoms were identified at least to genus level using SEM by using a 0.2 mL aliquot resuspended

from the fixed samples from individual slides and incubated with 5% hydrochloric acid for 24 h to remove organic material.

2.3 Results and discussion

The overall aim of this study was to identify and examine the process of biofouling in a number of different environments on environmental sensors and prominent commercial AF materials. It was envisioned that this would result relating the nature and extent of biofouling to disruption of environmental monitoring instrumentation. The estuarine and marine sites chosen in this study were considered to as representing two different biofouling environments.

2.4 Results and Discussion of Site 1: Poolbeg Marina, River Liffey Estuary

Biofouling in estuarine conditions is comparatively poorly studied and little is known about the species composition, settlement rate and sequence of biofilm formation that occurs on immersed surfaces in these conditions. Pelletier and co-workers recently evaluated the performance of chitosan and copper-based AF paints in the St. Lawrence Estuary (Canada) [19]. Interestingly, these authors concluded that both paints were equally ineffective against biofouling after two months immersion, suggesting that the use of expensive copper paints was not required in the conditions at their test site. This is in direct contrast to a marine environment, where copper is often reported as the only effective AF mechanism, outside of synthetic biocides.

Benthic diatoms and bacteria are also reported as significant components of attached biofilms on artificial surfaces in estuaries. Biofilm development on stainless steel and polycarbonate surfaces has recently been examined in the Delaware Bay using 16S rDNA libraries, fluorescence in situ hybridization (FISH), and denaturing gradient gel electrophoresis (DGGE) [20]. It was reported that alpha-proteobacteria in the *Rhodobacterales* clade dominated attached communities and different bacteria communities were initially associated with different materials. However, the composition of microbial communities gradually converged with time in estuarine waters. Diatom community structure in estuaries is also little studied, although seasonal variations in the fouling diatom community structure on stainless steel and polystyrene surfaces immersed in a tropical estuary have been reported [21]. The latter study suggested that the rapid onset of macrofouling disrupted natural development of the biofouling diatom community, such that the normally dominant diatom genus *Amphora* was replaced by *Navicula* species. Thus, it appears that a comparison between sensor and material performance in an estuarine and marine environment would lead to important insights into the differences in biofouling composition.

In this study, initial microfouling at Poolbeg Marina consisted of bacteria and microbial aggregates, while the resulting macrofouling layer became rapidly dominated by the invasive barnacle species, *Austroliminus modestus* (Synonym: *Elminius modestus*) (Darwin, 1854). In contrast, diatoms dominated initial microfouling at Lough Hyne Marine Reserve while calcareous macrofouling such as serpulid and cirripeds and the saddle oyster *Anomia ephippium* (Linnaeus, 1758), together with filamentous algae, dominated the later stage macrofouling.

2.4.1 *Sensor performance, Poolbeg Marina, Dublin*

Poolbeg Marina is located in the commercial centre of Dublin Port and the River Liffey estuary, opening into Dublin Bay, a shallow bay surrounded on three sides by Dublin City and open on the east to the Irish Sea. The effects of excess nutrient loading have been observed in Dublin Bay for almost a century and the area has become intensively developed in recent decades [22]. As such, the environmental conditions at this location are an important indicator of the environmental status of Dublin Bay and the site is a future candidate for long-term environmental monitoring programmes. However, to date no long-term continuous environmental monitoring programme is in place and this study was the first to collect environmental data using continuous monitoring at this location. In total some 20,400 environmental measurements were collected from each of 4 sensors over the deployment period. A brief summary of this data is presented in Table 2-5, where it can be observed that the site is well-oxygenated, with high variability in temperature and dissolved oxygen values.

Table 2-5: Summary of environmental variables measured at Poolbeg marina, Dublin port, between September 2010 and May 2011.

	Water temperature (°C)	Sp-Cond (mS cm^{-1})	Dissolved Oxygen (%)	Dissolved O_2 (mg L^{-1})	Turbidity (NTU)	Salinity (ppt)
Mean	9.3	48446.8	99.6	9.3	5.2	20.3
S.D.	3.35	2702.35	5.11	0.83	4.82	0.76
Max	16.61	51549.00	162.90	14.19	293.60	34.8
Min	3.20	193.00	5.11	0.83	-6.20	0.02

High variability in turbidity measurements were also recorded and were correlated with rainfall, tidal conditions and commercial shipping activity (data not shown). Water temperature varied greatly (Max = 16.61 °C, Min 3.2 °C) at the location chosen over the deployment period, and the site remained well-oxygenated throughout the deployment period. A graph of these measurements over the whole deployment period is shown in Figure 2-9, where it can be seen that temperature is lowest in mid-winter at the site when the surface of the river was frozen.

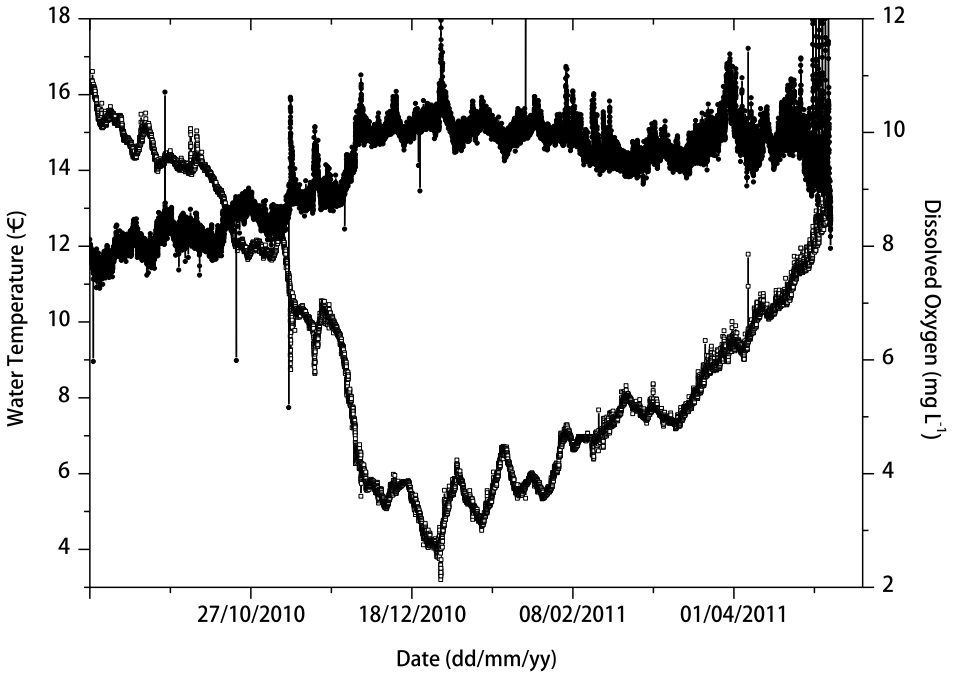

Figure 2-9: Graph of temperature and dissolved oxygen values at Poolbeg marina over the deployment period at a depth of 2.5 m below the surface. (Dissolved oxygen = solid symbols, Temperature = hollow symbols).

As well as the temporal variability in environmental conditions, this site also had high spatial variability, as indicated by profiles of the water column. An example of this is shown in Figure 2-10, where the variability in both salinity and water temperature can be observed. This variability in salinity values is typical of an estuarine site such as Poolbeg [23, 24]. Indeed stratification in Poolbeg estuary is the subject of a recent three-dimensional hydro-environmental model of Dublin Bay [25]. The latter study concluded that stratification was magnified by freshwater inflow from the Liffey River, complicated by the tidal currents into and out of the Liffey Estuary.

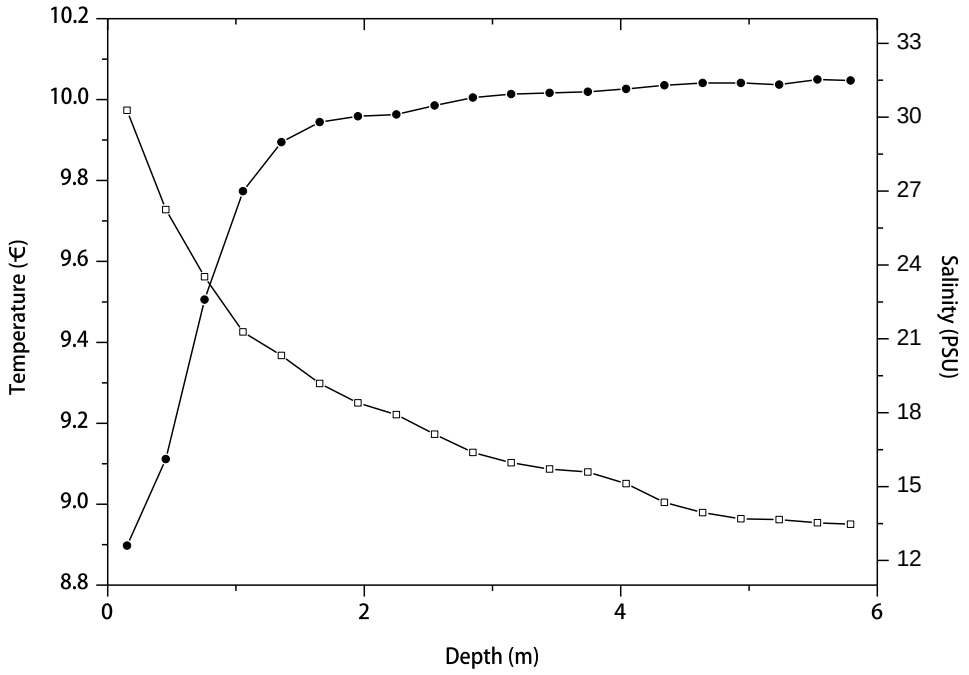

Figure 2-10: Water column profile from 0-6 m at the sensor deployment site illustrating stratification of the water column in terms of salinity values (profile taken on the 28/03/2011 14:51). (Salinity = solid circles, Temperature = hollow squares).

An example of turbidity and pH values area also shown in Figure 2-11, where periodic turbidity events resulting from sediment re-suspension are also shown.

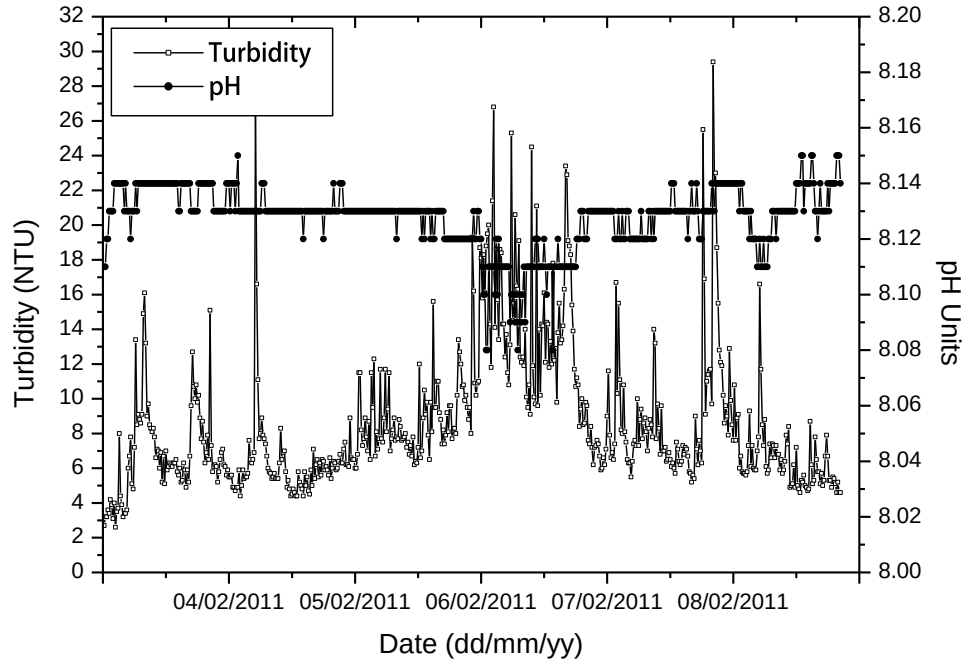

Figure 2-11: Graph of sample turbidity and pH levels recorded at Poolbeg marina during the study period.

2.4.2 *Biofouling in the Liffey Estuary*

Sensor power and data transmission requirements are easily met at the Liffey Estuary, thus biofouling is the most serious obstacle to long-term autonomous sensor deployment at this location. Knowledge of both the biofouling conditions, rate and species occurrence are of value in developing a suitable AF strategy for any environmental monitoring instruments deployed at such a location and for the estuarine monitoring in general.

The YSI 6600 V2 data sondes used in this study are designed for extended deployment in both freshwater and marine environments. These sondes are also "open" instruments, in which the installed sensors are directly exposed to the surrounding water body rather than having water pumped past the sensors. In addition, such instruments have been utilised extensively for estuarine and marine monitoring purposes [26, 27]. In common with other sensors, the validity of the data produced by these sondes is reliant on minimal interference from biofouling [2].

As of late 2011, optional AF kits are available from the manufacturer, consisting of copper sleeves and copper protective guards for each individual sensor, copper tape and "C-spray", a low surface energy coating supplied as a spray for areas difficult to coat with copper. Furthermore, the protective sensor guards are now available in copper alloy and membrane casings on optical dissolved oxygen sensors are now being manufactured from a similar copper/tin alloy. However, these additional biofouling protection measures were not yet available on the sondes in this study so settlement rates of biofouling on the sensing surfaces were assessed in the absence of any protection by biocidal means. During the 242-day deployment period at Poolbeg Marina, the sensor was continuously immersed, aside from removal for examination of the extent of biofouling. In agreement with other reports on estuarine biofouling, low initial biofouling rates (<0.5 mg cm^{-2} day^{-1}) were observed [19]. The mechanical wiper AF systems integrated into the sensors were thus able to provide adequate biofouling protection for optical sensors for the majority of the deployment duration.

Despite the ability of mechanical wipers to protect the sensing components of the deployed sondes from biofouling, the sonde casing was extensively colonised by biofouling during the deployment period. Macrofouling was dominated by *A. modestus* (Cirripedia; Thoracica, Class: Maxillopoda, Subclass: Thecostraca, Superorder:

Thoracica, Order: Sessilia, Family: Austrobalanidae, Genus: Austrominius) and colonisation of the sensor surface by this species occurred within weeks of immersion. Growth was initially observed on topographic features present on the sonde casing. These features consisted of label edges, indentations, laser markings and tooling marks resulting from the manufacturing process. *A. modestus* rapidly propagated from these locations, eventually dominating the macrofouling community attached to the sonde casing. Figure 2-12 illustrates the initial settlement pattern of this species after 8-12 weeks of deployment. The relationship between gregarious settlement of *A. modestus* and surface textures on the sonde casing can be observed.

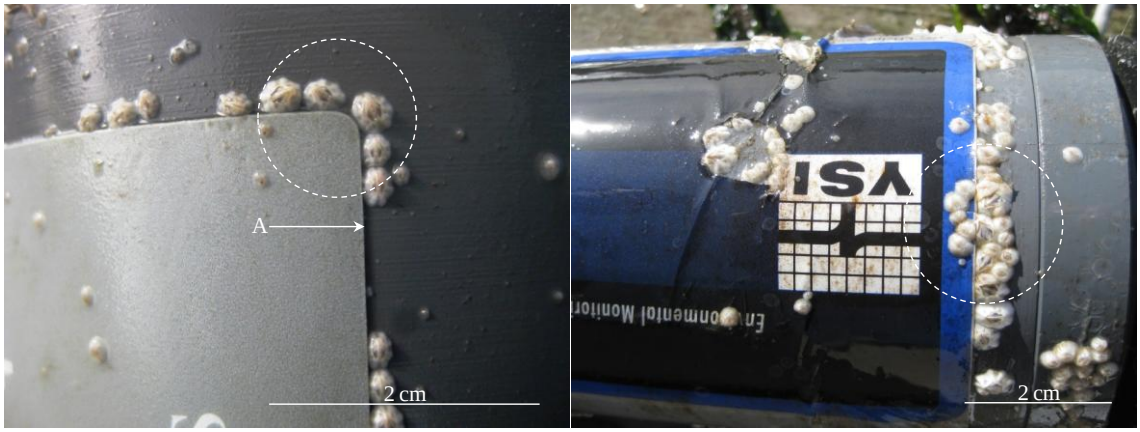

Figure 2-12: Digital images of the sonde casing deployed at Poolbeg marina. The barnacle species Austroliminus modestus has initially gregariously settled on the polymer casing (right, circled), aligned with surface topography on the casing (arrowed). This topography is a 750 µm edge created by a manufacturing label. Barnacles have begun to further colonise the casing from these initial settlement points after 60 d (left).Scale bar ~ 2 cm.

Colonisation of immersed surfaces in the estuary of the River Liffey by *A. modestus* is not surprising given the reported high growth rates of this species within estuaries throughout Europe [28, 29] . This species is a small (< 13 mm diameter), four-plated, Australasian barnacle that was first introduced to Britain in the 1940s, from where it spread to continental Europe and Ireland [30, 31]. It is eurythermal and euryhaline, with a high reproductive capacity, long settlement period, capability to utilise a wide range of food and ability to withstand turbid waters [30]. Thus, the environmental conditions in the Liffey Estuary would seem ideal for *A. modestus* to dominate the macrofouling community. The final extent of colonisation of the sensor casing at the end of the deployment period in April 2011 can be seen in Figure 2-13. Most (>90 % coverage) of the available surface area has been colonised, although effects of initial macrofouling growth associated with surface features can still be observed.

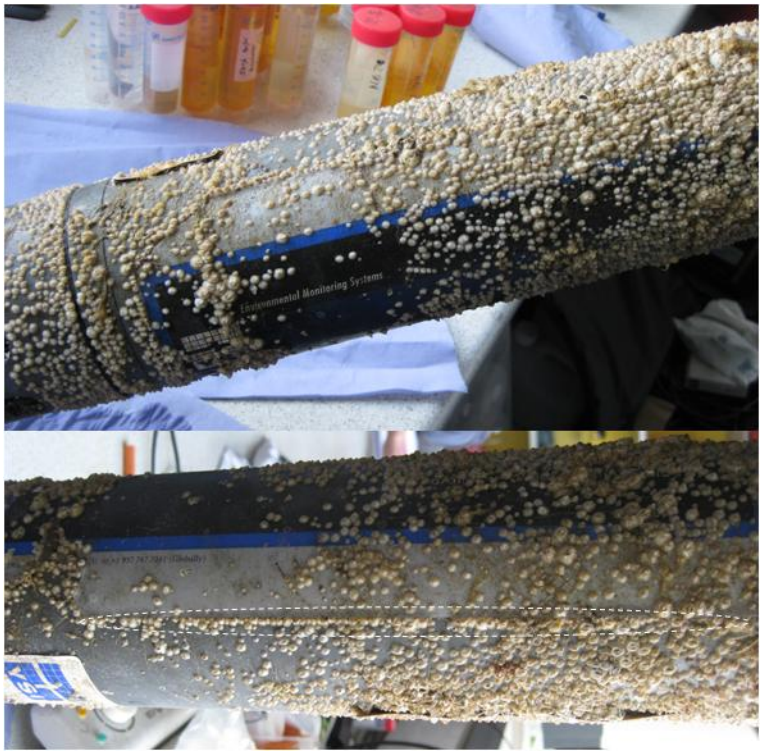

Figure 2-13: Digital images of Austrominius modestus settlement on the casing of an environmental sonde at the end of the deployment period at Poolbeg Marina. The influence of surface features on initial settlement patterns can still be observed (circled).

Gregarious settlement among individuals of *A. modestus* has been suggested in early studies by Knight-Jones and Stevenson, who noted that field observations by their peers suggested that preferential settlement of this species occurred alongside surface projections [32]. Additionally, investigation the presence of pre-existing biofilm growth on the attachment strength of *A. modestus* indicates that cypris larvae of this species have higher attachment strength on relatively thin, dense biofilms associated with high shear, in comparison to relatively thick, less dense biofilms associated with low shear [33]. This is an advantage for cyprids in an estuarine environment such as the Liffey Estuary, where stable but relatively thin biofilms develop and where high shear forces from hydrodynamic flow rates exist across surfaces.

Influences of surface topography on barnacle adhesion has been investigated in detail on environmentally inert marine coatings [34-38]. Many early studies indicated that barnacle cyprid settlement preferentially occurred on rough surfaces and indicated that adhesion strength would be greater on such surfaces. However, recent studies have examined the influence of microtextured surfaces on both cyprid behaviour and retention of adult barnacles. From these studies it has been determined that *Balanus improvisus* preferentially settles on smooth surface, with surface texture with profile heights within

a topographic range of 30–45 µm reducing settlement and cyprid recruitment by 92% as compared with smooth surfaces [35]. However, cyprids of *Semibalanus balanoides* are reported to settle preferentially on resin tiles with a surface texture in the range of 0–0.5 mm [39]. From the results of these studies and the present results it can be concluded that optimisation of texture design for reduced barnacle colonisation is required to improve the AF performance of current environmental sensors.

2.4.3 *Microfouling development in the Liffey Estuary*

Materials deployed alongside sensors at Poolbeg Marina, in the Liffey Estuary were periodically assessed for extent and composition of microfouling over the deployment period. Microfouling of materials was analysed from the same depth as the sensors and within a lateral distance of 0.5 m in order to avoid any undue disturbance to sensor measurements by the deployed panels. Deployed materials were removed periodically at 6, 13 26, 47 and 84 d into the study, beginning at the time of sensor deployment. These times depended upon access to the marina and sensor validation procedures, and were not chosen based on any prior knowledge of the biofouling regime at this location.

SEM visualisation of microfouling at Poolbeg Marina indicated that bacteria were the dominant microfouling organisms attached to materials throughout the study period. This is in agreement with the studies of Moss and co-workers who examined the bacterial biofouling community monthly over 1 year for 7-day incubations during peak tidal periods in East Sabine Bay, Florida [40]. These researchers reported that bacterial community structure appeared to be stable during fluctuating environmental conditions despite changes in salinity and in dissolved oxygen. Bacterial species were not identified in this study but it is reported that members of the *Roseobacter* clade of the alpha-proteobacteria and the *Alteromonas* group of the gamma-proteo bacteria are associated with primary colonisation of surfaces exposed in coastal environments [20]. Representative images of microfouling on immersed PDMSe and control glass slides is shown in Figure 2-14, where the progression from individual bacterial cells to microfouling aggregates can be observed.

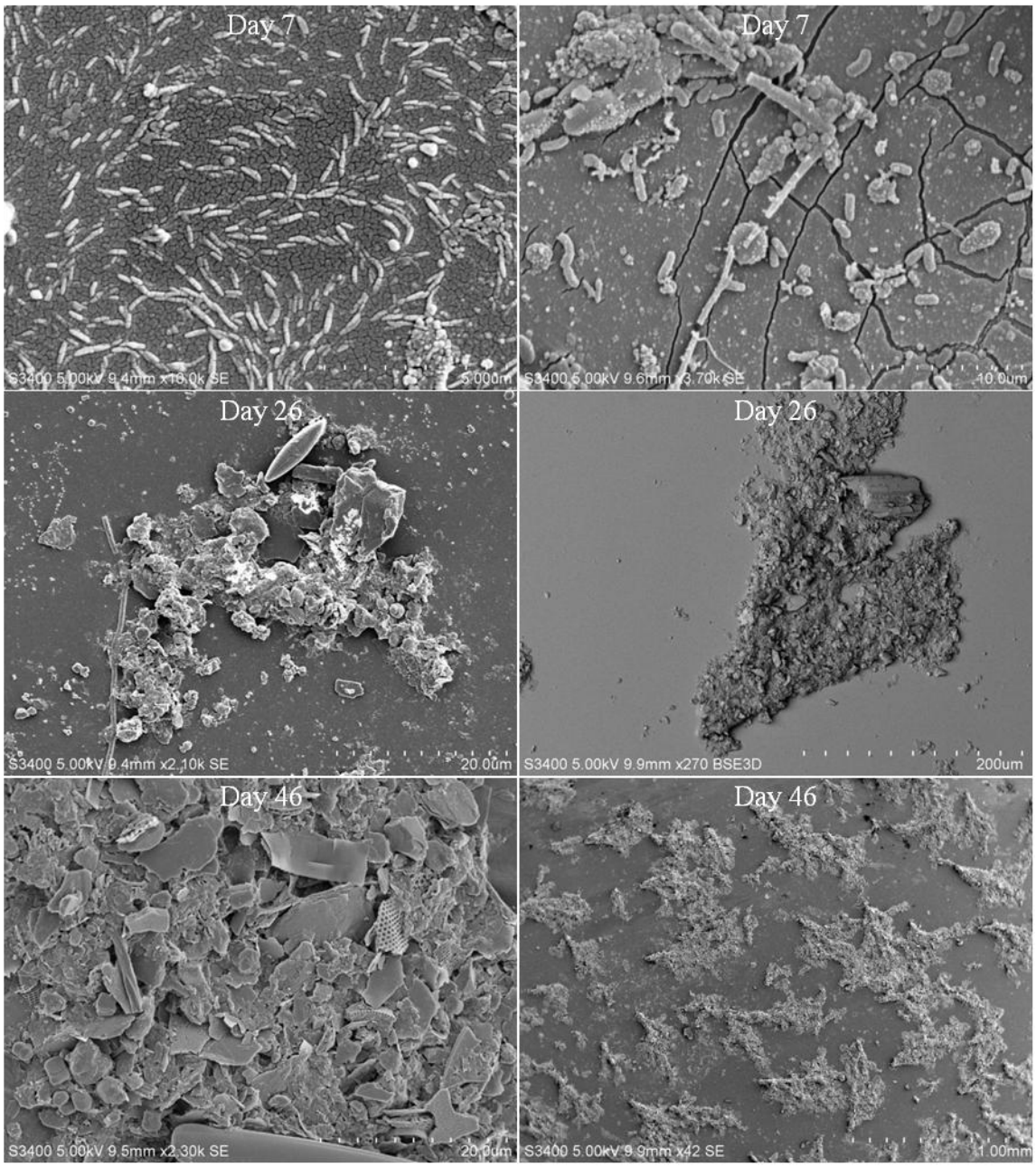

Figure 2-14: Scanning electron micrographs of fouling on a glass (left) and PDMSe surface (right) immersed at Poolbeg Marina, Dublin Port. Rod-shaped bacterial cells are seen to have attached to glass surfaces after 7 days, while bacterial cells are less abundant on PDMSe surfaces. By day 26, diatom cells are visible on both surfaces and biofouling has begun to develop into surface flocculation. By day 46, biofouling is extensive and consists of large amounts of diatom frustule debris, entrapped in microbial polymers, particularly on glass surfaces and large surface flocs have developed on PDMSe materials.

Importantly, it was observed in this study that bacterial cells did not adhere as individual cells to all deployed surfaces. Instead microbial aggregates formed part of the initial microfouling biofilm as illustrated by scanning electron micrographs of biofouling at Day 46 of deployment in Figure 2-14. These microbial aggregates rapidly established and appeared to be orientated with flow direction. After 26 days substantial

aggregates were present on all coatings not containing biocides. Biofouling aggregates have been reported for foul-release coatings in estuarine waters previously by Pelletier and co-workers, although they did not observe the formation of the aggregates or examine the composition in detail [19].

SEM analysis of microbial aggregates in this study indicated that these structures were composed of microbial cells and organic matter, bound together with filamentous structures. BSE- SEM analysis indicated the presence of fragments of silica diatom frustules within these aggregates, with few intact individual frustules. A microfouling layer had developed on all coatings after 46 d, however such aggregates were larger and covered a greater surface area on PDMSe-coated surfaces, while microfouling of the glass surface consisted of more intact diatom frustules and smaller aggregates. It could not be established if surface features seeded the formation of such aggregates on deployed materials or if the formation of such structures was a result of local hydrodynamic conditions.

Large numbers of diatom frustules were only apparent on materials after 46 d immersion. Materials removed at 46 d contained a number of identifiable frustules belonged predominantly to the genus *Cocconeis* or *Navicula* although other species were occasionally present in examined samples. Figure 2-15 illustrates some of the most common diatom frustules observed in microfouling at Poolbeg Marina in this study.

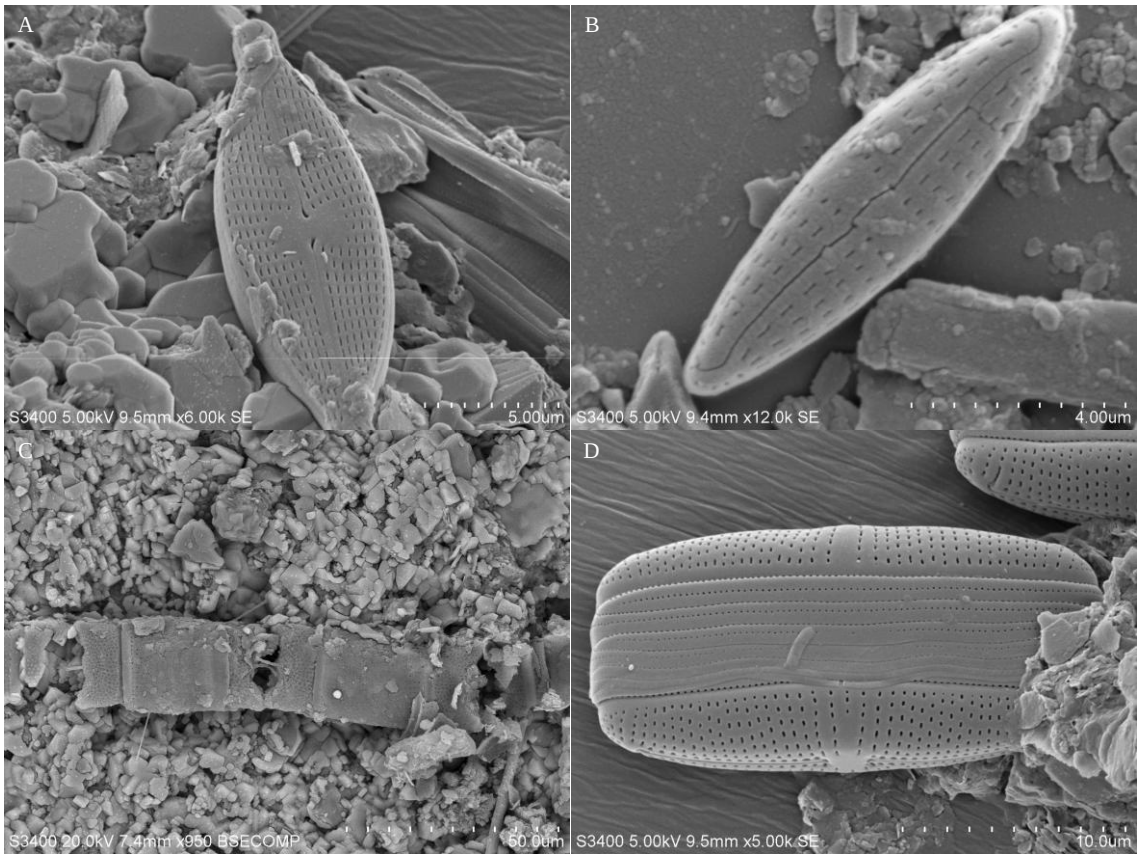

Figure 2-15: Scanning electron micrographs of diatom species observed on coatings deployed at Poolbeg marina. A = Navicula on PDMSe, B = Navicula on glass, C = Odontella aurita on Waterways AF, C = common unidentified diatom on PDMSe, possibly Paribellus.

All coatings and materials experienced biofouling at the end of the field trials, with the exception of the copper plate. Waterways commercial AF was initially an effective AF coating as indicated by mass increase and SEM. However, from day 26 – 46, an extensive biofilm had formed and an increase in mass was recorded. SEM visualisation indicated isolated cells attached to the surface within 7 days of immersion. However, cells remained isolated and microcolonies had not yet formed. Scanning electron micrographs of samples at day 26 indicated that the coating had now had large pores from leaching of the biocide. This is illustrated in Figure 2-16 where the porous nature of the coating is visible and initial colonisation by isolated bacterial cells is evident. At the termination of the trial, the measured mass increase of Waterways AF was comparable with that of the non-biocidal coatings and extensive barnacle adhesion to the surface had occurred.

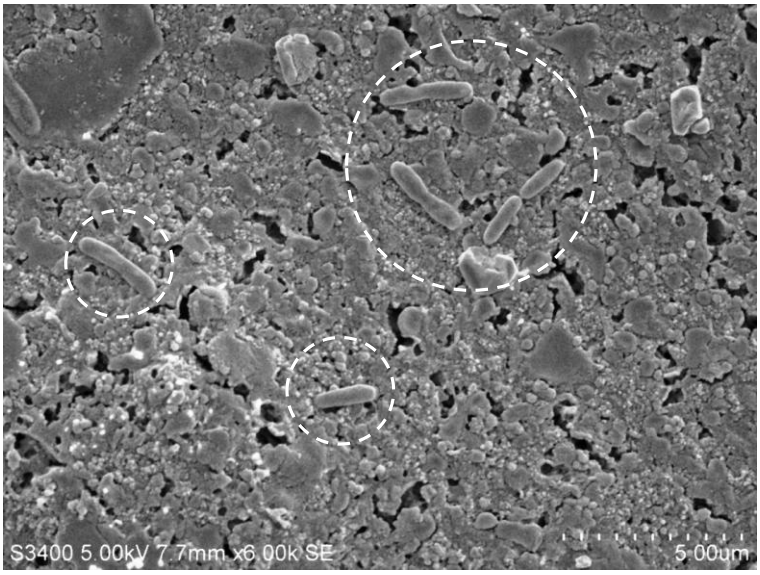

Figure 2-16: Scanning electron micrograph of bacterial colonisation (circled) on Waterways commercial AF after 14 d immersion at Poolbeg Marina. The porous nature of the coating is also visible.

Measurement of mass change associated with the other deployed materials indicated that both PDMSe and glass surfaces exhibited the greatest increases in mass, while copper plate performed best with a decrease in mass due to corrosion of the plate surface. The mass changes associated with PDMSe, glass and copper plate after 84 d at Poolbeg Marina is shown in Figure 2-17.

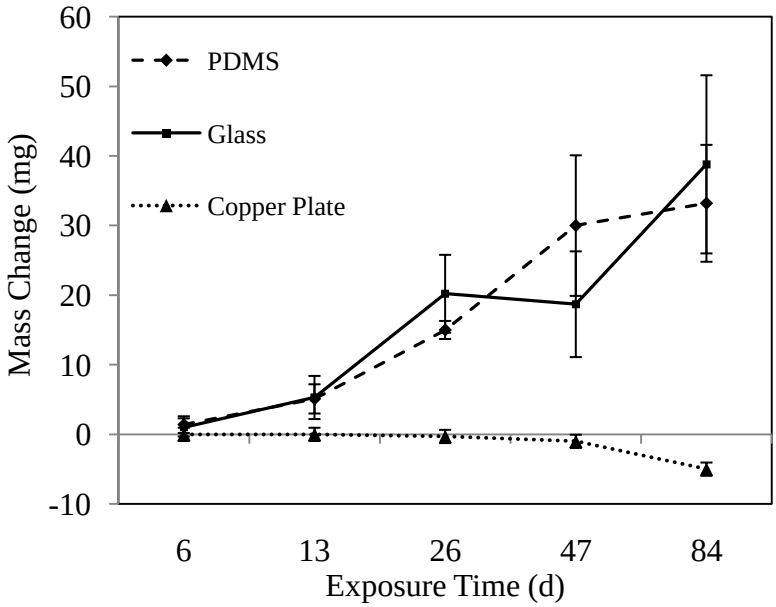

Figure 2-17: Graph of measured mass change associated with PDMSe, glass and copper surfaces at Poolbeg. Copper was the least fouled surface at the end of the exposure period, with a decrease in mass due to erosion of the plate, while glass exhibited the highest increases with 38.8 mg slide^{-1} ± 12.8 standard deviation.

In common, with the observations of macrofouling recruitment to the sensor casing at Poolbeg Marina, *A. modestus* dominated the macrofouling community on deployed AF coupons. The exception to this included both copper plate and smooth PDMSe surfaces. The deployed copper plates were completely devoid of visible biofouling, both by visual inspection and by SEM. Figure 2-18 illustrates the extent of the biofouling that occurred on materials after 84 days exposure at Poolbeg Marina.

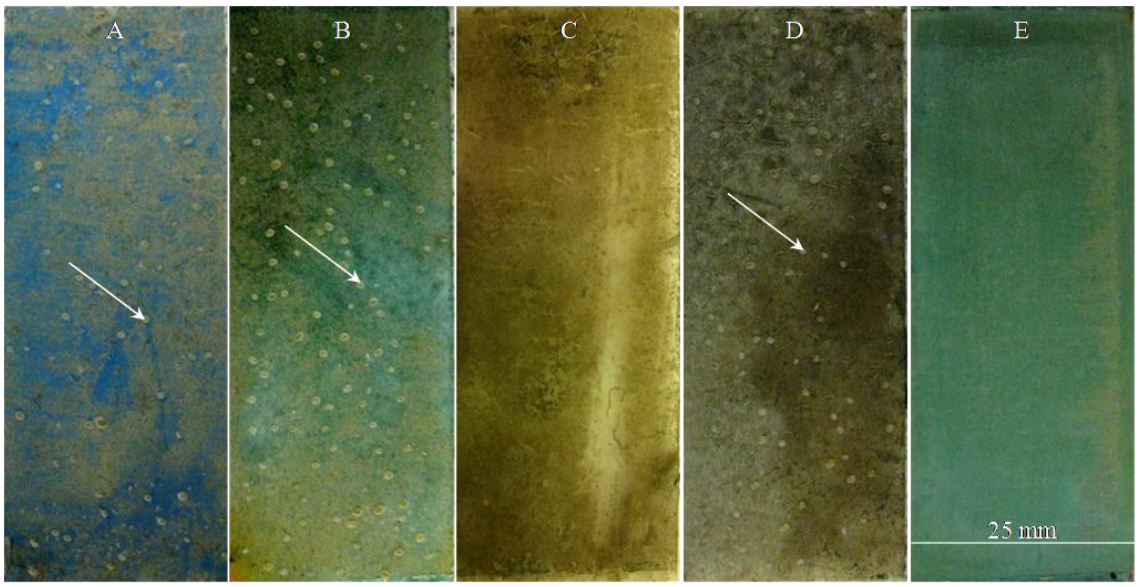

Figure 2-18: Digital images of deployed materials at Poolbeg Marina after 12 weeks. A=Waterways commercial AF, B=PDMSe incorporating Cu-microspheres C=PDMSe-coated slide, D = uncoated glass control and E= copper plate. Austrominius modestus can be observed on material A, B, and D (arrows).

Intact barnacles were enumerated on each material surface, the results of which are shown in Figure 2-19. Surprisingly with the exception of copper plate as a positive control, analysis of recruitment after 84 days indicated that slides coated with PDMSe containing Cu-microparticles had highest recruitment of barnacles, while glass surfaces were also heavily colonised. Smooth PDMSe surfaces were not heavily colonised perhaps indicating that the surface roughness caused by the presence of the particles was responsible for this recruitment. The copper particles were also either unavailable as a biocide due to coating with PDMSe or present in non-lethal concentrations at the surface of the coating.

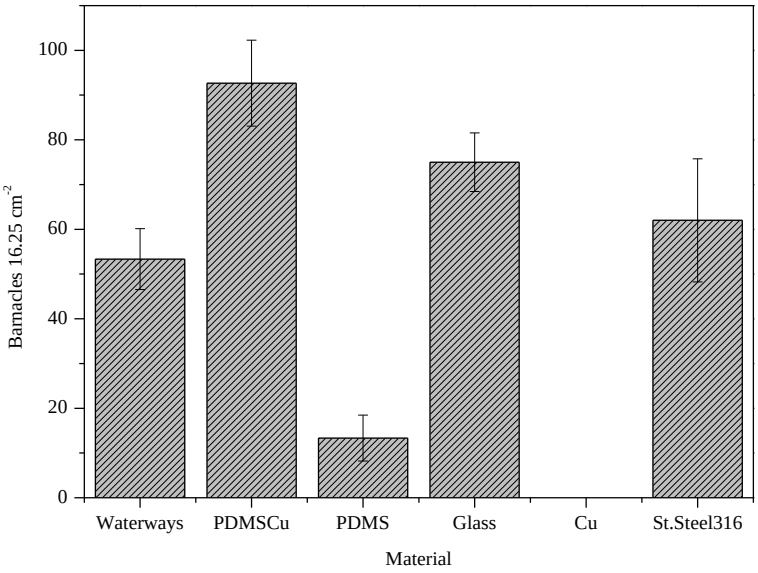

Figure 2-19: Recruitment numbers of the barnacle species Austrominius modestus to materials at Poolbeg Marina after 2 months. Values are the mean of 3 slides ± 1 standard deviation.

Interestingly, only stainless steel surfaces in this deployment were heavily colonised by other macrofouling organisms outside of *A. modestus*. The bryozoan, *Membranipora membranacea* was observed on all stainless steel surfaces after 84 d (Figure 2-20). Like *A. modestus*, this species is also invasive and appears to thrive in the environmental conditions in the Liffey Estuary.

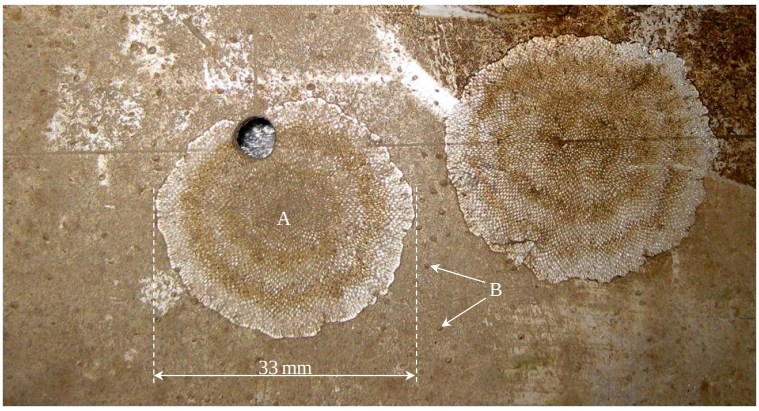

Figure 2-20: The Bryozoan species Membranipora membranacea (A) attached to 316 grade stainless steel at Poolbeg Marina at removal in April 2011. Juvenile barnacles of Austrominius modestus are also visible (B).

2.4.4 *Wettability measurements*

Wettability is one of the surface characteristics that is controlled by the chemical composition and roughness of a surface [41]. As such, analysis of contact angle as a means of examining surface properties has been extensively utilised in AF material development [42-45]. The relationship between water contact angle and surface free energy of polymeric coatings with the settlement and adhesion strength of various marine organisms has also been recently investigated [46, 47]. In this study, contact angle measurements were measured before deployment and on materials retrieved after 13 days.

With a contact angle of 90-120°, PDMSe incorporating copper particles was the most hydrophobic material deployed. The measured values of PDMSe are in agreement with published values [48]. All commercial AF coatings were slightly hydrophilic in nature, while cleaned glass was the most wettable of the surfaces deployed, with a CA of 20 ° prior to deployment.

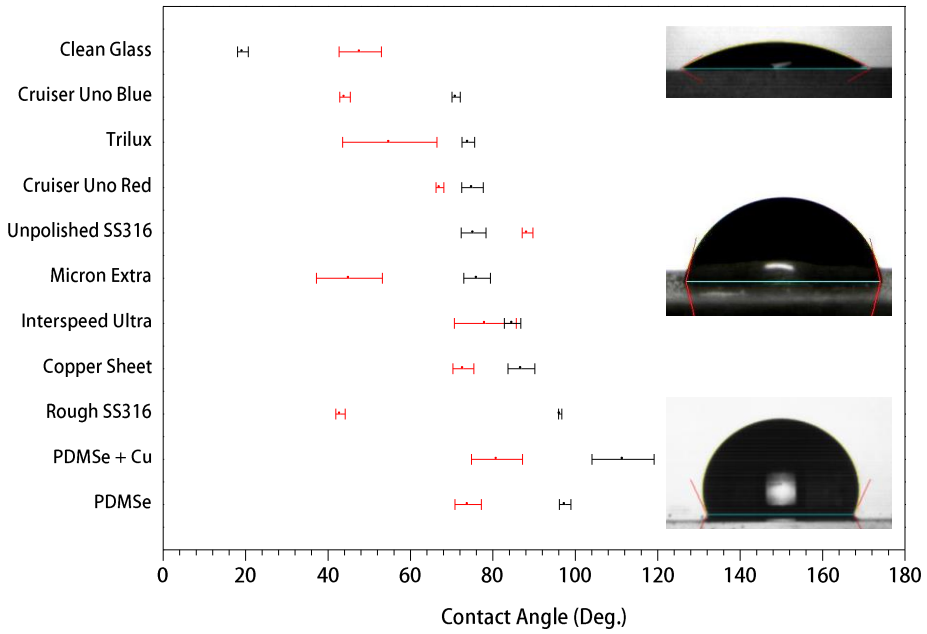

Figure 2-21: Graph of initial contact angle measurements (black symbols) and materials retrieved after 13 d deployment at Poolbeg Marina (red symbols). (Values are mean of n =3 measurements ± 1 standard deviation). Insets are digital images of representative contact angles on glass, Micron Extra and PDMSe surfaces.

In general, surfaces exhibiting high wettability such as the control glass slide had increased wettability after 13 d, while others such as the roughened stainless steel

surface exhibited lower wettability (Figure 2-21). Interestingly, unpolished stainless steel exhibited decreased wettability (Mean CA = 75.33 ° ± 3) before exposure than after exposure (Mean CA = 88 ° ± 1.29), while roughened stainless steel had a higher wettability before exposure (Mean CA = 96.32 ° ± 0.39) than after exposure (Mean CA = 43 ° ± 1.15).

2.5 **Results and Discussion Site 2: Lough Hyne Marine Reserve**

Lough Hyne Marine Reserve is Ireland's only (and Europe's first) statutory marine nature reserve in County Cork (51°50′ N, 9°18′ W). Research at this location was conducted under research permit R36-38/10 from the National Parks and Wildlife Service.

Established as a reserve in 1981, Lough Hyne is a unique semi-enclosed marine Lough with a surface area of approximately 0.5 km^2. Due to the narrow (<20 m) and shallow depth (~ 1 - 5 m) at the entrance to the Lough, an asymmetrical tidal cycle exists. Generally, it takes 4 h for the tide to flow into the Lough and 8.5 h to flow out again. This site is one of the most studied marine environments nationally and scientific research has been ongoing since the 19th century [16]. The Lough is regarded as marine in composition with little freshwater influx. These conditions, coupled with the unique tidal cycle produce an ideal natural laboratory to study marine biofouling aided by a detailed knowledge of the hydrodynamics of the Lough [10-12].

2.5.1 *Sensors performance at Lough Hyne*

The two sites studied at Lough Hyne (shown previously in Figure 2-3) were chosen in consultation with both available literature and scientists based at University College Cork currently conducting research within the Lough. Both sites were selected based on the large differences in hydrodynamic conditions and residence time between sites. The North Basin site consists of a low energy, low turbulence site with a long residence time, while the South Basin site consists of a high flow rate, high-energy environment with a short residence time.

The entrance/exit between Lough Hyne and the open ocean dominates conditions within the South Basin. Analysis of tidal inflow during the present study indicates that pulses of warm, oxygenated water are distributed into this basin in the summer season. As there is bi-directional water exchange between the open ocean and the Lough through the narrow entrance channel, it can be expected that there is also a bi-directional exchange of larvae between Lough Hyne and the Atlantic Ocean. Thus, the recruitment of biofouling organisms to surfaces within the Lough may vary with distance from the entrance [50], so biofouling of materials deployed within close proximity to the entrance to Lough Hyne should occur more quickly than materials deployed at a greater distance

from the entrance. Figure 2-22 illustrates data taken during this study at the entrance to Lough Hyne that demonstrates the influence of the tidal cycle and hydrodynamic flow on environmental conditions within the Lough. The temperature increase associated with tidal flow into the Lough can clearly be observed as can a corresponding increase in dissolved oxygen associated with greater turbulence.

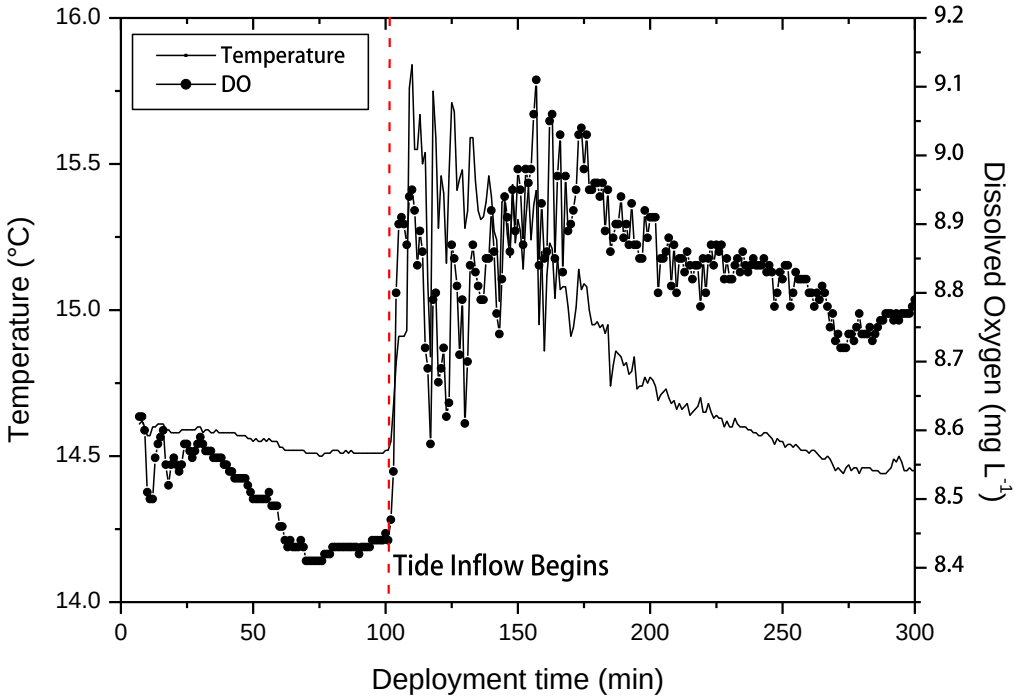

Figure 2-22: Graph of temperature and dissolved oxygen measurements on an incoming tide at the entrance to Lough Hyne at a depth of 10 m. A rise in both parameters within the water body is measured with change in tide.

In 2009, 2010 and 2011, test coupons were deployed at both locations within Lough Hyne at depths of 2 m and 10.5 m to examine biofouling on materials within the Lough. Simultaneous deployment of sensors in 2011 allowed both examination of the environmental parameters influencing biofouling rates and impact of biofouling on the deployed sensors.

2.5.2 *Sensor biofouling at Lough Hyne*

Environmental sondes were simultaneously deployed from 03/05/2011 until 01/07/2011 in both the North and South Basins of Lough Hyne with minimal disturbance except for battery renewal every 30 d and retrieval of biofouling coupons. The duration that each sonde spent out of the water was minimised during these periods and took less than 15 min to achieve.

Within 35 days of the 59-day deployment, turbidity measurements from sensors in the South Basin began to drift from values measured with a handheld sensor. This sensor is a nephelometer-type instrument that measures turbidity through an optical window. Additionally the sensor is fitted with an integrated mechanical wiper to remove fouling from the optical window. According to the manufacturer, the advantages of this sensor include (1) inhibition of both active and passive fouling; (2) nominal power consumption (3) removal of bubbles which result from out-gassing of environmental water, and (4) the fact that the sensor is mounted in the bulkhead of sonde with no interface hardware exposed to the environment. This should reduce the available area for adhesion of biofouling organisms to the surface and should present a design for optimum AF performance.

However, light-sensing devices such as this turbidity sensor need an unobstructed light path for both light source and receiver [6]. Any obstruction of the optical window will cause erroneous measurements. In this study, turbidity measurements increased from expected measurement values of <10 NTU to over 1000 NTU on the sensor deployed in the South Basin of Lough Hyne. An identical sensor deployed in the North Basin did not experience data disruption to the same extent and only experienced data drift outside of validation measurements in final days of the deployment. The difference between biofouling at the two sites as indicated by disruption of turbidity data measurements are shown in Figure 2-23 and Figure 2-24.

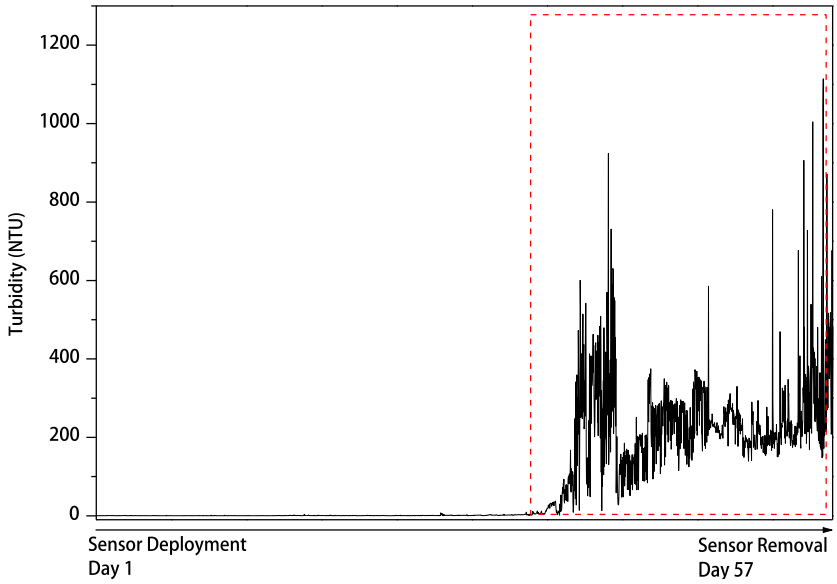

Figure 2-23: Graph of turbidity measurement disruption (red line) resulting from biofouling of the sensor deployed in the South Basin, Lough Hyne.

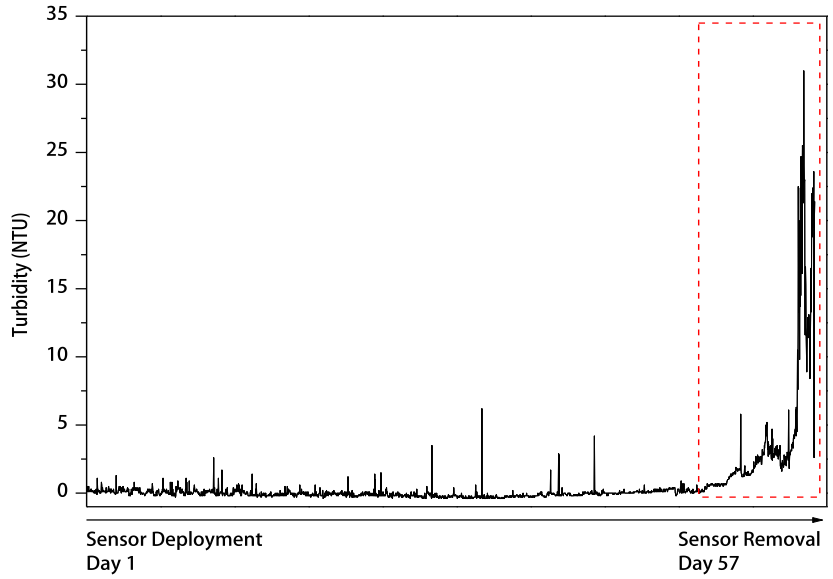

Figure 2-24: Graph of turbidity readings recorded over the study period in the North Basin of Lough Hyne. Erroneous data resulting from biofouling are highlighted (red line). Note the difference in scale between this figure and Figure 2-23.

Simultaneous removal and examination of the turbidity sensors from both sites indicated that erroneous data measurements were due to biofouling of both the acetal housing and sponge elements of the mechanical wiper present rather than the optical window. Filamentous algae growing on the mechanical wiper had developed to such an extent that filaments drifted in front of the optical window and thus affected sensor measurements, even when the mechanical wiper was at rest. Data drift of the deployed

turbidity sensors reflected the biofouling rates observed at each location in Lough as corroborated by examination of immersed test panels. Figure 2-25 illustrates the difference in biofouling between the two sondes at the end of the field trials.

Figure 2-25: Digital image of the sensors after removal. Ectocarpus siliculosus biofouling of the sonde deployed in the North Basin (upper sensor) is reduced compared to that of the South Basin (lower sensor).

Optical windows from deployed sensors could not be examined directly with microscopy as destructive analysis would have been required, however Figure 2-26 demonstrates biofouling of an identical but non-operational optical window since obtained from the sonde manufacturer.

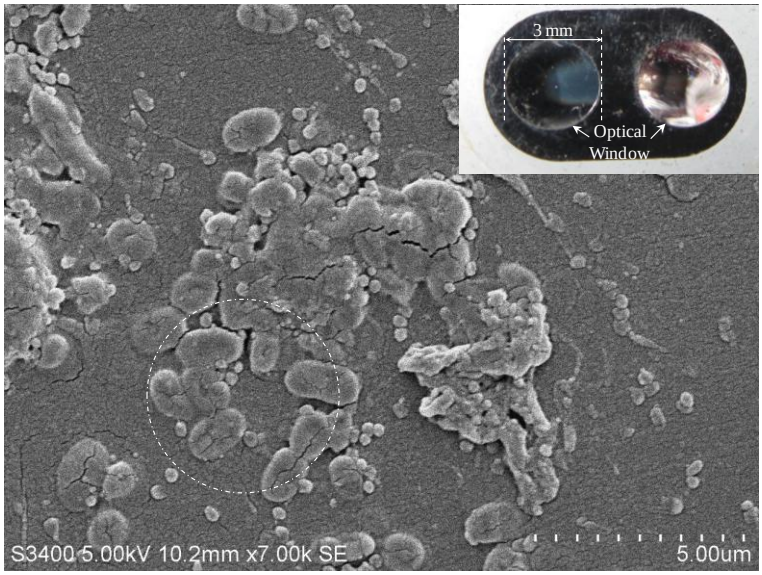

Figure 2-26: Scanning electron micrograph of an optical window of a turbidity sensor (Inset), illustrating microbial biofouling on the window surface (circled).

The only other sensor to display data drift resulting from biofouling was the pH sensor on the sonde deployed in the South Basin of Lough Hyne. A digital image of this sensor at the end of the study is shown in Figure 2-27.

Figure 2-27: Digital image of the glass bulb of the pH sensor deployed in the South Basin of Lough Hyne after 35 days. Biofouling is just visible on both the housing and glass bulb.

The pH sensor began to produce erroneous data readings beginning at approximately day 35 of the deployment. This sensor is a standard YSI 6589 pH probe with a guarded glass bulb, and fast response, signal-conditioning electronics. No AF protection is fitted

to the glass bulb and it appears that algal fouling significantly affects the operation of this probe when filamentous algae are present. The effects of biofouling on the pH data collected at this location is shown in Figure 2-28.

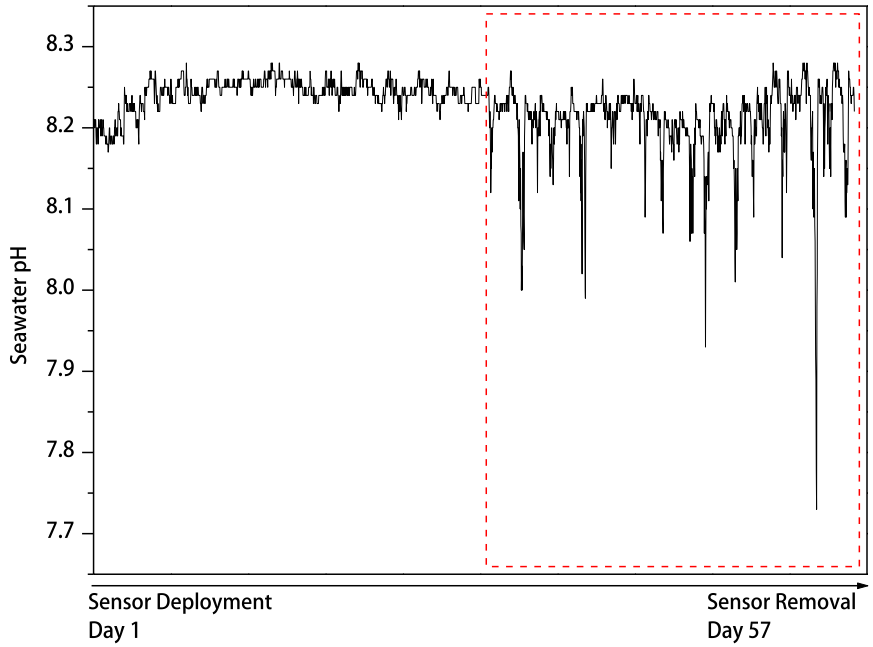

Figure 2-28: Graph of seawater pH values recorded on the sensor in the South Basin. The red line indicates erroneous readings resulting from biofouling of the pH membrane.

Few studies have examined the performance of pH sensors when exposed to biofouling in the marine environment. The influence of biofouling on glass pH electrodes has however been examined in freshwater systems using aquarium water in tandem with fouling coupons made from glass microscope slides [51]. Glass slides in this study were also immersed simultaneously with the pH sensor and an evaluation of the biofouling responsible for sensor failure was possible.

A decrease in the minimum daily pH values below that of true values was recorded in this study, perhaps resulting from respiration by the algae recorded on the deployed test panels. The response of pH electrodes covered with biofilms has been considered diffusion limited, thus respiring algal attachment to the pH electrode results in decreased localised pH levels because of CO_2 production near the electrode [51]. The presence of a biofilm on the electrode may also result in a volume of solution being held close to the glass membrane, such that the buffering effects of this biofilm increase the response time of the electrode in a linear manner with increasing biofilm accumulation on the electrode [51].

With the recent debate regarding global acidification of ocean waters [52, 53], it would appear that careful measurement and valid data collection are vital aspects of pH measurement. Thus, the ability to distinguish data produced from a biofouled sensor and valid measurements is vital. The optimal design of the current generation of pH meters precludes the use of mechanical wipers, although rotating brushes may yet have some success. Thus, the surface of pH meters requires novel AF solutions, particularly in areas in which biofouling resulting from the attachment of microalgae such as diatoms is extensive.

In common with initial sites of initial settlement and development of *A. modestus* at Poolbeg Marina in the River Liffey estuary, macrofouling of sensors at Lough Hyne also developed from localised topographic features on the sensor casings. In the case of Lough Hyne, macrofouling predominantly consisted of polychaetes such as *Pomatoceros triqueter*. Examples of this are shown in Figure 2-29.

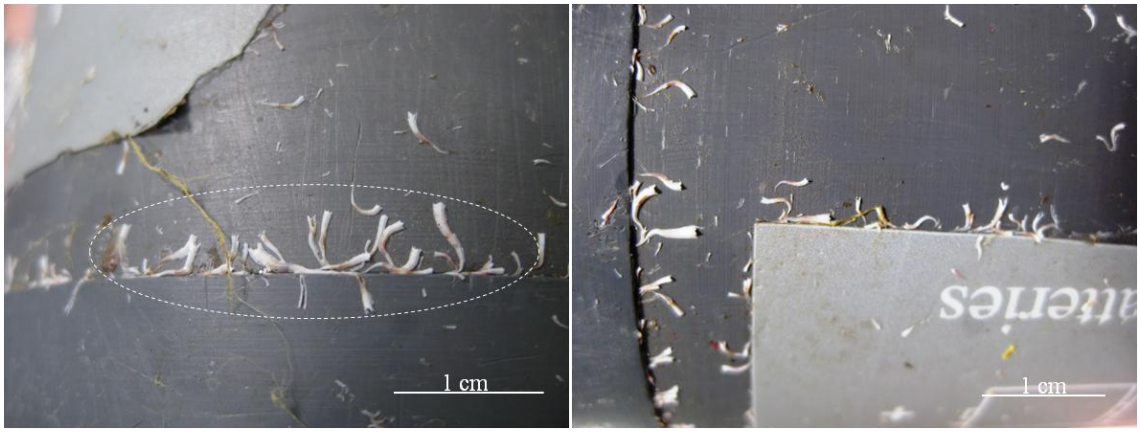

Figure 2-29: Digital images of macrofouling development on sensor casings deployed at Lough Hyne marine reserve during 2011. Initial settlement and growth points of Pomatoceros triqueter (circled, left image) are associated with the presence of topographic features on the sonde casing.

2.6 **Material performance at Lough Hyne**

Commercial AF coatings did not remain intact during continuous immersion at Lough Hyne and were frequently observed to separate and flake away from the glass substrates. This may be related to the lack of a tie-coat between the glass substrate and the coating. This material performance resulted in non-reproducible results for these coatings, thus complete analysis of biofouling is reported for transparent materials (PDMSe and glass surfaces) for this site.

2.6.1 *Spectrophotometric analysis of biofouling at Lough Hyne*

One of the major drawbacks of current techniques used for assessment of biofouling is that cell numbers are often determined using microscopy or culture techniques. These techniques are time-consuming and involve extensive sample preparation. In this study spectrophotometric analysis was assessed alongside these techniques as a rapid means of analysing biofouling on transparent materials at Lough Hyne. The potential of techniques for quantifying biofouling involving spectrophotometric analyses have been examined previously [54, 55]. Marrs and co-workers analysed Chl *a* absorption, corrected for degradation products, as a means of quantifying biofilms and concluded that the technique was non-destructive and could assess the performance of AF technologies for the protection of marine optical sensors [55]. These studies indicated that spectrophotometric techniques have the potential to provide a rapid alternative to microscopic counting of attached bacterial and diatom cells.

Previously, spectrophotometric analyses of biofouling has been conducted on undisturbed biofilms, while staining with DAPI (4,6 - diamidino - z - phenylidole) or AO is used to enumerate microbial cells [56]. In this study, the possibility of combining both techniques by performing spectrophotometric analyses on biofilms stained with AO was assessed. Initial coating of slides with transparent PDMSe to give a final coating thickness of ~50 µm had no measurable effect on the transmission properties of the materials. These measurements before deployment are shown in Figure 2-30.

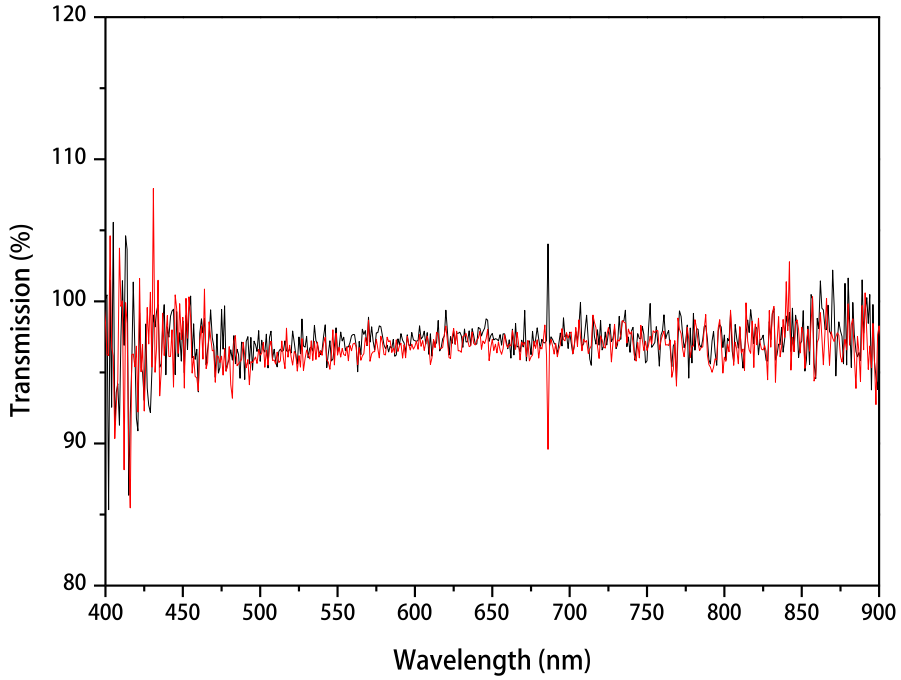

Figure 2-30: Graph of initial measurements of transmission of visible light and Near IR wavelengths(400-900 nm) through PDMSe-coated slides and PDMSe incorporating copper microparticles prior to deployment. Transmission measurements are referenced against a clean uncoated glass slide. (PDMSe-coated glass = black Line, PDMSe + Cu µparticles = red line)

Spectroscopic analyses of biofouling on microfouled slides resulted in maximum loss in transmission occurring at wavelengths of 460-470 nm. Examination of the transmission characteristics of AO stained slides from the two locations at Lough Hyne corroborated observed differences in biofouling rates of deployed sensors. Biofouled coupons from a depth of 2 m in the South Basin demonstrated transmission losses (~ 60%), while glass slides at the North Basin site demonstrated < 20% loss. This is consistent with the results obtained from sensor performance and subsequent microscopic analysis of deployed materials. However, the reproducibility of spectrophotometric measurements was affected by biofilm spatial heterogeneity on slides. Typical transmission spectra obtained using the described methods are shown in Figure 2-31, where the loss of transmission resulting from biofouling at each location and depth can be observed.

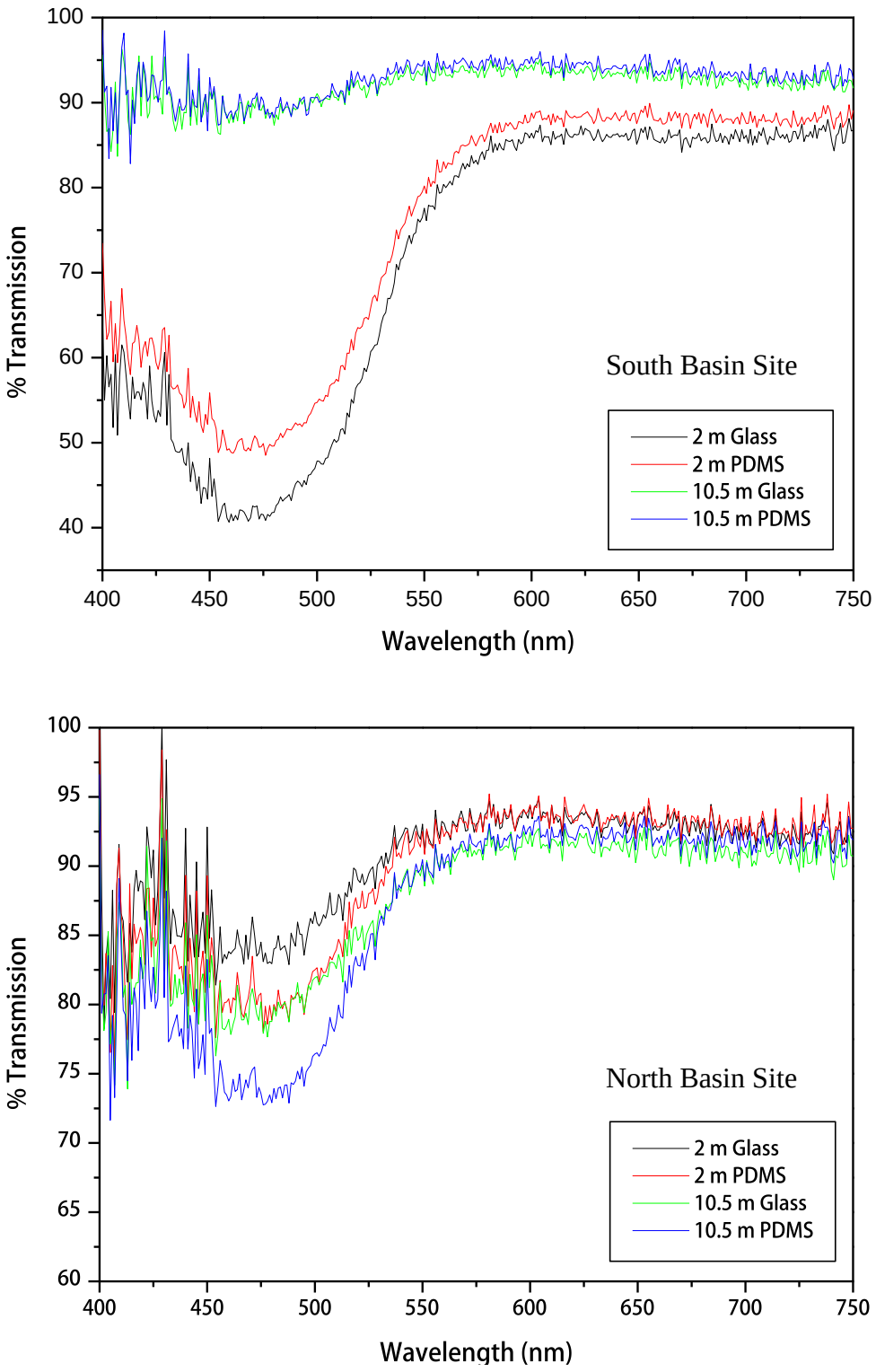

Figure 2-31: Graphs demonstrating loss in transmission resulting from biofouling of PDMSe-coated and plain glass control slides stained with AO. Data are shown for both the South Basin (top) and North Basin sites at the depths indicated. Slide samples removed from the South Basin at a depth of 2 m after 28 d exposure show greatest lost in transmission.

Although the above initial results indicated that spectrophotometric methods of biofilm analyses on transparent materials is a potentially rapid and non-destructive means of analysing biofouling, the method suffers from a number of disadvantages related to

reproducibility of results [55]. In their study, Marrs and co-workers analysed live biofilms primarily consisting of algal growth on exposed coupons. This resulted in characteristic absorption peaks by photosynthetic pigments, particularly chlorophyll *a* in the region of 675 nm, thus making this wavelength the most suitable for quantitative analysis. However, in this study, biofilms were fixed and stained with AO and no loss in transmission at the wavelengths of photosynthetic pigments was observed. The greatest difficulties with this method are encountered in producing a consistent staining procedure as uniform staining did not occur across complete slides. This was related to microfouling heterogeneity on slides surfaces, which could only be assessed by microscopic examination thus negating the purpose of rapid assessment techniques. Thus, to further examine biofouling development on deployed materials and sensor materials, diatom cell enumeration using both epifluorescence and electron microscopy were also assessed as a means of quantifying biofouling at both locations within Lough Hyne.

2.6.2 *Microfouling of materials at Lough Hyne*

Marine microbial community composition and development on commercial and novel AF materials have recently been examined in a number of detailed studies [57, 58] However, information is lacking on species composition and life history of many biofouling diatom species. Microscopy analysis of transparent materials deployed at Lough Hyne demonstrated a diverse microfouling community dominated by raphid diatom species.

Bacterial and diatom cells were present on all surfaces except copper plate at all locations and depths throughout the testing period. Examination by both epifluorescence and electron microscopy revealed a diverse microbial community, the composition of which was highly heterogeneous on deployed substrata. Although published studies have previously enumerated bacterial cells on surfaces using either image analysis of microcolonies or individual cell counts [59, 60], attached bacterial cells were not enumerated in this study. Due to the rapid growth conditions, particularly at the South Basin site, enumeration of bacterial cells on samples stained with AO for epifluorescence analysis proved difficult after only 3 days immersion. After this period, the presence of diatoms and other organisms frequently prevented accurate enumeration of bacterial cells on surfaces. While it was possible to enumerate bacterial cells in areas of deployed glass and PDMSe surfaces, stained debris and diatom cells prevented analysis in the majority of captured images. Figure 2-32 illustrates the extent of bacterial colonisation occurring on a glass surface at Lough Hyne after 14 days immersion (1st -14th June 2010).

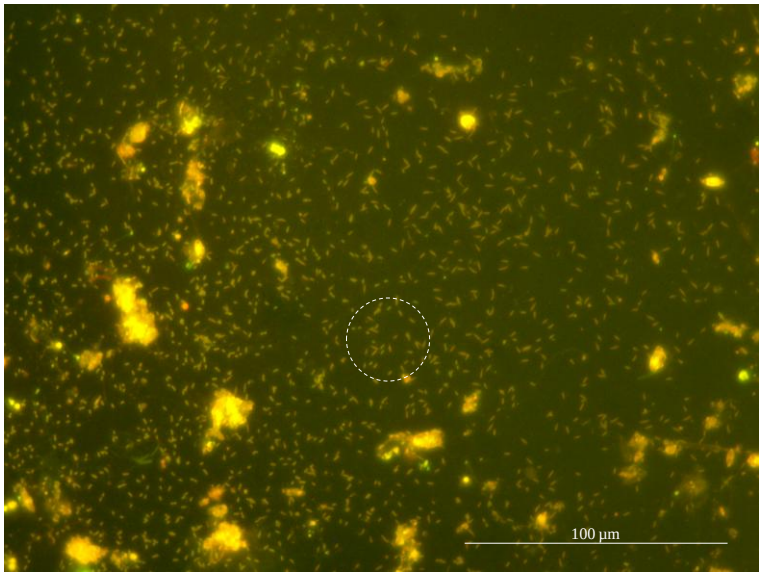

Figure 2-32: An epifluorescence micrograph of bacterial colonisation (circled) on a glass surface at the South Basin, Lough Hyne after 14 d immersion.

2.6.3 *Identification and enumeration of diatom attachment*

Diatom biofouling of PDMSe-coated slides and plain glass slides were examined in detail at Lough Hyne. Diatoms are often reported as the earliest eukaryotic colonisers of surfaces in the marine environment and a number of previous studies have investigated diatom biofouling of artificial materials for different immersion periods [57, 61, 62]. This study found that diatom cells dominated the initial biofilm on illuminated surfaces at both test sites chosen within Lough Hyne. Settled diatoms were counted *in situ* in this study rather than the methods utilised by Swain and co-workers where biofilms are removed from the surface and cells subsequently enumerated in a counting chamber [57, 58]. Indirect enumeration methods have been evaluated by Patil and co-workers who concluded that removal of diatom cells by brushing prior to enumeration in a counting chamber minimised losses compared to the use of the hard scraper [61]. Other studies utilising intact biofilms have categorised microscopy images based on the number of diatom cells present [63].

As the aim of this study was to examine the relationship between microbial adhesion and surface properties, attached biofilms were examined *in situ* on surfaces rather than after removal. Removal of sections of the biofilm disrupts examination of the community structure and precludes analysis of the relationship between settled organisms. *In situ* analysis allows examination of intact biofilms, an important factor when considering the development of the succession of a microfouling biofilm. Due to

the choice of methods, high variability in diatom abundance measurements were found on examined materials. High abundance of diatom cells was measured at the South Basin site at 2 m and 10.5 m depths on both PDMSe-coated and glass surfaces. Examples of diatom abundance on both surfaces after exposure in the South Basin for 14 d are shown in Figure 2-33 and Figure 2-34.

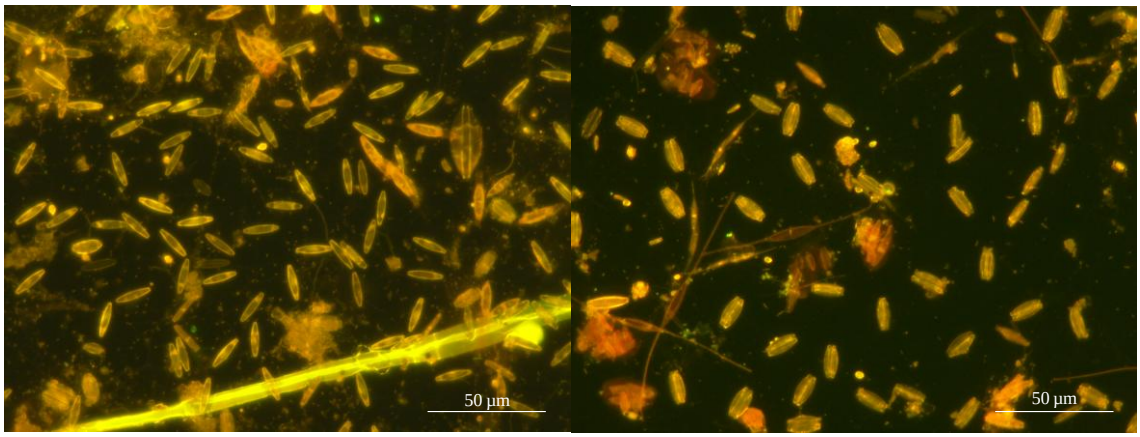

Figure 2-33: Epifluorescence micrographs of diatom attachment to PDMSe (left) and glass surfaces (right) in the South Basin of Lough Hyne (2 m depth, 14 d immersion).

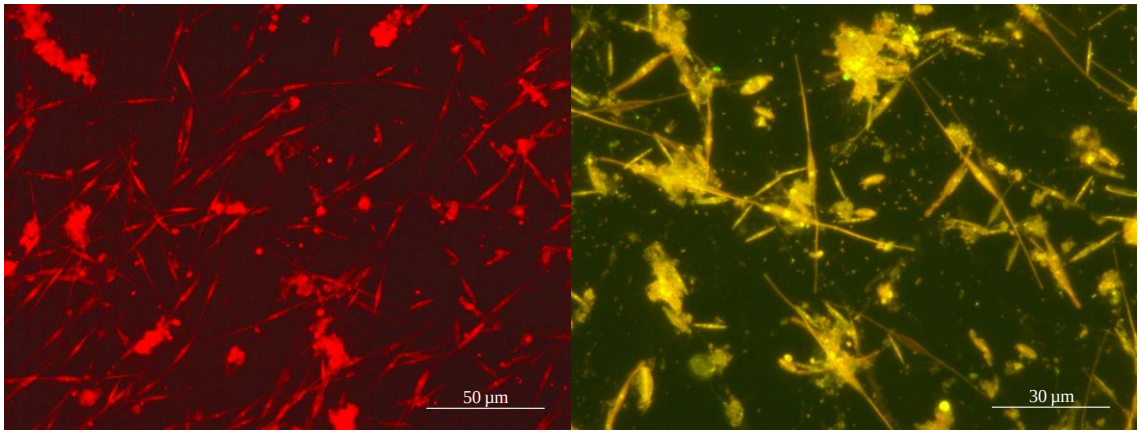

Figure 2-34: Epifluorescence micrographs of diatom attachment to PDMSe (left) and glass surfaces (right) in the South Basin of Lough Hyne (10.5 m depth, 14 d immersion).

Analyses of PDMSe and glass surfaces deployed in the North Basin indicated that diatom attachment was lower than in the South Basin, particularly at a depth of 10.5 m where the attached diatom community was dominated by both *Cylindrotheca* and *Cocconeis* species. Examples of diatom adhesion to glass and PDMSe surfaces at both depths of 2 and 10.5 m are shown in Figure 2-35 and Figure 2-36. The slow establishment of diatom cells on surfaces at 10.5 m at the North Basin site is evident.

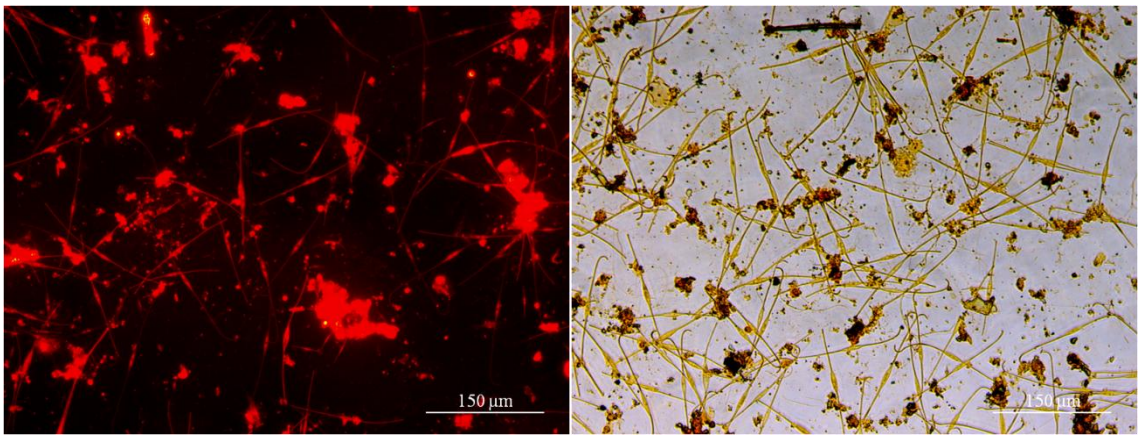

Figure 2-35: Epifluorescence micrographs of diatom attachment to PDMSe (left) and light micrographs of a glass surfaces (right) in the North Basin of Lough Hyne (2 m depth, 14 d immersion).

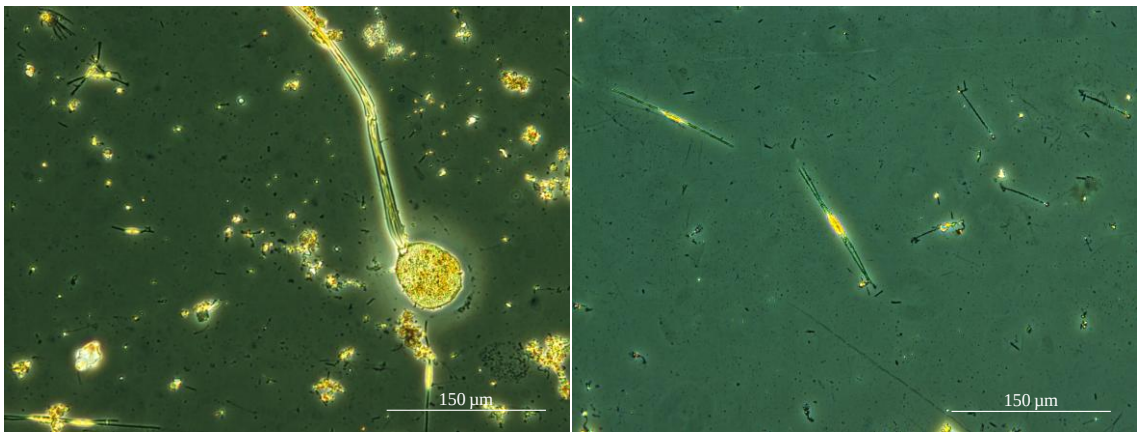

Figure 2-36: Epifluorescence micrographs of diatom attachment to PDMSe (left) and glass surfaces (right) in the North Basin of Lough Hyne (10.5 m depth, 14 d immersion).

As can be observed in the above images, the diatom *Cylindrotheca closterium* dominated the early diatom biofilms examined at the two locations and depths examined in Lough Hyne. *Cylindrotheca* is recently reported as the most common diatom genus on two fluoropolymer and silicone-based foul-release coatings (Intersleek 7001 (IS700) and Intersleek 9001 (IS900)) with as much as 5 cells mm^{-2} [64]. This species

was also noted during enumeration of attached diatom cells *in situ* on a foul-release coating (Intersleek 700) over a 16-day time period in Australian waters (Cairns and Williamstown) [63]. The authors of the latter study utilised a methodology that involved fixation followed by staining of organisms with a solution of 20 μg ml^{-1} Hoechst 33342, prior to capturing 20 haphazard images of stained cells using epifluorescence microscopy. Images were then imported into Photoshop® before photosynthetic organisms on the slide surface were counted. A similar methodology was followed in this study, however, AO was used instead of Hoechst 33342, meaning that all organisms were stained. Images were then processed using ImageJ software. It was found that the reproducibility of this technique relies upon the specific diatom biofouling community structure present on exposed materials, for instance slides with a high proportion of filamentous algae were not reproducible as diatom cells associated with these filaments. Meanwhile slides with relatively low diatom abundance and which were dominated by a particular diatom species, e.g. *Cocconeis* were easily counted. Large variances in diatom cells counts were also found for longer immersion times, again related to the presence of algal filaments, primarily *Ectocarpus sp*. Diatom cell counts for deployment of glass and PDMSe materials for the period of 1st – 14th June 2010 are presented in Figure 2-37. High variance values resulting from differences in cell numbers between counts is evident. This can be related to the spatial heterogeneity of diatom colonies on the surface, indicating that cells occur in clumps rather than randomly dispersed over the available surface area.

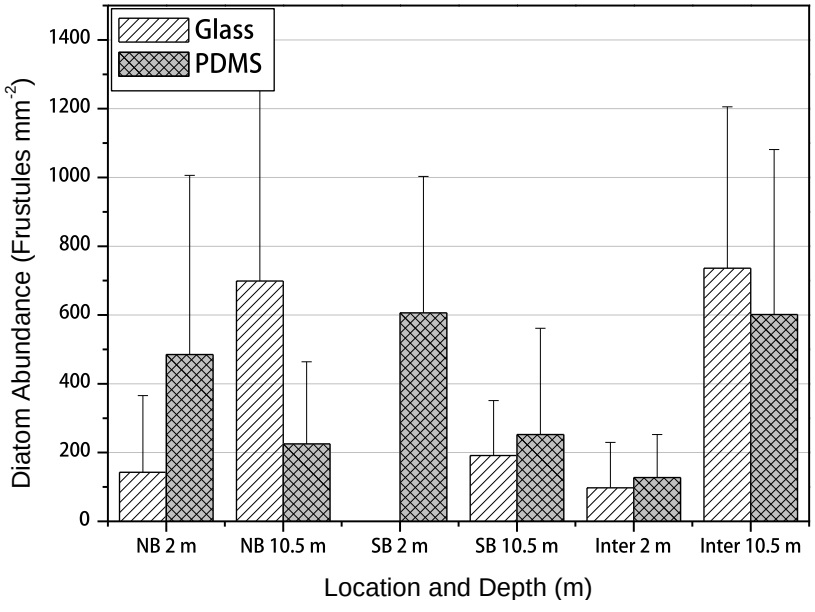

Figure 2-37: Diatom frustule abundance on transparent materials deployed at Lough Hyne at a depth of 2 and 10.5 m from the 1st -14th June 2010.

Further analysis of deployed materials in June 2011 demonstrated higher numbers of diatoms on PDMSe surfaces when compared to glass surfaces at all locations, however ANOVA demonstrated that the difference was not significant ($\alpha = 0.05$). This data is shown in Figure 2-38.

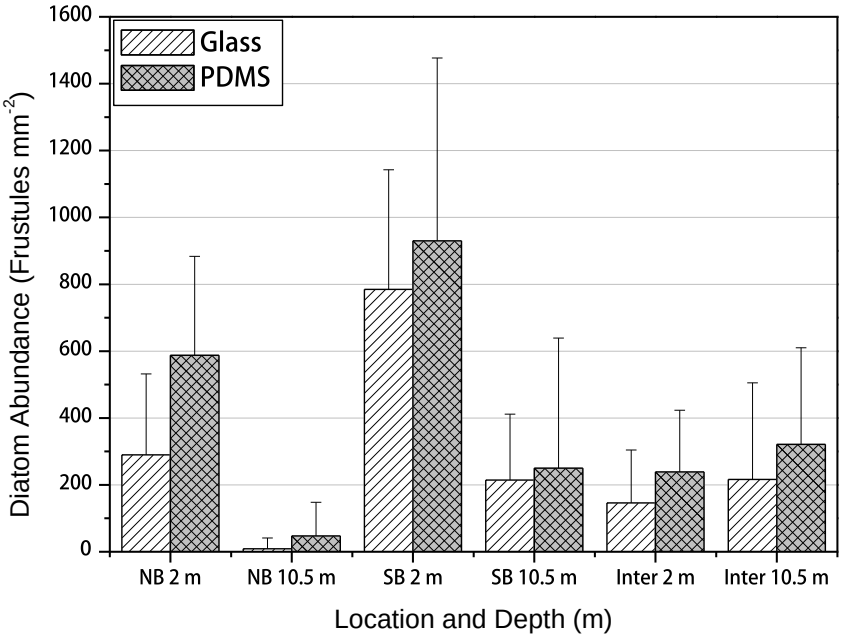

Figure 2-38: Diatom frustule abundance on both glass and PDMSe surfaces deployed at Lough Hyne at a depth of 2 and 10.5 m from 14th – 30th June 2011.

Comparison of samples with both SEM and epifluorescence microscopy demonstrated that smaller diatom (< 5 µm) frustules were generally underrepresented in samples examined solely using epifluorescence microscopy. However, SEM was complicated by large cell aggregates where cells numbers could not be accurately recorded. Direct enumeration of intact undisturbed diatom frustules was conducted in consultation with those methods proposed in the literature. However, it was found in this study that the attachment rate of diatoms to the surface occurred rapidly such that cell abundance at locations with the highest growth rates and diatom recruitment could not be accurately determined after periods of immersion greater than 14 d. Thus, removal of cells from materials prior to microscopic analysis is should be used when sufficiently large numbers of diatoms are present on the substratum. Figure 2-37 shows an example of a mature microfouling community on a glass substrate at Lough Hyne after 21 d

deployment. *In situ* analyses of individual diatom cell abundance is not possible due to the high cell densities.

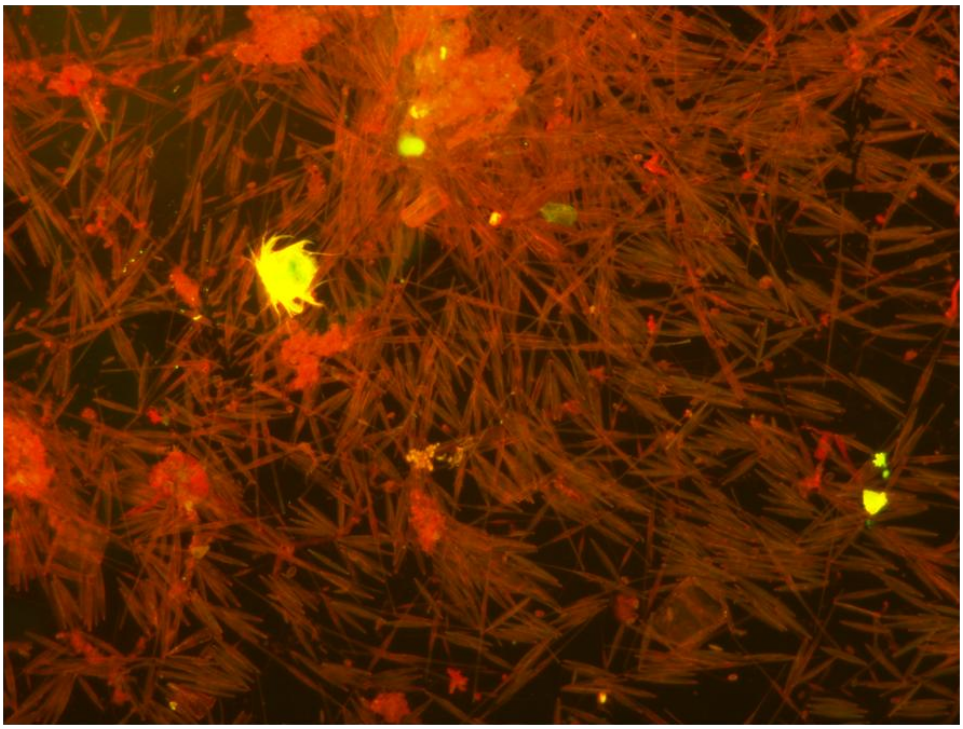

Figure 2-39: Epifluorescence micrograph of diatom growth stained with AO on a glass substrate in the South Basin after immersion for 21 days in July 2010. Diatom cells have become too abundant to enumerate using image analysis.

2.6.4 *Species composition of diatom biofouling at Lough Hyne*

While extensive records of planktonic diatom species exist at Lough Hyne ([15] and references therein), few data from previous studies are available on the benthic diatom community within Lough Hyne. No reports before the present study are available on the performance of AF materials at Lough Hyne and the benthic diatom community associated with foul-release materials at this location. A single description is available for epiphytic and benthic diatom communities at Lough Hyne and this is associated with the hydroid *Sertularia operculata* [65]. The latter study identified 70 separate diatom species associated with *S. operculata* of which *Cocconeis scutellum* was the most common.

A similar result was observed for artificial surfaces examined in this study where analyses of relative abundance between diatom genera indicated that *Cocconeis*, *Amphora* and *Cylindrotheca* were dominant on surfaces at most locations within Lough Hyne. The results of this are shown for the North Basin in Figure 2-40.

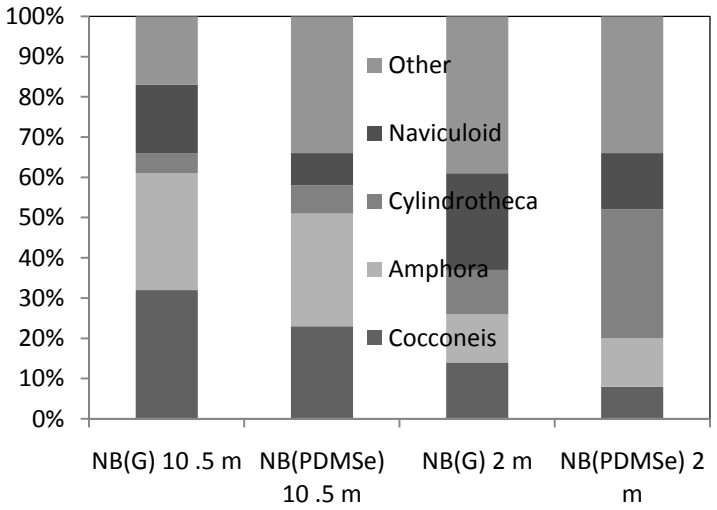

Figure 2-40: Graph of relative abundance of diatom frustules on glass (G) and PDMSe surfaces immersed in the North Basin at Lough Hyne at depths of 2 and 10.5 m from 1st – 14th June 2011.

Diatom species diversity varied with season and deployment period, however as the deployments proceeded it became apparent that diatom species of the genus *Cocconeis* (Ehrenberg, 1837) were problematic biofouling diatoms at Lough Hyne and often represented the highest diatom abundance on deployed materials. Interestingly, this has recently been reported in Australian and Indian waters where this genus is also reported as a prolific coloniser of foul-release coatings [21, 63]. This indicates that *Cocconeis* may be a worldwide coloniser of FRCs, however very few data are available on the life history of this genus. Figure 2-42 shows a number of scanning electron micrographs of individual cells of *Cocconeis* species attached to both glass and PDMSe surfaces at Lough Hyne. The adnate adhesion strategy in which the cells are lying in close proximity to the surface is evident.

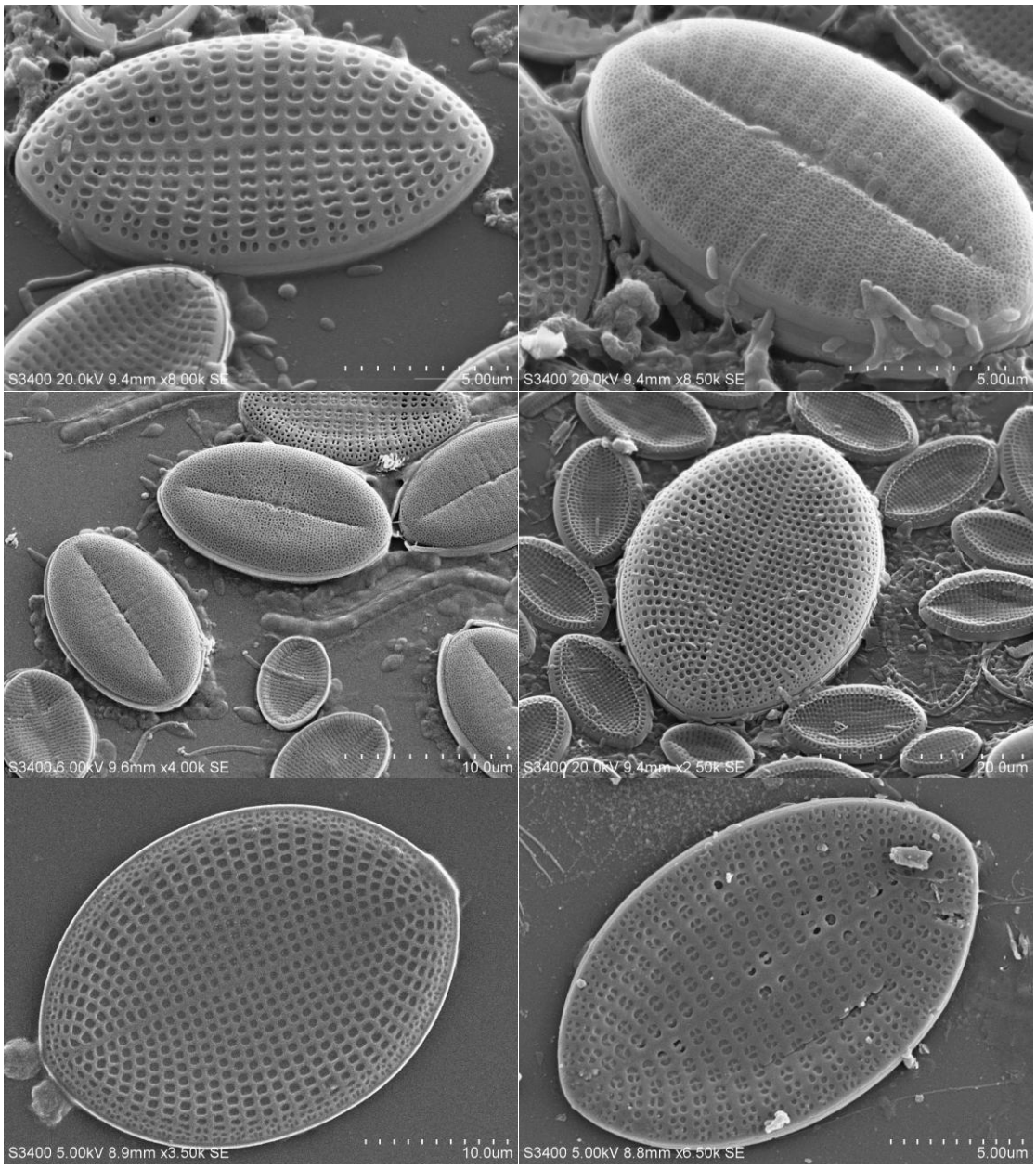

Figure 2-41: Scanning electron micrographs of individual species of diatom genus, Cocconeis, the dominant benthic diatom species attached to deployed test materials at Lough Hyne Marine Reserve.

It is known that cells of the *Cocconeis* genus are solitary and heterovalvar with a concave raphe valve. Cells adhere prostrate on the substratum with one frustule composed of an araphid valve and the other a raphid valve, and have a reduced cell width resulting in an optimal configuration for colonisation of AF materials. Molino and co-workers determined using time lapse microscopy that *Cocconeis* cells demonstrated an initial period of motility on the substratum surface, gliding until they eventually 'selected' a position to permanently adhere, presumably through the secretion and accumulation of a permanent adhesive [63]. Figure 2-42 illustrates an example of

colonisation of a PDMSe surface by *Cocconeis* species after 14 d immersion period in the North Basin at Lough Hyne. It can be seen that cells of this genus dominate the diatom community and initially attach and disperse on the surface as single cells.

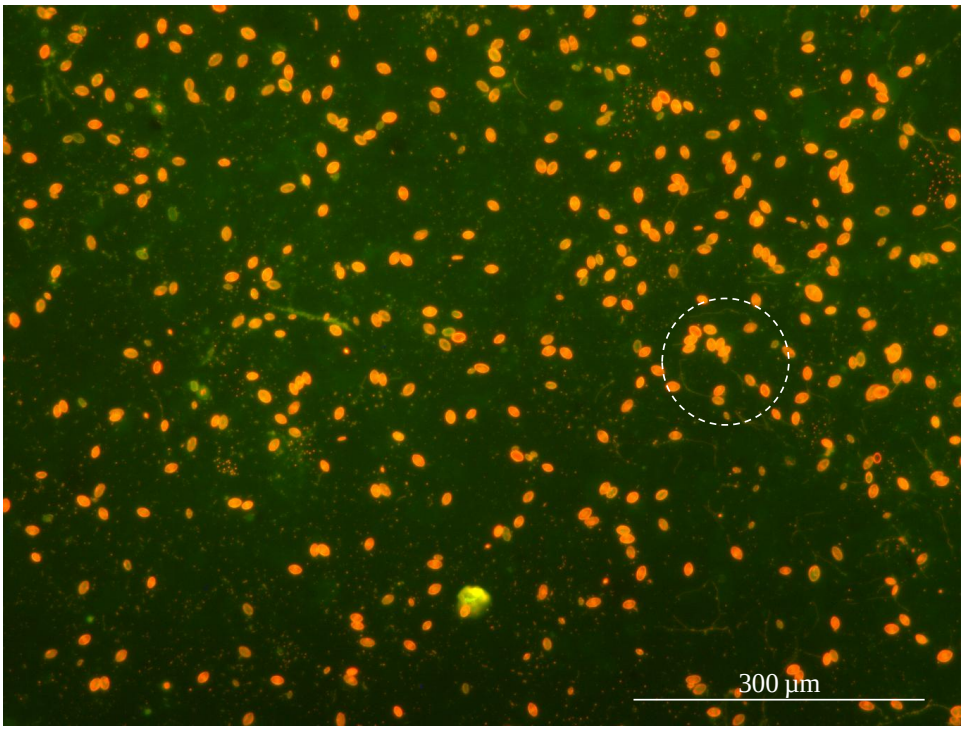

Figure 2-42: An epifluorescence micrograph of diatom colonisation of a PDMSe surface at Lough Hyne after 14 d deployment at a depth of 2 m. Early microcolonies of cells of Cocconeis are visible (circled).

After a period of 4 weeks cells of *Cocconeis* were found to have almost 100 % coverage of both PDMSe and glass surfaces formed a monolayer of cells on deployed surfaces. An example of a scanning electron micrograph demonstrating the extent of the surface coverage by this genus is presented in Figure 2-43.

Figure 2-43: A scanning electron micrograph of a PDMSe-coated glass slide after 28 d immersion. Total colonisation of the surface by diatoms of the Cocconeis genus is almost complete.

In agreement with the observations of Molino and other workers examining the life cycle of this species, individual mother cells have been observed to be present on the surface. These researchers demonstrated that under favourable conditions in the laboratory, individual mother cells can divide four times a day, each time producing a daughter cell that is capable of further exploration of the surface until adhesion occurs and these cells begin to produce daughter cells. This results in colonisation of the surface by a monolayer of *Cocconeis*, and by applying exponential growth rates and generation times would lead to complete colonisation of the area of a standard 25 x 75 mm microscope slide in approximately 100 h assuming a single cell has an area of attachment of 50 μm^2 and no mortality or predation effects.

The roles of light spectrum, nutrient availability, and culture conditions on the laboratory production of *Cocconeis scutellum scutellum* (Ehrenberg) and *C. scutellum parva* (Grunow) have very recently been examined [66] as has the effect of chlorine on based on inhibition of chlorophyll autofluorescence and esterase activity as probed by fluorescein diacetate (FDA) staining [67]. Production of bioactive substances was also investigated by analysing the ability of apoptogenic compounds able to influence the sex reversal of a decapod crustacean. The results produced the above study indicated

that *C. scutellum* can grow under wide ranging environmental conditions and use a varied light spectrum. These results were confirmed in the present field study on biofouling at Lough Hyne where it was found that *Cocconeis* species were initial colonisers of immersed surfaces. Cells of this genus often formed mono-species microcolonies on immersed that excluded other diatom species. The metabolite composition of both the ether and butanol extracts from *Cocconeis scutellum* was recently examined by gas chromatography-mass spectrometry (GC-MS) in a study which highlighted the potential of apoptotic compounds derived from benthic marine diatoms and the lack of research in this area [68]. Thus, this genus may possess some means of excluding other species or may be more tolerant of environmental conditions in the North Basin.

Table 2-6 summarises the distribution of diatoms attached to both PDMSe and glass surfaces in Lough Hyne at depths of both 2 m and 10.5 m depths in both the North and South Basins of Lough Hyne.

Table 2-6: Summary of the diatom species identified as present on PDMSe and glass surfaces at Lough Hyne marine reserve at depths of 2 m and 10.5 m in the North and South Basins from June 2010 and 2011.

	PDMSe								Glass							
Genus	SB 2 m		SB 12 m		NB 2 m		NB 12 m		SB 2m		SB 12 m		NB 2 m		NB 12 m	
Date	D1	D2	D1	D2	D1	D2	D1		D1		D2					
Amphora	+				+	+		+	+	*	+	+	+	+	+	+
Ardissonea										*						
Bacillaria					+					*				+		
Climaconeis		+			+			+	+	*						+
Cocconeis	+	+	+	+	+	+			+	*	+	+	+	+		+
Cylindrotheca	+	+		+		+	+	+	+	*			+	+	+	+
Licmophora	+	+	+						+	*	+					
Navicula	+							+		*						
Nitzschia									+	*		+				+
Opephora										*					+	
Paralia									+	*						
Psammodictyon					+					*						
Striatella	+	+							+	*						
Thalassiosira										*			+			
Stenoneis										*						+
Chaetoceros										*						+
Synedra	+	+								*						
Melosira	+	+							+	*						

Key: + = Genus present, D1 = 1-14th June 2010, D2 = 14th – 30th June 2011, SB = South Basin, NB = North Basin, * = Samples were not examined.

2.6.5 *Macrofouling of materials at Lough Hyne*

It was found that an initial visible algal biofouling layer developed on all deployed materials within 14 d immersion at Lough Hyne Marine Reserve. However, reflecting the microfouling trends observed and correlated with sensor data, macrofouling growth rates varied between the North and South Basins at Lough Hyne on deployed materials. Deployed panels in the North Basin exhibited a reduced rate of biomass accumulation compared with panels deployed in the South Basin (Figure 2-44). Macrofouling continued to develop over the study period until a mature biofouling community had established.

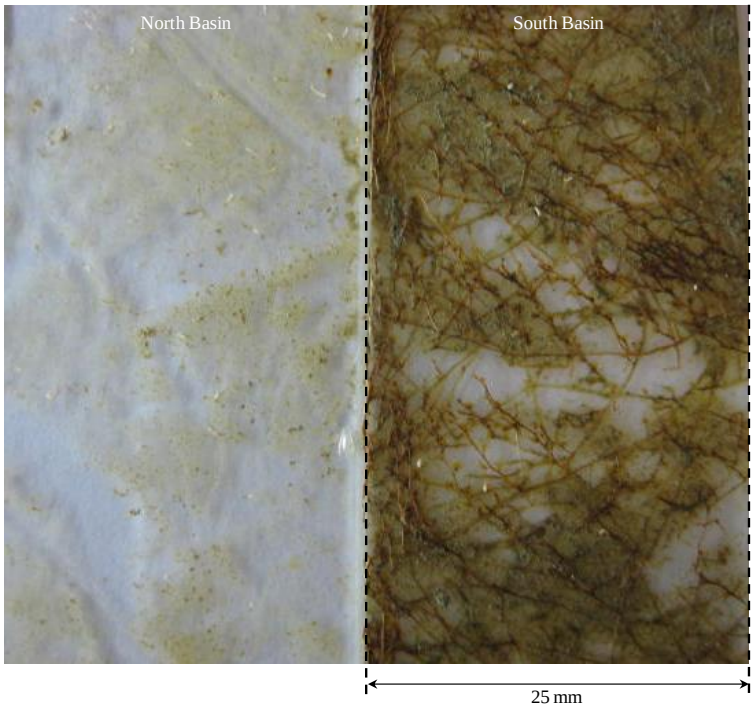

Figure 2-44: Digital images comparing algal biofouling of plain glass surfaces immersed in the North (left) and South Basin (right) of Lough Hyne for 21 d at 2 m depth from 08.05.2009 until 29.05.2009.

As the macrofouling community became established on materials, a diverse calcareous invertebrate population consisting primarily of the bivalve mollusc, *Anomia ephippium* and the polychaete worms such as *Pomatoceros* species was established. Individual juvenile barnacle species and bryozoans were also recorded; however, no single species dominated the settlement panels as at the Poolbeg Marina site. Figure 2-45 illustrates attachment of a polychaete (*Spirorbis* species) to a glass surface at Lough Hyne.

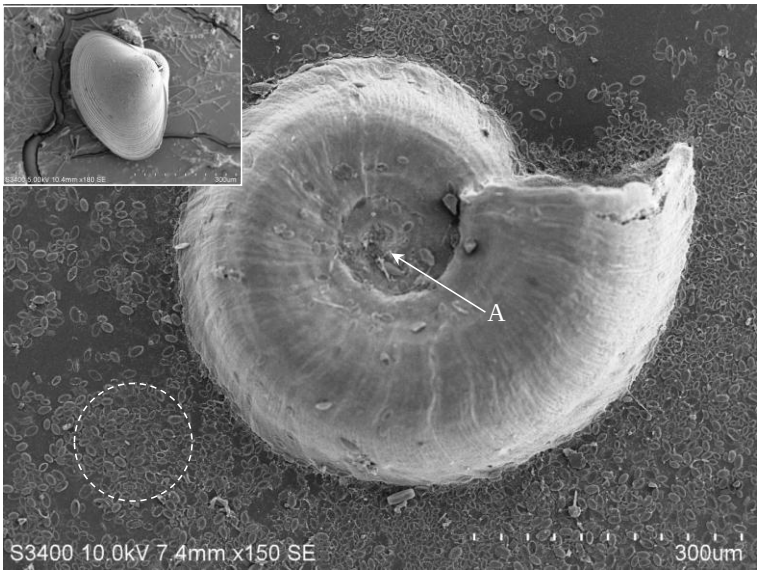

Figure 2-45: Scanning electron micrographs of macrofouling organisms on materials after 28 days. These include serpulid species (A) and bivalve adhesion (inset). Diatom microfouling is also visible on the surface (circled).

Extensive biofouling developed on all materials at Lough Hyne at termination of the deployment period. Figure 2-46 illustrates the development of a macrofouling layer on PDMSe coated slides after 38 days immersion. The spatial heterogeneity of diatom colonisation is visible as the brown discolouration presentation over the surface area of the slides.

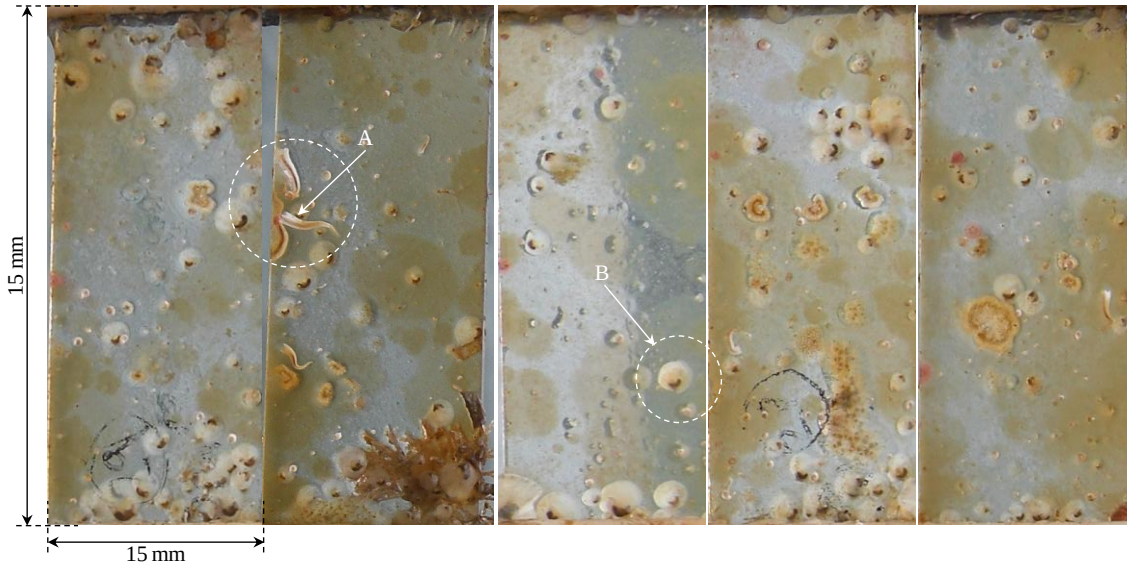

Figure 2-46: Digital images of macrofouling on a PDMSe-coated slides deployed for 38 d, South Basin Lough Hyne. A = the serpulid polychaete, Pomatoceros and B= Anomia. Brown discolouration is due to diatom settlement, note spatial heterogeneity of diatom colonisation of slides.

Watson and Barnes examined benthic recruitment of macrofouling organisms to slate panels at Lough Hyne from 1997-2002 and concluded that, in order of decreasing F statistic value, (and, therefore, likely magnitude of influence), season, site, year and depth had significant influence on recruitment rate to surfaces [50]. This study demonstrated that site selection within Lough Hyne is an important factor in determining the rates of macrofouling and hence microfouling rates. However, measurements of temperature, turbidity, dissolved oxygen, salinity and pH demonstrated no significant difference in measureable physiochemical parameters between the two sites. Therefore, differences in biomass adhered to deployed surfaces between the two sites is likely related to differences in delivery rates of biofouling propagules to the surface due to hydrodynamics.

2.6.6 *Evaluation of test panel design*

Assessment of material performance in field conditions is an important part of AF material testing [57, 69, 70]. Often materials are tested in laboratory assays involving single species regarded as representative of problematic biofouling species in the natural environment. While this is acceptable for screening of compounds or materials, fundamental data are also required on the behaviour of natural multispecies microfouling communities attached to artificial surfaces.

The test panels designed and manufactured in this study proved a reproducible and secure means of deploying test materials for biofilm analysis. Slides could be readily prepared for microscopy analysis and were easily transported and secured onsite. An additional advantage the design was the ability to readily apply coatings to slides using standard techniques such as dip-coating or spin-coating methods. Slides could then be evaluated using standard microscopy techniques such as CLSM, epifluorescence microscopy, transmission, biochemical assays or subdivided for electron microscopy. Figure 2-47 illustrates a number of test panels at the termination of deployment periods with *in situ* microfouling biofilms attached.

Figure 2-47: Digital images of the test panel and slides after various deployment periods in this study. Each holder was capable of deploying 12 replicate slides.

It has been reported that deployed panels in close proximity have less inter-panel variability than those further apart, although recruitment was reduced, due to panels masking one another. Keogh examined the influence of patch size on recruitment and concluded that the composition of small patches is determined mostly by recruitment,

while interspecific competition is most important on large substrata [71]. This has important consequences for the design of panels in biofouling studies, since panel size is unlikely to affect recruitment of species in any active way as it is improbable that cues have evolved for the selection of a given patch size.

In general, the performance of the test panels for deployment of coupons was satisfactory in this study, allowing rapid sample preparation for microscopy. However, in order minimise losses due to breakage and for greater statistical analysis a high level of replication is required. Dobretsov and co-workers have recently utilised a similar method involving microscope slide-sized coupons to test two FRC systems [64]. They reported using 84 replicate slides of each treatment (252 slides in total for each coating and a control). For each coating tested, the area for biofilm development was 0.16 m^2 giving a total area for biofilm growth in the experiment of 0.48 m^2.

2.7 **Conclusions**

This chapter has examined biofouling on different AF surfaces and performance of current multiparameter environmental sensing instruments. Marked differences in the microfouling communities on different commercial AF surfaces have been observed. Copper surfaces are the best performing AF surfaces, followed by the majority of commercial biocidal coatings tested, PDMSe did not perform well and results on this surface were comparable to plain glass control surfaces. However, results show that coating performance can be significantly influenced by test site, and that natural biofouling occurs large spatial and temporal differences occur in biofouling. The nature of biofouling at Poolbeg marina, an estuarine environment, is very different to that of a marine environment such as Lough Hyne. Within Lough Hyne, large variations in initial biofouling rates occur between the North and South basin sites. Thus, field testing of potential AF materials and when deploying environmental sensors for monitoring purposes, due consideration and measurement of biofouling rates must be undertaken in order to choose the optimum location for each requirement.

Three important observations on biofouling of current sensors have resulted from this work:

(a) Initial settlement of *Austrominius modestus* and other macrofouling organisms such as *Pomatoceros triqueter* are influenced by surface texture and presence of topographic features on manufactured sensor casings. These features act as a positive cue for gregarious settlement and development of macrofouling in both marine and estuarine environments. Thus optimisation of surface texture for AF performance should be investigated in greater detail.

(b) Raphid diatoms are a major component of biofouling communities at Lough Hyne and are earlier colonisers of immersed surfaces irrespective of season. Species of the diatom genus *Cocconeis* are prolific colonisers of artificial surfaces, often dominating the benthic diatom biofouling community.

(c) Algal biofouling negatively affects sensor performance even when protected by mechanical wiper AF technology. The presence of a mechanical wiper provides additional surface area for establishment of algal growth. Thus, such features require optimisation for AF performance, perhaps resorting to alternative technology where filamentous algae form a significant component of the biofouling community.

2.8 **References**

1 L. Delauney, C. Compère and M. Lehaitre, *Ocean Sci. Discuss*, 2009, **6**, 2993-3018.

2 L. Delauney and C. Compère, in *Marine and Industrial Biofouling*, ed. H. C. Flemming, P. S. Murthy and R. Venkatesan, Springer, 2009, p. 119-134.

3 P. W. Rundel, E. A. Graham, M. F. Allen, J. C. Fisher and T. C. Harmon, *New Phytol.*, 2009, **182**, 589-607.

4 J. H. Porter, E. Nagy, T. K. Kratz, P. Hanson, S. L. Collins and P. Arzberger, *Bioscience*, 2009, **59**, 385-397.

5 J. K. Hart and K. Martinez, *Earth-Sci. Rev.*, 2006, **78**, 177-191.

6 D. V. Manov, G. C. Chang and T. D. Dickey, *J. Atmos. Ocean. Technol.*, 2004, **21**, 958-968.

7 A. Whelan and F. Regan, *J. Environ. Monit.*, 2006, **8**, 880-886.

8 F. P. Chavez, D. Wright, R. Herlien, M. Kelley, F. Shane and P. G. Strutton, *J. Atmos. Ocean. Technol.*, 2000, **17**, 215-219.

9 J. Kitching, F. Ebling, J. Gamble, R. Hoare, A. McLeod and T. Norton, *J. Anim. Ecol.*, 1976, **45**, 731-758.

10 R. Bassindale, E. Davenport, F. J. Ebling, J. A. Kitching, M. A. Sleigh and J. F. Sloane, *J. Ecol.*, 1957, **45**, 879-900.

11 S. J. Lilly, J. F. Sloane, R. Bassindale, F. J. Ebling and J. A. Kitching, *J. Anim. Ecol.*, 1953, **22**, 87-122.

12 F. J. Ebling, J. A. Kitching, R. D. Purchon and R. Bassindale, *J. Anim. Ecol.*, 1948, , 223-244.

13 J. A. Kitching, *Adv. Ecol. Res.*, 1987, **17**, 115-186.

14 M. P. Johnson, M. J. Costello and D. O'Donnell, *Ophelia*, 1995, **41**, 137-151.

15 M. P. Johnson and M. J. Costello, *J. Plankton Res.*, 2002, **24**, 1305-1315.

16 J. Lawson, J. Davenport and A. Whitaker, *Estuar. Coast. Shelf Sci.*, 2004, **60**, 729-735.

17 R. McAllen, J. Davenport, K. Bredendieck and D. Dunne, *J. Exp. Mar. Biol. Ecol.*, 2009, **368**, 67-74.

18 W. Rasband, *1997–2007. ImageJ*.

19 E. Pelletier, C. Bonnet and K. Lemarchand, *Int. J. Mol. Sci.*, 2009, **10**, 3209-3223.

20 P. R. Jones, M. T. Cottrell, D. L. Kirchman and S. C. Dexter, *Microb. Ecol.,* 2007, **53**, 153-162.

21 S. Mitbavkar and A. C. Anil, *Biofouling,* 2008, **24**, 415-426.

22 T. G. O'Higgins and J. G. Wilson, *Estuar. Coast. Shelf Sci.,* 2005, **64**, 323-334.

23 J. H. Simpson, J. Brown, J. Matthews and G. Allen, *Estuaries and Coasts,* 1990, **13**, 125-132.

24 D. W. Stanley and S. W. Nixon, *Estuaries and Coasts,* 1992, **15**, 270-281.

25 Z. Bedri, M. Bruen, A. Dowley and B. Masterson, *Environ. Monit. Assess,* 2011, **16**, 369-384.

26 B. L. Peierls, R. R. Christian and H. W. Paerl, *Estuaries,* 2003, **26**, 1329-1343.

27 N. S. Hall and H. W. Paerl, *Mar. Ecol. Prog. Ser.,* 2011, **425**, 1-19.

28 S. Nehring, *Helgol. Mar Res.,* 2006, **60**, 127-134.

29 M. A. Robson, D. Williams, K. Wolff and J. C. Thomason, *Biofouling,* 2009, **25**, 215-227.

30 R. M. O' Riordan, S. Culloty, J. Davenport and R. McAllen, *Mar. Biodiv. Records,* 2009, **2**, 1-4.

31 D. J. Crisp, *J. Mar. Biol. Assoc. UK,* 1958, **37**, 483-520.

32 E. W. Knight-Jones and J. P. Stevenson, *J. Mar. Biol. Assoc. UK,* 1950, **29**, 281-297.

33 A. L. Neal and A. B. Yule, *J. Mar. Biol. Assoc. UK,* 1994, **74**, 251-258.

34 K. M. Berntsson, P. R. Jonsson, A. I. Larsson and S. Holdt, *Mar. Ecol. Prog. Ser.,* 2004, **275**, 199-210.

35 K. M. Berntsson, P. R. Jonsson, M. Lejhall and P. Gatenholm, *J. Exp. Mar. Biol. Ecol.,* 2000, **251**, 59-83.

36 S. Petronis, K. Berntsson, J. Gold and P. Gatenholm, *J. Biomater. Sci. Polymer Edn.,* 2000, **11**, 1051-1072.

37 N. Aldred, *Biofouling,* 2008, **24**, 351-363.

38 N. Aldred, A. Scardino, A. Cavaco, R. de Nys and A. S. Clare, *Biofouling,* 2010, **26**, 287-299.

39 J. M. Hills and J. C. Thomason, *Biofouling,* 1998, **12**, 57-69.

40 J. A. Moss, A. Nocker, J. E. Lepo and R. A. Snyder, *Appl. Environ. Microbiol.,* 2006, **72**, 5679-5688.

41 M. L. Carman, T. G. Estes, A. W. Feinberg, J. F. Schumacher, W. Wilkerson, L. H. Wilson, M. E. Callow, J. A. Callow and A. B. Brennan, *Biofouling*, 2006, **22**, 11-21.

42 A. Marmur, *Biofouling*, 2006, **22**, 107-115.

43 J. A. Finlay, M. E. Callow, L. K. Ista, G. P. Lopez and J. A. Callow, *Integr. Comp. Bio*, 2002, **42**, 1116-1122.

44 M. J. Huggett, B. T. Nedved and M. G. Hadfield, *Biofouling*, 2009, **25**, 387-399.

45 M. E. Callow, J. Callow, L. K. Ista, S. E. Coleman, A. C. Nolasco and G. P. López, *Appl. Environ. Microbiol.*, 2000, **66**, 3249-3254.

46 Y. Li, Y. H. Gao, X. S. Li, J. Y. Yang and G. H. Que, *Colloids Surf. , B*, 2010, **75**, 550-556.

47 J. A. Finlay, S. M. Bennett, L. H. Brewer, A. Sokolova, G. Clay, N. Gunari, A. E. Meyer, G. C. Walker, D. E. Wendt and M. E. Callow, *Biofouling*, 2010, **26**, 657-666.

48 D. Armani, C. Liu and N. Aluru, *Re-configurable fluid circuits by PDMS elastomer micromachining*, IEEE, Orlando. FL., 1999.

49 G. McHale, N. J. Shirtcliffe, S. Aqil, C. C. Perry and M. I. Newton, *Phys. Rev. Lett.*, 2004, **93**, 36102-36104.

50 D. I. Watson and D. K. A. Barnes, *Mar. Biol.*, 2004, **145**, 201-214.

51 W. A. Munro, C. L. P. Thomas, I. Simpson, J. Shaw and J. Dodgson, *Sensors Actuators B: Chem.*, 1996, **37**, 187-194.

52 K. Caldeira and M. E. Wickett, *Nature*, 2003, **425**, 365-365.

53 K. C. Hester, E. T. Peltzer, W. J. Kirkwood and P. G. Brewer, *Geophys. Res. Lett.*, 2008, **35**, L19601-L19606.

54 L. Jacobs, E. E. De Bruyn and T. E. Cloete, *Water Sci. Technol.*, 1996, **34**, 533-540.

55 S. J. Marrs, R. M. Head, M. J. Cowling, T. Hodgkiess and J. Davenport, *Estuar. Coast. Shelf Sci.*, 1999, **48**, 137-141.

56 K. G. Porter and Y. S. Feig, *Limnol. Oceanogr.*, 1980, **25**, 943-948.

57 F. Casse and G. W. Swain, *Int. Biodeterior. Biodegrad.*, 2006, **57**, 179-185.

58 K. A. Zargiel, J. S. Coogan and G. W. Swain, *Biofouling*, 2011, **27**, 955-965.

59 P. J. Molino, S. Childs, M. R. E. Hubbard, J. M. Carey, M. A. Burgman and R. Wetherbee, *Biofouling*, 2009, **25**, 149-162.

60 A. Kerr and M. J. Cowling, *Philos. Mag.*, 2003, **83**, 2779-2795.

61 J. S. Patil and A. C. Anil, *Biofouling*, 2005, **21**, 181-188.

62 M. E. Callow, in *Studies in Environmental Science*, ed. L. V. Evans and K. D. Hoagland, Elsevier, Amsterdam, 1986, p. 1-20.

63 P. J. Molino, E. Campbell and R. Wetherbee, *Biofouling*, 2009, **25**, 685-694.

64 S. Dobretsov and J. C. Thomason, *Biofouling*, 2011, **27**, 869-880.

65 F. E. Round, J. F. Sloane, F. J. Ebling and J. A. Kitching, *J. Ecol.*, 1961, **49**, 617-629.

66 V. Zupo, C. Patalano and P. Messina, *J. Phycol.*, 2011, **47**, 1433-1444.

67 Y. V. Nancharaiah, M. Rajadurai and V. P. Venugopalan, *Environ. Sci. Technol.*, 2007, **41**, 2617-2621.

68 M. Nappo, S. Berkov, C. Codina, C. Avila, P. Messina, V. Zupo and J. Bastida, *J. Appl. Phycol.*, 2009, **21**, 295-306.

69 C. Bressy, C. Hellio, J. Marechal, B. Tanguy and A. Margaillan, *Biofouling*, 2010, **26**, 769-777.

70 K. Efimenko, J. Finlay, M. E. Callow, J. A. Callow and J. Genzer, *ACS Appl. Mater. Interfaces*, 2009, **1**, 1031-1040.

71 M. J. Keough, *Ecology*, 1984, **65**, 423-437.

3 Investigation of Physical AF Mechanisms of Shark Dermal Denticles

3.1 **Introduction**

Chapter 2 has demonstrated that surface texture can provide settlement cues for biofouling organisms such as the barnacle *Austrominius modestus* in the environment. Initial field studies suggest that surface topography on materials exposed to settlement of *A. modestus* can promote gregarious settlement of this species. This is in contrast to a number of recent publications that have proposed that bio-inspired engineered surface texture can prevent or reduce the settlement of problematic biofouling organisms under certain conditions [1-3].

The use of engineered surface texture for biofouling reduction inspired by sharkskin and other surfaces are reported [4-9]. One of these surface textures, Sharklet AF™, is described as being inspired by specific topographic features associated with sharkskin and is reported as an effective deterrent to a number of biofouling organisms. These organisms include the common biofouling alga *Ulva* (synonym: *Enteromorpha*) and the bacterium *Staphylococcus aureus*. Although seemingly inspired by sharkskin, this surface texture has little relationship to published descriptions of sharkskin [10]. Furthermore, few reports exist on whether natural sharkskin has any natural AF defences attributable to the physical structure of the surface.

3.1.1 *Biomimetic design and AF surfaces*

The approach to design of surface textures like Sharklet AF™ is based upon a concept known as biomimetics. Biomimetics is the use of concepts and material characteristics present in nature to inspire novel improvements to existing engineered materials, or indeed to mimic ideas from nature to produce completely novel solutions to engineering problems [11, 12]. Historically, the biomimetic approach to material design has been fruitful and many successful materials and concepts have inspired by close observation of the natural world, including such ubiquitous concepts and materials as powered flight and Velcro [12].

Designing novel AF solutions using biomimetics is an appealing prospect, as many marine organisms appear to have some intrinsic ability to resist epibiosis through chemical and/or physical means [13]. Biomimetic design inspired by sharkskin began with the observation that the skin of this group was not smooth as anticipated but instead

exhibited microscopic features called placoid scales. These structures are now known as dermal denticles [14].

Curiosity concerning the reasons why sharkskin would exhibit dermal denticles and particularly the work of Bechert [16, 17] led to detailed experiments on drag reduction created by the presence of dermal denticles. Investigation of the hydrodynamic properties of mechanical riblets similar to those of dermal denticles indicated that riblets present on dermal denticles produced hydrodynamic flow patterns. .It has been subsequently determined that fast-swimming shark species gain an additional 8-10% swimming efficiency due to dermal denticle riblets [18].

Attempts have been made to exploit the drag reducing properties of riblets in various applications such as the Fastskin® body suit designed by swimwear company Speedo® as a drag reducing whole body swimsuit [12]. However, the successful transferral of hydrodynamic properties created by dermal denticles to artificial surfaces is complex [19]. Efforts to re-create drag reduction by use of dermal denticle-like riblets on large artificial surfaces such as the hulls of ships and aeroplane fuselages has proven to be a major challenge [20].

Despite speculation that dermal denticles and riblets may have dual functionality in drag reduction and AF [21], inhibition of biofouling by either the microtopographic architecture of the denticle surface, the presence of riblets or by the hydrodynamic conditions created close to the skin surface is a possibility that has not been considered in detail experimentally. Any ability to control hydrodynamics and boundary layer conditions using surface features is intriguing as it may affect the ability of biofouling propagules to contact a surface, particularly with regard to vortex generation and recirculating cross-flow as created by surfaces exhibiting riblets [21].

One of reasons why dermal denticles have not been tested for AF ability is related to the lack of suitable synthetic sharkskin for testing purposes. Models of artificial surfaces used to generate data on fluid dynamics are prohibitively expensive, time consuming and to produce and generally not suitable for exposure in the environment. This prohibits assessment of the effect of riblets in field trials. Thus in order to test effects of structures like dermal denticles on microbial adhesion, an inexpensive means of producing synthetic skin must be found. Replication of a sharkskin surface using moulds produced from the natural skin surface may offer this possibility.

3.1.2 *Aims and objectives*

The aim of this chapter is to evaluate dermal denticles of natural and artificial sharkskin for AF ability. The objectives are:

(1) Characterise the physical structure, geometry and quantify the extent of epibiosis from natural dermal denticles.

(3) Generate synthetic sharkskin to test physical mechanisms of AF.

(4) Evaluate the AF potential of artificial sharkskin surfaces.

3.2 **Materials and Methods**

3.2.1 *Reagents*

Polydimethylsiloxane (PDMSe) (Sylgard 184 kit, Dow-corning, Farnell, Ireland), Araldite epoxy resin kit (Epoxy resin kit R1030, Agar Scientific, Stanstead, UK), ethanol (Cooley Distillery, Ireland), microscope slides (Corning, NY), Petri dishes and 50 ml centrifuge tubes (Sarstedt, Ireland), trichloro(1H,1H,2H,2H-perfluorooctyl)silane (97%, Sigma-Aldrich, Dublin, Ireland) and clear silicone-based adhesive (Aquatics online, Bridgend, UK).

3.2.2 *Sharkskin collection*

Mature specimens of the common catshark, *Scyliorhinus canicula* were collected from local anglers. Dead specimens were collected from fishing boats near Baltimore Harbour, County Cork, Ireland (51°29’ N; 09°22’ W). Several adult specimens ranging from 600-660 mm total length were collected, placed in a cool box, an immediately transported to the laboratory, where measurements of total length were taken and each specimen frozen to -18 °C to await analysis.

3.2.3 *Sample preparation for electron microscopy*

Sharkskin samples for microscopy (1 cm^2) were removed from the body with a scalpel. The skin surface was removed from underlying collagen layers and other tissues and mounted on glass slides for examination by light microscopy. Samples for scanning electron microscopy were analysed by drying skin samples at ambient temperature for one hour before mounting on 15 mm diameter aluminium stubs with double-sided carbon adhesive tabs. Microbial biofilms were prepared for analysis by fixation in gluteraldehyde (2.5% v/v) and dehydration in an ethanol series (30-100%). After several days, the un-fixed samples exhibited small shrinkage artefacts when imaged in SEM but thereafter appeared to remain stable for months. Samples were coated with gold (Edwards 150B sputter-coater).

3.2.4 *Denticle characterisation*

Dimensions were measured from dermal denticles at four locations on the shark body from SEM images processed using ImageJ image analysis software [22]. To measure the dimensions of dermal denticles, scanning electron micrographs were imported into ImageJ and a scale set using the embedded scale bar present in SEM images. Measurements of maximum denticle length and width, abundance (denticles mm^{-2}), and tip angle (°) were made. Contamination of dorsal and ventral surfaces of individual denticles was also quantified by importing SEM images into ImageJ.

3.2.5 *Artificial skin fabrication*

Sharkskin samples from four selected locations on *S.canicula* were replicated in epoxy resin and PDMSe for subsequent biofouling assessment using methods previously outlined for fabrication of artificial Lotus leaves [23]. A schematic of this process is shown in Figure 3-1.

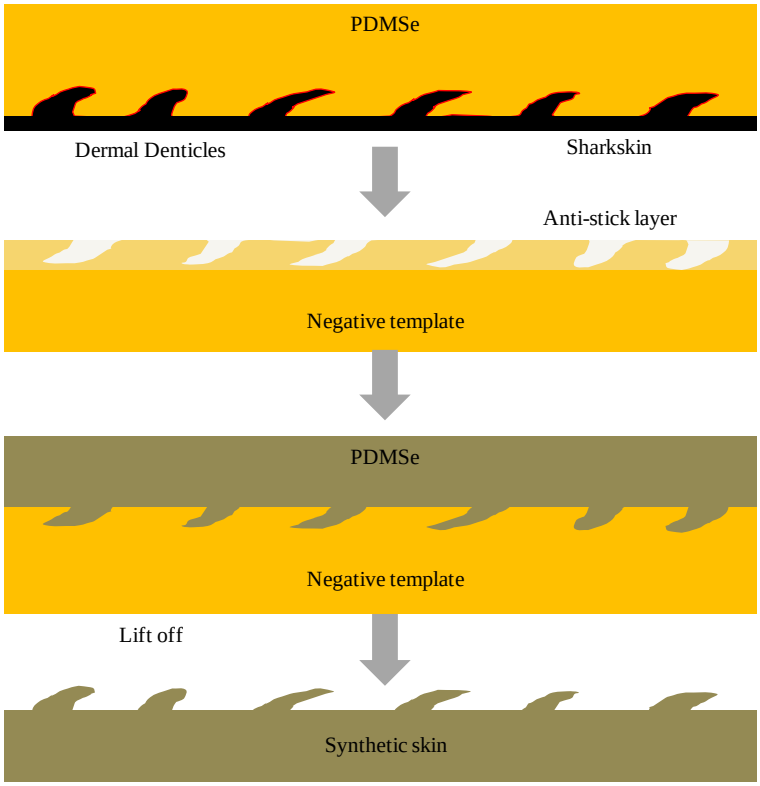

Figure 3-1: Schematic of the methodology to produce artificial skin from the catshark Scyliorhinus canicula in PDMSe.

3.2.6 *Negative template production*

Artificial sharkskin was created in epoxy resin and PDMSe using negative templates prepared from natural sharkskin removed from *S. canicula*. These negative templates were produced in PDMSe by mixing 10 parts by mass of PDMSe resin and 1 part by mass curing agent Poly(methylsiloxane). This mixture was then hand stirred for 2-4 min and degassed under vacuum using a dessicator for 20-30 min. Approximately 10 cm² sections of frozen sharkskin were removed from the shark body. These skin sections were rinsed with de-ionised water and allowed to dry. Skin samples removed in this way were approximately 0.5 - 1 mm in depth. Skin sections were allowed to reach room temperature (18-25 °C) and excess water removed by gentle heating in a vacuum oven (Technico, Chennai). To prevent curling and warping, skin samples were placed on microscope slides, sealed with clear nail varnish, and allowed to dry slowly at 20 °C for 2 days.

Skin samples were then placed in the bottom of clean sterile Petri dishes, dermal denticles upward. Degassed PDMSe was then poured over the skin to a depth of 4-5 mm and transferred to an oven to cure at 50 °C for 24 h. After curing, sharkskin could be removed from the template by flushing with de-ionised water. Occasionally isolated denticles were trapped within the templates but were removed with the first use of the template.

3.2.7 *Synthetic sharkskin production*

Artificial sharkskin was produced from negative templates by first depositing a self assembled monolayer of trichloro(1*H*,1*H*,2*H*,2*H* -perfluorooctyl)silane on template surfaces. The structure of this compound is shown in Figure 3-2. To do this, negative templates were placed in a dessicator under vacuum with 10-20 µL of silane for 40 min at 40 °C. Once completed, templates were removed and immediately filled with mixed and de-gassed PDMSe. This mixture was then cured as described previously.

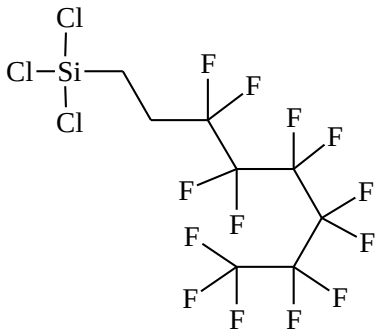

Figure 3-2: The chemical structure of trichloro(1H,1H,2H,2H -perfluorooctyl)silane used in this study.

3.2.8 *Epoxy artificial skin*

Artificial sharkskin in epoxy resin was produced in an identical manner to that described for PDMSe, except that epoxy was substituted for PDMSe in the final step. The epoxy resin used was obtained from a microscopy embedding epoxy resin kit and mixed as per manufacturer's instructions (Araldite CY 212/DDSA/BDMA; 20 mL/22 mL/ 1.1 mL). Mixed epoxy resin was cured at 60 °C in a vacuum oven set at 200 mbar for 24 h.

3.2.9 *Field testing of artificial skin*

Artificial skin samples were assessed for biofouling growth in November 2010 at Lough Hyne Marine Reserve, Cork, Ireland (for description of the Lough and associated research on the population of *S.canicula* present, see [24]). Skin samples were mounted on poly(methylmethacrylate) discs cut from Petri dishes, using non-toxic silicone adhesive. Prior to field trials, samples were submerged in de-ionised water for 1 week to removal any residual contamination resulting from the production process. Discs with attached artificial skin were mounted on a stainless steel backing panels and suspended in high flow areas in the South Basin of Lough Hyne Marine Reserve (14 d at 1 m depth). Other samples were suspended in low flow in the North Basin of Lough Hyne for the same period. Samples in the high flow environment were securely anchored in order to keep samples orientated parallel to mean flow direction. On removal, samples were gently rinsed in clean seawater to remove any loosely attached fouling, preserved with 2.5% (v/v) gluteraldehyde in 50 mL centrifuge tubes, and transported back to the laboratory for biofouling assessment.

3.2.10 *Characterisation of denticle fouling*

Biofouling was assessed on both dorsal and ventral surfaces of synthetic and natural sharkskin using image analysis. Backscattered electron SEM (BSE-SEM) images taken at x2K provided contrast between the denticle surface and fouling. Images were processed in ImageJ software and biofouling calculated as a percentage of the denticle surface. Mass changes were also measured on artificial sharkskin after deployment.

3.3 **Results and discussion**

Dermal denticles are reported to provide several advantages to sharks and rays, including protection from predators and ectoparasites, reduction of mechanical abrasion, accommodation of bioluminescent and sensory organs, and reduction of frictional drag [25]. Acting as a deterrent to the attachment of ectoparasites is thought to be one of the primary functions of dermal denticles. This deterrence has been proposed as a primary function for at least three major ecological classes, including schooling sharks of low to moderate speed (*Squalus, Triakis, Deania*) and those on demersal sharks on sandy and muddy substrates (*Centrophorus, Oxynotus, Squatina, Hemiscyllium, Ginglymostoma, Galeus, Scyliorhinus, Mustelus*) [26]. This function was proposed based on the absence of observed parasites in captured specimens, however the mechanism(s) by which dermal denticles could prevent attachment of ectoparasites has not been explained.

3.3.1 *Denticle morphology in S. canicula*

S. canicula, a representative of the largest order of extant sharks, is a member of the *Galeomorphs* and belongs to the order *Carcharhiniformes*, family *Scyliorhinidae*. Thus, *S. canicula* is not accurately called a dogfish, having closer morphological similarity to the catsharks. *S. canicula* was used in the present study as it is abundant in European inshore waters [27], is readily available and a representative member of active but slow-swimming sharks [10]. Swimming speeds for this and similar species are reported as being in the region of 0.24 ms^{-1} in aquaria, although no precise figure can given for speeds outside of captivity [28]. This swimming speed categorises *S. canicula* as a comparatively slow swimming shark. Examination of the muscle fibre has indicated that this species is capable of a maximum speed of 7.8-12.9 fish lengths s^{-1} [29].

Scanning electron microscopy of skin from four locations on the body of *S. canicula* indicated distinct variation in denticle morphology at the different locations. While retaining the tridentate shape and a true plate-like crown with longitudinal riblets reported in the literature for similar species [14], the average shape of dermal denticles were more elongated than typically reported. This was particularly evident on skin samples examined from the anterior of *S. canicula*. A typical dermal denticle isolated from the skin surface of *S. canicula* is shown in Figure 3-11. This denticle is from the anterior of the body and is fully developed.

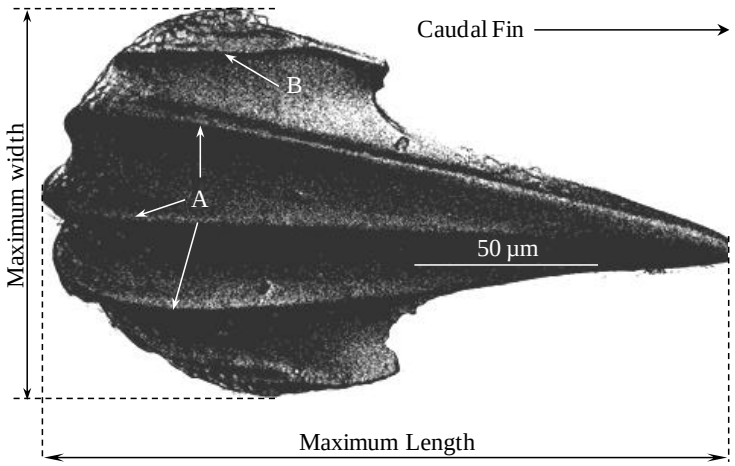

Figure 3-3: Scanning electron micrograph of an isolated dermal denticle from the skin of Scyliorhinus canicula. The denticle is positioned so that the head of the shark is to the left while the tail is to the right of the image. Riblets are present (A), including a central riblet with two flanking riblets converging at the denticle point. Initial formation of further riblets can also be observed (B).

Figure 3-4 illustrates a digital image of a dermal denticle acquired with a light microscope, and demonstrates the overlapping nature of dermal denticle from *S. canicula*. The attachment base of dermal denticles to the underlying skin surface is also evident; allowing some degree of pivotal movement of individual dermal denticles while swimming, however, the changes in the range of movement capable among individual dermal denticles was not examined further in this study.

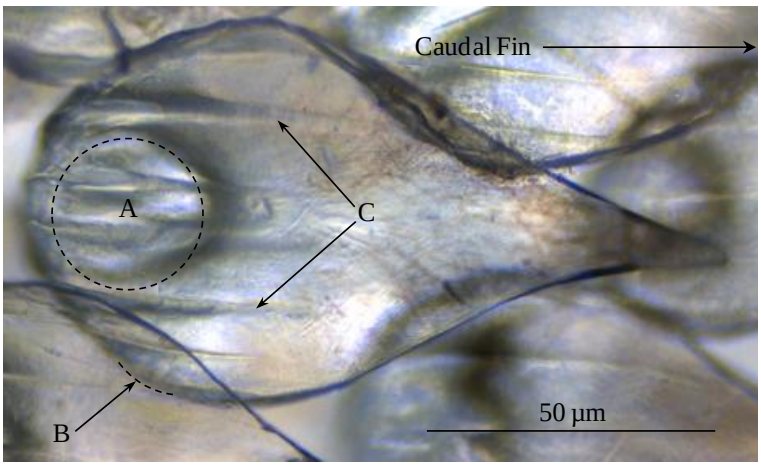

Figure 3-4: Digital light microscopy image of dermal denticles attached to the skin surface of S. canicula. The attachment area of the denticle can just be seen (A), while B highlights the degree of overlap between denticles. The riblets on the dorsal surface of the denticle can also be distinguished (C).

Examination of dermal denticles from *S. canicula* generally indicated that denticles were arranged in the pattern shown in Figure 3-5. This alignment of dermal denticles is in agreement with published descriptions indicating that numerous horizontally arranged layers of collagen fibre bundles are present under the skin surface, often crossing at an angle of 40–70°. The placement of these collagen fibre bundles control alignment and association of denticles on the skin surface.

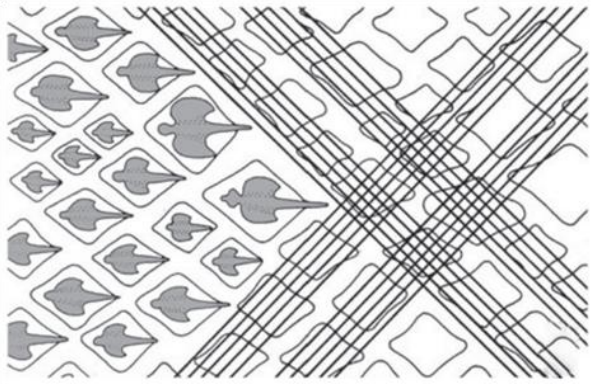

Figure 3-5: A schematic of dermal denticle arrangement on the skin surface of S. canicula. The angle of the fibre bundles in relation to the orientation of the denticles can be seen. (Figure adapted from Meyer and Seegers [10])

The internal structure of examined dermal denticles is shown in Figure 3-6. A thin-section through the denticle illustrates both the internal structure and the bristling angle of individual dermal denticles from the skin surface.

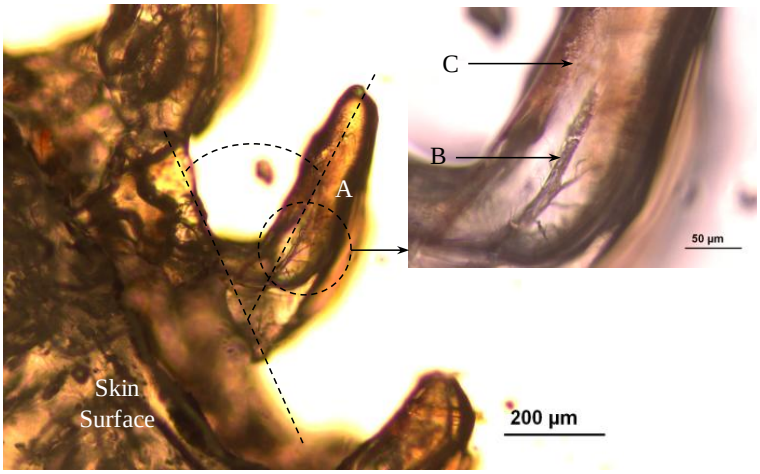

Figure 3-6: A light micrograph of a thin section through the skin surface and dermal denticles of S. canicula. Enlargement of the internal structure is also shown (circled, inset). A= Dental papilla, B = dentine and C = enamel (enameloid). The bristling angle between the skin surface and the denticle is also evident.

Dermal denticles were present on all examined skin samples. Measurement of denticle dimensions indicated a variation in denticle shape, packing density and ratio of maximum denticle length to width at different locations on the skin. A progressive reduction in denticle length from 729 ± 201 µm at the head to 332.8 ± 40.5 µm (errors ± standard deviation) at caudal fin was evident. A reduction was also recorded in the ratio of maximum length to width and large dermal denticles were typically more elongated with a larger ratio of length to width. Physical manipulation of dermal denticles revealed a degree of scale bristling reported by Lang and co-workers [15], however the extent of this bristling could not be examined in detail on fixed skin samples. Estimation of the bristling angle indicated a range of 25-70 °.

Profiles of the riblets on the dorsal surface of dermal denticles also varied with skin location, becoming progressively more pronounced from posterior to anterior of the shark. This is in agreement with previous reports from two pelagic carcharhinids, where it was suggested that strong indications of reduced ridge (riblet) dimensions, particularly heights and spacing, on the dorsum are present along the anterior portion of the body that may be related to water velocity at these locations [25]. This is illustrated in Figure 3-7.

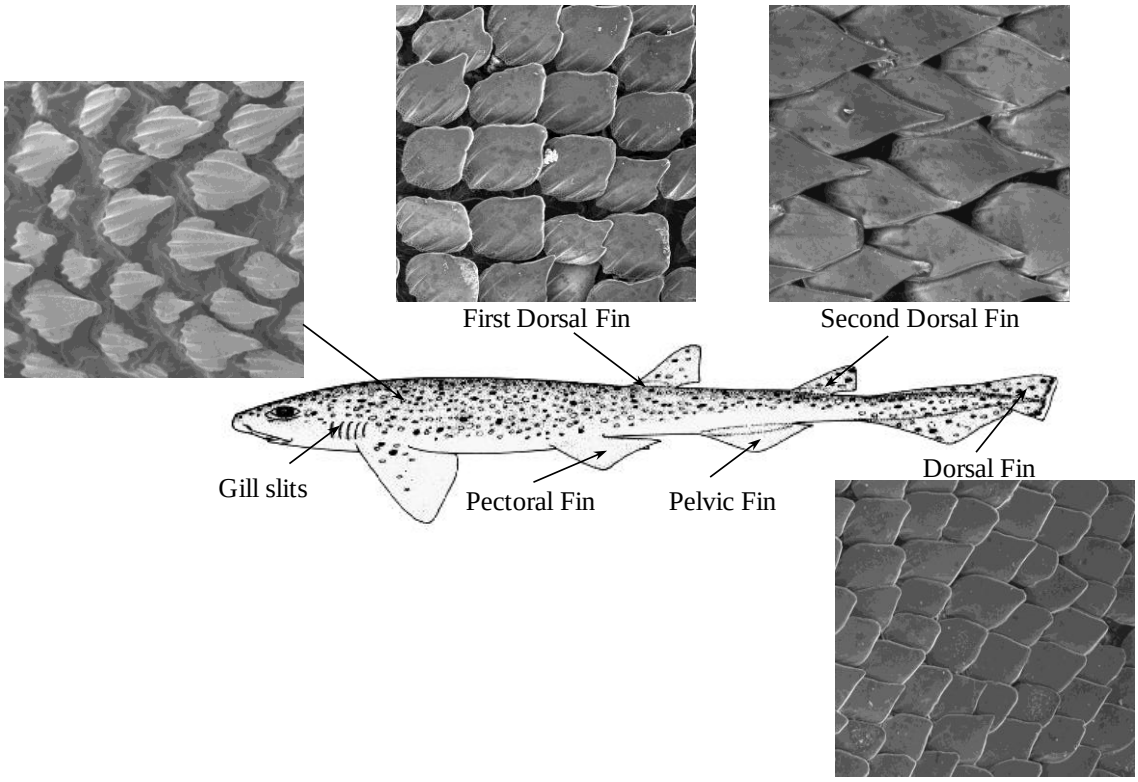

Figure 3-7: A schematic of denticle morphology and anatomy at positions on the body of S.canicula, showing representative scanning electron micrographs of typical denticle morphology at each location.

A progressively increasing number of riblets were observed on denticles from the tail towards the head. This was also noted by Reif who demonstrated that as the skin surface area increases with growth, the resulting spaces are often covered by larger scale crowns [26]. It was proposed that in order to maintain consistent riblet spacing, new riblets may be added, resulting in a decoupling of scale width and riblet spacing. This is in agreement with the results of the present study where more riblets were found on dermal denticles isolated from the anterior of individuals of *S. canicula.* In general, riblets were less pronounced on the dorsal surface of denticles isolated from the tail and extremities (fins) of the shark.

Thus it is concluded that riblet height and spacing on dermal denticles from *S. canicula* remain ontogenetically constant in spite of an increasing overall scale width in agreement with dermal denticle measurements completed elsewhere [25]. The riblet heights of shark species most strongly selected for high-speed swimming are generally less than 30 µm and have spacing values of less than 100 µm, consistent with optimal theoretical values for optimum hydrodynamic efficiency [25]. Measured values for *S.canicula* in this study were outside of these values on dermal denticles isolated from the anterior region of the body, yet were generally within these values on smaller dermal denticles. As denticles became larger at the anterior of the shark, this spacing began to widen with larger spacing between riblets at the base of the denticle. This data is summarised in Table 3-1.

Table 3-1: Summary of the principle dimensions and denticle morphology with regard to location on the surface of S. canicula (Data taken from n = 150 dermal denticles in each position except for denticle density mm^{-2} where data was collected from n = 36 counts)

Location on shark	Denticle Surface Area (mm^2)	Denticles mm^{-2} ± SE (n = 36)	$\bar{x}$ length (µm) ± SE	$\bar{x}$ width (µm) ± SE	Width:Length	Mean tip angle (Deg) ± SE
Head	0.19 ± .086	3.66 ± 1.33	729 ± 201	417.76 ± 92	1:1.8	27.8 ± 5.2
1st Dorsal Fin	0.11 ± .064	7.66 ± 1.46	470.8 ± 77.4	320.2 ± 41	1:1.5	39.7 ± 8.4
2nd Dorsal Fin	.06 ± .0046	19.2 ± 2	336.3 ± 36.5	233.8 ± 21	1:1.4	61.5 ± 6.7

Caudal Fin	.05 ± .0038	17.28 ± 2.61	332.8 ± 40.5	244 ± 32.6	1:1.4	59.1 ± 9.3

The relationship between the length and width of dermal denticles from locations along the body surface of *S. canicula* is indicated in Figure 3-8.

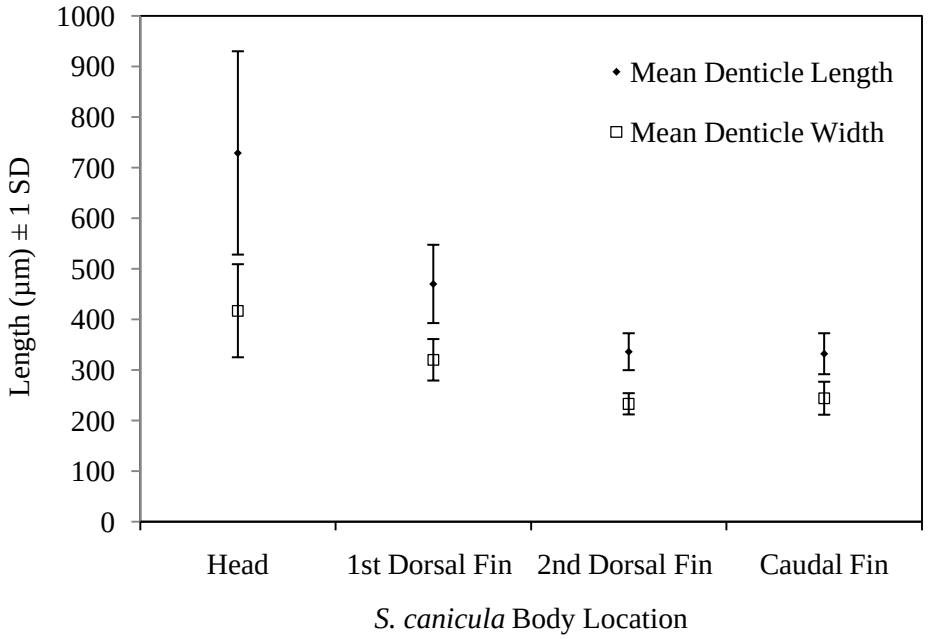

Figure 3-8: Graph of the relationship between denticle length and width over the skin surface of S. canicula. A trend of decreasing maximal denticle length and width is observed when measured from the anterior to posterior of the body.

Towards the anterior of the shark, denticle length measurements demonstrated a bimodal distribution. This is likely due to new dermal denticles protruding through the skin surface gradually replacing the older, larger denticles. Light microscopy occasionally indicated that larger dermal denticles in this area were degraded and were bleached in appearance. This distribution is shown in Figure 3-9.

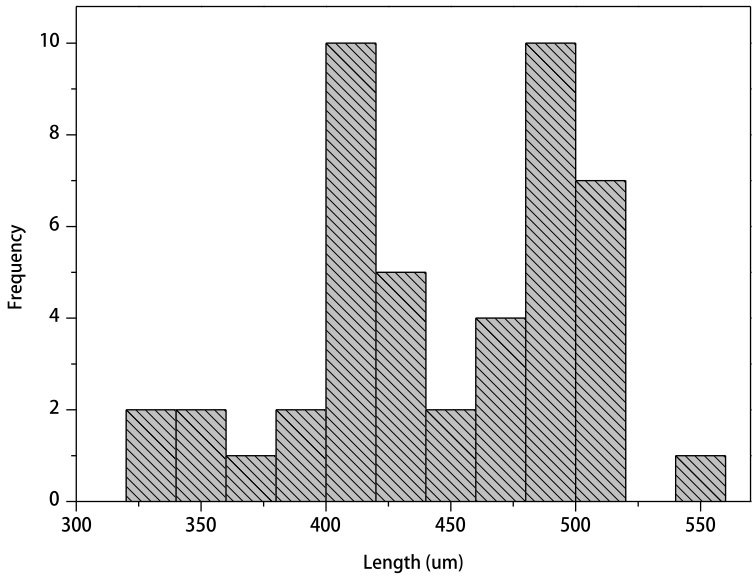

Figure 3-9: A typical bimodal distribution curve of denticle length at the head position of a specimen of S. canicula, demonstrating the two populations of dermal denticles are present.

3.3.2 *Denticle surface texture*

Scanning electron microscopy examination of dorsal surfaces from individual dermal denticles indicated the presence of surfaces grooves consistent with mechanical abrasion. The majority of these surface features were positioned approximately parallel to the longitudinal axis of denticles. These features are consistent with mechanical damage, perhaps caused by contact with rocks or other sharks. These features may even result from contact between dermal denticles during feeding [31]. Contact between overlapping denticles may also occur when the skin surface flexes during forward swimming motion of the shark.

It has been postulated that the microtopography or microtexture of marine organisms may have some function in preventing the adhesion of fouling organisms [32], particularly in regard to periodic grooved features which may reduce the binding energy between the surface and adhering bacteria. Although the features seen on the denticle surfaces may have some, as yet unspecified, role in preventing microorganism attachment, the lack of consistence waviness, isotropy or other consistent textural parameters does not support this view.

In addition to grooved surface topography, ectodermal pits were also noted on the dorsal surface of many but not all dermal denticles examined. These pit structures are unexplained although a correlation between the mass of individual dermal denticles and

the presence of ectodermal pits has been measured [33], indicating that crown thickness controls the presence of absence of these features. Examples of both mechanical abrasion and ectodermal pits are shown in Figure 3-10.

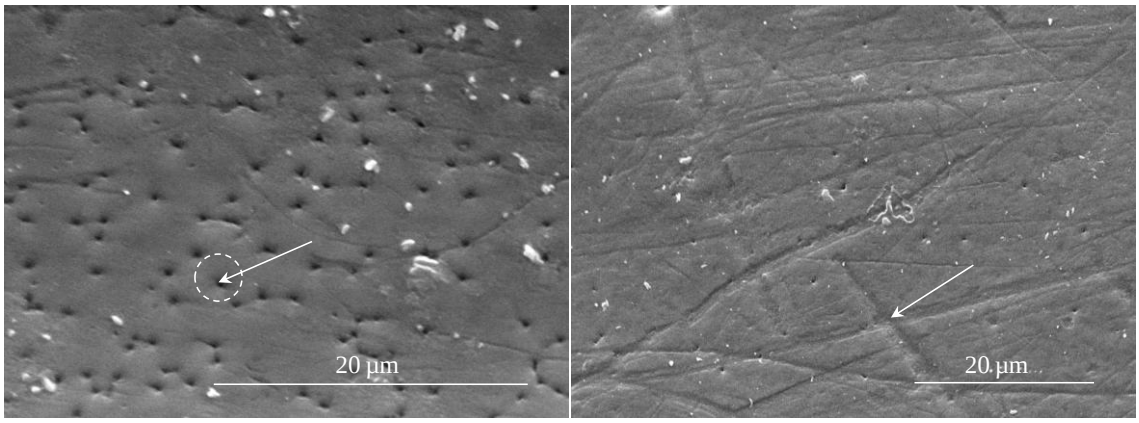

Figure 3-10: Scanning electron micrographs of microtopographic detail on the denticle surface demonstrating ectodermal pits (left) and linear surface grooves (right).

3.3.3 *Further denticle characterisation*

While light and electron microscopy have been utilised previously to characterise dermal denticles, these methods suffer from a number of disadvantages when characterising the 3D structure of shark dermal denticles. Therefore, a number of alternative techniques were attempted to gather a comprehensive overview of denticle morphology and microbial colonisation of the skin of *S. canicula*. These techniques included Scanning white light interferometry (SWLI), a versatile technology that provides a noncontact, 3-D method of measuring surface roughness, profilometry, optical sectioning and 3D modelling of individual dermal denticles. In generally, due to the complex nature of dermal denticles these methods did not produce valid additional data for analysis of denticle morphology. An example of this is shown in Figure 3-11 using white light interferometry (WLI) results of dermal denticles *in situ* on the skin of *S. canicula*. This technique is a noncontact, 3-D method of measuring surface roughness. Although a recognisable representation of the denticle surface has been reproduced, the number of missing data points precludes any detailed analysis of the surface texture and roughness associated with these structures.

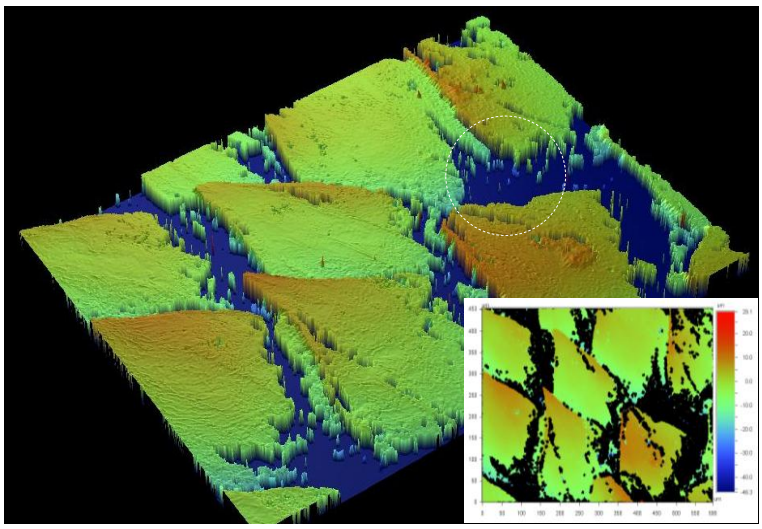

Figure 3-11: Digital image of a 3D model of dermal denticles generated using white light interferometry (inset). Missing data points resulting from the overlapping nature of the denticles are in blue (circled).

3.3.4 *Microfouling of S.canicula dermal denticles*

Although a number of published reports exist on chemical antimicrobials in sharks [34], few studies have examined physical mechanisms of epibiosis prevention on outer surfaces of this group. There are limited reports of biofilm development on dermal denticles and the degree to which *S. canicula* undergoes microbial colonisation in general. Prevention of external parasites has been suggested as a primary function of dermal denticles in sharks. However, the mechanisms by which dermal denticles can reduce parasitic attachment are not known although reports exist on *S. canicula* dermal parasitic infestation in Irish waters [35].

Inhibition of epibiosis by the egg case of *S. canicula* has been attributed to heavy metal scavenging or a Fenton-like reaction on the outer surface of this structure [36, 37]. Chemical antimicrobials originating from dermal denticles have not been examined although such compounds would originate in mucilage secretions from the skin surface rather than from dermal denticles *per se*. Chemical compounds isolated from the tissues of sharks have demonstrated potent antimicrobial activity. Of these, squalamine, a compound previously isolated from the tissues of the dogfish shark (*Squalus acanthias*) and the sea lamprey (*Petromyzon marinus*), has been demonstrated to exhibit broad-spectrum antiviral activity against human pathogens [38].

Gram–positive bacteria are thought to be an important component of the bacterial flora on the skin of sharks and *Vibrio spp*. in particular have been associated with skin flora and even systemic infection in sharks in captivity [40, 41]. However, in general commensal bacterial communities associated with sharks are also poorly studied. Among teleost fishes, in which the commensal bacterial flora has received considerable attention, the skin often has in excess of 10^2–10^7 cells cm^{-2} of skin [39]. The largest taxa of these bacteria are represented by *Achromobacter, Pseudomonas, Flavo-bacterium* and *Cytophaga* species and coryneform organisms. Therefore data on localisation and quantification of microbial communities associated with *S. canicula* will be of use in future studies examining commensal bacterial communities.

3.3.5 *Fouling of denticle dorsal surfaces*

Quantification of biofilm growth by standard methodologies such as crystal violet staining or carbohydrate and protein analysis proved difficult due to the topographic and chemical nature of sharkskin. Thus, the extent of microbial growth on dorsal surfaces of dermal denticles of *S. canicula* was quantified using image analysis techniques. Examination of the dorsal surfaces of dermal denticles isolated from *S. canicula* identified bacterial microcolonies on the surface, but these were a small percentage of the overall surface area of denticles. Not all surface contamination could be identified as biological in origin; hence, contamination of denticle surfaces is referred to as fouling. Images for fouling analysis were processed from the central region of the denticle surfaces. High contrast levels between surface fouling and the denticle surface when imaged with BSE-SEM, allowed percentage area calculation from images. A disadvantage of this method was that no distinction could be made between fouling by mucilage secretions originating from the skin surface and microbial EPS unless individual bacterial cells could be identified. An example of this method is shown in Figure 3-13.

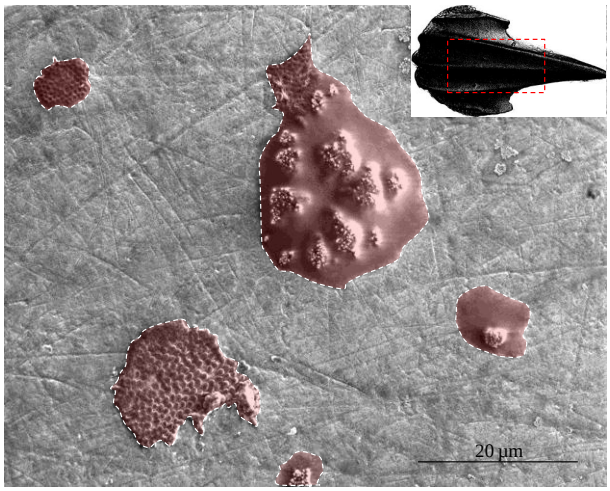

Figure 3-12: Scanning electron micrograph of the dorsal surface of a dermal denticle of S. canicula, demonstrating surface fouling of the denticle (highlighted). Calculation of fouling as a percentage of the total image surface area was used as a means of estimating surface fouling. The portion of the denticle surface imaged for fouling analysis is also shown (inset).

The results of this analysis are presented in Figure 3-13, where denticle fouling is presented as a percentage of the total image area. Dermal denticles from the anterior of *S. canicula* demonstrate the least amount of dorsal surface fouling, while a progressive reduction in surface fouling is observed from the first dorsal to the caudal fin.

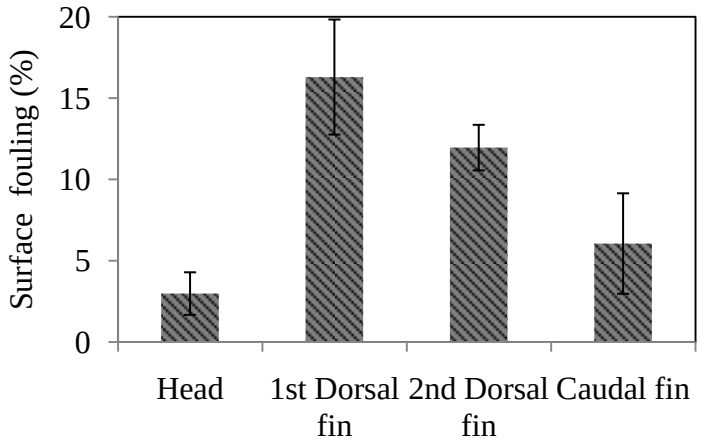

Figure 3-13: Graph of percentage fouling of dorsal surfaces from dermal denticles isolated from S. canicula at the locations indicated. (Mean from 10 images ± standard deviation)

Microbial cells encapsulated in EPS were associated with particular features on the denticle surface particularly surface features present at the anterior of dermal denticles. Unusually, diatom frustules were rarely present. Figure 3-14 illustrates the typical texture associated with the anterior end of a dermal denticle, in which a number of surface indentations are observed. The function of these structures is unknown but can be speculated to have a function in retaining mucilage secretions on the denticle surface or anchoring denticles to the underlying skin. A number of examined denticles exhibited microbial colonisation of these features and retention of debris and diatom cells.

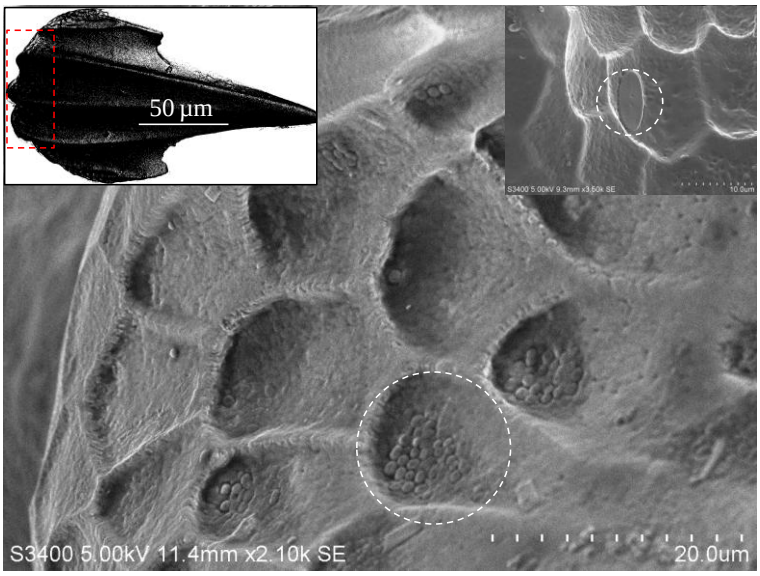

Figure 3-14: Scanning electron micrograph of the posterior of a dermal denticle (inset) isolated from S. canicula demonstrating microbial attachment (circled) on textures present. Diatom cells were also present in such structures (Inset right, circled).

3.3.6 *Microbial colonisation of denticle ventral surfaces*

Microbial biofilms were present on all examined ventral surfaces; however, colonisation was generally confined to areas closest to the attachment point of the skin surface and was progressively reduced towards the tip of dermal denticles. Figure 3-15 demonstrates variation in both surface texture and biofilms associated with the ventral surface of a dermal denticle. Bacterial strains were not identified in this study, but cells were rod-shaped and were present as a monolayer on the surface.

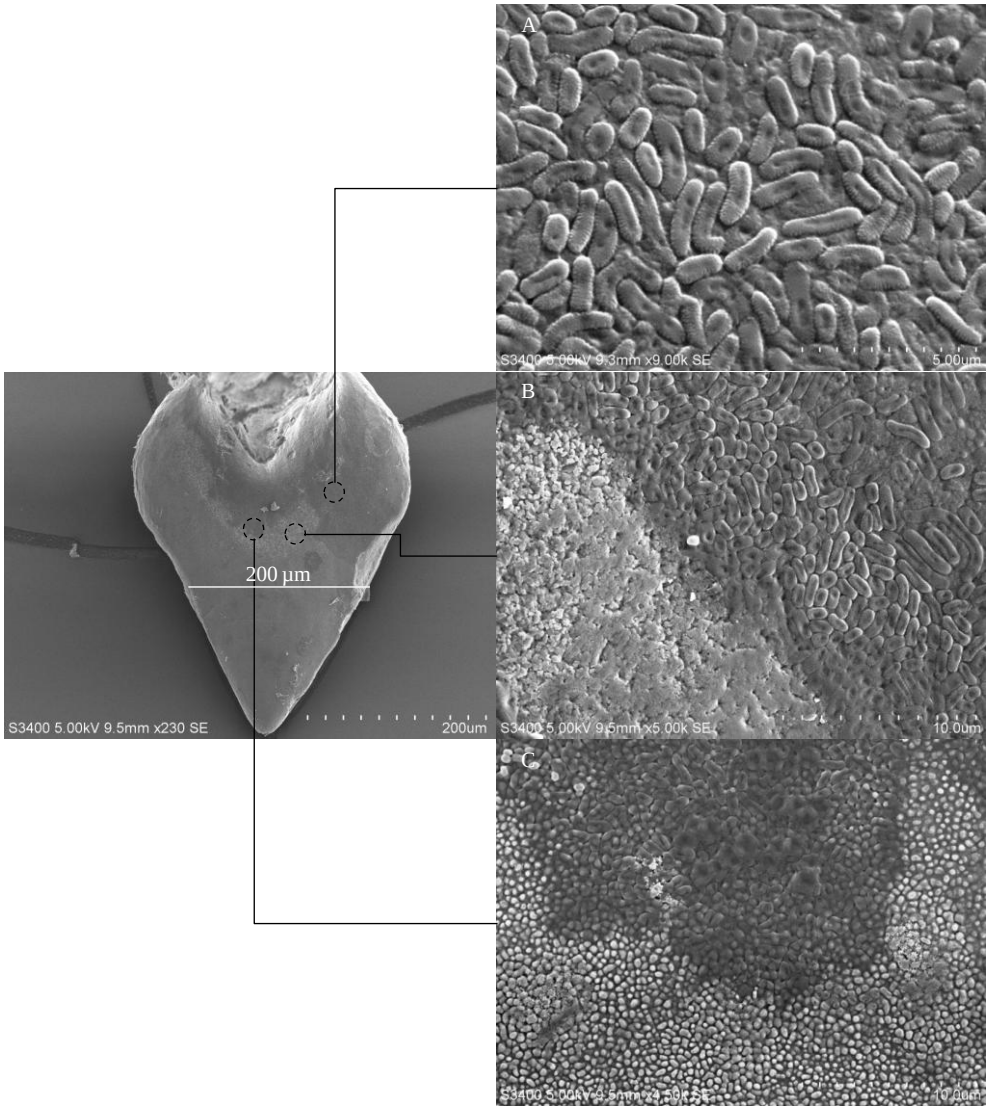

Figure 3-15: Scanning electron micrographs of the ventral surface of an isolated dermal denticle of S. canicula (left). Microbial cells adhered to the surface are generally rod-shaped and are in the form of a microcolony on the surface (A). (B) Demonstrates the transition from microbial colonisation to the clean denticle surface. Pitting and damage to the denticle surface is evident. (C) Shows the surface microtopography that is present on the surface towards the anterior of the denticle consisting of a unique surface topography composed of nanometre-scale surface nodules.

From the examined surfaces of natural dermal denticles, it can be concluded that dermal denticles of *S. canicula* undergo extensive microbial colonisation. However, this colonisation is not distributed uniformly across either denticle surfaces or the skin surface of the shark. Microbial colonisation is reduced towards the anterior of individual dermal denticles and on the both the head and tail sections of the shark.

3.3.7 *Artificial skin fabrication*

Artificial skin was produced from a negative template created using the skin of *S.canicula.* This technique is used in micro-fluidics to create topographically complex structures [42] and has been used to successfully to re-create the structure of lotus leaves in artificial materials [23]. Cured PDMSe has the capability to reproduce topographic features in the order of 20 nm in dimension [43] and thus is adequate to reproduce features of the dimensions of dermal denticles.

Initial difficulties encountered at the onset of producing artificial skin related to gas bubble formation in negative templates was overcome. This was done by curing the PDMSe in a vacuum and gently agitating trapped bubbles with a rubber cell scraper. This is an effective method of producing synthetic skin with embedded dermal denticles characteristic of the original template. Figure 3-16 illustrates the process of producing synthetic skin at various stages of fabrication. This method resulted in surfaces that could be readily assessed for biofouling, yielding exact replicas of the larger, non-overlapping dermal denticles.

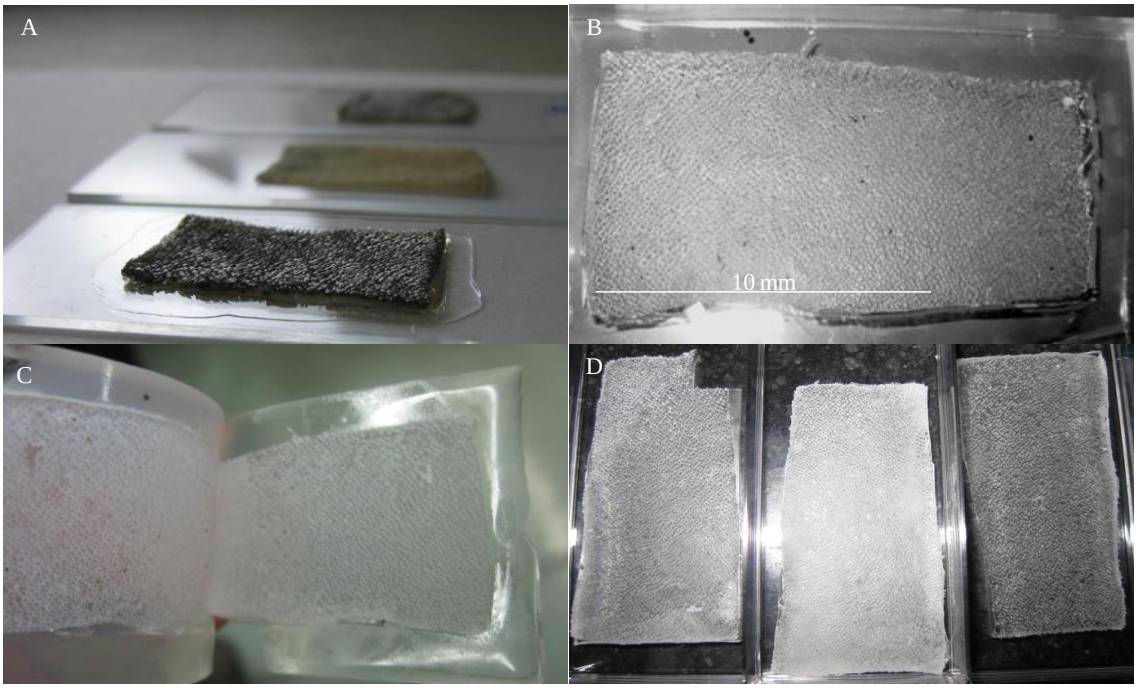

Figure 3-16: Digital images of the fabrication process for artificial sharkskin, showing (A) adhesion of an area of sharkskin to a glass slide surface to prevent warping and shrinking, (B) the negative template produced from casting PDMSe over the surface, (C) separation of artificial skin samples from the negative template after silanisation and (D) artificial skin samples prepared for characterisation and testing.

Difficulties were encountered in producing accurate artificial skin from negative templates in which dermal denticles had a high degree of interlocking. Examination of the skin after production of a negative template indicated that PDMSe became entrapped between denticles. This is illustrated in Figure 3-17, where PDMSe has cured between dermal denticles and subsequent removal of the elastomer results in retention of the elastomer in these areas.

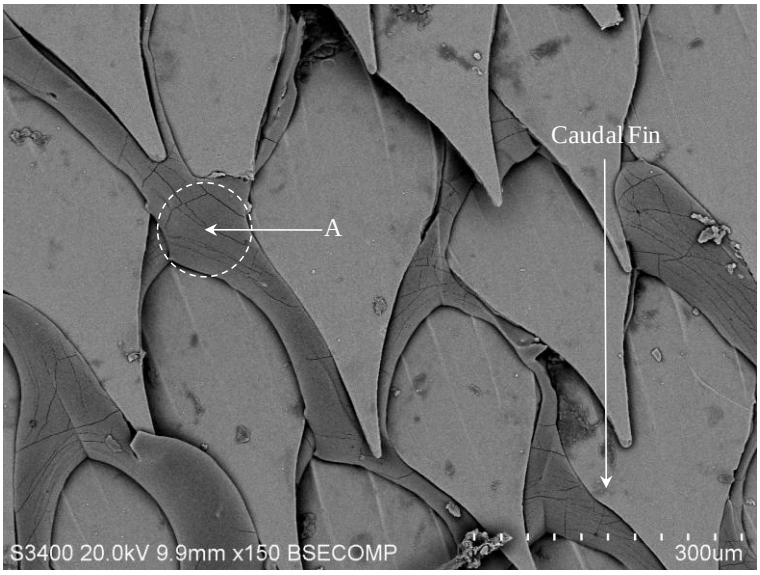

Figure 3-17: Scanning electron micrograph of cured PDMSe retained within the natural sharkskin surface used to produce the negative template for artificial skin fabrication (A).

Areas of the skin of *S. canicula* with larger dermal denticles exhibiting less overlap were more easily replicated and were reproduced exactly (Figure 3-18).

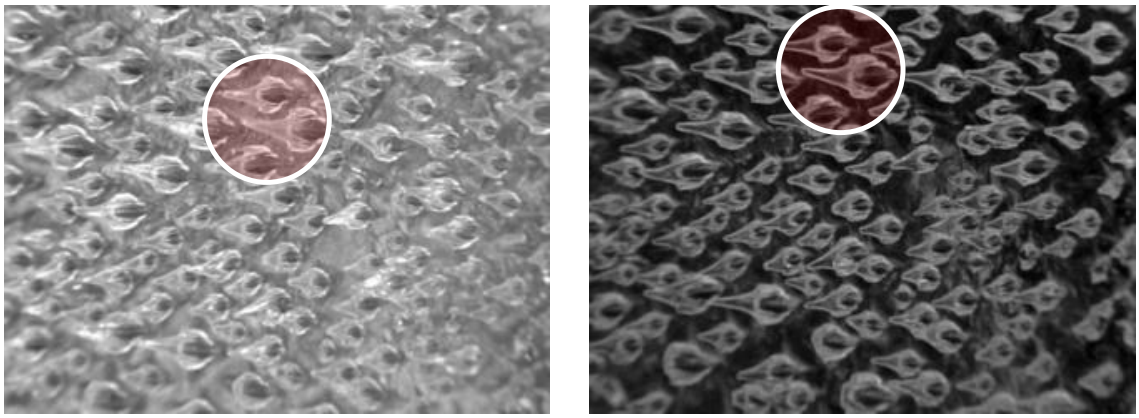

Figure 3-18: Digital images (mag. x 400) of natural sharkskin (left) and epoxy replicate of the same surface (right) created using real skin surface as a negative template for creating a mould. The circled area represents the same dermal denticle as imaged on both surfaces.

Figure 3-19 illustrates artificial skin reproduced in both epoxy and PDMSe where the detail and accuracy provided by the casting process is visible if dermal denticles do not overlap.

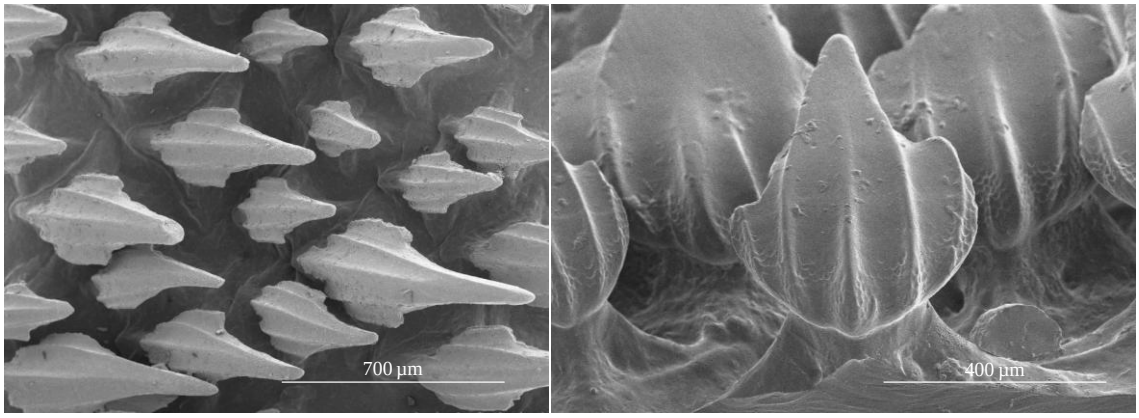

Figure 3-19: Scanning electron micrographs of dermal denticles from the anterior of S. canicula reproduced in epoxy (left) and PDMSe (right).

A comparison of artificial skin reproduced from both areas with large overlap and from areas exhibiting large individual dermal denticles is shown in Figure 3-20 where cross-sections through the reproduced demonstrate the surface texture produced.

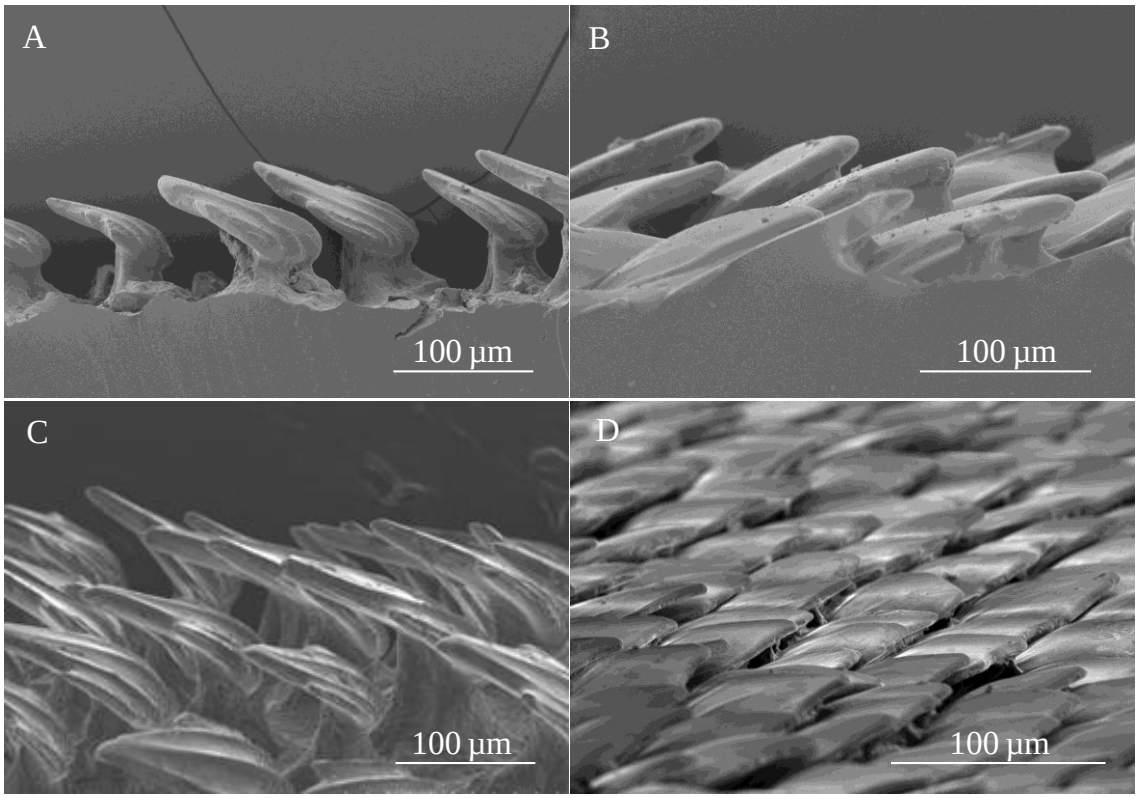

Figure 3-20: Scanning electron micrographs of cross-sections through the artificial skin surface at the 1st dorsal fin (A and C) showing PDMSe replicate (A) and real surface (C) and PDMSe replicate at the caudal fin (B) and real surface (D).(Scale bar = 100 µm).

3.3.8 *Biofouling of synthetic sharkskin*

Biofouling of synthetic sharkskin was assessed at two sites, the North and South Basins of Lough Hyne Marine Reserve as shown in Chapter 2, Section 2.2.3. These two test sites were chosen based on known hydrodynamic conditions at each location. The South Basin is a high-energy environment with full exposure to tidal flow in excess of 3 ms^{-1}; while the North Basin is a low energy environment with negligible current. Both sites had full light exposure and were exposed at a depth of 1 m in open water to minimise disturbance from wave action.

Assessment of the extent of surface biofouling during field or laboratory trials of novel materials is usually carried out by colorimetric, gravimetric, visual or biochemical tests (carbohydrate, protein, uronic acid, DNA); or by laboratory based single cell assays. These tests are routinely carried out on materials with a known surface area, while few methods have been developed for the analysis of topographically complex surfaces. Due to the unique nature of the surfaces generated in this study, established methodologies for assessment of biofouling were not possible. In view of this, microscopy visualisation coupled with mass changes of materials were used a means of biofouling assessment on synthetic sharkskin.

Synthetic skin produced with smaller dermal denticles had a measured reduction in accumulated mass after 14 d immersion compared with artificial skin with larger, non-interlocking dermal denticles. The effect of hydrodynamic conditions was also examined although no clear correlation between mass increase and flow rate could be measured in this experiment. The results of measurement of change mass of the samples is shown in Figure 3-21.

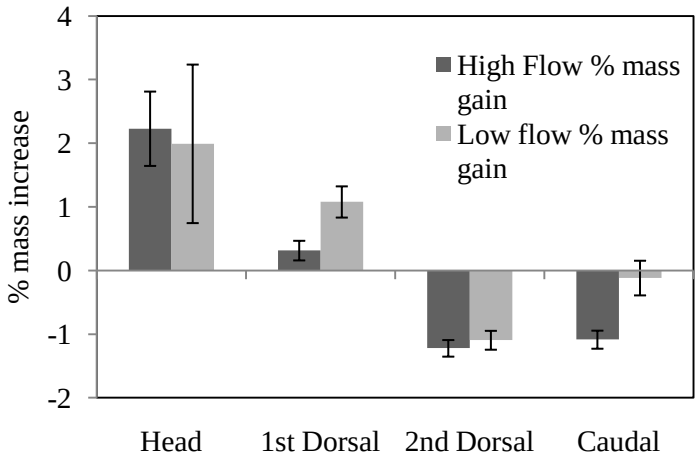

Figure 3-21: Graph of percentage mass increase associated with artificial skinskin reproduced from various locations on the shark body. The mass changes are normalised to the mass change of a smooth surface exposed at the same time. Artificial skin produced from templates of the dorsal and caudal fins show reduced mass increase when compared to a smooth control at high flow rates.

Table 3-2 summaries the results obtained from ANOVA of mass changes associated with artificial skin produced from four locations on the shark body. A significant difference in mass change was measured between artificial skin produced using negatives templates of skin produced at the caudal fin and between artificial sharkskin produced from the head of *S. canicula.*

Table 3-2: ANOVA results generated from comparison of the data on mass gain of artificial skin replicates at locations on the body of S. canicula

Mass change	Sum of Squares	df	Mean Square	F	Sig.
Between Groups	36.243	3	12.081	8.089	.001
Within Groups	29.871	20	1.494		
Total	66.114	23			

Scanning electron micrographs of cross sections through artificial skin of both types indicated that surfaces with larger dermal denticles accumulated greater debris between and underneath the dermal denticles present. This is likely related to the isolated nature of individual dermal denticles promoting greater sedimentation in the larger spaces beneath such structures. Artificial skin with smaller, interlocking denticles had a higher degree of overlap which may have resulted in reduced accumulation of sediment and

explain the reduced mass associated with these surfaces. However, such surfaces also had measurably less mass increase compared with that of smooth controls, an increase that remains unexplained by increased sedimentation rates and debris entrapment with denticles.

Synthetic sharkskin exposed in a high energy environment exhibited the same overall trend as samples exposed in the low energy environment, namely greater mass increases on surfaces with larger mean dermal denticle sizing and less interlocking as seen at head and 1st dorsal fin locations. Mass change in synthetic skin when exposed to high flow was less than that experienced by a smooth surface under the same conditions, indicating that dermal denticle configuration and spacing may have a role either in increased fouling release or perhaps reduced adhesion of contamination and biofouling.

A distinct difference in diatom attachment was observed between natural sharkskin and artificial sharkskin. Dermal denticles examined on the skin of *S. canicula* had few diatom frustules present while exposed artificial skin was heavily colonised by diatoms. Small benthic diatoms of genus *Cocconeis*, *Nitschia* and *Navicula* were prevalent on surfaces, and planktonic species including *Paralia* and *Minidiscus* were found in debris agglomerates under denticles. Larger denticles with less dense packing provide a greater illuminated surface area and more refuge from shear forces for diatom cells and may explain the greater diatom colonisation of these surfaces.

However, the fact that natural dermal denticles and synthetic sharkskin had differing degrees of diatom colonisation indicates a fundamental difference in the reaction of biofouling to these surfaces. Natural sharkskin must contain further mechanisms to colonisation not contained in synthetic skin. It can be speculated that this is related to self cleaning of denticles through mechanical contact as evidenced by the presence of mechanical damage on the surface of natural denticles. Differences in hydrodynamic regimes between the two surfaces or the presence of a specific commensal bacterial community on the shark surface may also have a role. Lastly, PDMSe is a hydrophobic, elastomeric material (Young's Modulus = 1.84 MPa at 23 °C) very different to the chemical nature of natural sharkskin and furthermore algae have been demonstrated to adhere particularly well to this material. Therefore fundamental differences in surface chemistry and flow over such surfaces may also have some role in the observed differences in diatom adhesion on each surface type. Figure 3-22 is an example of an electron micrograph of a cross section through elastomeric artificial skin. Microalgae

and debris fouling of the synthetic PDMSe sharkskin are evident. Diatom species belonging to the genus *Cocconeis* were particularly prevalent on dorsal surfaces of the synthetic denticles.

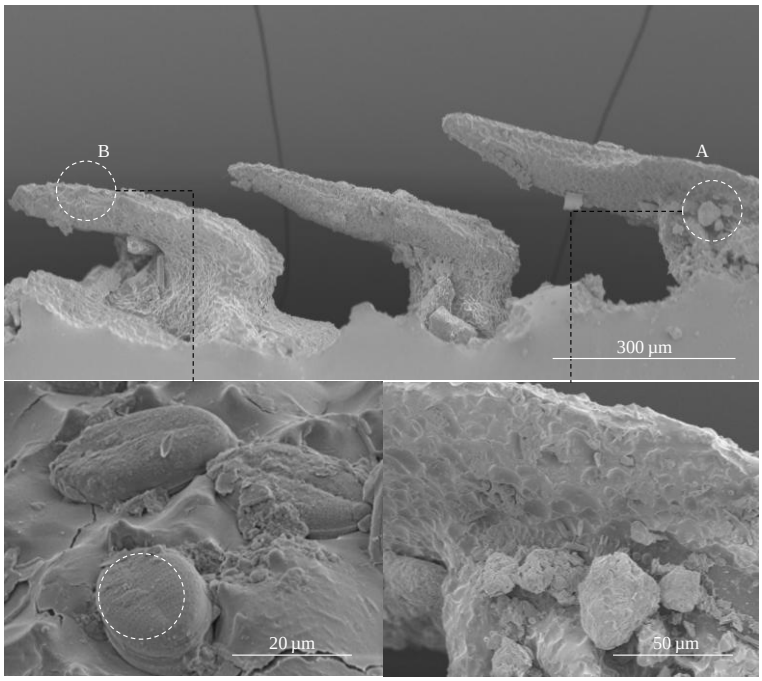

Figure 3-22: Scanning electron micrographs of a cross section through field deployed synthetic PDMSe sharkskin. A = diatom biofouling of the surface, while B = accumulated debris on the ventral surface of synthetic denticles.

Attempts were made to observe flow patterns over both real and synthetic sharkskin at different locations using hydrogen bubble flow visualisation as per other studies on riblet hydrodynamics [44]. However, little additional information could be gained on the hydrodynamics of fluid flow over the surface due the small dimensions of the dermal denticles and limited camera resolution of the available equipment.

3.3.9 *Modelling of denticle structure*

A final observation of this study is that data provided here can be utilised to produce a model suitable for computational fluid dynamics (CFD) modelling hydrodynamic conditions created by dermal denticles of *S. canicula*. Dermal denticles are rigid structures, albeit with a certain degree of flexibility of movement in relation to the skin surface caused by a unique pivotal attachment system. This may have fundamentally different influences on hydrodynamics at the dermal denticle surface that would require complex fabrication methods to reproduce in synthetic surfaces.

A model such as this will provide additional information on shear forces present over the dorsal surface of dermal denticles and may provide insight into whether such forces are sufficient to remove attached microorganisms. Figure 3-23 illustrates initial progress towards this objective in which a model of an individual dermal denticle has been created.

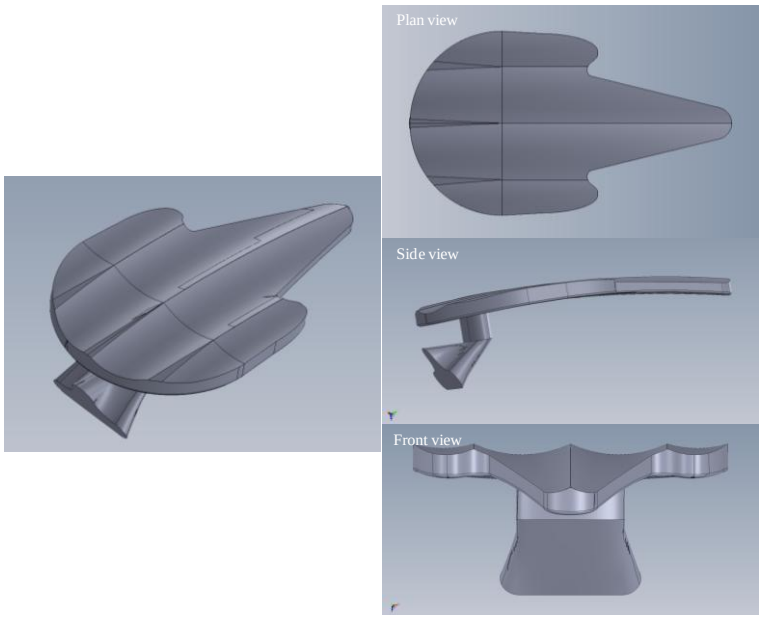

Figure 3-23: Digital images of a model dermal denticle created in Solidworks CAD software. The model was created by Patrick Rowesome of the Energy And Environmental Flow Modelling Group at DCU using the dimensions of dermal denticles measured in this study.

3.4 **Conclusions**

The aim of this work has been to examine dermal denticles of natural sharkskin for physical mechanisms epibiosis prevention and reduction. Few previous reports are available on the extent of microbial colonisation on either natural sharkskin or synthetic sharkskin. This work has demonstrated for the first time that dorsal and ventral surfaces of dermal denticles isolated from *Scyliorhinus canicula* exhibit extensive microbial biofilms. This colonisation varies between these two surfaces and the dorsal surface has less colonisation, perhaps resulting from greater exposure to higher hydrodynamic shear forces. This study has also examined variability in morphology of dermal denticles of *S. canicula* and has demonstrated that dermal denticles of this species retain many structural similarities to dermal denticles of other species reported in the literature.

This study has also produced synthetic sharkskin surfaces with dermal denticles in PDMSe using simple fabrication methods. It has been demonstrated that natural sharkskin can be used as a negative template for production of artificial sharkskin over limited surface areas. Assessment of biofouling on artificial sharkskin exhibiting dermal denticle indicated these surfaces may have some role in reducing biological growth. However, the effect seen is minimal and results are complicated by both the available area of synthetic sharkskin available at present and lack of suitable assays to assess microbial growth on topographically complex surfaces.

The presence of linear topographic grooves on the dorsal surface of denticles also indicates that mechanical abrasion may have a role in removal of attached organisms. Behavioural traits of the species, contact with the environment or contact between dermal denticles during swimming motion may cause these features. While physical mechanisms of epibiosis reduction or prevention are not conclusively eliminated in *S. canicula,* any effects are weak in nature and perhaps supplemented by chemical means.

3.5 **References**

1 K. Efimenko, J. Finlay, M. E. Callow, J. A. Callow and J. Genzer, *ACS Appl. Mater. Interfaces,* 2009, **1**, 1031-1040.

2 A. J. Scardino, H. Zhang, D. J. Cookson, R. N. Lamb and R. d. Nys, *Biofouling,* 2009, **25**, 757-767.

3 A. J. Scardino, D. Hudleston, Z. Peng, N. A. Paul and R. de Nys, *Biofouling,* 2009, **25**, 83-93.

4 M. L. Carman, T. G. Estes, A. W. Feinberg, J. F. Schumacher, W. Wilkerson, L. H. Wilson, M. E. Callow, J. A. Callow and A. B. Brennan, *Biofouling,* 2006, **22**, 11-21.

5 J. F. Schumacher, M. L. Carman, T. G. Estes, A. W. Feinberg, L. H. Wilson, M. E. Callow, J. A. Callow, J. A. Finlay and A. B. Brennan, *Biofouling,* 2007, **23**, 55-62.

6 J. F. Schumacher, N. Aldred, M. E. Callow, J. A. Finlay, J. A. Callow, A. S. Clare and A. B. Brennan, *Biofouling,* 2007, **23**, 307-317.

7 K. K. Chung, J. F. Schumacher, E. M. Sampson, R. A. Burne, P. J. Antonelli and A. B. Brennan, *Biointerphases,* 2007, **2**, 89-94.

8 J. F. Schumacher, C. J. Long, M. E. Callow, J. A. Finlay, J. A. Callow and A. B. Brennan, *Langmuir,* 2008, **24**, 4931-4937.

9 S. P. Cooper, J. A. Finlay, G. Cone, M. E. Callow, J. A. Callow and A. B. Brennan, *Biofouling,* 2011, **27**, 881-892.

10 W. Meyer and U. Seegers, *Basics of skin structure and function in elasmobranchs: a review*, Wiley Online Library, 2011.

11 A. J. Scardino and R. de Nys, *Biofouling,* 2011, **27**, 73-86.

12 B. Bhushan, *Phil. Trans. R. Soc. A.*, 2009, **367**, 1445-1486.

13 M. Salta, J. A. Wharton, P. Stoodley, S. P. Dennington, L. R. Goodes, S. Werwinski, U. Mart, R. J. K. Wood and K. R. Stokes, *Phil. Trans. R. Soc. A.*, 2010, **368**, 4729-4754.

14 W. C. Hamlett, *Sharks, skates, and rays: the biology of elasmobranch fishes*, Johns Hopkins University Press, Baltimore, 1999.

15 A. Lang W, P. Motta, P. Hidalgo and M. Westcott, *Bioinspir. Biomim.*, 2008, **3**, 1-9.

16 D. W. Bechert, M. Bartenwerfer, G. Hoppe and W. Reif, *Drag reduction mechanisms derived from shark skin*, American Institute of Aeronautics and Astronautics, Inc., New York, 1986.

17 D. Bechert W., G. Hoppe and W. Reif, *On the drag reduction of the shark skin*, AIAA Shear Flow Control Conference Paper 85-0546, 1985.

18 B. Dean and B. Bhushan, *Phil. Trans. R. Soc. A.*, 2010, **368**, 4775-4806.

19 H. M. Toussaint, *The Fast-Skin™ bodysuit: Hip, hype, but does it reduce drag during front crawl swimming?*, 20th International Symposium on Biomechanics in Sports Swimming, University of Estremadura, Caceres, Spain, 2002.

20 P. Ball, *Nature,* 1999, **400**, 507-509.

21 D. W. Bechert, M. Bruse, W. Hage and R. Meyer, *Naturwissenschaften,* 2000, **87**, 157-171.

22 W. Rasband, *1997–2007. ImageJ*.

23 M. Sun, C. Luo, L. Xu, H. Ji, Q. Ouyang, D. Yu and Y. Chen, *Langmuir*, 2005, **21**, 8978-8981.

24 D. Sims, J. Nash and D. Morritt, *Mar. Biol.,* 2001, **139**, 1165-1175.

25 W. Raschi and C. Tabit, *Aust. J. Mar. Freshwater Res.,* 1992, **43**, 123-147.

26 W. E. Reif, *Courier Forschungsinstitut Senckenberg,* 1985, **78**, 1-255.

27 J. R. Ellis and S. E. Shackley, *J. Fish Biol.,* 1997, **51**, 361-372.

28 R. M. N. Alexander, *The chordates*, Cambridge University Press, London, 1981.

29 N. A. Curtin and R. C. Woledge, *J. Exp. Biol.,* 1988, **140**, 187–197.

30 T. Miyake, J. L. Vaglia, L. H. Taylor and B. K. Hall, *J. Morphol.,* 1999, **241**, 61-81.

31 E. J. Southall and D. W. Sims, *Proc. R. Soc. B,* 2003, **270**, S47-S49.

32 A. V. Bers and M. Wahl, *Biofouling,* 2004, **20**, 43-51.

33 W. Raschi and J. Elsom, *Comments on the structure and development of the drag reduction-type placoid scale*, Ichthyological Society of Japan, Tokyo, 1986.

34 K. S. Moore, S. Wehrli, H. Roder, M. Rogers, J. N. Forrest, D. McCrimmon and M. Zasloff, *Proc. Natl. Acad. Sci. U. S. A.,* 1993, **90**, 1354-1358.

35 A. C. Henderson and J. J. Dunne, *The Irish Naturalists' Journal,* 1998, **26**, 104-107.

36 J. C. Thomason, J. Davenport and A. Rogerson, *J. Mar. Biol. Assoc. UK,* 1994, **74**, 823-836.

37 J. C. Thomason, S. J. Marrs and J. Davenport, *J. Mar. Biol. Assoc. UK,* 1996, **76**, 777-792.

38 M. Zasloff, A. P. Adams, B. Beckerman, A. Campbell, Z. Han, E. Luijten, I. Meza, J. Julander, A. Mishra and W. Qu, *PNAS,* 2011, **108**, 15978-15983.

39 R. W. Horsley, *J. Fish Biol.,* 1977, **10**, 529-553.

40 D. J. Grimes, J. Stemmler, H. Hada, E. B. May, D. Maneval, F. M. Hetrick, R. T. Jones, M. Stoskopf and R. R. Colwell, *Microb. Ecol.*, 1984, **10**, 271-282.

41 S. Bertone, C. Gili, A. Moizo and L. Calegari, *J. Fish Dis.*, 1996, **19**, 429-434.

42 J. R. Anderson, D. T. Chiu, R. J. Jackman, O. Cherniavskaya, J. C. McDonald, H. Wu, S. H. Whitesides and G. M. Whitesides, *Anal. Chem.*, 2000, **72**, 3158-3164.

43 X. M. Zhao, Y. Xia and G. M. Whitesides, *J. Mater. Chem.*, 1997, **7**, 1069-1074.

44 J. Wang, S. Lan and G. Chen, *Fluid Dyn. Res.*, 2000, **27**, 217-229.

4 Investigation of Surface Texture from Marine Decapod Crustaceans for Prevention of Epibiosis and Biofouling

4.1 **Introduction**

The surface texture profile of natural surfaces from the marine environment such as the periostracum of bivalve molluscs and the skin of the pilot whale have been demonstrated to have anti-settlement properties against epiphytes [1-4]. Meanwhile, the surface topography of others such as tropical sea stars has been discounted from having any role in protection of the surface from epibiosis [5]. Thus, the role of surface texture in protecting many marine species epibiosis is still unclear.

Crustaceans (Crustacea) are a large group of both marine and land-dwelling arthropods, characterised by the presence of a hard protective shell or exoskeleton. Colonisation of the outer layer of the exoskeleton, known as the epicuticle, may be advantageous for epibionts in the marine environment because the movement and feeding activities of large crustaceans will guarantee the arrival of food. However, colonisation by epibionts may negatively affect the health and survival rates of the host organism (basibiont) [6, 7]. Therefore, crustaceans are likely to have developed a number of mechanisms to reduce or prevent such settlement. Thus, members of this group are among the marine organisms currently under examination for epibiosis prevention mechanisms with the aim of utilising analogous mechanisms in non-toxic biomimetic AF strategies for synthetic surfaces [8-11]. There are reports that specific crustacean species such as *Cancer pagurus* (Class: Malacostraca, Order: Decapoda, Infraorder: Brachyura, Family: Cancridae), possess anti-settlement defences against epibiontic organisms [12]. These defences have been related to the topographic profile of the exoskeleton; however, the mechanisms by which surface texture can prevent epibiontic colonisation are unclear. Few data exist on whether trends in the surface profile of crustacean species are specific to individual species or if similarities in the topographic nature of the crustacean carapace exist independent of individual species.

4.1.1 *The exoskeleton of Cancer pagurus*

The crustacean exoskeleton (also referred to as an integument) is recognised as having remarkable mechanical properties of strength and flexibility [13]. These properties result from the composition and structure of the exoskeleton, which is composed of a nanocomposite organic matrix combined with an inorganic mineral [14]. The exoskeleton of *Cancer pagurus* is a heavily biomineralised structure consisting of varying amounts of chitin (15–40%) and proteins (20–40%), combined with $CaCO_3$ (20–50%) as an

inorganic strengthening mineral [15]. The exoskeleton of this species is shown in Figure 4-1, including individuals exhibiting limited epibiosis.

Figure 4-1: Digital images of Cancer pagurus. Carapaces of healthy individuals (A) often remain relatively free from epibionts. Some species such as polychaete worms (B, circled) and cirriped species (C, circled) are known epibionts of C. pagurus. Note that epibiosis primarily occurs along edges of the carapace (arrowed, C)

The exoskeleton is heterogeneous in both chemical composition and structure. Four discrete layers are usually present, an epicuticle, exocuticle, endocuticle and an innermost membranous layer. The first three layers of this exoskeleton are heavily calcified, with calcite crystals and amorphous $CaCO_3$, while the outer epicuticle is a thin waxy layer providing a permeable barrier to the external environment [15]. Epibiosis occurs on the epicuticle which consists of tanned lipoproteins impregnated with calcium salts, and possible trace amounts of chitin and lamellar organisation [15]. There is still however some debate over the composition of the epicuticle and the reliability of the histochemical techniques that have been utilised to determine the lack of chitin in this layer are questioned [16]. Therefore, the chemical composition may vary between species and within individuals of the same species.

4.1.2 *The exoskeleton of Homarus gammarus*

The European lobster, *Homarus gammarus* is a common crustacean species with an overlapping habitat range to that of *C. pagurus* [17]. While there are limited reports of the epibiont community associated with both the embryos and adults of the American lobster, *Homarus americanus* [18], there are no detailed published reports to the author's knowledge concerning the epibiont community associated with *H. gammarus*. Additionally, few data are available on the surface texture of this species and the topographic profile of this species has not been previously examined for epibiosis prevention mechanisms. A digital image of *H. gammarus* is shown in Figure 4-2 where the different areas of the exoskeleton are labelled.

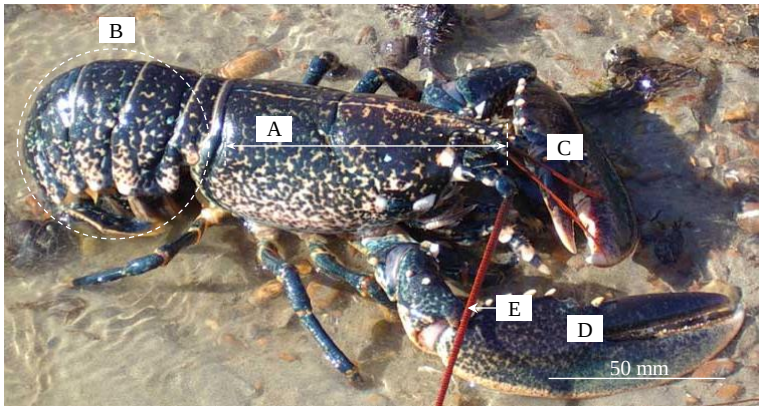

Figure 4-2: Digital image of the European Lobster, Homarus gammarus. A = carapace, B = tail and abdomen, C= crusher claw, D = pincher claw, D = antennae.

While moulting of the exoskeleton is responsible for periodic removal of epibionts, the inter-moult stage of many marine decapod crustaceans is considered to be of sufficient duration for a substantial epibiont community to develop [19]. Periods between moults can be several months in duration for adult decapods, particularly during periods of poor food supply or low temperature [20]. It has been suggested that crustaceans with longer inter-moult duration (i.e. older individuals or ovigerous females) host more epibionts than those with shorter inter-moult periods; however, reports are not conclusive on this [21]. Also, while moulting of the exoskeleton has a role in removing established epibionts; it is unclear if mechanisms of preventing larval or propagule settlement and adhesion to the epicuticle exist among crustacean species.

Chitin, a major component of the exoskeleton (the chemical structure of which is shown in Figure 4-3), is reported to possess some antimicrobial properties, especially when deacetylated to chitosan [22]. The exo- and endocuticular layers contain varying amounts of chitin, which is used as a support mucopolysaccaride. Chitosan is a static or cidal agent of microbial growth and has been shown to have antifungal properties against plant pathogenic fungi such as *Fusarium solani* [23]. However, chitin is not found in pure form in the exoskeleton of crustaceans and is reported to be always associated with proteins, although the exact nature and form of protein association has not been firmly established [16].

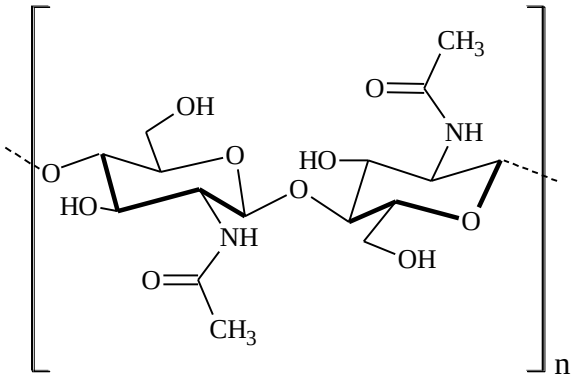

Figure 4-3: Chemical structure of chitin, the second most abundant nitrogen-bearing biopolymer in nature, and a major constituent of crustacean exoskeletons.

Aside from the reported antimicrobial activity of chitin, it is also reported that specific crustacean species possess antimicrobial peptides (AMPs) in the bloodstream that have

a broad range of activity against both Gram-positive and Gram-negative bacteria [24]. Of these, penaeidins, a family of AMPs isolated from the hemolymph of shrimps *Penaeus vannamei*, are reported as particularly effective against both fungi and bacteria, and especially Gram-positive bacteria [25]. However, while these peptides have potent fungicidal activity against filamentous fungi, they are inactive against yeasts such as *Candida albicans* or *Saccharomyces cerevisiae* [26]. Nonetheless while AMPs in the hemolymph and hemocytes of crustaceans are active in preventing or reducing infection, it is unclear if AMPs can have any role in prevention of epibiosis at this stage.

4.1.4 *Physical mechanisms of defence against epibiosis in decapod crustaceans*

Extensive epibiont colonisation of the crustacean exoskeleton may negatively affect the survival and health of the host organism (basibiont) [7]. Therefore, a number of alternate strategies to chemical means of controlling epibiont colonisation have developed among crustaceans. Complex behavioural patterns such as burrowing, avoidance of light and grooming appendages on many decapod crustaceans are reported as being involved in reducing epibiosis [20]. Grooming, the physical removal of epibionts using specialised setal brushes and combs, has been reported for a number of species, especially from chemosensory appendages. The morphology of the grooming limbs has been examined in detail for several species [27]. However, as pointed out by Bauer [20], many decapod species that do not appear to have general body grooming specialisations are nonetheless clean. Thus, other mechanisms other than grooming may be utilised to prevent epibiosis.

Physical defences may also include surface texture. Indeed topographic texture specific to the exoskeleton of some crustacean species have been reported to have some AF ability, mainly acting as anti-settlement cues for marine macrofouling organisms such as barnacles and macro-algal spores [12, 28]. In work by Bers and Wahl, comparison of the macrofouling rates of epoxy replicas of the exoskeleton of *C. pagurus* with smooth epoxy control surfaces indicates that a decrease in macrofouling organism recruitment to the surface occurs due to the topographic nature of the surface [12]. Other crustacean carapaces have not been examined in detail for mechanisms of defence against epibiosis. Therefore, a comparison of epibiosis and biofouling of epoxy replicates of the epicuticle of several species is required to understand if this effect is unique to *C. pagurus*. The micro-topographic structures reported for *C. pagurus* are also poorly

described, and the morphology of the structures is relatively unknown. Furthermore, the effects of the presence of such structures on microfouling community development on the carapace of *C. pagurus* are unknown.

4.2 **Aims and objectives**

The aim of this chapter is to characterise mechanisms of epibiosis reduction or prevention utilised by marine crustacean species.

The objectives of this work are to:

(1) Investigate the epicuticle surface texture of two crustacean species, *C. pagurus* and *H. gammarus* in detail, and assess these properties for prevention of epibiosis.

(2) Compare the surface texture from each species and determine if similarities exist in surface texture, dimensions and orientation.

(3) Produce artificial materials exhibiting an identical surface texture to *C. pagurus* and *H. gammarus* and examine the formation of microfouling communities on these materials.

(4) Determine if a unique microfouling layer associates with each surface type and the extent to which this influences the overall biofouling of the surface.

4.3 **Materials and Methods**

Inter-moult individuals of *C. pagurus* (carapace length, 140 – 200 mm) and *H. gammarus* (carapace length, 200 – 300 mm) were collected from local fishermen at Barlogue Creek, Cork, captured using crab pots. Captured individuals were examined for macrofouling and diseased individuals exhibiting any evidence of shell necrosis were discarded. Six specimens were killed by deep freezing (-15 °C) as per Becker and co-workers [9] to prevent alteration of the surface structure.

4.3.1 *Characterisation of the exoskeleton morphology*

Sections from different areas of the exoskeleton were divided into sections approximately 1 cm^2, and were prepared for SEM as described in Chapter 2, Section 2.2.12.

4.3.2 *Energy dispersive X-ray Spectroscopy (EDS-SEM)*

EDS-SEM elemental analysis of the exoskeleton of *C. pagurus* was conducted using a Hitachi S3400 SEM, Oxford PentaFet EDS detector, and INCA suite software version 4.12. Operating conditions included a probe current of 50 mA and an accelerating voltage of 25 keV. Samples were prepared for EDS-SEM by mounting air-dried samples that had been rinsed in de-ionised water (18 Ω milli-Q) to remove salt crystals; on 15 mm diameter aluminium stubs using double adhesive carbon tabs and carbon sputter coated (Agar Auto carbon coater, Agar Scientific). EDS software was calibrated to a cobalt reference standard for quantitative analysis.

4.3.3 *Wettability measurement*

Wettability of the carapace was analysed by measurement of the static contact angle of a droplet of ultrapure water (5 µL) on sections of carapace from both species as described in Chapter 2.

4.3.4 *Production of artificial carapaces*

Nine sections of artificial exoskeleton were produced in epoxy resin using the methodology shown in Figure 4-4. Surfaces were rinsed with de-ionised water and

gently scrubbed with a fine toothbrush to remove as much biofilm as possible. SEM evaluation of the surface before and after such treatment revealed negligible effects of this treatment on the surface topography of the samples; provided a soft brush with little applied force was used. For experiments on exoskeletons lacking an intact textured epicuticle, the surface was abraded using P600 grade "wet and dry" sandpaper while wet. Exoskeletal sections were carefully rinsed with de-ionised water to remove any adhered particles and surface contamination prior deployment in field trials. A schematic overview of the production and testing process is shown in Figure 4-4.

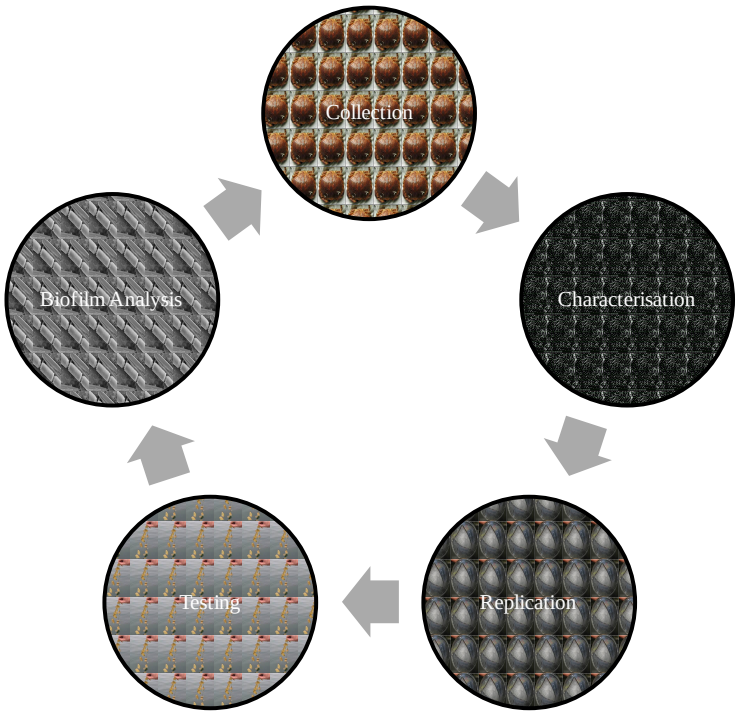

Figure 4-4: Schematic of the general production and testing procedure of the synthetic crustacean carapace used in this study.

4.3.5 *Characterisation of microbial growth on exoskeletal sections*

Sections of carapace of both *C. pagurus* and *H. gammarus* and epoxy replicas of both surfaces were simultaneously examined for biofilm growth by immersion in the marine environment. Diatom settlement on each surface type was quantified by examining the orientation and number of diatom frustules present on the epicuticle surface after a 14-d immersion in the South Basin of Lough Hyne Marine Reserve (N51.50061º W009.29802º ± 6 m) (For map of this location see Chapter 2, Section 2.2.3.). A number of methods for securing the synthetic carapace sections for field-testing were attempted, including suspending sections on rope and stainless steel. Samples of both the real

carapace of each species and artificial replicas were finally adhered poly(methylmethacrylate) disks using silicone adhesive. Upon removal, samples were preserved (2.5% (v/v) gluteraldehyde, Sigma-Aldrich, Tallaght, Dublin) and placed in sterile centrifuge tubes and transported to back to the laboratory for analysis. Samples were prepared for SEM using the same techniques as described in Chapter 2 Section 2.2.12.

4.3.6 *Enumeration of diatom frustules*

Intact diatom frustules present on both natural and artificial carapace sections were counted and identified with SEM (x 600 magnification) using a secondary electron (SE) detector. A working distance (WD) of 10 mm for 15 random fields of view (RFOV) from 6 replicate surfaces, with no applied tilt and rotation was used. Only the central 1 cm^2 of each sample was imaged to avoid edge effects on microbial recruitment to surfaces. The resulting images were then processed with ImageJ software [29] and gridlines were constructed to give 10,000 μm^2 area grids based on the embedded scale bar within each image. Total visible intact diatom frustules were then enumerated within each grid and multiplied to give frustule abundance (frustules mm^{-2}).

4.3.7 *Visualisation of Diatom settlement of carapaces*

Visualisation of settlement distribution of benthic diatoms over a larger area than that of a single SEM image was accomplished by taking 100 individual Scanning electron micrographs (x 750 magnification). These were acquired in a raster grid pattern of 10 x 10 images and combined to create an image montage. Individual images were gridded into 4 sections and intact diatom frustules were counted within each quadrant. Visualisation of the distribution of frustules was accomplished by applying a colour hue to individual images based on total frustule counts within that image. An illustration of this process is shown in Figure 4-5.

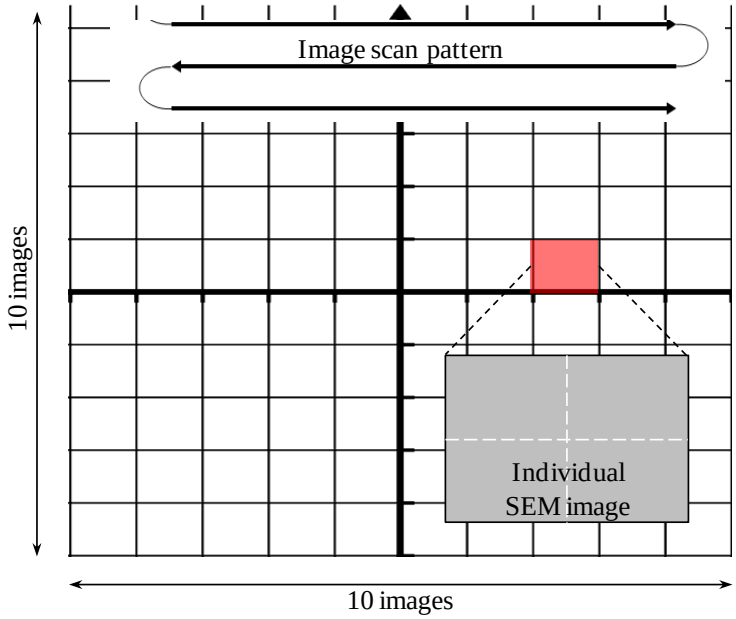

Figure 4-5: Schematic of the methodology for visualisation of spatial distribution of diatom settlement over a large surface area. An image montage consisting of 100 SEM images (mag. x 750) was created using the scanning pattern indicated. Each individual image was divided into 4 quadrants and diatom frustules counted within each quadrant. A colour was then applied that depended upon the frustule abundance within each quadrant.

4.3.8 *Diatom species identification*

To distinguish diatom cell settlement patterns on individual carapace sections and distinguish species type, diatoms were identified to species level wherever possible, and to genus level otherwise using the classification system of Round and co-workers [30].

4.4 **Results and discussion**

The aim of this work was to gain insight into epibiosis prevention or reduction mechanisms utilised by crustaceans. This can then inform development of novel biomimetic AF strategies. Surfaces such as the epicuticle of the crustacean carapace are of particular interest when considered in terms of biomimetic AF; as such surfaces bear closest resemblance to artificial hard surfaces. Surface texture has been reported to influence diatom adhesion to hard natural substrates such as sand particles [31-33], but few data are published on cell anti-settlement mechanisms arising from surface texture of the crustacean epicuticle. Furthermore, few data are available on host-symbiont specificity; i.e. if certain diatom species are associated with the epicuticle of specific crustacean species.

It has previously been reported that "the chitinous skeleton of crustaceans are nutrient surfaces that encourage bacterial attachment and growth and hence undergo extensive colonisation" [34]. However, to the author's knowledge, few studies have reported the effect of commensal bacterial communities on subsequent diatom adhesion to these surfaces. The ecological context and significance of any relationship between bacterial colonisation of the surface and subsequent diatom adhesion has also not been established, despite the fact that diatoms are reported as the dominant micro-algae on copepods and other small crustaceans [10].

4.4.1 *Surface texture of the carapace of C. pagurus*

The surface texture of the examined epicuticle of *C. pagurus* and *H. gammarus* was dissimilar both in dimensions and morphology of the surface features present. However, epicuticles from both species exhibited a distinct microscale surface texture superimposed on a larger macrostructure. The dorsal carapace of *C. pagurus* consisted of a hierarchical microtopography consisting of needle-like microscale features superimposed on larger oval structures elevated above the surrounding epicuticle, with occasional pits containing sensory setae as shown in Figure 4-6.

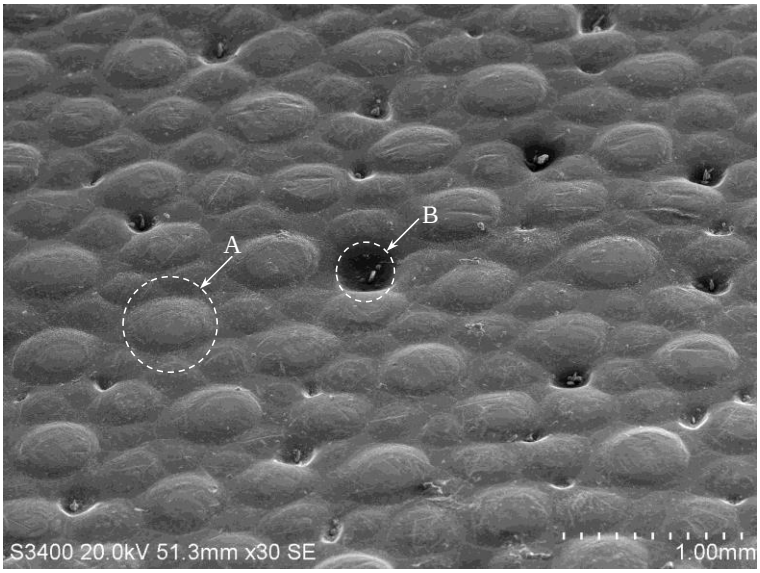

Figure 4-6: A scanning electron micrograph of the microtopographic dorsal carapace surface of C. pagurus. Raised areas are visible (A). Isolated surface pits are visible in carapace surface (B).

Examination of the raised oval features present on the carapace of *C. pagurus* with BSE-SEM to provide elemental contrast indicated that circular sections of the carapace were different in composition to the surrounding epicuticle. This contrast is shown in Figure 4-7.

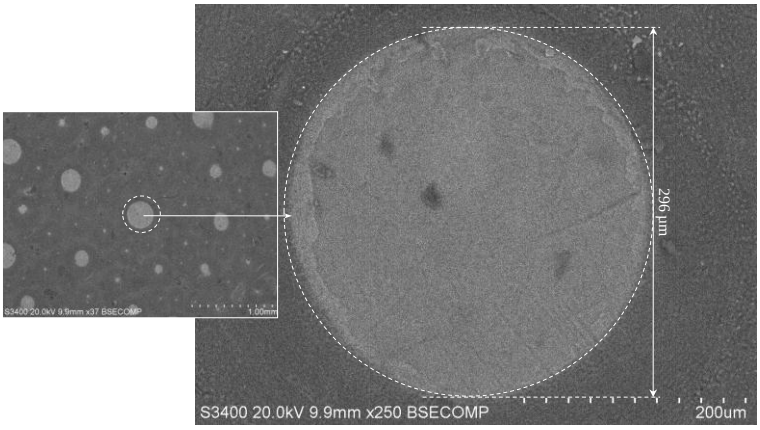

Figure 4-7: BSE scanning electron micrographs taken in compositional mode of elevated areas of the epicuticle of C. pagurus. Areas of lighter colour indicate a concentration of elements of higher atomic number. These structures were present over both the entire dorsal surface of the carapace, however variation in the diameter of these areas occurred (inset).

The dimensions of raised areas of the carapace of *C. pagurus* varied with total width of the carapace from examined individuals. The raised areas were found to have a mean diameter of 475 µm (from an individual of 130 mm total carapace length, total width 85

mm) on a section of exoskeleton removed from the central area of the dorsal carapace (Figure 4-8). However, variation exists in these dimensions, depending on location on the epicuticle, with smaller features towards the edges of the carapace and within damaged areas of the surface.

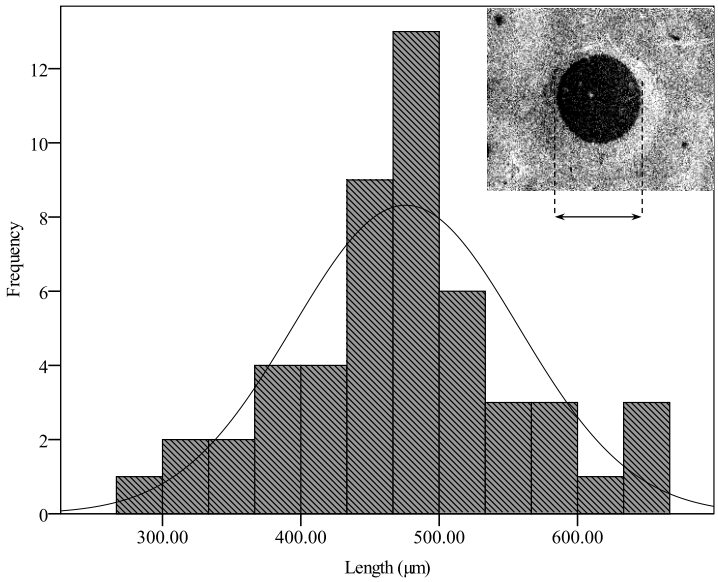

Figure 4-8: Size distribution histogram of the raised features of the epicuticle of C. pagurus as measured using SEM and ImageJ software. An approximate normal distribution of feature size is observed (Mean = 475.80 µm, Standard deviation = 81.538, n =51).

With the exception of the raised sections shown in Figure 4-6, the remaining surface area of the carapace of *C. pagurus* contains microscale needle-shaped structures. These are shown in Figure 4-9. These features have been referred to as spicules in recent publications on *C. pagurus* in AF studies [12] but were previously termed microtrichia in the first published study to examine the epicuticle of *C. pagurus* in detail [35]. To avoid confusion, the term microtrichia will be used in the present study.

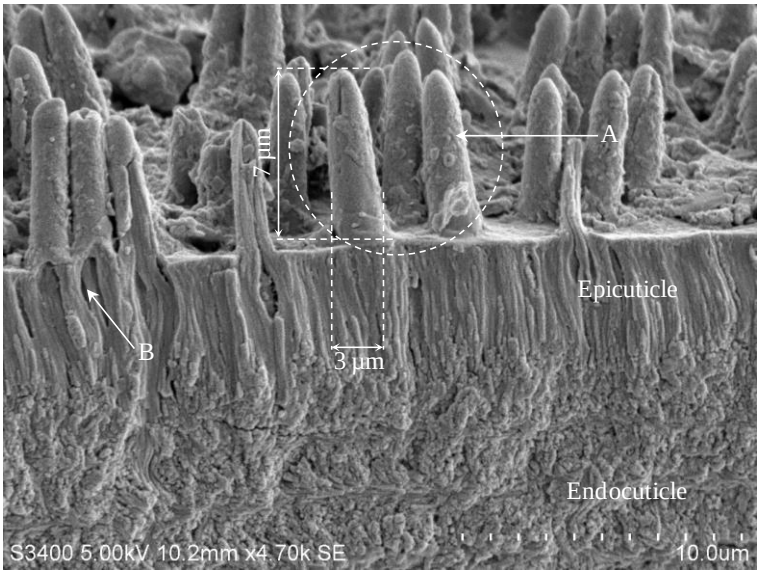

Figure 4-9: Scanning electron micrograph of a vertical cross-section through the carapace of C. pagurus. Microtrichia are visible (A) embedded in the epicuticle and approximate dimensions are indicated. Pore canals leading from the epicuticle into the microtrichia are also visible (B).

In this study, microtrichia were found to be high aspect ratio (approximately 10:1), circular, tapered, rigid structures. In specific areas of the carapace of *C. pagurus* and particularly at the boundary of raised sections of exposed epicuticle, the microtrichia were not perpendicular to the surface. Instead, in these areas the microtrichia curved towards the surface and were often in pairs with adjoining attachment points to the surface. This has not been previously reported for these structures and is shown in Figure 4-10.

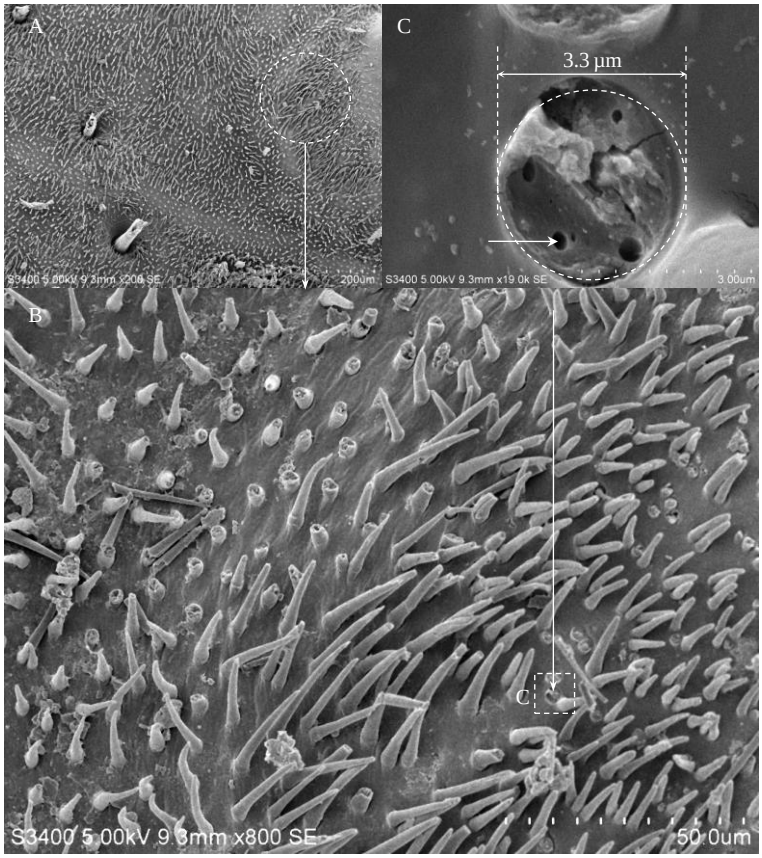

Figure 4-10: A series of scanning electron micrographs showing microtrichia at the boundary between the raised areas of the carapace (A). An enlargement of the highlighted area demonstrates curvature of the microtrichia (B) and damage to individual spicules resulting in visualisation of the pore canals within the base of the microtrichia as described by Hegdahl and co-workers [35] *(C, arrowed).*

The internal structure of microtrichia was revealed in both cross-section and in areas where microtrichia had been removed from the surface of the epicuticle. Circular pore canals connecting individual microtrichia to the endocuticle were visible in Scanning electron micrographs of completely removed microtrichia (Figure 4-10). The function of such pores remains unclear but it has been reported that they most likely have an important role in the transport of calcite to and from the crustacean cuticle [35].

Damaged microtrichia were also evident on the dorsal surface of *C. pagurus*, and only remained intact in depressed areas of the carapace. In contrast, examination of the ventral surface of the exoskeleton of *C. pagurus* revealed a greater abundance of microtrichia, the majority of which were intact. Raised areas of the ventral surface were less prominent on the ventral carapace surface and exposed areas of the epicuticle were smaller in diameter, thus resulting in the greater surface coverage of microtrichia. Figure 4-11 illustrates an area of the epicuticle of *C. pagurus* where the microtrichia have been undergone mechanical damage.

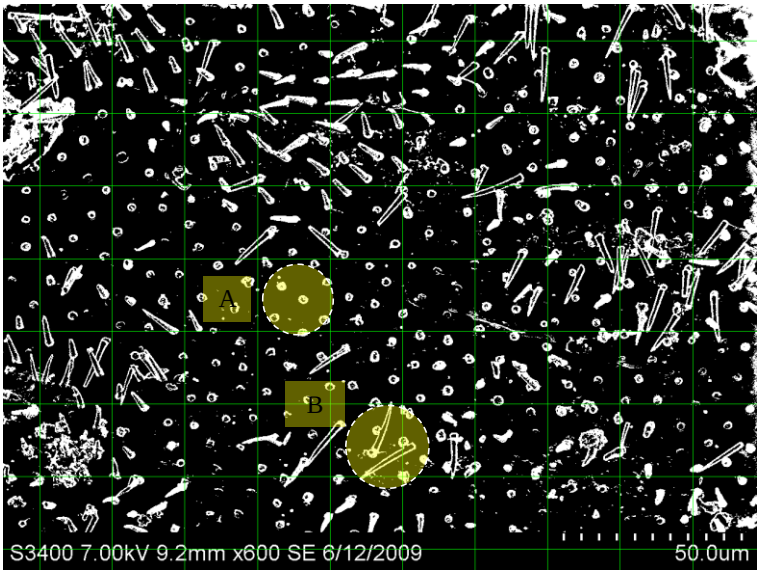

Figure 4-11: A scanning electron micrograph (threshold adjusted in ImageJ) of the dorsal surface of C. pagurus demonstrating damage to microtrichia present (A) microtrichia are missing or broken at the base (B). Examination of the lower carapace surface revealed that the majority of microtrichia were.

To gain insight into the dimensions of the microtrichia on the carapace of *C. pagurus*, the distance between microtrichia and the packing density of these structures was calculated from a number of sections. The results of this analysis are presented in Figure 4-12 and Figure 4-13 where it can be seen the average distance between microtrichia was 8.4 µm and approximately 16 x 10^3 microtrichia cm^{-2}. These dimensions are important for cell settlement as the measured distances will determine the dimensions of cells which can adhere directly to the surface between microtrichia and those that will remain suspended above the surface on microtrichia.

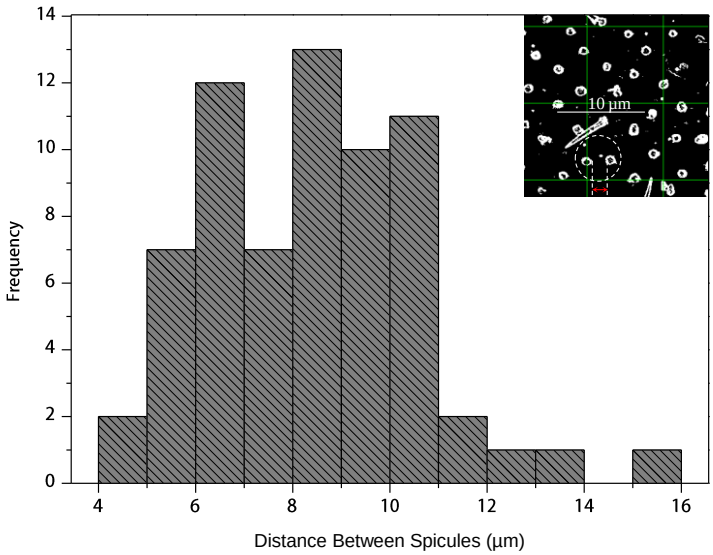

Figure 4-12: Histogram of distances between microtrichia on the surface of C. pagurus. The nearest neighbour distance between each structure has a mean of 8.4 µm ± 2.09 S.D. (n =70).

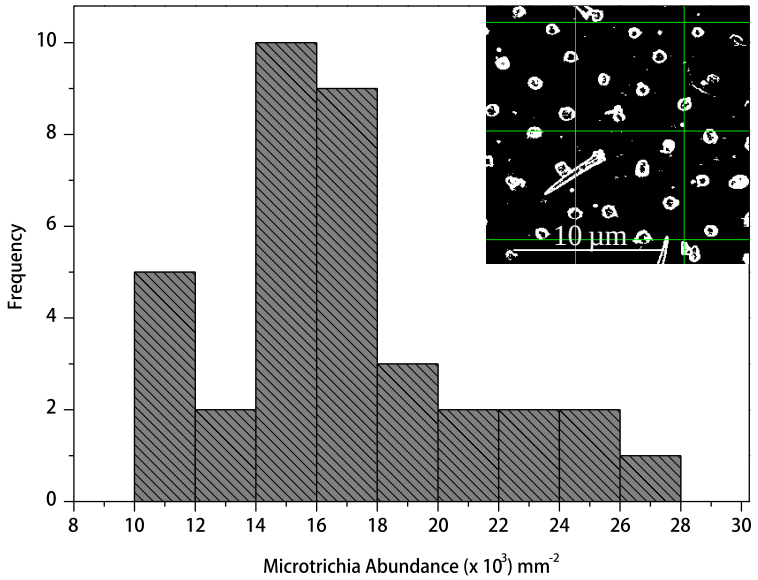

Figure 4-13: Abundance of microtrichia on the surface of C. pagurus (Mean = 8 microtrichia 500 µm^{-2})

A vertical cross section was made through the carapace of *C. pagurus* in order to understand the nature of the internal structure of the carapace and the relationship between external microtopography and internal structure. This indicated that the raised sections of the epicuticle originated from within the endocuticle, the thickest and most heavily calcified area of the cuticle [15]. This is shown in Figure 4-14, where the endocuticle can be observed to protrude through the exocuticle until it exits through the epicuticle.

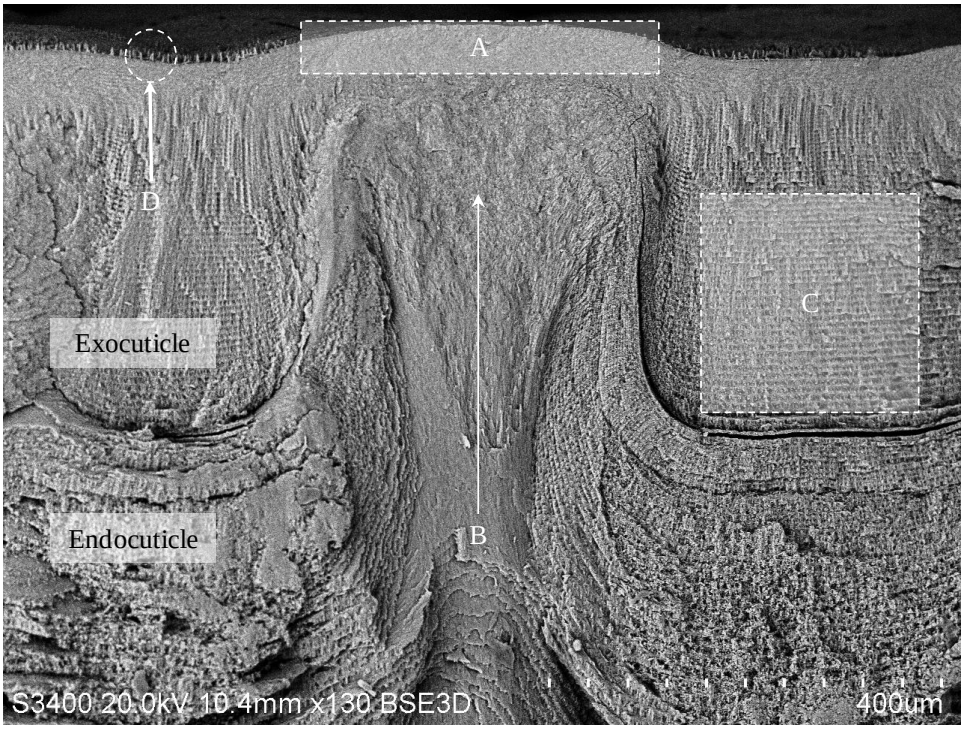

Figure 4-14: A scanning electron micrograph of a vertical cross-section through the carapace of C. pagurus. The structure of the features resulting in raised areas of the carapace with different elemental composition can be visualised (A). Protrusion of the endocuticle through the exo- and epicuticle is responsible for the features observed (B). Note the lamellar structure of the exocuticle (C). Microtrichia are just visible on the surface of the epicuticle (D).

Protrusion of the endocuticle layer through the epicuticle would explain the differences in elemental composition observed in BSE-scanning electron micrographs of the external surface of the epicuticle.

4.4.2 *Surface texture of H. gammarus*

In contrast to *C. pagurus*, the macrotopographic features of the carapace of *H. gammarus* consisted of surface depressions rather than elevated features. This surface structure has not previously been reported or described to the author's knowledge. Surface depressions measured in this study were found to have a variable diameter and often contain sensory setae similar in appearance to those described for *Homarus americanus*. Linear scratches were also present on the surface of *H. gammarus* consistent with mechanical damage to the cuticle, perhaps though contact with rocks and other materials on the seabed during the lifecycle of the organism. An example of the macrotopography of the epicuticle of *H. gammarus* is shown in Figure 4-17.

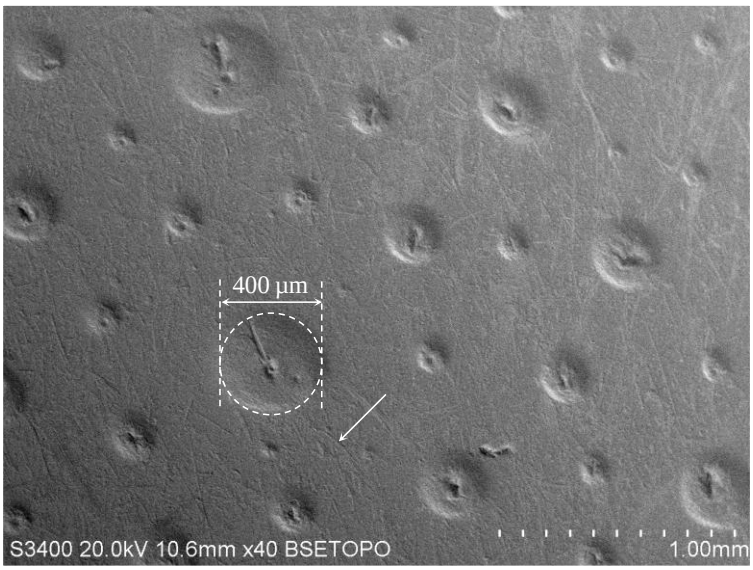

Figure 4-15: Scanning electron micrograph of the macroscale surface texture of H. gammarus showing the surface pits present (mag. x40).Surface scratches from mechanical abrasion are also evident (arrowed).

A number of cross-sections through the carapace of *H. gammarus* were taken in order to measure the approximate depth of the surface depressions. An example of the internal structure of the carapace of *H. gammarus* is shown in Figure 4-16, where the profile of the surface depressions can be observed.

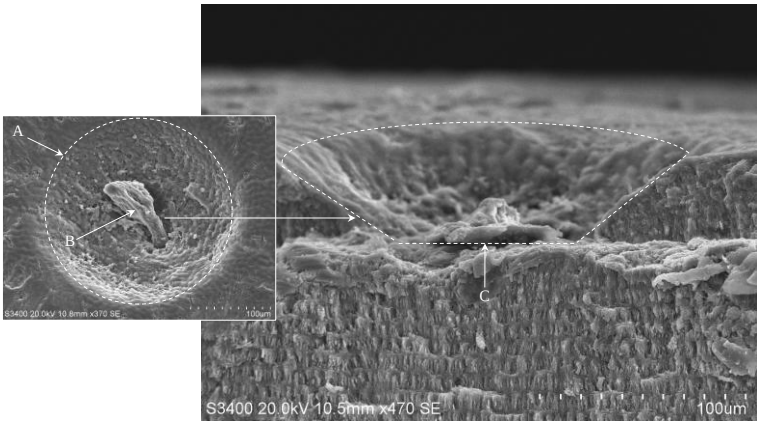

Figure 4-16: Scanning electron micrographs of a surface depression in the carapace of H. gammarus in top view (A, inset) and vertical cross section through the surface of the carapace of H. gammarus. Sensory setae are often present in such pits (B). The depth of each pit is ranges between 30 – 60 µm (C).

Measurement of the diameter indicated a bimodal distribution with larger numbers of smaller depression and another population of larger surface depressions. This distribution is shown in Figure 4-17.

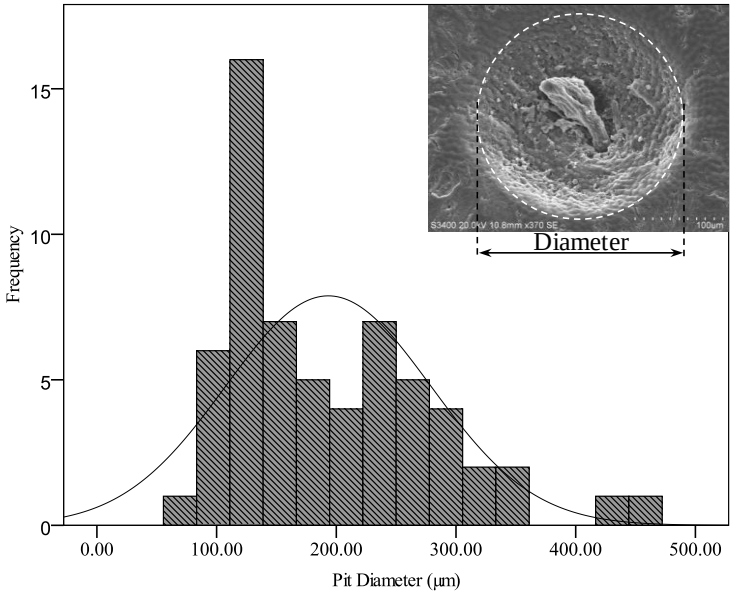

Figure 4-17: Size distribution of the diameter of the surface pitting on a 400 mm total length specimen of H.gammarus.

The microscale surface texture of *H. gammarus* consists of an undulating pattern of repeating surface features. This micro-structure has not been previously reported and the function and nature of the surface are unknown. Analysis of this microtopographic structure on a number of specimens suggested that the amplitude and distance between

these features varied both on the carapace of single specimens of *H. gammarus* and between individuals examined.

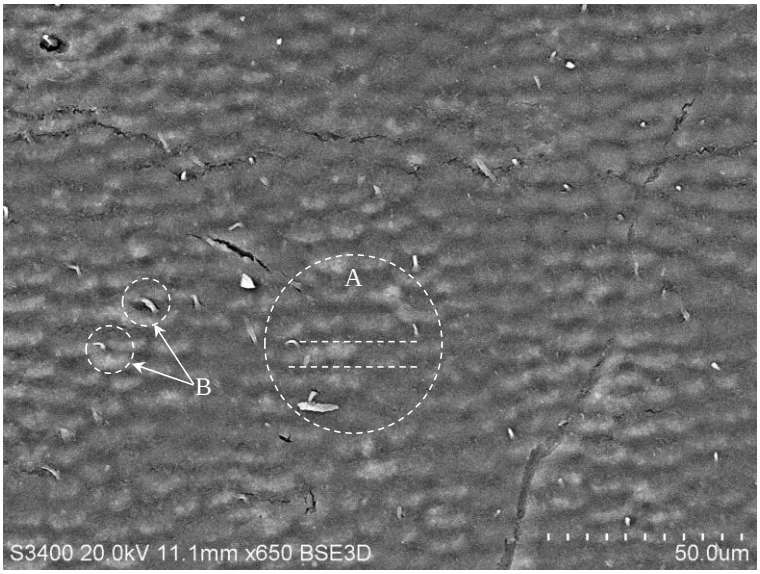

Figure 4-18: Scanning electron micrograph of the micro-rippled structure of the carapace of H. gammarus (circled, A). Small setae are also visible on the surface (B).

Further magnification indicated that the individual features of with this texture exhibited the remains of setae of nanoscale dimensions. These are illustrated in

Figure 4-19: A high-resolution scanning electron micrograph of individual features within the microtexture of H. gammarus, the remains of sensory setae (circled) and the surface nanostructure can be observed.

4.4.3 *Carapace wettability measurements*

Wettability of both natural and artificial surfaces was measured using the sessile drop CA method described previously (Chapter 2, Section 2.2.10.). Of the natural surfaces, the ventral surface of *C. pagurus* exhibited the highest wettability with a mean CA of 10.79 °, while the carapace of *H. gammarus* had a mean CA of 94.6 °. Epoxy replicas of the carapaces were less wettable than the natural surfaces with contact angles ranging from 90 ° - 102 °. The increased wettability of the carapace of *C. pagurus* is likely due to the presence of microtrichia and the described elevated surface features causing droplet spreading, while decreased wettability of *H. gammarus* can be attributed to air entrapped in surface depressions beneath the droplet as described by the Cassie-Baxter wettability model [36]. The presence of polyanionic sites and acid mucopolysaccharides together with calcium in the epicuticle are also likely to increase wettability [9].

Reproducing a similar sessile drop CA method to that used by Becker and co-workers [9] did not result in satisfactory wettability measurements. Frequently sections of both the real and artificial carapaces were not sufficiently flat to give identical contact angles on both left and right sides of sessile droplets as viewed with CA analyser and problems were encountered due to the curvature of the carapace surface. Following the methodology established by Becker and co-workers, measurements were considered for data evaluation if the difference between the right and left angle of the sessile drop did not exceed 5°. This was repeated on 3 separate sections from each of both the natural and artificial carapaces. In addition, analysis of the CA of a sessile drop over time revealed that liquids used in CA measurements were absorbed into the surface with time resulting in an unstable sessile drop CA. The ventral surface of C. pagurus demonstrated the greatest wettability with absorption of the sessile droplet into the porous surface over time. Becker and co-workers reported that certain crustacean species maintain a characteristic carapace surface wettability despite molecular fouling and colonisation processes. The contact angle of both epoxy replicas and the natural surfaces of both *H. gammarus* and *C. pagurus* are shown in Figure 4-20.

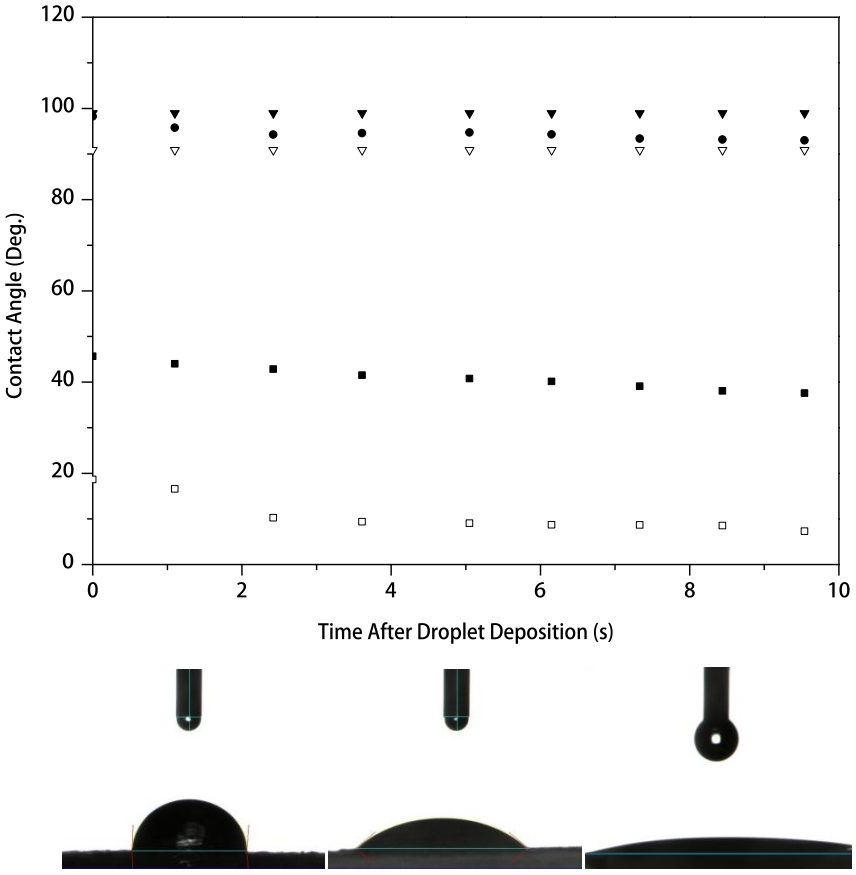

Figure 4-20: Contact angle (CA) measurements with respect to time (s) on textured surfaces. ▼ = C. pagurus epoxy replica, ▵ = H. gammarus epoxy replica, • = H. gammarus natural surface, ■ = C. pagurus natural surface, □ = C. pagurus ventral surface. Digital images of contact angle measurements demonstrate adsorption of the droplet into the surface over time.

A number of studies have reported that surface wettability influences substratum preferences and/or attachment strength of fouling organisms on artificial materials [37, 38]. It was expected that contact angle measurements of the exoskeleton surface of the *H. gammarus* and *C. pagurus* would yield useful information regarding the wettability of the surface and hence the adhesive characteristics of the surface. Contact angle has been previously examined as possible AF mechanism of decapod crustacean exoskeletons, where it was shown that crustaceans create and maintain highly characteristic surface wettabilities [9]. However, the authors of the latter study concluded that surface wettability is of little relevance for AF defence in crustaceans. Measurement of contact angle on the carapace of *C. pagurus* and *H gammarus* in this study has resulted in similar conclusions.

Microbial colonisation occurred within hours on both artificial and epoxy replicas of the epicuticle of both *C. pagurus* and *H .gammarus* following immersion. Bacterial cell numbers were observed to rapidly rise on the epicuticle surface compared to epoxy replicates, and a bacterial film consisting mostly of large rod-shaped cells (mean length 1.72 µm ± 0.27, n = 50 measured cells) developed on the exoskeleton samples of *C. pagurus* and *H. gammarus*. This bacterial film was less extensive on epoxy replicas of the surface within the study period indicating that the organic casing of the real sections of both species encouraged microbial growth. Quantification of bacterial cell abundance was complicated by the presence of surface topography and spatial heterogeneity of the attached microbial population; therefore estimates of surface coverage were made. Bacterial colonisation of the surface of *C. pagurus* is shown in Figure 4-21**.**

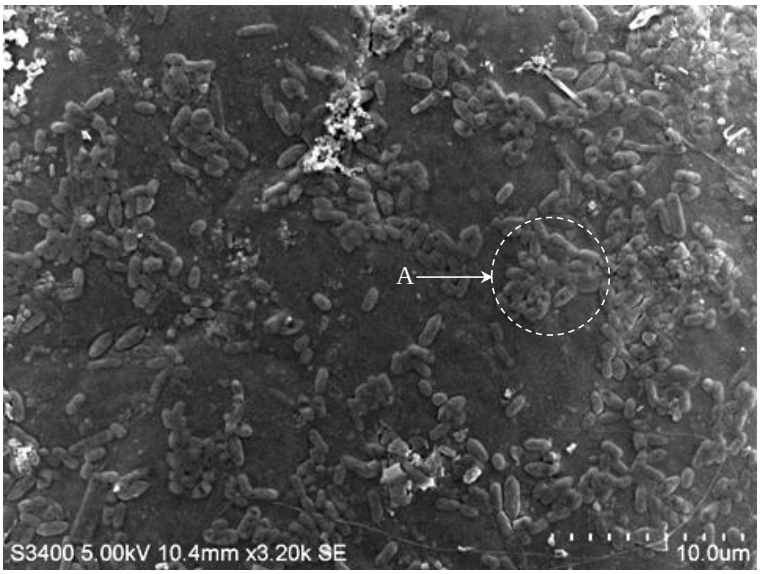

Figure 4-21: Scanning electron micrograph of bacterial cell microcolonies formed on a section of carapace isolated from C. pagurus and immersed in the marine environment for 7 d.

Given the abundance of chitin in marine waters and the occurrence of specialised chitinous (or chitinoclastic) bacteria involved in the decomposition of chitin structures [39], it is likely that the majority of the bacteria initially attached to the immersed sections of crustacean epicuticle are involved in decomposition of the epicuticle. It is still not known if this bacterial colonisation is host specific, although there are reports that the *vibrio* genus and especially *Vibrio harveyi* appear to preferentially colonise crustacean carapaces and may even have specific proteins for attachment to chitin [40, 41]. There are

also reports that crustacean exoskeletons may be used as a growth substrate by the *vibrio* genus, species of which have been shown to possess chitinolytic enzymes [42].

The bacterial layer that developed on *H. gammarus* was more extensive than that of *C. pagurus* and 100 % surface coverage was achieved after a 14-21 d immersion period. Bacterial colonisation had become so extensive that diatom cells were often found to be embedded in the underlying bacterial layer. Such an extensive microbial layer may reduce the survival rate of photosynthetic organisms like diatoms by preventing both motility and photosynthesis. However, few reports are available on the effects of an extensive bacterial layer on diatom survival. Figure 4-22 illustrates biofilm growth on the surface of *H. gammarus* where the extensive bacterial colonising layer can be seen. Diatom EPS trails are clearly visible on the surface of this bacterial layer indicating that diatoms are motile on the bacterial understory, even becoming embedded in the bacterial biofilm.

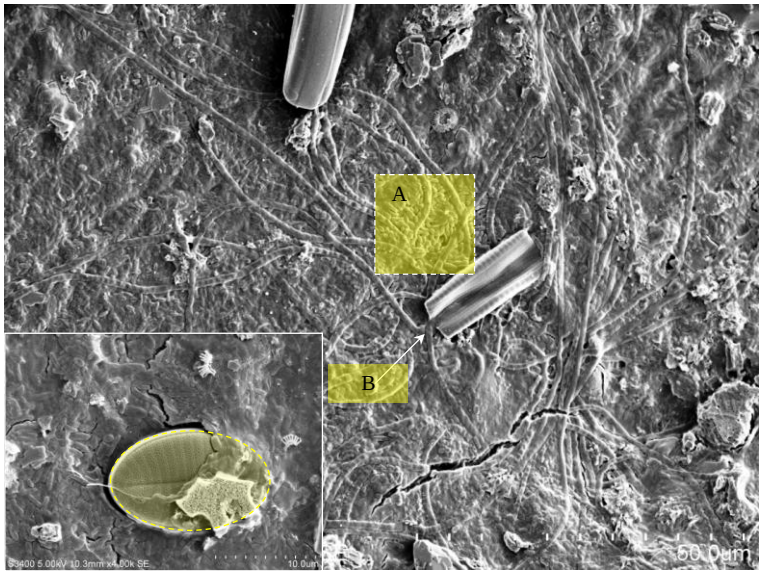

Figure 4-22: Scanning electron micrographs of microbial growth on H. gammarus after 14 d immersion in the marine environment. Surface coverage by a bacterial biofilm is complete (A) and EPS trails from exploring diatoms are visible (B). The microbial layer is so extensive that diatom frustules are enveloped in the underlying microbial layer (inset).

4.4.5 *Diatom settlement on natural and artificial carapaces*

Diatoms are known colonisers of crustaceans [10]. Previously reported studies on the external epibionts malacostracan species (*Amphipoda, Hoplocarida, Decapoda*) from the Gulf of Thailand, recorded the presence of diatoms on 18 out of a total of 47 crustacean species [43]. In this study, diatom frustules belonging to 34 genera were identified on epoxy and real sections of carapace exposed to the natural microfouling community at Lough Hyne marine reserve. Of these, *Tabularia, Amphora, Cocconeis, Navicula* and *Achnanthes* were the most dominant genera observed and were present on all surfaces.

SEM analysis indicated the presence of the first diatom frustules on all immersed surfaces within hours of immersion, concurrent with bacterial colonisation of the surface. Enumeration of diatom frustules on each surface type was used as an indication of the micro-algal biofouling rate of each surface. Attempts at automated image analysis did not yield reproducible results, so frustules were counted manually using the cell counter plugin for ImageJ. The methodology followed has a degree of error associated with it as the surfaces in question were not completely heterogeneous, therefore the surface area of each grid used to enumerate cells varied slightly depending on the topographic profile of the surface. Large diatom cells also occasionally prevented smaller frustules from being identified in areas of very high frustule density. Raphid diatoms were the most common benthic diatom group attached to the exposed surfaces. While centric diatoms were present, the overall abundance of this group was low in comparison and confined to planktonic aggregates that had become attached to the surface. Table 4-1 summarises attachment of diatom genera to each surface type.

Table 4-1: Summary of attached diatom genera on each surface type exposed.

	C. pagurus, Raised areas	*C. pagurus microtrichia*	*H. gammarus Epicuticle*	*H. Gammarus Pit*	*C. pagurus Epoxy*	*C. p Epoxy microtrichia*	*H.gammarus Epoxy Epicuticle*	*H. gammarus Epoxy pit*
Centric Group								
Minidiscus	-	+	+	+	+		+	
Melosira	+	+	+	+				
Biddulphia			+	+				
Plagiogramma		+	+	+				
Paralia		+	+	+				
Thalassiosira		+	+	+	+		+	
Cyclotella			+					
Araphid group								
Neosynedra		+	+	+				
Catacombas		+	+	+				
Licmophora	+	+	+	+	+		+	
Thalassionema		+	+	+				
Striatella		+	+	+				
Grammatophora		+	+	+	+		+	
Hyalosynedra		+	+	+				
Tabularia		+	+	+	+		+	
Raphid group								
Rhoicosphenia		+	+	+				
Achnanthes	+	+	+	+	+	+	+	+
Cocconeis	+	+	+	+	+	+	+	+
Climaconeis		+	+	+				
Diploneis		+	+	+				
Navicula	+	+	+	+	+		+	
Pleurosigma		+	+	+				
Amphora	+	+	+	+	+	+	+	+
Psammodictyon		+	+	+				
Nitzschia		+	+	+	+		+	
Cylindrotheca	+	+	+	+	+	+	+	+
Plagiotropis		+	+	+				
Gomphonemopsis		+	+	+	+			
Lyrella		+	+	+				
Gyrosigma			+	+				
Mastoglia			+	+				
Opephora			+	+				
Odontella			+	+				
Donkinia			+	+				

Key: + = genus present

4.4.6 *Diatom settlement on Cancer pagurus*

Diatom colonisation of both sections of ventral and dorsal surfaces of the carapace of *C. pagurus* occurred within hours of immersion at Lough Hyne Marine Reserve. Diatoms were counted on the carapace of *C. pagurus* from two categories of surface type, (a) areas of intact microtrichia and (b) raised areas of carapace. These two categories reflect both differing composition and microtopography between the two areas. Diatom frustules were enumerated (mag x 750, SEM) within these areas at intervals of 7 d and 14 d after immersion Table 4-2 summarises the diatom frustule numbers associated with each surface type after 7 and 14 d immersions periods.

Table 4-2: Summary of diatom abundance to each surface type after 7 and 14 day immersion times. Counts are taken from n =15 random fields of view of each surface type taken at a magnification X 750 using scanning electron microscopy (SEM). Samples labelled "raised" refer to images taken on raised areas of both actual and epoxy replicas of the carapace, while "microtrichia" refer diatoms counted on areas of intact microtrichia.

	Mean Frustule Abundance	Standard Deviation	Standard Error	Min	Max
Day 7 *C. pagurus* Raised Natural	5.53333	4.20657	1.08613	0	15
Day 7 *C. pagurus* Raised Epoxy	20.1333	8.27101	2.13556	8	38
Day 7 Microtrichia Natural	25.4667	8.40805	2.17095	16	44
Day 7 Microtrichia Epoxy	13.6667	4.76095	1.22927	5	23
Day 14 *C. pagurus* Raised Natural	7.46667	4.53347	1.17054	2	17
Day 14 *C. pagurus* Raised Epoxy	20.2667	9.14539	2.36133	8	36
Day 14 Microtrichia Natural	32.4667	12.7999	3.30493	13	56
Day 14 Microtrichia Epoxy	29.4667	13.0924	3.38043	12	54

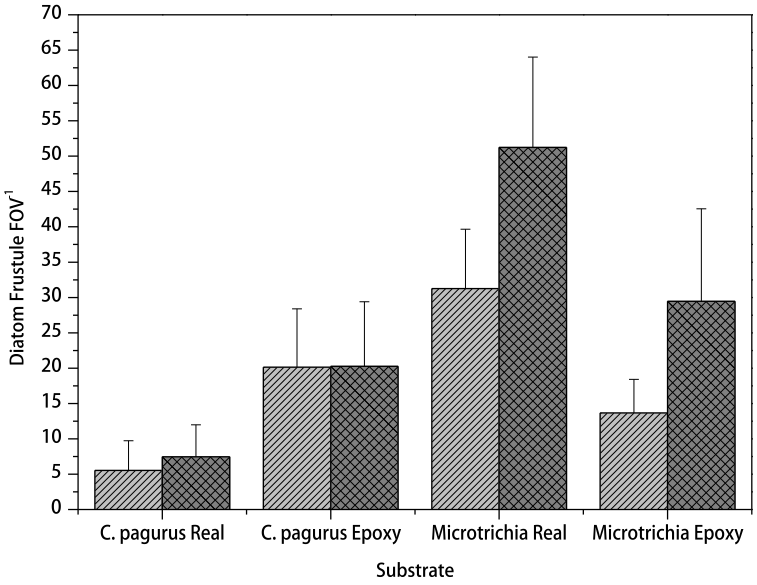

Figure 4-23: Graph summarising total diatom frustule abundance on both epoxy replicas and real samples of C. pagurus carapace, counted after immersion for 7d (light hatching) and 14 d (dark hatching) (Mag.x 750). Frustules were counted on raised areas of the carapace and locations containing intact microtrichia (Error bars represent ± 1 standard deviation, 15 random fields of view (FOV) of each surface type).

Figure 4-23 summarises diatom abundance on each surface type after 7 and 14 days immersion. Frustule counts on both topographic feature types present from sections removed from the carapace of *C. pagurus* indicated that the raised areas had significantly reduced diatom frustules (mean = 5.53 ± 4.20) per field of view compared with areas containing intact microtrichia (mean = 20.1 ± 8.27). A difference between diatom abundance on both epoxy replicates of the carapace and sections of the actual carapace of *C. pagurus* was also measured. Diatom frustules were significantly more abundant on the actual surface of *C. pagurus* than on replicas of the same surface. The reasons for this have not been conclusively established, however it is speculated that the presence of the substantial bacteria layer on the exoskeleton increased the ability of diatom species to adhere to the surface. This is likely due to exopolymeric substances facilitating the adhesion of diatom cells, topographic cues due to the physical presence of bacterial cells or induction of diatom adhesive polymers by chemical cues produced by bacteria. Induction of larval settlement by a microfouling layer of bacteria and diatoms has been shown previously [44] [45], however few data are available concerning promotion of diatom settlement by a bacterial biofilm. This is supported by the reduced abundance of diatom frustules on the epicuticle of *H. gammarus* after immersion for an identical period to that of *C. pagurus*, the surface of which does not develop complete bacterial biofilm layer as rapidly as *C. pagurus.*

Diatom frustule abundance on areas of both epoxy and real carapaces sections populated with intact microtrichia was higher than the raised areas. Diatom frustules existed in two distinct orientations on surfaces exhibiting intact microtrichia: frustules were either positioned between structures of resting on top of microtrichia (Figure 4-24 and Figure 4-25). Frustules that were observed on top of microtrichia were elevated from the surface. This may be an important aspect of the epibiontic defences of *C. pagurus* as the contact area between adhered diatom frustules and the surface is much reduced, and cells do not contact the surface in a preferable orientation for strongest adhesive contact. Furthermore, it has been demonstrated that current velocities and shear stress are important considerations in determining the relative abundances of diatoms species in micro-habitats, especially among rough or colonised surfaces [46]. This may indicate that the presence of surface features on the epicuticle of *C.pagurus* may be an important mechanism for control of micro-habitat and hence the attached benthic diatom community. Figure 4-24 illustrates how larger diatoms can be suspended above the carapace surface of *C. pagurus* by microtrichia, decreasing the available surface area for adhesion and perhaps increasing removal rates due to hydrodynamic shear forces.

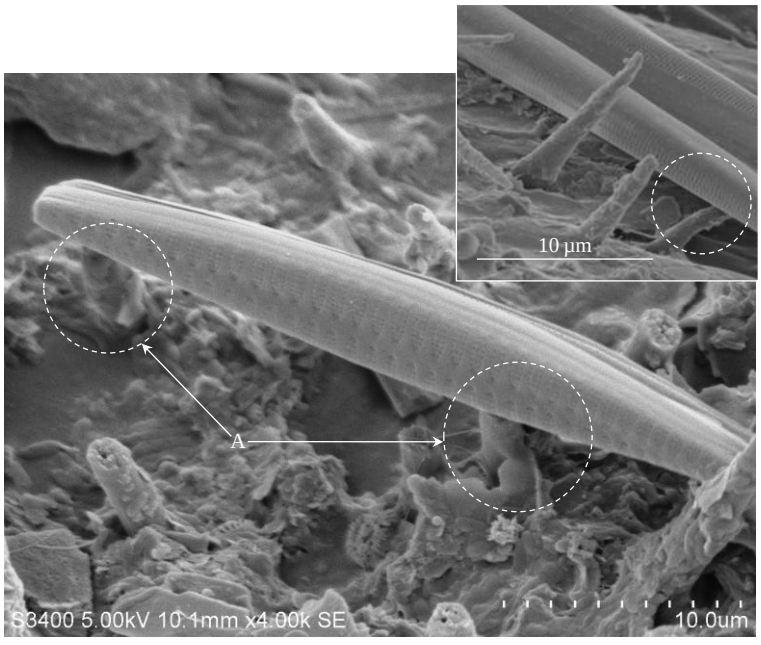

Figure 4-24: Scanning electron micrographs of a diatom frustule (Tabularia species.) suspended above the epicuticle surface of C. pagurus on microtrichia (A). Deformation of microtrichia when compressed by a diatom frustule could also be observed on occasion (inset).

Diatom frustules were also located between microtrichia on the carapace of *C. pagurus*. For the most part, smaller raphid species such as *Amphora* and *Navicula* were present in areas containing intact microtrichia, and it is possible that the present of microtrichia

select for smaller species such as these. Diatom species with a pedunculate attachment strategy involving the use of an adhesive stalk or foot such as those of *Achnanthes* and *Licmophora* were also abundant on areas densely populated with microtrichia. It is not clear why diatoms of this guild should be more abundant on such surfaces but can probably be related to the ability of the cell to remain elevated above the surface features. This is illustrated in Figure 4-25 where smaller diatoms can be observed on the carapace between microtrichia. Larger stalked diatoms are able to adhere to these surface types as well, presumably by resting on the microtrichia and then secreting an adhesive pad to anchor on the surface.

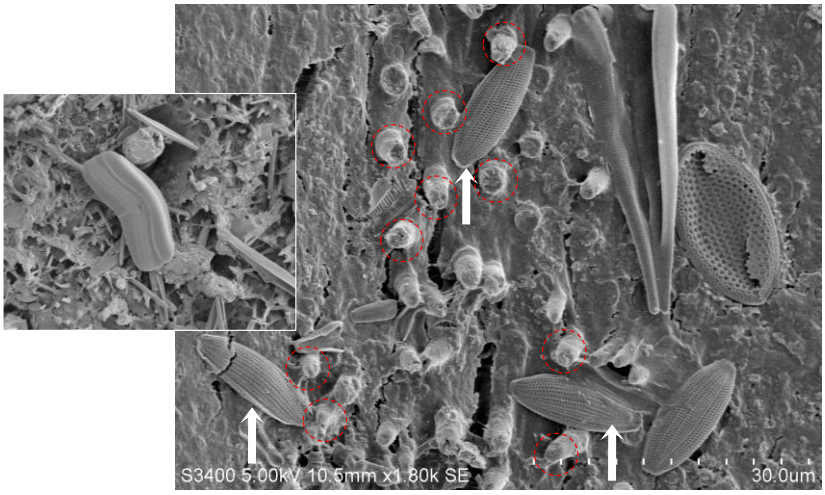

Figure 4-25: Scanning electron micrographs demonstrating positioning of diatoms (Amphora sp) between microtrichia (circled in red) on the carapace of C. pagurus. Diatom species with stalked adhesion strategies (e.g. Achnanthes sp.) were also in higher abundance on areas with microtrichia on the carapace (inset).

Examination of spatial heterogeneity is complicated by the small surface areas that can be imaged with high-resolution microscopy techniques such as SEM. Image montaging and colour-coded mapping of diatom frustules across a large section of the epicuticle highlighted areas reduced in diatom frustule attachment. Due to the small size of diatom frustules in relation to the surface area of the epicuticle, it was necessary to montage a number of SEM images of the surface to produce a better visualisation of frustule distribution on the carapace. Frustules within individual images could then be enumerated and a false colour image produced based on frustule abundances on the surface. Figure 4-26 illustrates an image montage composed of 100 individual Scanning electron micrographs showing diatom cells adhered to the surface of *C. pagurus.*

Figure 4-26: Visualisation of distribution of adhered diatom frustules from a sample of C. pagurus by montaging 100 scanning electron micrographs revealed the areas of reduced frustule density (circled). These areas corresponded to the spherulitic areas of increased elevation created by protrusion of the heavily calcified endocuticular material through the epicuticle.

False colour imaging of diatom abundance over a larger surface area reinforced the results obtained by enumeration of individual diatoms within random fields of view. A hue value of between 0 (red) and 125 (blue) degrees, and a saturation value of 0.75 was applied to each pixel depending on the cell abundance value at that pixel. Red areas correspond to areas of greater diatom abundance while blue areas correspond to areas of less abundance. The circled areas correspond to areas of the carapace in which the epicuticular layer is absent. In general diatom abundances are lower near or on these areas, while the highest abundances are found with surface pits on the carapace of *C. pagurus*. This is illustrated in Figure 4-27.

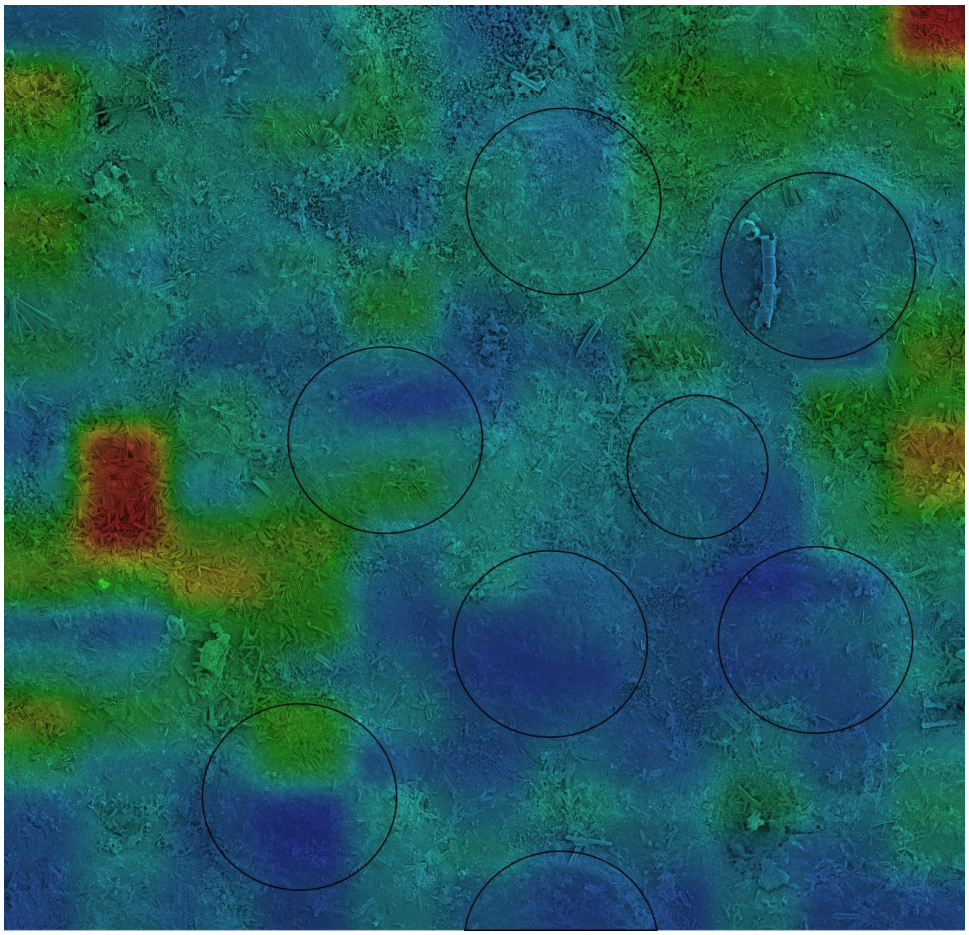

Figure 4-27: Abundance of diatom frustules as revealed by artificial colour mapping of the surface based on cell abundance.. Higher abundances produce lower hue values: the maximum density produces red and the minimum density produces blue. Areas of high frustule density (Red) correspond with surface pits on the carapace. Areas that are blue in colour correspond to areas with reduced diatom frustule abundance. This image is constructed of a montage of 100 individual SEM images.

During SEM analysis a narrow beam of mono-energetic electrons is focused within an area of interest of a specimen. A variety of signals are generated when these primary electrons hit the sample and scanning electron micrographs are predominantly generated by detection of lower energy secondary electrons generated after the collision of the primary electrons with the sample itself. As a result of the interaction between the primary electrons and the specimen, X-rays are also emitted which possess energies characteristic of each element. Energy dispersive X-ray (EDX) microanalysis is able to record all the X-ray energies simultaneously, thus giving information about the local chemical composition. EDX microanalysis can be used to determine the presence of metal ions that are important constituents biological structures and has been utilised to determine the composition of biological adhesives [47] and examine biocorrosion [48]. A similar technique involving energy dispersive X-ray fluorescence (EDXRF) has also been recently utilised to examine the accumulation of elements (S, As, Br, Sr, Cd, Hg, Pb) in two populations of *C. pagurus* [49]. Boßelmann and co-workers combined EDX with atomic absorption spectroscopy (AAS), thermogravimetric analysis and X-ray powder diffraction to examine the elemental composition and crystalline structure of the American lobster *Homarus americanus* and *C. pagurus* [50]. However, these workers did not differentiate between separate areas on the epicuticle or examine the elemental composition of the microtrichia relative to the epicuticle in general.

SEM analysis of the cross-section of both crustacean species revealed a heterogeneous composition containing discrete layering consistent with that reported in the literature [14, 50]. Due to the absence of diatom frustules on specific areas of the exoskeleton of *C. pagurus*, further analysis of the composition of these areas was conducted to determine differences in the elemental composition of these areas. EDS-SEM analysis indicated that C, O and Ca were the principal elements of the cuticle of *C. pagurus* (Figure 4-28). This composition was in agreement with previously published reports on the composition of the cuticle [13, 15, 50]. However, variation in the relative abundance of each element occurred at different locations on specific surface features. Analysis of the areas of corresponding to lowest diatom abundance revealed that the differences in composition indicated by BSE detection (Raised areas, Figure 4-28) were due to variation in the calcium content of these areas of the carapace. Elevated Ca and O concentrations were seen at these locations when compared to microtrichia-free areas of epicuticle.

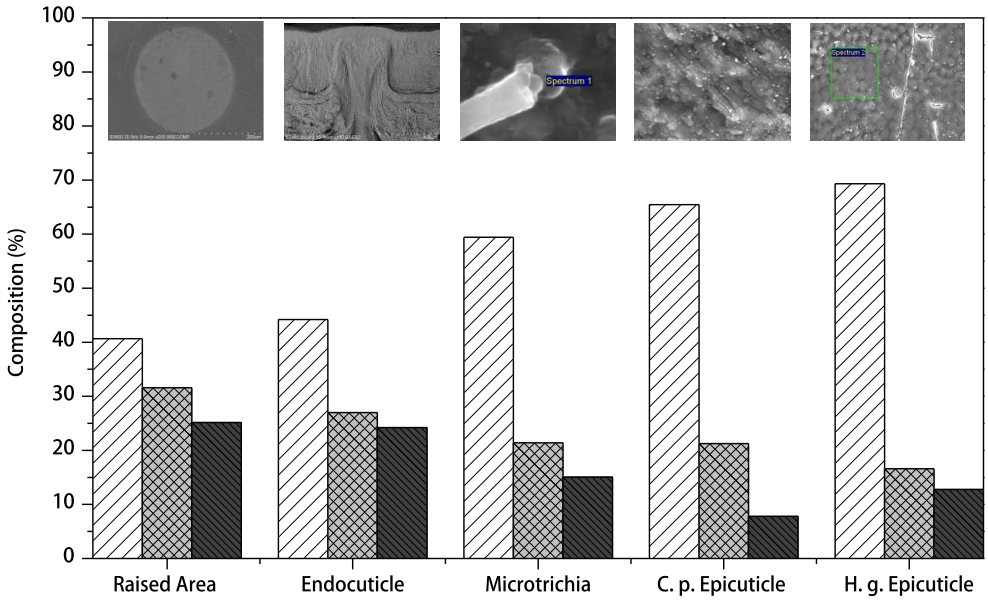

Figure 4-28: Comparison of the elemental composition between areas of the exoskeleton of C. pagurus and H. gammarus (Carbon = light hatching left column, Oxygen, middle column and Calcium dark hatching, right column). The epicuticle of H. gammarus demonstrates greatest Carbon content while the endocuticle of C. pagurus has the greatest Ca content. Inset scanning electron micrographs show the location of analysis.

The adhesion of biofouling organisms to heavily calcified materials such as the exoskeleton of crustaceans is of importance, as it has been demonstrated that Ca^{2+} has a crucial role in adhesion of diatoms and bacteria to exposed surfaces in the marine environment [51]. Thus the highly calcified areas of the exocuticle exposed on the surface of the exoskeleton of *C. pagurus* correspond to the areas of reduced diatom adhesion is unexpected as it is known that calcium ions have an important role in facilitating adhesion of both bacterial and diatom cells to a surface. Cations in general have an important role in neutralisation of the electrical double layer and Ca^{2+} can decrease electrostatic repulsion during the initial stage of cell adhesion to a negatively charged substratum. Research into the effects of Ca^{2+} on a *Pseudomonas* strain has indicated contradictory influences on cell adhesion, one that promoted interaction of a primary adhesive polymer with the substratum, and a second influence that disrupted the structure of a secondary adhesive polymer. Therefore the relationship between the concentration of specific cations in solution and the ability of bacteria to adhere to surfaces is complex. It is possible that dissolution of $CaCO_3$ structures from areas of exposed endocuticle may have a role in both releasing diatoms these surfaces or perhaps discourage initial settlement.

In addition to analyses of C, O and Ca content of the epicuticle, trace elements were also recorded. Figure 4-29 demonstrates trace element composition of the carapaces of both *C. pagurus* and *H. gammarus*.

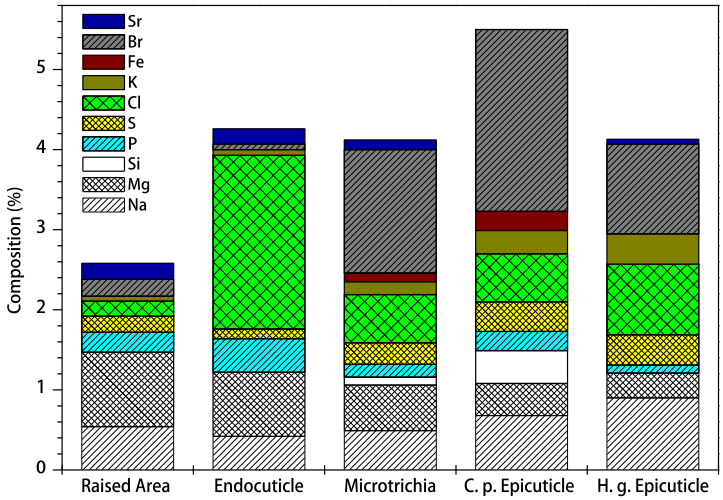

Figure 4-29: Graph of % composition of trace elements present in the epicuticle of C. pagurus and H. gammarus measured using EDX.

Analysis of the trace elements present on each surface type indicated trace amounts of S and Mg in most samples as expected. However, no unusual metals were present that would indicate any biocidal effects from metal adsorption by the carapace of *C. pagurus* or *H. gammarus*. It is possible that some as yet unidentified secondary metabolite is preventing biofouling of these areas, or it is possible that diatom cells naturally avoid elevated areas such as this that may increase the likelihood of remove due to copepod grazing or removal from hydraulic shear forces.

4.4.9 *Influence of microtrichia on macrofouling*

Several cirripede crustacean species have been noted as colonisers of the carapace of intermoult *C. pagurus*. These include *Balanus balanus, Balanus crenatus, Chelonibia patula, Chirona hameri, Austrominius modestus*, and *Verruca stroemia* [52]. There is a suggestion that barnacle species such as *B. crenatus* and *A. modestus* principally inhabit grooves or depressions in the carapace of either *C. maenas* or *C. pagurus* and are less common on raised or smooth regions of the carapace [53]. However, the reasons for this are unknown. Several species of spirorbid polychaete (*Janua pagenstecheri, Spirorbis rupestris, and S. tridentatus*) have also been described as inhabiting the external carapace of *C. pagurus* [53].

Bers and Wahl found that an artificial replica of the topography of the epicuticle of *C. pagurus* significantly repelled the barnacle *Balanus improvisus* during the first 3 weeks of immersion, but that the effects became non-significant thereafter [12]. However, the authors did not offer a satisfactory explanation of how the surface topography of *C. pagurus* may have generated this effect.

In this study, careful removal of the attached organisms, facilitated SEM examination of the underside of some adhered macrofouling organisms. It was found that microtrichia present on the surface of *C. pagurus* were incorporated into the mineralised structures of calcareous biofouling organisms. Subsequent removal of the biofouling organisms resulted in removal of the microtrichia which remained intact on the epicuticle of *C. pagurus* in the majority of cases. This resulted in a series of pore-like features in the adhesive surface of removed macrofouling organisms (Figure 4-30). This may have some role in early mortality of biofoulers such as polychaetes or barnacle species as microtrichia may penetrate the thin walls of early colonising calcareous organisms. Surviving organisms initially settling in areas lacking or exhibiting damaged microtrichia, may eventually overcome the effects of microtrichia by secreting tubes or walls of sufficient thickness that the microtrichia no longer effect growth. Therefore, the structural characteristics of the epicuticle of *C. pagurus* may select for certain macrofouling organisms by excluding those with thin base plates.

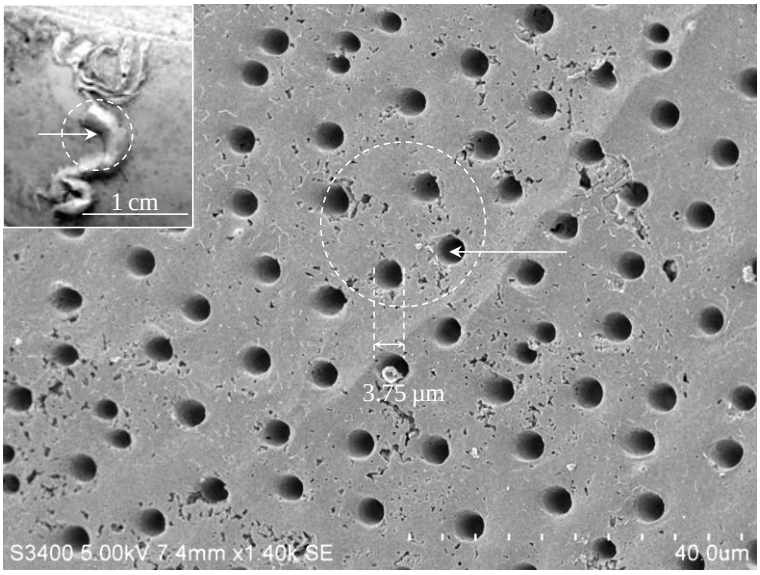

Figure 4-30: Scanning electron micrograph showing the adhesive surface of a serpulid worm (digital image, inset) after removal from the surface of C. pagurus. The circular holes visible in the surface are a result of the removal of microtrichia from the calcified skeleton of the attached organism.

However, once an organism has attached and developed significantly to overcome any initial inhibitory effects of the microtrichia, it may require greater force to remove the organism as the microtrichia may act as anchors to the surface. Removal of individuals of *Pomatoceros* spp from the surface did not always result in intact microtrichia remaining on epicuticle of *C. pagurus*. In certain areas, particularly where the microtrichia were not perpendicular to the plane of the epicuticle, the microtrichia remained embedded with the basal plate of the removed organism (Figure 4-31).

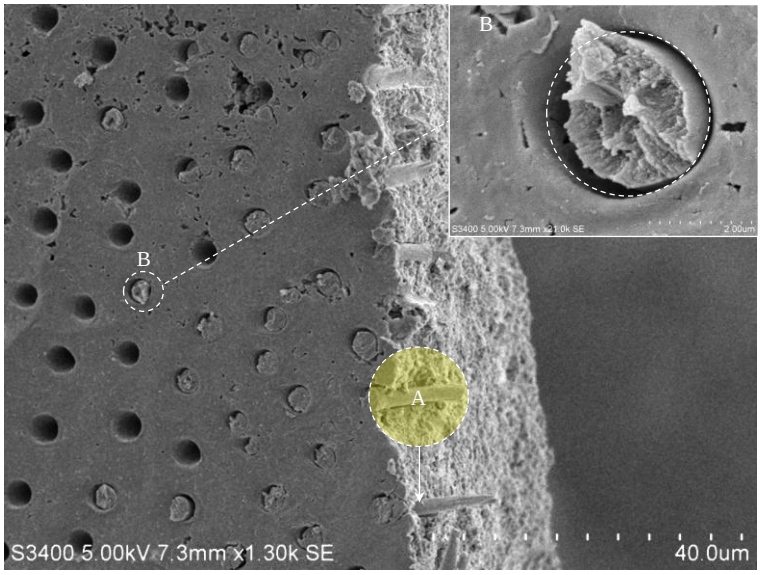

Figure 4-31: Scanning electron micrographs showing retention of microtrichia with the calcareous tube of Pomatoceros. Intact microtrichia can be observed at a fracture through the surface of the tube (arrowed). Such microtrichia have been broken from the surface of the carapace during removal (inset).

Further investigation of the effects of microtrichia on macrofouling organisms is required. It has been observed in previously studies such as that of Gregg [54] that the nature of the surface affects the orientation of the axes of barnacle species and that grooved patterns were duplicated in the basal plate morphology of attached barnacles. A similar result from this study is shown in Figure 4-32.

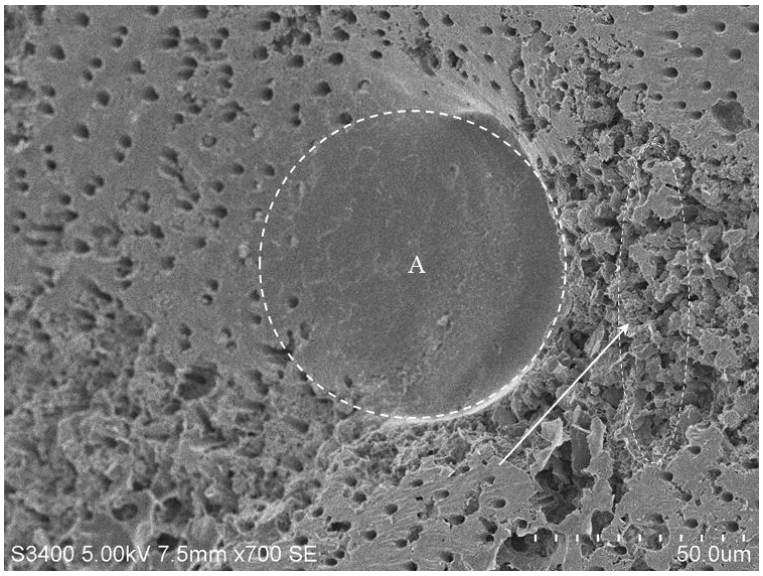

Figure 4-32: A scanning electron micrograph of the base a calcareous biofouling polychaete after removal from the carapace of C. pagurus. The indentation resulting from the raised areas of the carapace is seen (A) and damage to the calcareous shell after removal from the microtrichia (arrowed).

The carapace of *H. gammarus* was categorised into two surface types, plain epicuticle and surface cavities or pits. The relative abundance of diatom frustules was analysed for each category on both real and artificial epoxy replicas of the carapace exposed to a natural microfouling community for 14 d.

Overall, diatom abundance was greater on the real sections *H. gammarus* than the produced epoxy replicas. Diatom abundances were highest in cavities present on the carapace of *H. gammarus* both in natural and epoxy replicates of the carapace. The concentration of diatoms found within surface cavities is demonstrated in Figure 4-33.

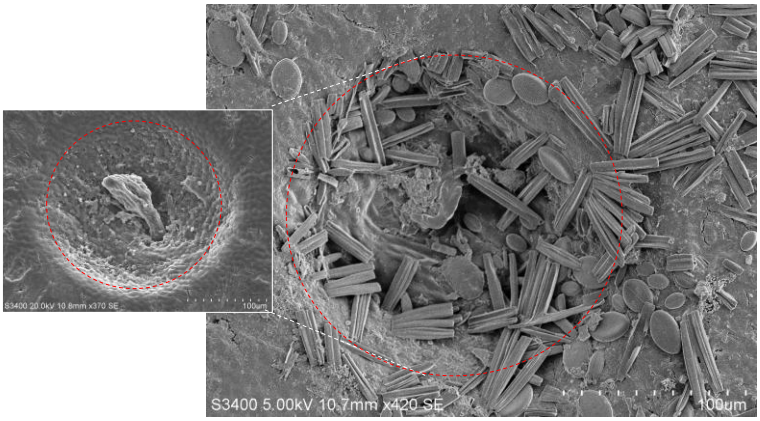

Figure 4-33: Scanning electron micrographs of diatom abundance in surface pits present on the carapace of H. gammarus after 14 d exposure to a natural microfouling community. The original unexposed pit (inset) has become colonised a diverse benthic diatom biofilm.

It is unclear why pits on the surface of *H gammarus* would have increased diatom settlement. Possible reasons may include retention of cells within cavities due to hydrodynamic flow. Surface depressions are known to have the opposite effect on hydrodynamic flow velocity when compared with protruding features such as those observed on *C. pagurus*. The velocity of flow is calculated to reduce when flowing over and into a depression. An adverse pressure gradient is created that leads to a separation of flow at the upstream edge of the depression and vortical flow within the cavity [55]. The velocity of vortices within the depressions are approximately a tenth of mainstream flow and periodically become unstable and are shed from the depression, leading to replacement of bulk replacement of fluid within the depression. This process potentially results in greater delivery of microorganisms to microscale depressions [55]. The dimensions and depth of the depressions measured on *H. gammarus* in this study are

such that the depth is always equal or less than the diameter of the depression in any direction of flow. This produces a single vortex within the cavity with a rapid inward current and slow outward current. A simple diagram of this effect is shown in Figure 4-34.

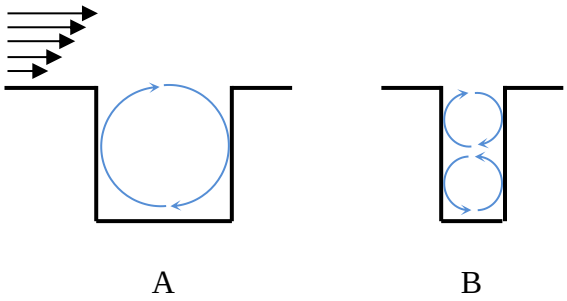

Figure 4-34: Schematic of representation of flow over a shallow depression where (A) the depth of the depression is equal to or less than the diameter or (B) where the depth is greater than the diameter. The arrows indicate flow direction. Figure adapted from Abelson and Denny [55].

Increased diatom abundance within cavities on the surface of *H. gammarus* may also be related to decreased shear forces within these layers, or the cavities may offer niche protection from predation. Motile diatom cells may also be simply become trapped within surface cavities during surface exploration. However, no quantitative studies are available to address transport rates of diatom cells to surface cavities or depressions, and a thorough analysis of the effects of hydrodynamic forcing on the accumulation of biofouling propagules and organisms under these circumstances is required.

The effects of epicuticle removal on epibiosis in *C. pagurus* were examined by removal of the epicuticle. Mechanical abrasion of the exoskeleton surface was carried out and removal of the surface microtrichia and much of the outer epicuticle layer was confirmed using SEM. After 14 days exposure, the abraded exoskeleton surfaces were very different in appearance to previously immersed intact sections of exoskeleton. The exocuticle layer directly underneath the epicuticle had eroded, leaving a porous surface. This layer originally was composed of chitin-protein fibres stacked in layers of continuously changing orientation [15], hardened by quinone tanning and calcification with mineral crystals situated between the fibres [35]. However, after marine exposure, the surface had degraded and the organic material had been removed.

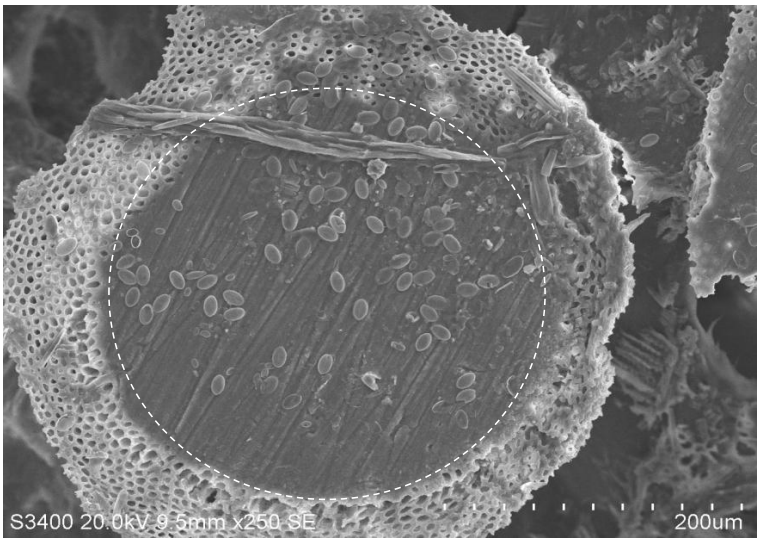

Figure 4-35: Scanning electron micrograph of the carapace of C. pagurus with epicuticle after 14 d deployment. The heavily calcified areas of the endocuticle remain intact (circled).

Microbial colonisation of the exoskeleton with epicuticle removed was reduced compared with that of the carapace sections containing an intact epicuticle. The dense microbial layer which had previously formed on the intact epicuticle was no longer evident and diatom abundances were much less on the exposed exoskeletal layer. Diatom cells that did attach consisted of adnate cell forms mainly from the Genus *Cocconeis*. Diatom species abundance and diversity were reduced on this surface and species attached to the surface, as indicated by intact frustules, were mainly dominated by *Cocconeis*. An example of this settlement is shown in Figure 4-36 where diatoms of the genus Cocconeis are visble.

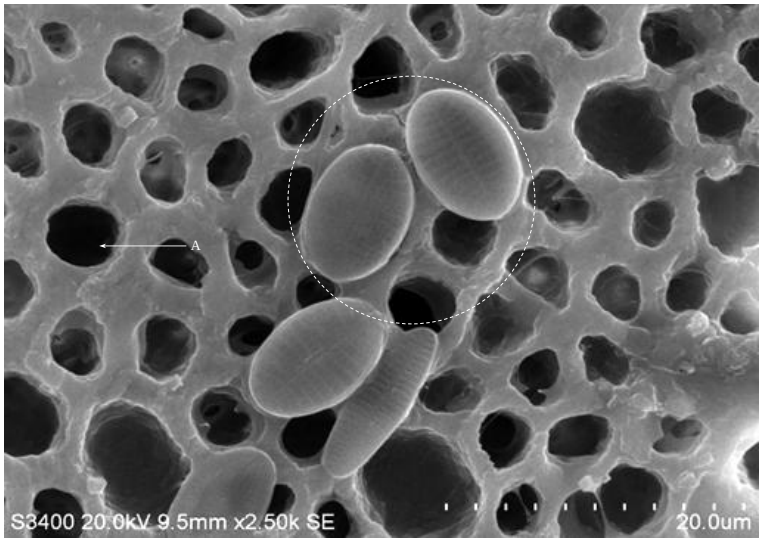

Figure 4-36: Scanning electron micrograph of diatom adhesion to the porous surface (A) of the eroded cuticle of C. pagurus. Diatoms adhered to the surface were from the Cocconeis genus.

The fact that raphid diatoms are capable of adhesion to a porous surface as shown in Figure 4-36 illustrates the ubiquitous nature and adhesive tenacity of this biofouling group. While the effect of this surface structure on the rate of diatom removal could not be tested, the fact that diatoms can adhere to such surface offering very little adhesive planar surface area demonstrates the versatility of adhesion among diatoms.

4.5 **Conclusions**

The aim of this work has been characterisation of possible epibiosis defences of two marine decapod crustaceans attributable to surface texture of the epicuticle. The surface texture of exoskeletons of both *H.gammarus* and *C. pagurus* has been characterised, and this study has demonstrated that the topographic profile of both species differs in both texture and scale of topography. This is the first complete characterisation of the topographic nature of the epicuticle in *H. gammarus* and the first time that sections of the exoskeleton of both species have been compared in terms of fouling rate.

The natural epicuticle of *C. pagurus* and *H .gammarus* undergo rapid bacterial colonisation which may increase subsequent diatom adhesion compared to epoxy replicates of the surface. Despite this, two areas are comparatively less fouled on the epicuticle of *C.pagurus*, the elevated spherulitic areas, which differ in composition and appearance to the rest of the carapace, and areas containing sharp mineralised needle-like structures (microtrichia). Microtrichia are highly abundant in the areas of depressed elevation on the epicuticle of the exoskeleton. The elevated areas are heavily calcified where the endocuticular layer extends to the external surface of *C. pagurus*. Mapping of diatom frustule distribution on the surface of the epicuticle has highlighted these areas as having a lower abundance of attached diatoms than surrounding areas.

Overall a substantial microfouling community developed textures of both *C. pagurus* and *H. gammarus*, and although some AF ability may be related to microtrichia preventing secure attachment of diatom cells in *C. pagurus*, a diverse diatom community was capable of adhesion to both surfaces. Spacing between microtrichia is sufficient to allow colonisation of smaller diatom species between structures, and this colonisation may facilitate later colonisation by macrofouling organisms.Microtrichia may still have a role in the prevention of macrofouling organisms, particularly calcareous organisms such as serpulid worms or cirripede species in early stages. However, once such organisms become established, the length scale of the microtrichia appears insufficient to affect growth, and indeed the presence of microtrichia may increase the adhesive bond of such species to the surface.

4.6 **References**

1 C. Baum, W. Meyer, R. Stelzer, L. G. Fleischer and D. Siebers, *Mar. Biol.*, 2002, **140**, 653-657.

2 A. J. Scardino and R. de Nys, *Biofouling*, 2004, **20**, 249-257.

3 A. J. Scardino, D. Hudleston, Z. Peng, N. A. Paul and R. de Nys, *Biofouling*, 2009, **25**, 83-93.

4 A. V. Bers, E. R. Dıaz, B. A. P. da Gama, F. Vieira-Silva, S. Dobretsov, N. Valdivia, M. Thiel, A. J. Scardino, C. D. McQuaid and H. E. Sudgen, *Biofouling*, 2010, **26**, 367-377.

5 J. Guenther, *Biofouling*, 2007, **23**, 1-11.

6 M. Wahl, *Mar. Ecol. Prog. Ser.*, 1989, **58**, 175-189.

7 M. Wahl, *Biofouling*, 2008, **24**, 427-438.

8 K. Becker and M. Wahl, *J. Exp. Mar. Biol. Ecol.*, 1996, **203**, 245-258.

9 K. Becker, T. Hormchong and M. Wahl, *Hydrobiologia*, 2000, **426**, 193-201.

10 K. R. Carman and F. C. Dobbs, *Microsc. Res. Tech.*, 1997, **37**, 116-135.

11 L. Savoie, G. Miron and M. Biron, *J. Crust. Biol.*, 2007, **27**, 30-36.

12 A. V. Bers and M. Wahl, *Biofouling*, 2004, **20**, 43-51.

13 C. Sachs, H. Fabritius and D. Raabe, *J. Struct. Biol.*, 2006, **155**, 409-425.

14 D. Raabe, C. Sachs and P. Romano, *Acta Materialia*, 2005, **53**, 4281-4292.

15 R. Roer and R. Dillaman, *Am. Zool.*, 1984, **24**, 893-909.

16 R. H. Hackman, in *Chitin and benzoylphenyl ureas*, ed. J. E. Wright, Kluwer Academic Publishers, Dordrecht, The Netherlands, 1987, p. 1-33.

17 E. Moland, E. M. Olsen, K. Andvord, J. A. Knutsen, N. C. Stenseth and B. Sainte-Marie, *Can. J. Fish. Aquat. Sci.*, 2011, **68**, 1197-1210.

18 M. S. Gil-Turnes and W. Fenical, *Biol. Bull.*, 1992, **182**, 105-108.

19 A. J. Scardino and R. de Nys, *Biofouling*, 2011, **27**, 73-86.

20 R. T. Bauer, *J. Crust. Biol.*, 1989, **1**, 49-73.

21 R. Y. Bernier, A. Locke and J. M. Hanson, *Aquatic Invasions*, 2009, **4**, 105-110.

22 F. Shahidi, J. K. V. Arachchi and Y. J. Jeon, *Trends Food Sci. Technol.*, 1999, **10**, 37-51.

23 D. F. Kendra and L. A. Hadwiger, *Exp. Mycol.*, 1984, **8**, 276-281.

24 J. A. Tincu and S. W. Taylor, *Antimicrob. Agents Chemother.*, 2004, **48**, 3645-3654.

25 D. Destoumieux, P. Bulet, D. Loew, A. Van Dorsselaer, J. Rodriguez and E. Bachère, *J. Biol. Chem.*, 1997, **272**, 28398-28406.

26 D. Destoumieux, P. Bulet, J. M. Strub, A. van Dorsselaer and E. Bachère, *Eur. J. Biochem*, 1999, **266**, 335-346.

27 J. Fleischer, M. Grell, J. T. Høeg and J. Olesen, *Mar. Biol.*, 1992, **113**, 425-435.

28 E. Ralston and G. Swain, *Bioinspir. Biomim.*, 2009, **4**, 015007-015011.

29 W. Rasband, *1997–2007. ImageJ*.

30 F. E. Round, R. M. Crawford and D. G. Mann, *The diatoms: biology & morphology of the genera*, Cambridge University Press, Cambridge, UK, 1990.

31 A. R. Miller, R. L. Lowe and J. T. Rotenberry, *J. Ecol.*, 1987, **75**, 693-709.

32 B. Cooksey, K. E. Cooksey, C. A. Miller, J. H. Paul, R. W. Rubin and D. Webster, in *Marine Biodeterioration: an interdisciplinary study.*, ed. J. D. Costlow and R. D. Tipper, Naval Institute Press, Annapolis, M. D., 1984, p. 167-169.

33 M. E. Krejci and R. L. Lowe, *J. N. Am. Benthol. Soc.*, 1986, **5**, 211-220.

34 J. M. N. Sieburth, H. L. Pratt, P. W. Johnson and D. Scales, *Microbial seascapes: a pictorial essay on marine microorganisms and their environments*, University Park Press Baltimore, MD, 1975.

35 T. Hegdahl, J. Silness and F. Gustavsen, *Zool. Scr.*, 1978, **6**, 89-99.

36 A. B. D. Cassie and S. Baxter, *Trans. Faraday Soc.*, 1944, **40**, 546-551.

37 M. L. Carman, T. G. Estes, A. W. Feinberg, J. F. Schumacher, W. Wilkerson, L. H. Wilson, M. E. Callow, J. A. Callow and A. B. Brennan, *Biofouling*, 2006, **22**, 11-21.

38 J. A. Finlay, S. M. Bennett, L. H. Brewer, A. Sokolova, G. Clay, N. Gunari, A. E. Meyer, G. C. Walker, D. E. Wendt and M. E. Callow, *Biofouling*, 2010, **26**, 657-666.

39 C. E. Zobell and S. C. Rittenberg, *J. Bacteriol.*, 1938, **35**, 275-287.

40 M. T. Montgomery and D. L. Kirchman, *Appl. Environ. Microbiol.*, 1994, **60**, 4284-4288.

41 M. T. Montgomery and D. L. Kirchman, *Appl. Environ. Microbiol.*, 1993, **59**, 373-379.

42 B. L. Bassler, C. Yu, Y. C. Lee and S. Roseman, *J. Biol. Chem.*, 1991, **266**, 24276-24286.

43 K. Becker, *J. Crust. Biol.*, 1996, , 92-104.

44 T. Harder, C. Lam and P. Y. Qian, *Mar. Ecol. Prog. Ser.*, 2002, **229**, 105-112.

45 T. Harder, in *Marine and Industrial Biofouling Vol. 4, XII*, ed. H. C. Flemming, R. Venkatesan, P. Sriyutha Murthy and K. Cooksey, Springer, Heidelberg, New York., 2009, p. 219-231.

46 R. J. Stevenson, *Ecology*, 1983, **64**, 1514-1524.

47 L. Petrone, N. L. C. Ragg, L. Girvan and A. J. McQuillan, *Biofouling*, 2009, **85**, 78-96.

48 I. B. Beech, *Int. Biodeterior. Biodegrad.*, 2004, **53**, 177-183.

49 S. Barrento, A. Marques, B. Teixeira, M. L. Carvalho, P. Vaz-Pires and M. L. Nunes, *Food Chem. Toxicol.*, 2009, **47**, 150-156.

50 F. Boßelmann, P. Romano, H. Fabritius, D. Raabe and M. Epple, *Thermochimica Acta*, 2007, **463**, 65-68.

51 G. G. Geesey, B. Wigglesworth-Cooksey and K. E. Cooksey, *Biofouling*, 2000, **15**, 195-205.

52 D. J. Heath, *Zool. J. Linn. Soc.*, 1976, **59**, 59-67.

53 G. D. Stentiford, *ICES J. Mar. Sci.*, 2008, **65**, 1578-1592.

54 J. H. Gregg, *Biol. Bull.*, 1948, **94**, 161-168.

55 A. Abelson and M. Denny, *Annu. Rev. Ecol. Syst.*, 1997, **28**, 317-339.

5 Diatom Biofouling of Bio-inspired Textured Synthetic Surfaces

5.1 **Engineered surface topography**

Surface textures consisting of microtopography or nanotopography of controlled dimensions are reported to influence initial settlement, attachment strength and retention of a range of cell types [1-3]. Thus, development of engineered surface topography (EST) of regular, three-dimensional topographic features of precise dimensions is an attractive proposition for incorporation into novel non-toxic AF strategies. Fabrication methods developed in the electronics industry for production of nanoscale and microscale features such as photolithography, laser ablation and e-beam lithography allow production of a large variety of engineered surface textures. Both nanometre and micrometer scale surface topographies produced in this way have been tested for influence on settlement and adhesion strength of a variety of cell types [2, 4-9]. EST of specific dimensions is reported to influence settlement of common biofouling organisms on engineered surfaces, including specific bacterial species [10], algal spores [5, 11] and invertebrate larvae [12].

Several considerations are regarded as important in the development of surface topography for control of biofouling. These include control of aspect ratio of surface features (ratio of width to height of a feature) [13], forces generated on a cell wall when in contact with surface features (force gradients) [11], theoretical attachment points available to colonising cells [14-16] and containment of exopolymeric substances from expanding cell colonies [10]. The dimensions and texture of surface features and the material properties of the substrate on which the textures are generated control these characteristics. Understanding the fundamental impact of these factors on material performance not only has relevance for the future development of non-toxic AF materials, but is also of importance when improving existing biocidal coatings and materials.

5.1.1 *Engineered texture fabrication*

A number of methods of fabricating nano and micro-scale texture on material surfaces have been used to examine biological response to engineered surface texture. These include femtosecond laser ablation [17, 18], photolithography with PDMSe or poly(ethylene glycol) (PEG) [19], nanolithography, microcontact printing and chemical etching [20, 21]. Anselme and co-workers have recently published a review of current methods used to produce nano- and microscale surface topography [22]. To understand the

role of surface texture alone on cell behaviour, the method of surface texture fabrication must allow control of both topography and avoid modification of surface chemistry where possible. The techniques currently available that provide controlled manipulation of surface texture without loss of control over surface chemistry are summarised in Table 5-1. A number of the techniques listed such as photolithography offer control of both nano- and micro-scale surface features, but are time-consuming and often expensive to produce.

Table 5-1: Summary of techniques capable of surface topography modification while retaining original surface chemistry. (Table modified from [22])

Technique	Modification of topography	Modification of chemistry	Lateral resolution	Advantages	Disadvantages
Photolithography	Yes	No	40 nm (EUV)	Widely used, any shape possible	Best resolutions require a synchrotron and are expensive
Transfer from self-assembled polymer film	Yes	Can be avoided	50 nm	Different substrates possible	Usually only one type of shape: hexagonally packed pegs
Polymer demixing	Yes	Yes, but there are ways this can be avoided	Sub-micron	Very easy to make, nanometric heights	Little shape control, only worm-like or island structures
Nanoimprint lithography	Yes	No	100 nm	Topography without chemistry	Low resolution
Colloidal lithography	Yes	No, but possible if desired	50 nm	Even spacing	Lack of shape flexibility, can only have hexagonally packed
Surface roughening	Yes	No	Not easily controlled, nanometric	Uniform surface with controlled chemistry	The surface structure cannot be controlled
Anodic oxidation of metals	Yes	No	15 nm for nanotubes	Controlled chemistry, easily tunable sizes	Small range of structures that can be produced
Electrospinning	Yes	No	Dependent on fibre size	Can use a wide variety polymers, mimics ECM	Only one type of shape: bed of fibres
E-beam lithography	Yes	No	15 nm	Good resolution	Very slow because each feature has to be made separately; expensive

5.1.2 *Diatom settlement on engineered surface topography*

While the effects of surface texture produced using many of the techniques listed in Table 5-1, have been extensively examined on bacterial strains and mammalian cells, very few reports exist on the influence of engineered surface texture on recruitment, adhesion and behaviour of raphid benthic diatoms. This is surprising since, as has been demonstrated in the preceding chapters; raphid diatoms are prolific colonisers of immersed surfaces and are an important group of biofouling organisms. Several reports are available on the influence of textured artificial surfaces on diatom adhesion in laboratory studies [16] and on natural surfaces in field studies [23]. However, there is lack of data regarding the effects of EST on development of natural multispecies diatom communities in the marine environment. This is surprising as surface texture is likely to be an important factor for raphid diatoms seeking optimum locations for colonisation on surfaces. This should be particularly relevant to raphid diatom species developing from perhaps a single initial colonising cell to form a monolayer of cells over all the available surface area [24]. The diatom genus *Cocconeis* contains a number of species for which surface topography is likely to influence settlement. The development of this genus on a surface is illustrated in Figure 5-1 where it can be seen that cells are closely associated when abundant on the surface. How settlement and adhesion of cells types such as this are influenced by the physical presence of other cells has not been previously explored, and little is known about how the physical cues provided by surface texture influence settlement in these and similar organisms.

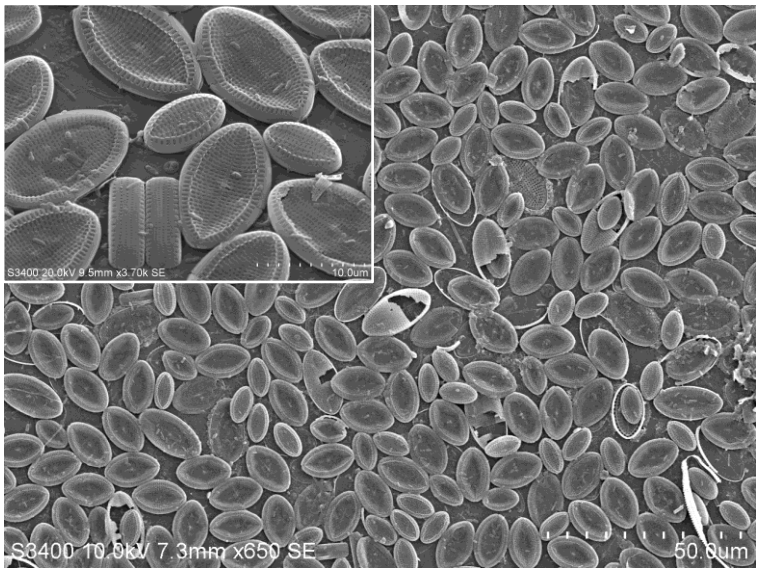

Figure 5-1: Scanning electron micrographs of raphid diatoms (genus primarily Cocconeis) attached to the surface of a glass optical window. Cells can be seen to form a monolayer on the surface in which different cell sizes exist, bound cohesively together by EPS (inset).

Investigation of recruitment of raphid species to surfaces with different surface textures can inform optimisation of surface texture on AF materials such as silicone elastomer materials used as foul release coatings. Any ability to influence both recruitment or exploratory behaviour and retention of cells on the surface using surface textures will provide important information for future development of these materials.

5.2 **Aims and objectives**

Expanding on results from previous chapters, in which textured natural surfaces have been demonstrated to affect settlement and adhesion of diatom species, the aim of this chapter is to assess settlement of raphid diatoms on engineered textured surfaces.

The objectives of this chapter are to:

(1)Design and production of textured surfaces with surface texture capable of preventing settlement of raphid diatoms. These surfaces will be designed using current theories regarding optimum surface design for AF.

(2)Assessment of settlement of the common and problematic biofouling raphid diatom species, *Amphora coffeaeformis* to textured elastomer surfaces in laboratory studies.

(3)Assessment of influences of surface texture on settlement and adhesion of a natural diatom community structure in field tests.

(4)Assessment of applicability of current theoretical models developed to describe settlement of macroalgal spores and other biofouling propagules to predict raphid diatom adhesion to synthetic textured surfaces.

5.3 **Materials and Methods**

Prior to production of engineered surface textures using the techniques described in this section, a number of alternative methods of texture fabrication were trialled. These included computer numerical control (CNC) micro-milling, laser ablation, polymer printing, polymer casting, silicon etching, and nanocasting techniques. However none of these methods provided sufficient control of the dimensions of surface features without alteration of surface chemistry – a necessity for examining the role of surface texture alone on diatom behaviour. Ultimately, photolithography was considered the most successful method of producing precisely controlled and reproducible surface textures.

5.3.1 *Texture design*

Engineered surface textures presented in this section were fabricated using the facilities at the Tyndall Institute, Cork, with funding provided under a National Access Programme grant (NAP 181). Transferral of initial design sketches into CAD and production of the master wafers were conducted by members of the fabrication team at the Tyndall Institute.

Surfaces were designed based on available literature regarding design of textures capable of inhibiting settlement of biofouling organisms. Designs incorporated attachment point theory [15, 16] whereby surface textures of dimensions smaller than those of a settling cell were able to reduce initial cell settlement. Textures were designed specifically to investigate settlement of the benthic and problematic biofouling diatom species, *Amphora coffeaeformis* in laboratory studies. This species is a small, biraphid diatom species that is frequently utilised in diatom adhesion experiments in biofouling studies. The structure and dimensions of this species as visualised using SEM is shown in Figure 5-2, where the texture and morphological features of the frustule of this species can be seen.

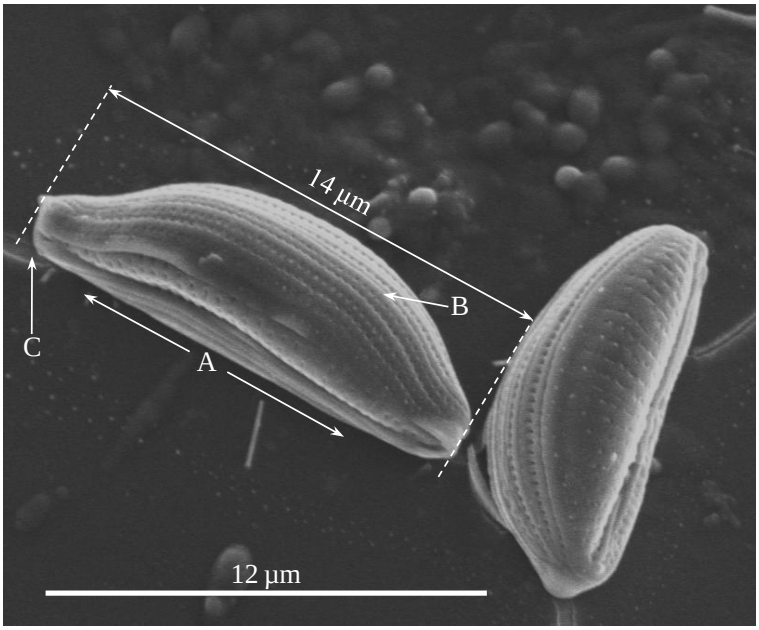

Figure 5-2: Scanning electron micrograph of cells of Amphora coffeaeformis (PCC, Plymouth, UK culture # 545). Cells are in girdle view , (A) = raphe, (B) girdle bands and (C) EPS trail originating from raphe.

The mean dimensions of *A. coffeaeformis* are reported as approximately 14 x 7 µm [16]. Five distinct surface textures with feature dimensions smaller than the mean dimensions of *Amphora coffeaeformis* were designed based on mean cell dimensions given. Textures have a designed height of 6 µm, with 6 µm spacing between features unless otherwise stated. Textures have been designated as ED 1 – ED 5 respectively. In addition to examining attachment point theory, the alignment of blocks within each texture was varied to examine movement of diatoms within texture and orientation of cells with respect to each texture. The arrangement and designation of each texture is shown in Figure 5-3.

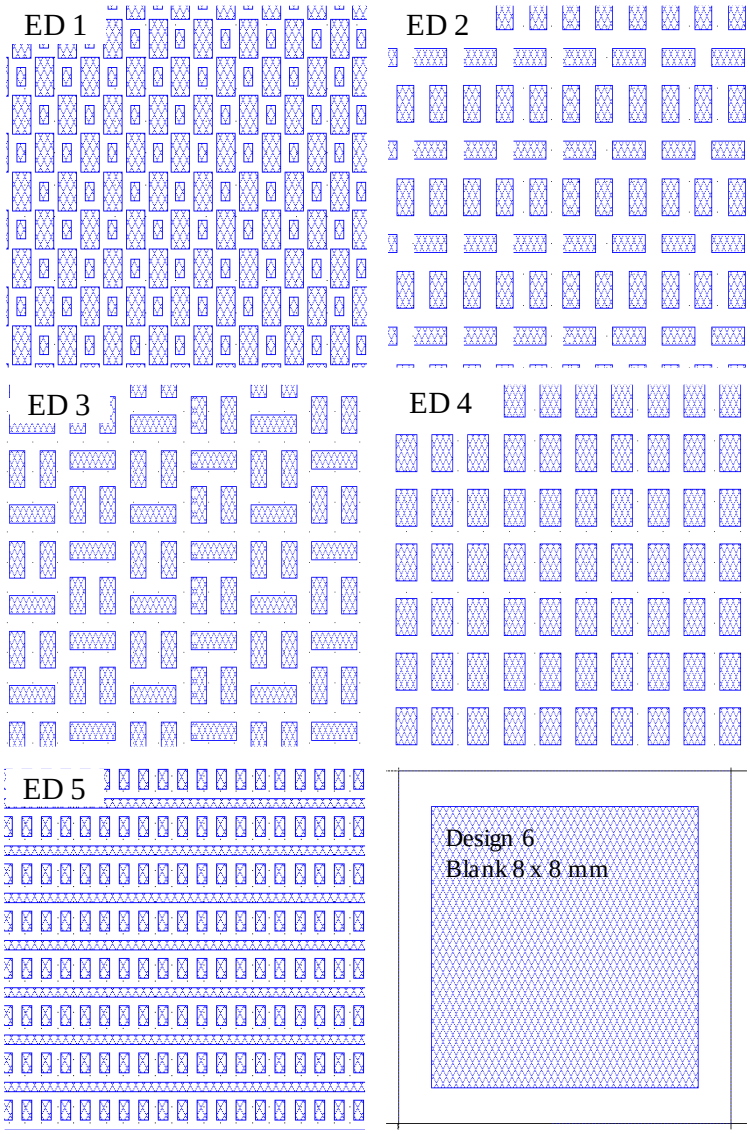

Figure 5-3: Drawing of the layout of the 5 designed surface textures used in this study. All surface features are shaded and project outward from the surface a distance of 6 µm. (Drawings produced by Richard Murphy of the Tyndall Institute, Cork.)

The larger features of textures designated as ED 2 and ED 5 shown in Figure 5-3 are 12 µm in length and 6 µm in width, while ED 1 has 12 x 6 µm features with smaller 3 x 6 µm blocks interspaced between these. ED 4 retains the 12 µm block length but varies block width by dividing the textured area into 3 with each third populated with 6, 8 and 10 µm width features. ED 5 incorporates a continuous feature of 6 µm in width over the area of the textured surface. The larger blocks of ED 3 are 18 µm in length.

5.3.2 *Master fabrication*

The patterns were initially etched in silicon wafers (100 mm Ø, 525 µm thickness). The designs in Figure 5-3 were etched into silicon wafers at the Tyndall National Institute, Cork, under a National Access Programme grant (NAP grant Number 181). An arrangement of patterned surfaces, surrounded by a 2 mm border, was produced as shown in Figure 5-4. This design allowed space for removal of individually textured surfaces for analysis as required. This wafer design produced up to 9 replicas, each of 1 cm^2 area for each designed texture.

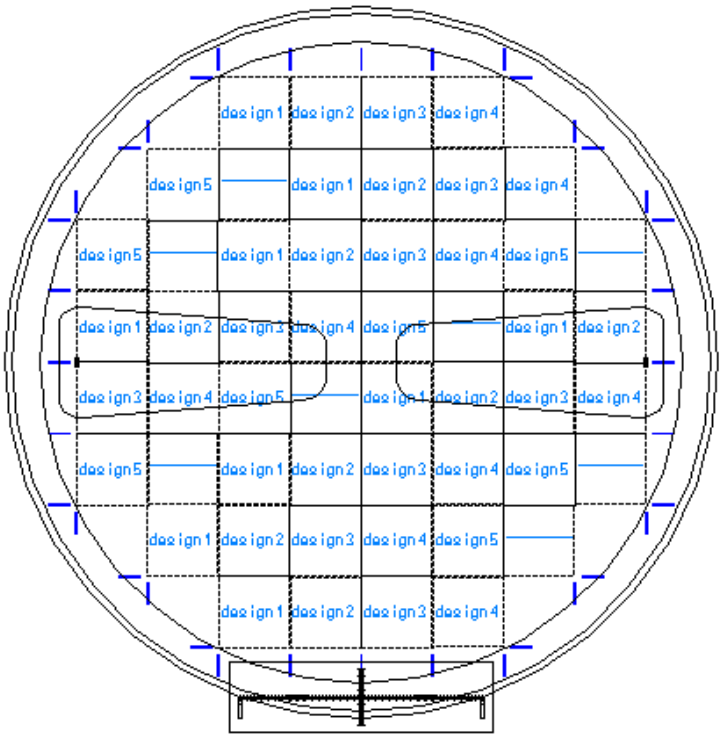

Figure 5-4: Schematic of the layout of the silicon wafer for production of the PDMSe textured surfaces. Nine replicates of the five textures plus a control smooth surface were produced on one PDMSe cast from the master wafer. (Drawing produced by Richard Murphy of the Tyndall Institute, Cork).

5.3.3 *Production of textured PDMSe*

Etched silicon wafers were utilised as a negative template for production of patterned PDMSe. Textured surfaces were generated by curing poly(dimethylsiloxane) elastomer (PDMSe) on the master template. An elastomer kit, SYLGARD 184 (Dow corning, Farnell, Ireland) containing base and curing agent were utilised in this study. Cured elastomer was produced by mixing base resin and curing agent (10:1 w/w).

5.3.4 *Wafer preparation*

The wafer template was prepared for production of textured PDMSe by vapour deposition of a semi fluorinated self-assembled monolayer (SAM) on the cleaned wafer surface using trichloro(1H,1H,2H,2H-perfluorooctyl)silane (TCPFOS). 10 µL of TCPFOS was placed onto absorbent paper and placed into a dessicator in a fume hood. The silicon wafer was then placed in the dessicator, facing away from the filter paper. The dessicator was then evacuated for 1800 s, causing the SAM to deposit on the wafer. (Note: the same dessicator was used exclusively for all experiments involving silanising agents and was no longer suitable for any other experiments).

5.3.5 *Textured PDMSe production*

To produce textured PDMSe from the etched master silicon wafer, the wafer was removed from the dessicator and placed on a flat tinfoil sheet, approximately 20 mm larger in diameter than the wafer. The excess overlap of the tinfoil sheet was then turned upwards to produce a barrier around the wafer. Thoroughly mixed and degassed PDMSe was then poured onto the wafer surface until a uniform layer of PDMSe to a depth of 3 mm over the surface of the wafer was created. The wafer and PDMSe was subsequently transferred to a clean desiccator and a vacuum created to remove any bubbles in the uncured elastomer. PDMSe was cured in a drying oven at 50 ºC for 24 h. Once fully cured the excess tinfoil and PDMSe at the edges of the wafer were removed with a scalpel and the cured PDMSe carefully removed from the wafer. This procedure could be repeated up to 10 times without the need to clean the etched wafer.

5.3.6 *Electron microscopy of produced surfaces*

Surfaces produced by the above methods were checked for defects by SEM. Random textures were removed using a scalpel and mounted on 15 mm diameter Al stubs using carbon tabs. Surfaces were made conductive by Au sputter-coating (Edwards 150B).

5.3.7 *Contact angle measurements*

Wettability of the designed textures were measured using static contact angle using deionised ultrapure water as described in Chapter 2, Section 2.2.10.

5.3.8 *Computational fluid dynamics (CFD) modelling*

CFD modelling of shear stresses and hydrodynamic influences resulting from the presence of microtopography on the surface were conducted by Dr. Yan Delauré of the Energy and Environmental Flow Modelling Group at Dublin City University. The exact dimensions of the surfaces as manufactured were re-drawn by Dr. Delauré in Solidworks 3D CAD design software. The Solidworks drawings of ED 1 used for modelling of flow over surfaces is shown in Figure 5-5.

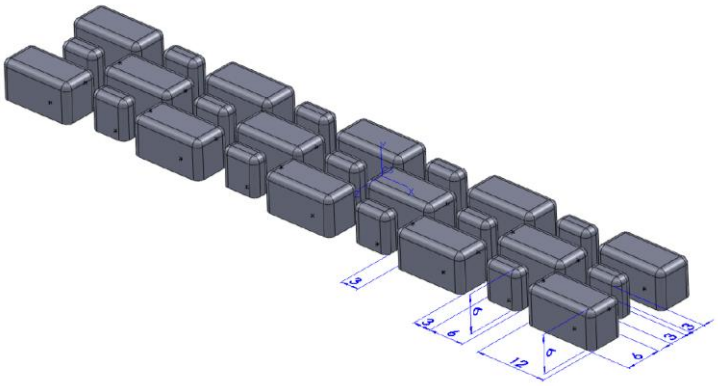

Figure 5-5: A schematic of ED 1 as drawn in Solidworks CAD software for CFD modelling (all dimensions are in µm).(Drawing produced by Dr. Yan Delauré of the Energy and Environmental Flow Modelling Group, Dublin City University)

The steady flow over ED 1 was modelled using a Semi-Implicit Method for Pressure Linked Equations (SIMPLE) solver for incompressible flow. The fluid considered was liquid water at standard atmospheric conditions. The computational domain is sketched in Figure 5-6 and x, y and z are used here for the streamwise, wall-normal and transverse directions. The open boundary at the top was modelled as a pressure condition to allow fluid flow through the surface and avoid acceleration as a result of the reduction in the cross section surface area above the obstacles.

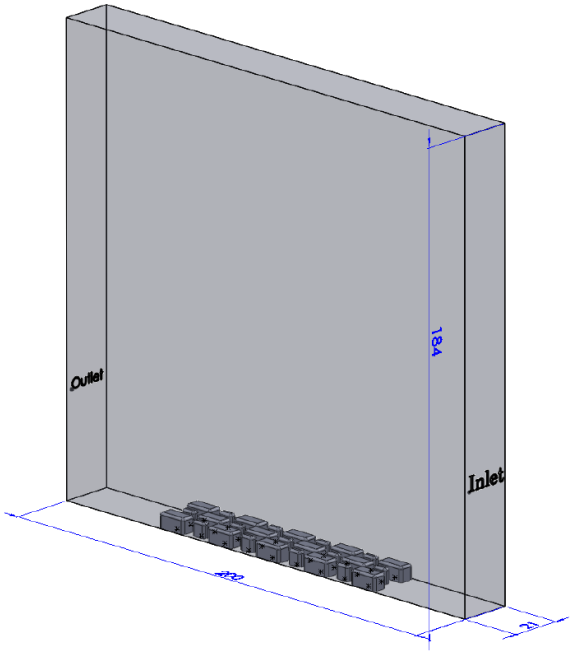

Figure 5-6: The computational domain used for calculation of fluid dynamics across ED 1. (All dimensions are in μm). (Drawing produced by Dr. Yan Delaure of the Energy and Environmental Flow Modelling Group, Dublin City University).

Plane symmetry conditions were set for the front and back surfaces to approximate an infinite array. Based on a free stream velocity $u_0 = 1m\ s^{-1}$ and a body length $L = 1\ m$, the flow Reynolds number $Re: 10^6$ indicated turbulent flow. The velocity at the inlet was calculated from the law of the wall. Since at this Reynolds number the domain extends five wall units ($y^+ = yu_\tau/\nu = 5$) above the bottom surface, the flow was considered to be in the viscous sublayer and the inlet condition was specified according to $u^+ = y^+$. The non-dimensional velocity u^+ was defined by $u^+ = u/u_\tau$ where $u_\tau = sqrt(\tau_w/\rho)$ is the friction velocity and τ_w is the shear stress at the wall. The outlet surface was also specified as a pressure boundary.

The wall roughness height due to the 6 μm surface features was much smaller than the wall unit, estimated as: $23\ \mu m$. This was assumed to have very little impact on the flow within the buffer-layer and the logarithmic layer where most of the turbulent kinetic energy was generated, and the flow was assumed to be dominated by viscous processes. The study was therefore limited to laminar flow and, as discussed above, the forcing was achieved by setting a velocity inlet condition with a viscous sublayer profile.

Two different meshes for CFD modelling were considered. For the initial mesh, the computational domain was decomposed into 1 μm^3 cubic cells. A two level refinement

was applied to cells within $15\ \mu m$ of the bottom surface. This refinedment involved spliting cells evenly in all directions for each level of refinement. The two level refinement therefore yielded cubic cells of length/height/width equal to $0.25\ \mu m$. A bottom and side view of this initial mesh is given in Figure 5-7. A second refined mesh was generated by applying a further one level refinement to cells within $9\ \mu m$ of the bottom. To limit the cell count, the underlying mesh was generated with cells stretched in the x direction with a 1.7 aspect ratio. The initial mesh was made up of : 4×10^6 cells while the refined one included : 6.7×10^6 cells.

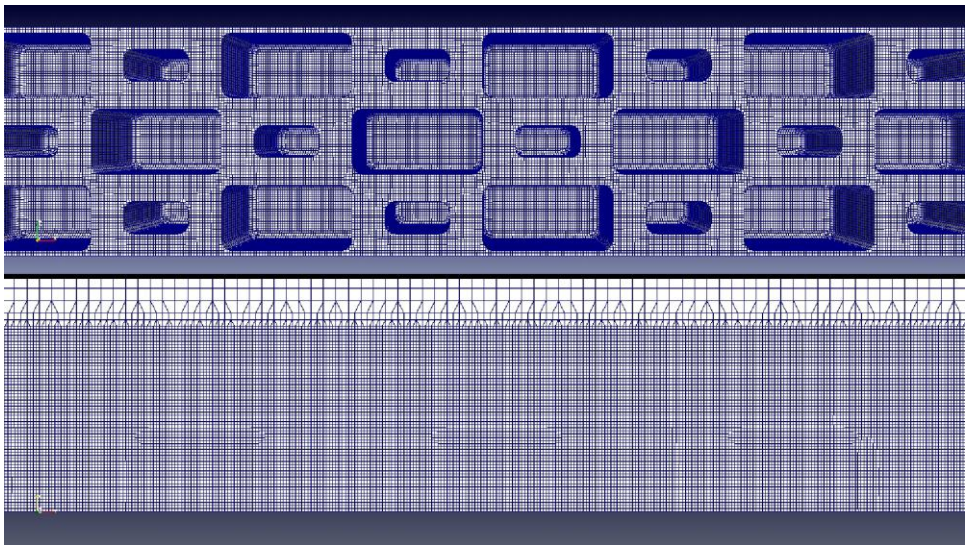

Figure 5-7: Bottom and side view of the initial mesh used for calculation of the hydrodynamic conditions across each feature. (Drawing produced by Dr. Yan Delaure of the Energy and Environmental Flow Modelling Group, Dublin City University).

5.3.9 *Laboratory assays for A. coffeaeformis settlement*

Starter cultures of *A. coffeaeformis* cells were shipped overnight from the Plymouth Culture Collection of Marine Algae (PCC, Plymouth, UK) (cell culture collection number PLY # 547). Cells were cultured in 50 mL of 0.45 µm filtered, autoclaved (121 °C, 15 min), natural seawater collected from Lough Hyne Marine Reserve (LHMR) (Lat N51.50061º; Long W009.29802º ± 6 m) enriched with Guillard's F/2 medium [25]. The growth medium was initially prepared by adding the constituents to 950 mL of filtered seawater and then a final volume of 1000 mL before autoclaving. Later experiments were conducted with Guillard's F/2 medium obtained directly from the Plymouth Culture Collection (PCC, Plymouth, UK). Autoclaved medium was allowed to cool

fully and then agitated on a reciprocating shaker (SSL2, Stuart, UK) for 24 h before addition of cells. The constituents of Guillard's F/2 medium are listed in Table 5-2.

Table 5-2: The main additives of Guillard's F/2 medium used for culturing Amphora coffeaeformis in this study.

Component	Stock Solution	Quantity in 1000 mL	Molar Concentration in Final Medium (M)
$NaNO_3$	75 g L^{-1} dH_2O	1 mL	8.82 x 10^{-4}
NaH_2PO_4 H_2O	5 g L^{-1} dH_2O	1 mL	3.62 x 10^{-5}
Na_2SiO_3 $9H_2O$	30 g L^{-1} dH_2O	1 mL	1.06 x 10^{-4}
Trace metal solution			
$FeCl_3$ $6H_2O$	-	3.15 g	1.17 x 10^{-5}
Na_2EDTA $2H_2O$	-	4.36 g	1.17 x 10^{-5}
$CuSO_4$ $5H_2O$	9.8 g L^{-1} dH_2O	1 mL	3.93 x 10^{-8}
Na_2MoO_4 $2H_2O$	6.3 g L^{-1} dH_2O	1 mL	2.60 x 10^{-8}
$ZnSO_4$ $7H_2O$	22.0 g L^{-1} dH_2O	1 mL	7.65 x 10^{-8}
$CoCl_2$ $6H_2O$	10.0 g L^{-1} dH_2O	1 mL	4.20 x 10^{-8}
$MnCl_2$ $4H_2O$	180.0 g L^{-1} dH_2O	1 mL	9.10 x 10^{-7}
Vitamin solution			
Thiamine HCl (Vit. B1)	---	200 mg	2.96 x 10-7
Biotin (Vit. H)	0.1 g L^{-1} dH_2O	10 mL	2.05 x 10-9
Cyanocobalamin (vit.	1.0 g L^{-1} dH_2O	1 mL	3.69 x 10-10

A commercial algal incubation chamber was unavailable for this study, thus a system consisting of daylight fluorescent lamps (10,000 lux, Amazon.co.uk) in conjunction with a timer and shelf system was used to grow diatom cultures. Cultures were grown in static conditions in 250 mL borosilicate flasks (VWR, Ireland). Growth conditions included a light regime of 16:8 h (light : dark) cycle at a temperature of 20 ± 3 °C and cells were allowed to reach log phase growth (7-10 days) before use in adhesion assays. Cell numbers were estimated by counting in the central area of an improved Neubauer bright-line hemocytometer (0.1 mm depth, BlauBrand, Wertheim, Germany).

Cells were prepared for short-term (3 h) settlement assays on textured surfaces by removing the growth medium and washing twice in artificial seawater (Instant Ocean, Aquarium Systems, Sarrebourg, France), thereby preventing cell division during the course of the experiment. Cells were diluted with seawater to give a chlorophyll *a* content of approximately 0.3 μg ml^{-1}. Cells were removed by gently scraping the cells from the bottom of the flask using a sterile 16 cm rubber cell scraper (Sarstedt, Ireland). The resultant suspension was filtered through 35-μm stainless steel gauze in order to

produce a suspension of mostly single cells before use in settlement assays. For longer growth assays on textured surfaces, cells were re-suspended in 250 mL of fresh medium. Cells and fresh medium were then added to undivided PDMSe casts from the master wafer in borosilicate crystallising dishes (140 mm diameter, Schott Duran, Germany). Cells were then returned to original static growth conditions.

5.3.10 *Laboratory assessment of A. coffeaeformis attachment*

Short-term (3 h) adhesion assays for *A. coffeaeformis* on textured surfaces were carried out by modification of the assay reported by Holland and co-workers [26]. Textured PDMSe surfaces produced from the master wafer were rinsed with deionised water and dried before division into standard microscope slide sized (25 x 75 mm) sections with a scalpel blade. Each PDMSe cast thus produced full sections, each containing at least duplicates of each textured surface and smooth control surfaces. After division, the segments were placed in clean dry 127.8 x 85.5 mm non-treated sterile quadriPERM® cell culture dishes (Nalge Nunc International, Rochester, NY, USA) to which 7 mL of prepared diatom cell suspension was added. Cells were allowed to settle under culture conditions without agitation. Surfaces were then removed from the culture dishes and rinsed by dipping twice sequentially in beakers containing 50:50 deionised H_20/filtered seawater and finally just deionised H_20. This process removed any loosely bound cells and any remaining salt crystals. Surfaces were then fixed prior to analysis with gluteraldehyde (2.5% v/v, Sigma-Aldrich, Tallaght, Dublin) in deionised H_2O.

5.3.11 *Enumeration of attached A. coffeaeformis cells*

Visible cells were enumerated using a combination of light microscopy and SEM. Light microscopy was carried out using an Optika microscope (Optika microscopes, Ponteranica, Italy) equipped with phase contrast at x400 magnification. Sample preparation for SEM analysis was conducted as described previously (Section 5.3.6). Diatom cells were counted in 3 x 100 µm wide transects across each textured surface (ED 1 – ED 5) from three separate randomly chosen replicates on each wafer. Transect 1 was from the central portion of the design while transects 2 and 3 were approximately 0.25 cm from the edge of each designed surface. The described methodology is shown schematically in Figure 5-8.

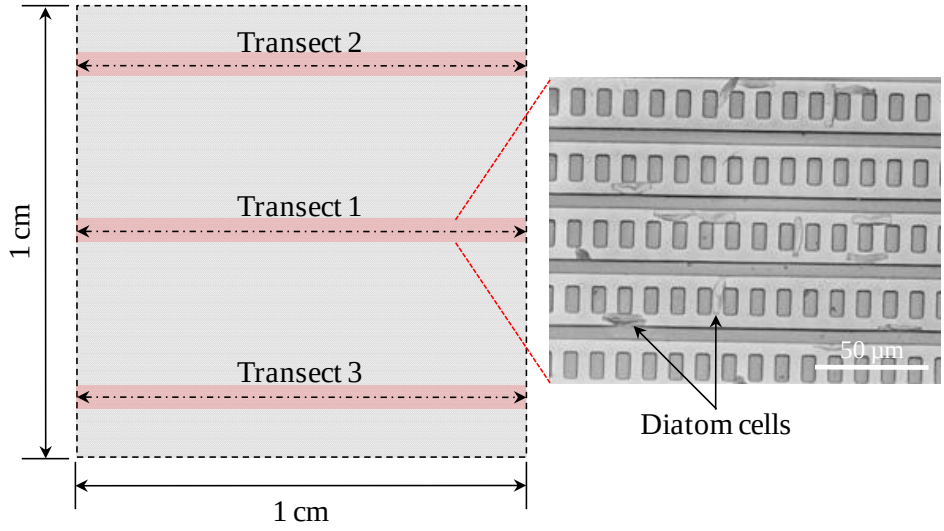

Figure 5-8: Schematic of the methodology used for enumeration of Amphora coffeaeformis cells in transects on each textured surface.

5.3.12 *Field assessment of textured surfaces*

Assessment of the influence of textures ED 1– ED 5 on the settlement on a natural diatom community was carried out by field exposure of complete PDMSe wafer casts containing all surface textures in the marine environment. Field-testing was carried out at Lough Hyne Marine Reserve (Research permit # R36 – 38/10). A number of field moorings had previously been deployed for purposes of continuous monitoring of water quality within the reserve and examination of the spatial variation in biofouling of surfaces (See Chapter 2 for site descriptions). These moorings were modified to allow attachment of PDMSe textured surfaces. Environmental data on a number of parameters were collected simultaneously using YSI 6600 V2 (2) (YSI Hydrodata, UK) multi parameter sondes, measuring pH, conductivity, salinity, temperature, turbidity, depth, dissolved oxygen (See chapter 2 for further details).

PDMSe wafer casts containing textured surfaces were fitted within Petri dish lids (92 mm diameter), adhered using silicone adhesive, and the Petri dish lid bound to a transparent PMMA backing panel also using silicone adhesive (350 x 250 mm). Panels were suspended horizontally and vertically in the water column. Results are reported for surfaces exposed for 7 d from the 3rd to 10th April 2011 and for 14 d from the 1-14th June 2011.

5.3.13 *Preservation of microbial biofilms*

Biofouling on textured surfaces was preserved by immersion in filtered (0.45 µm) natural seawater to remove cells and debris that had weakly settled on the surface. Surfaces were immersed once in a container of deionised water, to remove salt crystals and finally in Lugol's (iodine/potassium iodide) solution (Sigma-Aldrich Ireland Ltd) for 120 s before transportation to the laboratory for analysis.

5.3.14 *Diatom frustule enumeration*

Diatom frustules on the surface of each design were enumerated using a light microscope (x400 magnification) and using SEM as per Section 5.3.6. In order to check accuracy of LM counts, a number of designs were counted in transects using both LM and SEM. No differences were observed for counts using both methods unless high numbers of small centric diatoms (2-5 µm diameter) such as *Paralia* or *Minidiscus spp.* were present on the surface. Transects across the complete area of each design were made, using the surface texture as a guide. Any diatom frustules crossing or touching the edge of the line were included in the count. Three transects were made at approximately 0.25 cm from each texture edge and in the middle of each texture. Three replicates were chosen at random from each wafer cast to be enumerated. Diatom genera present were identified from Round and co-workers [27].

5.3.15 *Statistical analysis of settlement*

Intact frustule counts were square-root-transformed to ensure normality of variance and analysed with 1-way ANOVA followed by the Tukey HSD *post hoc* test using statistical software SPSS statistics 17.0.

5.4 **Results and discussion**

A number of methods of producing microtopographic surface features were assessed for cost and ability to control surface features in this study. Ultimately, photolithography was the method of choice despite the costs involved. This method offered greatest control over features sizes and the absence of defects resulting from manufacturing processes compared with laser texturing and polymer printing.

5.4.1 *Pattern fidelity*

Textured PDMSe surfaces were produced from silicon wafers as part of the agreement with the Tyndall Institute under the NAP 181. However, due to inconsistent quality of the textured surfaces and texture defects large surface areas, the initial patterned wafers were discarded, and a new set of silicon master wafers fabricated. Textured surfaces were subsequently produced in the lab at Dublin City University. SEM examination showed that textured surfaces subsequently produced were defect free over >99% of the texture, with the exception of ED 1 where the smaller features of this design were occasionally absent from the texture. Texture defects involving pairing and sagging of the individual PDMSe blocks also observed as described by Whitesides and co-workers [28]. Figure 5-9 demonstrates an example of the problems encountered in fabricating controlled surface texture from the original master wafers. In this example, the surface features have been retained in the silicon wafer, in the process separating from the elastomer surfaces, resulting in a "footprint" of the original texture without the desired height. Retention of PDMSe within the silicon wafer surface necessitated cleaning of the master wafer surface using Piranha etch (sulphuric acid and hydrogen peroxide) for 2 h followed by deionised water.

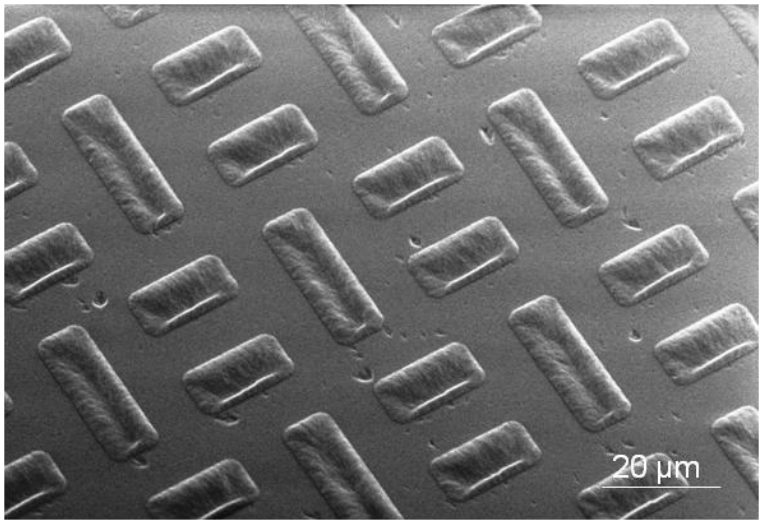

Figure 5-9: Scanning electron micrograph of a defective surface texture. The PDMSe blocks are only represented by a footprint as the polymer has been retained within the silicon wafer used to create the texture.

Accurate productions of textured PDMSe surfaces are shown in Figure 5-10. As can be observed, all larger features were faithful to the designed surfaces, however defects were observed irregularly in ED 1 where the smaller (6 x 3 µm area) features were not reproduced. It is suggested that this may relate to the entrapment of microscale gas bubbles within the master wafer although thorough de-gassing of PDMSe was always completed. An area of ED 1 with defects is shown in Figure 5-10.

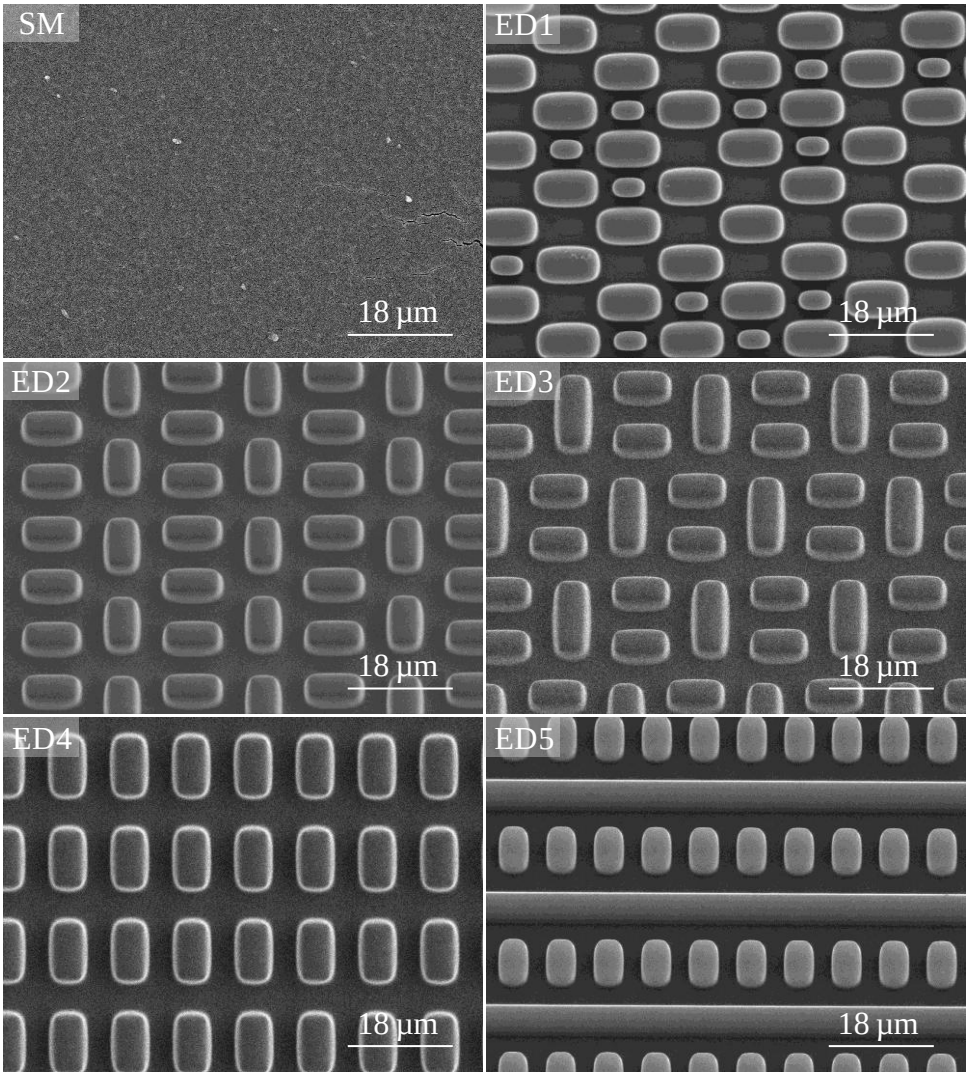

Figure 5-10: Scanning electron micrographs of the textured surfaces produced in PDMSe.

The principle dimensions and calculated planar areas of produced features are shown in Table 5-3

Table 5-3 Principle dimensions of the individual surface textures as produced. All designs were produced over an area of 1 cm^2 apart from ED 4A-C, which were produced on 0.33 cm^2.

	ED 1	ED 2	ED 3	ED 4A	ED 4B	ED 4C	ED 5	SM
Feature height (µm)	6	6	6	6	6	6	6	-
Planar surface area (cm^2)	1	1	1	0.33	0.33	0.3	1	0.8
Recessed fraction	0.375	0.72	0.65	0.66	0.619	0.58	0.4	NA
Bas-relief fraction	0.625	0.277	0.35	0.33	0.38	0.416	0.6	NA
Surface area ratio	2.875	1.833	2	2	2.14	2.25	1.4	NA
Total surface area (cm^2)	2.875	1.833	2	0.66	0.706	0.742	1.4	1

In the above table, the terms recessed fraction and bas-relief refer respectively to the surface area of the texture that is below the feature height and to the surface area of features that project above the background.

5.4.2 *Wettability of textured surfaces*

Sessile drop measurement of the CA of each texture indicated decreased wettability (increased CA) compared to that of a smooth PDMSe surface. This was expected and can be attributed to incomplete wetting of the surface beneath the liquid droplet as per the Cassie-Baxter wetting model of surface wetting [29]. Carman and co-workers reported a similar result from measured water contact angles on the structured PDMSe fabricated, where an increase in CA of 20% was measured over a smooth surface [4]. Petronis and co-workers also reported similar results from investigation of textured silicon elastomers on settlement of *Balanus improvisus* [12]. The latter study utilised both a Wilhemy plate and sessile drop technique to analyse surfaces, however as the texture was only producible on one surface in the present study, the Wilhemy plate technique was not utilised. The increased contact angles of textured surfaces compared to a smooth PDMSe surface are shown in Figure 5-11.

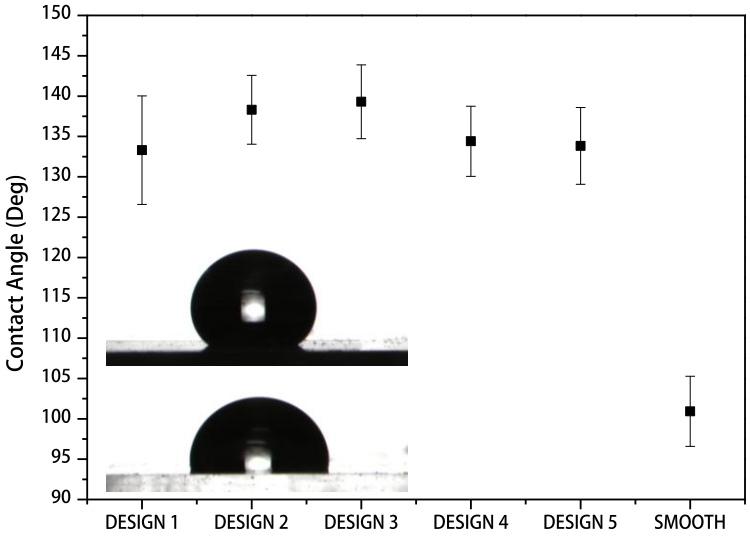

Figure 5-11: Graph of the contact angle on textured surfaces ED 1 – ED 5 as measured with a sessile drop of deionised water (error bars ± 1 SD of the mean, n = 3). The digital images (inset) show droplet formation on the textured surface (upper image) and a smooth PDMSe surface (lower image).

The wetting regimes of a textured surface such as those produced in the present work where air pockets are trapped beneath the droplet are described by the Cassie-Baxter equation for a wetting model:

$$\cos\theta_{\mathrm{CB}} = r_f f \cos\theta_{\mathrm{Y}} + f - 1 \qquad \text{Equation: 5-1}$$

Where θ_{CB} is the apparent contact angle which corresponds to the stable equilibrium state, r_f is the roughness ratio of the wet surface area, θ_{Y} is the Young contact angle and f is the fraction of the solid surface area wet by the liquid. This wetting regime always increases the contact angle of a textured surface compared to a smooth surface. Thorough wetting of the textured surfaces prior to short-term settlement assays ensured that differences in cell settlement behaviour caused by initial differences in CA were minimised.

However, long-term growth assays of *A. coffeaeformis* cells for 84 h on surface textures indicated that respiration rates and the gaseous exchange of actively dividing cells were influenced by surface textures. Smooth PDMSe surfaces developed large gaseous bubbles on the surface after growth assays of 84 h. Due to the nature of the surface and lack of hydrodynamic shear forces, these bubbles continued to develop until cell growth was affected in the surface areas directly under the bubbles. It is known that bubble formation on a solid surface immersed in water is dependent on surface heterogeneities,

effecting both bubble nucleation and formation [30]; however, the effect of this phenomenon on respiring algal cells and for AF studies has not been reported in detail. The effect of surface texture on gas bubble formation is shown in Figure 5-12 where bubble entrapment near the surface of textured PDMSe can be observed. Larger bubbles attached to smooth control surfaces are clearly seen while smaller bubbles suspended above the surface, presumably adhered to the feature tops of surface textures are also evident.

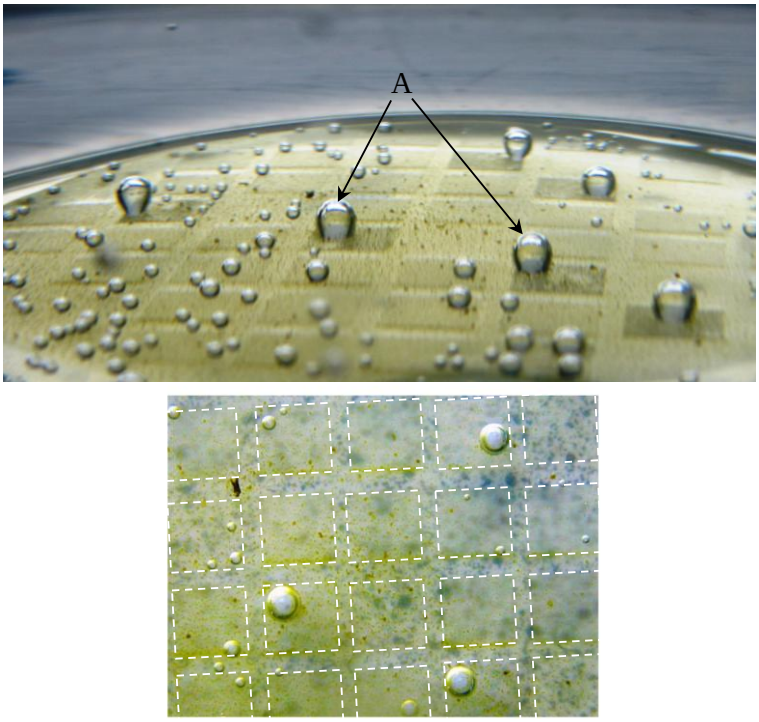

Figure 5-12: A digital image of an adhesion assay involving Amphora coffeaeformis cells growing on textured surfaces for 84 h. Bubbles resulting from respiration are visible on smooth controls (A). The lower image shows a plan view of the textured surface in which the textured areas have been outlined (dotted line).

Under natural conditions, the entrapment of gas bubbles as shown in Figure 5-12 is unlikely, as turbulent mixing over the surface would ensure adequate gas exchange. However, this effect has not been previously reported to the author's knowledge and is an important consideration when designing assays for testing growth of photosynthetic cells over longer experimental periods. The observation of entrapped bubbles was not be examined further, although future studies should investigate this in detail on textured surfaces, perhaps using AFM [30]. Therefore, laboratory assays are only reported for those of 3 h duration in the present work.

CFD analysis of textures was conducted to understand the possible influences of surface texture on hydrodynamic flow over the surface, and in particular any increase in shear stress created by the topographic features. The results here are presented for ED 1, as this texture had the best anti-settlement performance against *A. coffeaeformis*.

CFD analysis of the shear stress resulting from laminar flow of the designed surfaces indicated that a maximum shear force was present on the edges of designed features. Results shown correspond to the refine mesh unless otherwise stated. The wall shear stress contour plots over the bottom wall and textured surfaces shown in Figure 5-13 clearly indicate an increase in wall shear stress over the top surfaces of the designed texture and in particular over the fore and aft edges of the PDMSe features. Between the features, slow flowing cavity vortices are set up but these generate very small velocity gradients at the wall and stresses remain very low. The flow channelled between the rows of micro-structures is also too slow to induce any significant shearing. Also it should be noted that any such streamwise flow channelled between the rows would disappear if the flow was incident at an angle to the axis of the array.

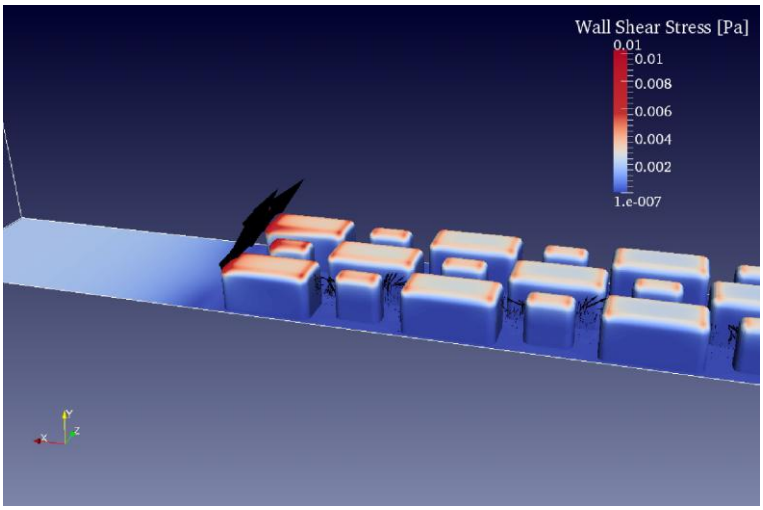

Figure 5-13: Contour plot of magnitude of Kinematic Wall Shear Stresses ($\tau_w = \nu|E \cdot \tilde{n}|$) over bottom surfaces and micro structures. E is the rate of strain tensor.(Drawing produced by Dr. Yan Delaure of the Energy and Environmental Flow Modelling Group, Dublin City University).

A change in the wall shear stresses along a streamwise curve, which follows the contour of bottom wall and texture boundaries, is shown in Figure 5-14. In this case, results obtained with both meshes are given showing reasonable grid independence. The plot clearly shows a significant increase in the stress over the top surface of the surface

features by comparison with the stress over the flat part of the bottom wall both upstream and downstream of the features. If the leading edge and trailing edge structures are ignored the increase in shear stress ranges from 38 % to 157 %.

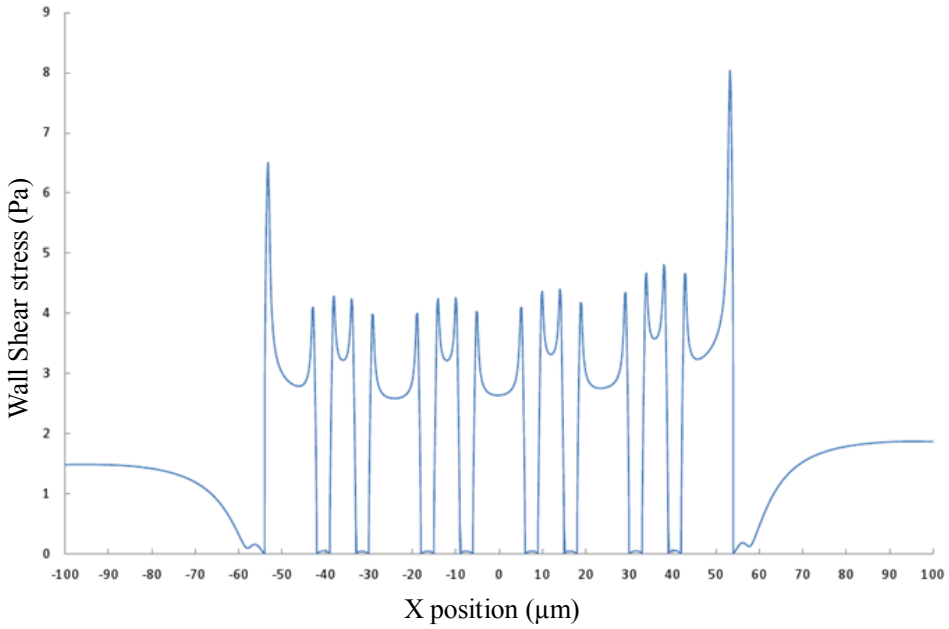

Figure 5-14: *Magnitude of Dynamic Wall Shear Stresses ($\tau_w = \mu|E \cdot \tilde{n}|$) over the bottom wall and and microtexture of ED 1 along the symmetry plane for the two meshes considered.*

5.4.4 *A. coffeaeformis settlement on textured surfaces*

Adhesion and settlement of the diatom species *Amphora coffeaeformis* has been examined on a variety of surfaces prior to the present study. These surfaces include non-solid gel surfaces [31], micro-textured polyimide biomimics [16], patterned self-assembled monolayers (SAMs) [32] and smooth PDMSe [26]. Superhydrophobic coatings (SHCs) are also reported to have been tested against an *Amphora* sp, though not specifically *Amphora coffeaeformis* [14]. Of tested materials and textures, non-solid gels had no appreciable effect on diatom adhesion and cells generally adhered more strongly to hydrophobic surfaces, including PDMSe (115°), than to glass. On patterned self-assembled monolayers (SAMs) of increasing hydrophobicity (water contact angles of 20–115°) *Amphora coffeaeformis* cells were removed in lower numbers on the most hydrophobic surfaces. However, Scardino and co-workers reported attachment of an *Amphora* sp. was lower on three tested SHCs than on glass surfaces.

In this study, laboratory-based 3 h settlement experiments indicated a reduction permanent adhesion of diatom cells to ED 1 compared to the other textured surfaces produced. However, the reduction was not significant when compared to a smooth control surface, indicating that *A. coffeaeformis* preferentially settled on textured surfaces. The results of adhesion assays of *A. coffeaeformis* cells to the textured surfaces after 3 h are presented in Figure 5-15.

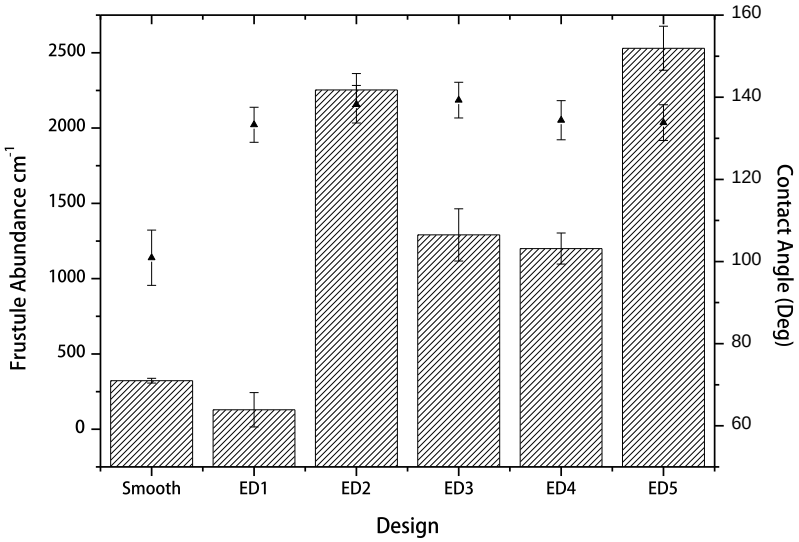

Figure 5-15: Mean cell counts of adhered Amphora coffeaeformis cells after a 3 h adhesion assay on produced engineered surfaces. ED 1 and the smooth control exhibited reduced adhesion compared to the other produced surfaces.

As shown in Figure 5-15, cell abundance was greatest on both ED 2 (Mean = 2252 ± 108 cells cm^{-2}) and ED 5 (Mean = 2530 ± 146 cells cm^{-2}), while settlement was reduced below that of a smooth surface on ED 1 (Mean = 129 ± 114 cells cm^{-2}). Representative light micrographs of diatom cells on both ED 2 and ED 5 are shown in Figure 5-16.

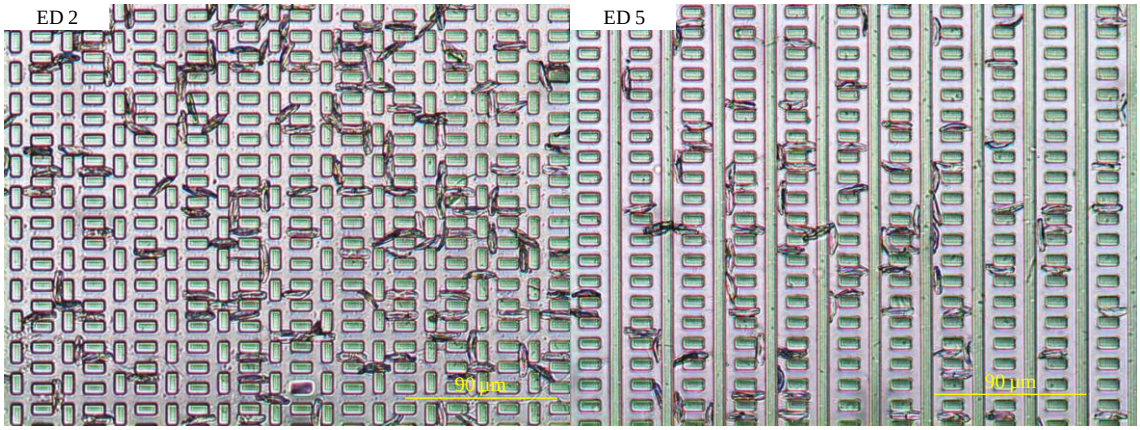

Figure 5-16: Representative digital images of diatom cells adhered to textures ED 2 and ED 5. Cells are visible and aligned with surface features.

Although ED 1 had the lowest number of adhered cells, the anti-settlement performance could have been improved as cells frequently settled within fabrication defects in the texture. Textured areas in which defects caused by the absence of the smaller (6 x 3 µm) surface features allowed diatom cells to adhere diagonally between the larger surface blocks with one raphe in contact with the surface. A representative light micrograph of cell adhesion to ED 1 is presented in Figure 5-17.

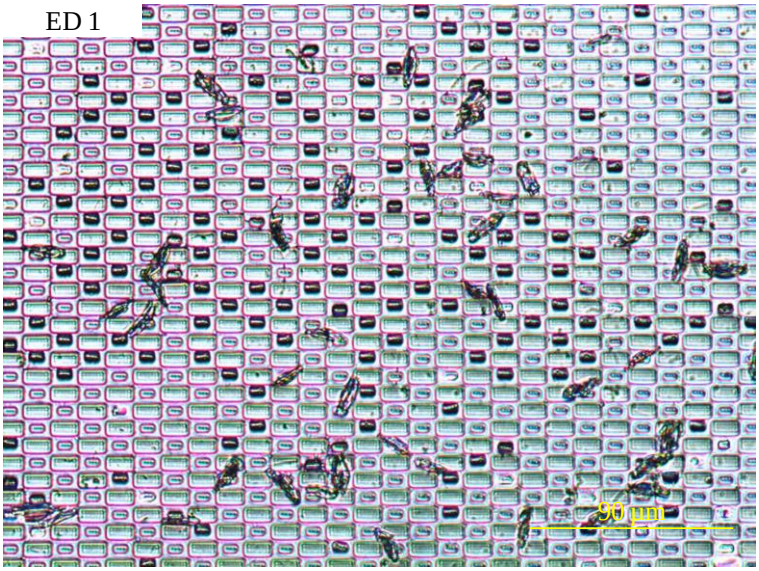

Figure 5-17: Representative digital light micrograph of settlement of Amphora coffeaeformis to ED 1. The smaller surface features are visible and on occasion have twinned with larger surface features as indicated by the darker surface features.

These results suggest that cell of *A. coffeaeformis* may preferentially settle between surface topographic features perhaps to gain protection from hydrodynamic shear forces, however the effects cell orientation on adhesion strength are unknown. ED 1 also represents the greatest disparity between individual features within a texture, and diatom cells encountering the surface may sense this instability and thus not permanently adhere to the textured surface. An additional consideration may involve instability of the 3 µm by 6 µm wide block, resulting in movement of the block during settlement. A representative Scanning electron micrograph of the adhesion pattern of *A. coffeaeformis* on texture defects of ED 1 is shown in Figure 5-18, where the orientation and adhesion of the cells using one raphe can be observed.

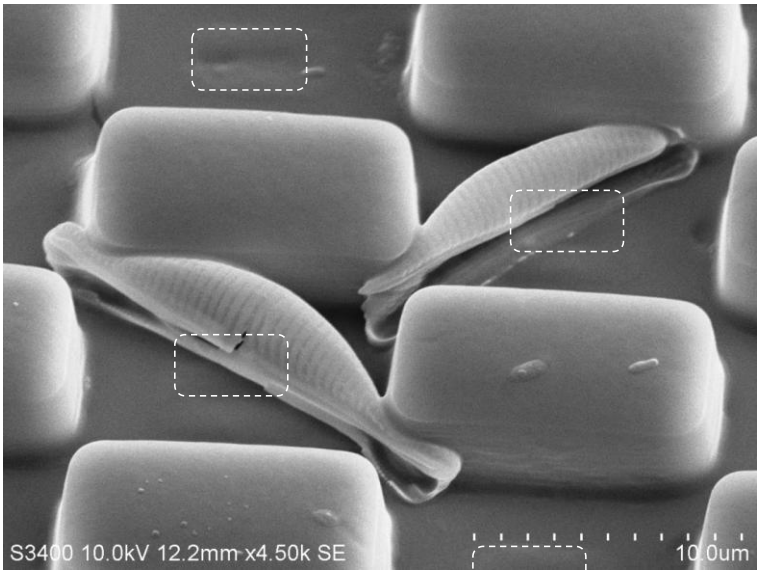

Figure 5-18: Scanning electron micrograph of cells of A. coffeaeformis settled in fabrication defects in the texture of ED 1. The texture has not been completely reproduced from the wafer and the smaller PDMSe features (represented by the dotted lines) are absent from the produced texture.

Analysis of a larger surface area of the texture as shown in Figure 5-19 demonstrates that the majority of cells attached to ED 1 are settled in spaces created by the absence of features within surface defects.

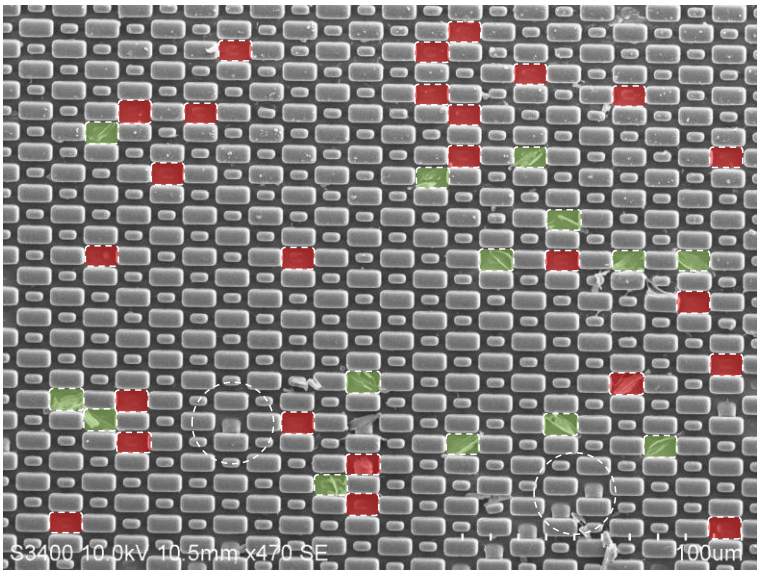

Figure 5-19: Scanning electron micrograph of a larger area of ED 1 demonstrating areas of missing 6 x 3 µm features (red) and where the texture defect resulted in cell settlement (green). The circled areas indicate instances of failure of the block to self-support (twinning of the features).

To assess differences in diatom settlement patterns in relation to texture features, 100 cells were counted from each textured surface. These were then categorised as situated either on top or between surface features. An example of the settlement of diatom cells categorised as being either on top or between texture features is shown in Figure 5-20.

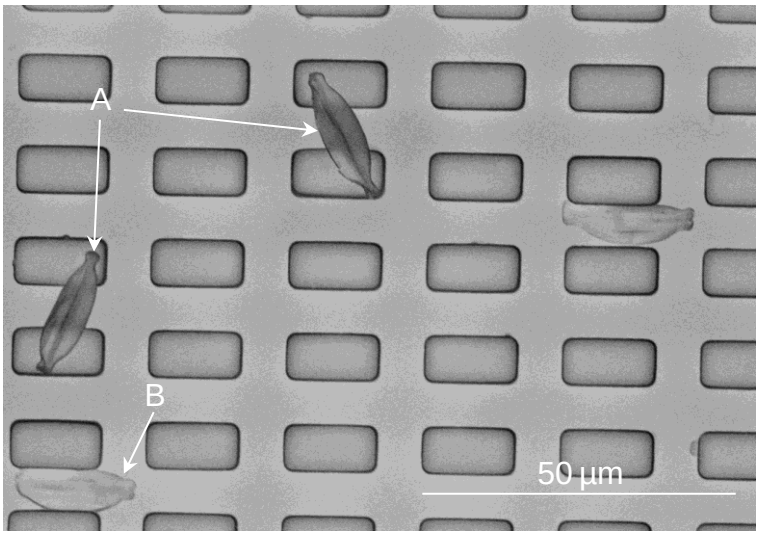

Figure 5-20: Scanning electron micrograph of ED 4 illustrating A. coffeaeformis adhesion on top (A) and between surface features (B).

The results of this analysis are presented in Figure 5-21, in which it can be seen the majority of diatom cells adhered between surface features rather than on feature tops.

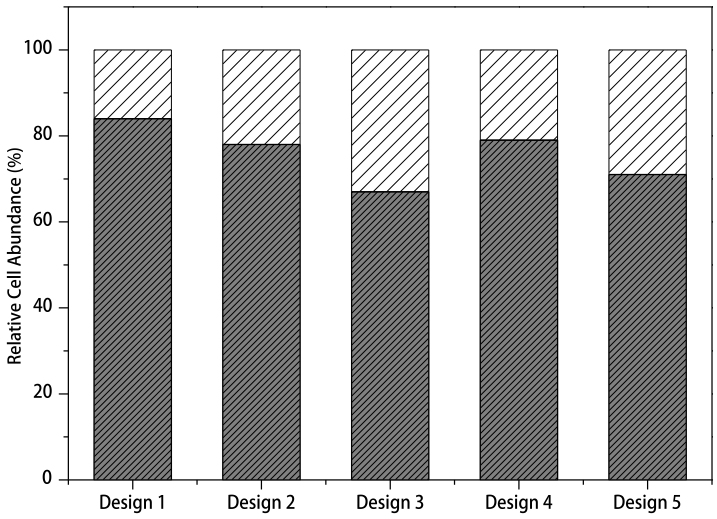

Figure 5-21: Graph of relative abundance of total diatom cells of A. coffeaeformis categorised as either remaining on surface features or between topographic features (Dark hatching = cells between features, light hatching = between features).

Cells were observed to settle between surface features at defects in ED 1 as discussed. In all other surface textures, the majority of cells settled between the surface features. Cells not between surface features may have been actively exploring the surface at termination of the experiment or were weakly adhered and easily disrupted from the original settlement position. Evidence of cell removal was noted when an adhesive plaque composed of EPS was observed on the surface but the cell was no longer apparent. An example of this is shown in Figure 5-22.

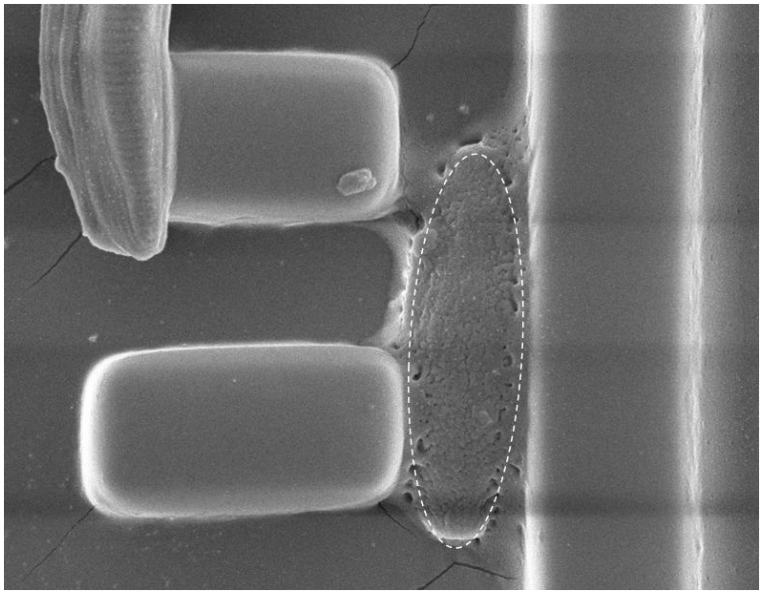

Figure 5-22: Scanning electron micrograph showing an adhesive EPS "footprint" of A. coffeaeformis (circled) indicating that a cell has been removed from the surface.

Cells adhered between features are more likely to have settled permanently to the surface, perhaps availing of protection from shear forces provided by the texture. Whether cells remain on top of features of between surface features has important implications for the number of attachment points and consequently for strength of adhesion and protection from shear forces.

5.4.5 *Comparison of observed diatom settlement patterns to theoretical models*

Initial results from adhesion assays involving *A. coffeaeformis* in laboratory studies have indicated that ED 1, consisting of a texture containing two distinct features, a large 6 x 12 µm block separated by smaller 3 x 6 µm blocks, can reduce settlement of this species. All other tested surface textures increased diatom adhesion compared to a smooth (non-textured) surface. The difference between ED 1 and the other tested

designs is that the spacing between features on this surface is sufficiently small to prevent cells from settling between features as on other surfaces. Cells of *A. coffeaeformis* were also observed to settle in texture defects, demonstrating ability to align between surface features. ED 2 and ED 5 have a slightly larger spacing and cell abundance reflects this as adhesion is significantly increased on these surfaces.

To gain a greater understanding of mechanisms underlying the observed settlement differences, the data were fitted to the theoretical models currently under development for the settlement and inhibition of *Ulva* spores and other microbial cells on topographically engineered surfaces. The models currently proposed include the Engineered Roughness Index (ERI) and an improved ERI_{II} [5] [33]. The ERI is a dimensionless ratio that demonstrates a negative correlation between attachment of zoospores of the algal species *Ulva linza*, wettability and texture of a surface. As such, larger ERI values should be indicative of reduced settlement of motile zoospores such as *Ulva*. The ERI combines a number of terms thought to be important for settlement of microorganisms, including Wenzel's roughness factor (*r*), the degrees of freedom of a texture (*df*) and the depressed surface area fraction ($1-\Phi_s$). The modified attachment model, ERI_{II}, substitutes the degrees of freedom (*df*) of the pattern with the number of distinct features in the pattern (*n*) [33]. Diatom settlement data from this study were fitted to both models for comparison. The original ERI is expressed mathematically as:

$$ERI_1 = (r \times df) / f_D \qquad \text{Equation 5-2}$$

Where *r* is the Wenzel roughness factor, f_D is the depressed surface fraction when compared to the planar projected surface area, and *df* refers to the degrees of freedom available to a settling cell (in the case of the ERI, motile spores of *Ulva*). This last term relates to the tortuosity of the surface, or the ability of a cell to follow linear surface features and attempts to quantify the degree of mobility of a cell on the surface. The degree of freedom of a surface containing recesses of a continuous and intersecting grid (movement in both x and y directions) is 2 while textures with continuous linear features have a degree of freedom of 1. The modified ERI_2 is expressed as:

$$ERI_{\mathrm{II}} = (r \times n)/(1 - \Phi) \qquad \text{Equation 5-3}$$

The degrees of freedom of the pattern have been replaced by the number of distinct features in the pattern (*n*), while the term $(1 - \Phi)$ refers to the depressed surface

fraction determined by the ratio of the depressed surface area between features and the projected planar surface area [34].

Fitting the data obtained from the this study to both of the above attachment models, resulted in no correlation between attached diatom cells and the theoretical attachment rates predicted by ERI models. In particular, the smooth PDMSe exhibited much lower adhered cells than would be expected if the adhesion of *A. coffeaeformis* were in agreement with prediction models. In contrast, ED 5 showed much higher adhesion rates than would be expected using the predictions resulting from the models. Figure 5-23 illustrates attachment of cells of *A. coffeaeformis* to textured surfaces in this study compared with those predicted by the ERI models.

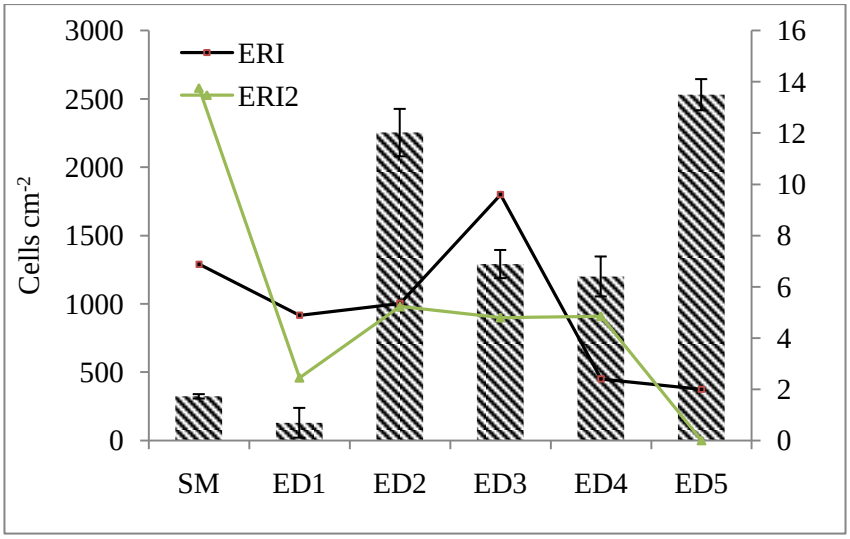

Figure 5-23: Graph of settlement Amphora coffeaeformis on textured surfaces compared with values predicted by the Engineered Roughness Index (ERI) models.

It is suggested that the inability of the ERI models to predict settlement patterns of *A. coffeaeformis* may result from fundamental differences in the attachment mechanisms and settlement behaviour of diatom cells when compared with motile zoospores of macro-algae. One of the most fundamental differences is that macroalgal zoospores are quadriflagellate, actively exploring a potential settlement site prior to physically contacting the surface [35, 36]. In contrast, diatom cells, lacking flagella or other obvious means of propulsion in the water column, are reported as passively contacting a surface. Diatoms become motile once in contact with a surface and then explore the surface before permanent adhesion [24, 37]. This fundamental difference may mean that theoretical

models capable of predicting settlement choices among algal spores may have no validity for predicting settlement choices among diatoms [35].

Another fundamental difference between diatoms and macro-algal spores such as Ulva is found in the presence and absence of a cell wall. Motile *Ulva* zoospores do not have a cell wall when in exploratory form. Zoospores only develop a cell wall once permanent adhesion to the surface and loss of the flagella has occurred [35]. This cell wall is somewhat flexible and may be able to conform to surface texture, although the degree of deformation possible without damage to internal organelles is not precisely known. Diatoms however are encased in a rigid silica frustule that may lessen the impact of external forces caused by interactions with surface texture. Recent examination the effects of sustained force on deformation of the frustule have highlighted the strength of this structure [38]. While mechanical strength and size were inversely related within a single species and between different species examined, the magnitude of the forces that frustules can withstand (equivalent to 100–700 tonnes m^{-2}) are remarkable. Therefore, stresses induced by surface texture on the cell wall of a diatom may not be sufficient for active discouragement of settlement.

Despite extensive laboratory-based examination of the effects of surface texture on recruitment of diatoms to surfaces, few reports of the influence of surface texture on diatom adhesion to texture in field studies are available. Field exposure was conducted on all textures in this study to examine the effects of textured PDMSe surfaces on the recruitment of a natural diatom community. All textured surfaces were fouled by bacteria and diatoms after 7 d exposure at Lough Hyne. The results of transects across the surface are presented in Figure 5-24.

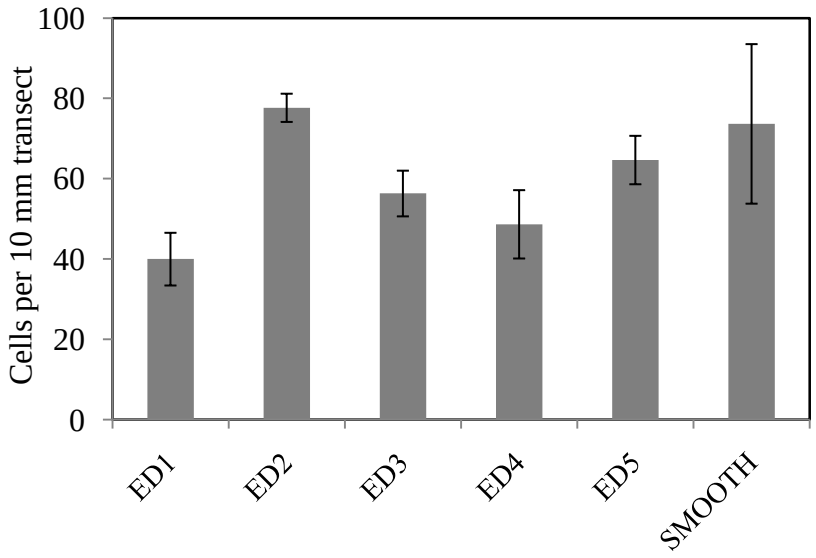

Figure 5-24: Total diatom frustules from the mean of three 1 cm length transects across each engineered design after 1-week exposure in Lough Hyne marine reserve (error bars represent ± 1 standard deviation). There is a significant difference (α= 0.05) between ED1 and the smooth surface, and between ED 2 and ED 4 as illustrated by a 1-way ANOVA followed by Tukey's Posthoc analysis.

Two diatom species, identified as *Cylindrotheca closterium* (Ehrenberg) and *Licomphora flabellata* (Greville), were initial colonising species on all textures. Figure 5-26 illustrates initial attachment of these two species to ED 4 within 7 d of immersion.

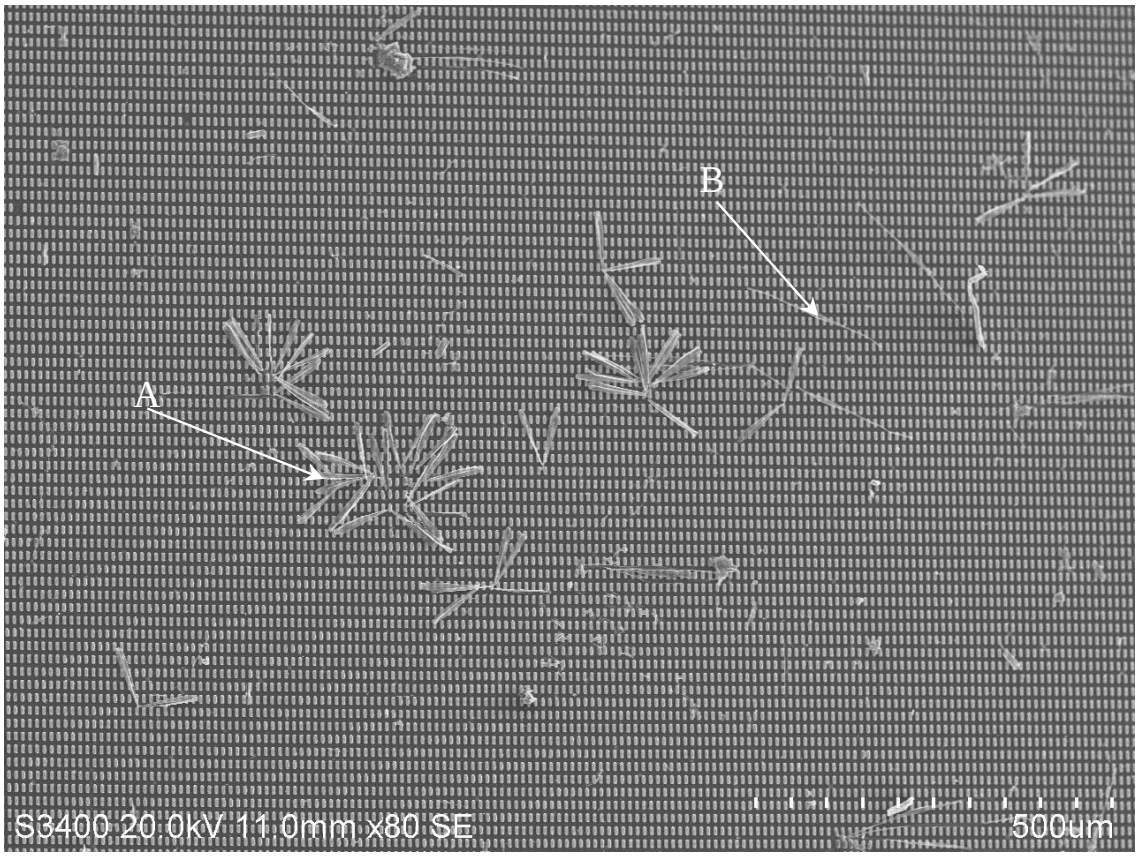

Figure 5-25: Scanning electron micrograph of ED 4 demonstrating colonisation of surface textures by L. flabellata (A) and C. closterium (B).

C. closterium and *L. flabellata* are reported as early colonisers of immersed surfaces and appear capable of colonisation prior to surface modification by a bacterial layer. *C. closterium* is described as an epipelic species (living freely on sediment surfaces) and a copious producer of EPS [39]. This species is attracting greater scientific interest due to the large-scale phenomenon of mucilage aggregate formation in the northern Adriatic Sea and other locations worldwide [40] and the EPS isolated from individuals has recently been examined in detail using AFM [41].

Although often regarded as solitary, many of the cells of *C. closterium* from this field experiment were observed to attach to the surface at a common EPS mucilage pad. This mucilage often contained trapped particles frustules of small planktonic centric diatom species, indicating the role that *C. closterium* may play in preparing the surface for subsequent colonisation by other diatom species. *L. flabellata* is a stalked diatom species that is frequently found as part of a mature epiphytic diatom community on macroalgae [27]. This species has a pedunculate attachment strategy and forms branched colonies that project up to several millimetres from the surface. The presence of surface

texture is thought to influence the location of initial adhesion of erect diatom species such as *Licmophora*. This observation is drawn from the fact that many cells were observed to attach on bas-relief features rather than recessed areas. Figure 5-26 illustrates this attachment in individuals of *Licmophora abbreviata* where focal adhesion to individual surface features has occurred.

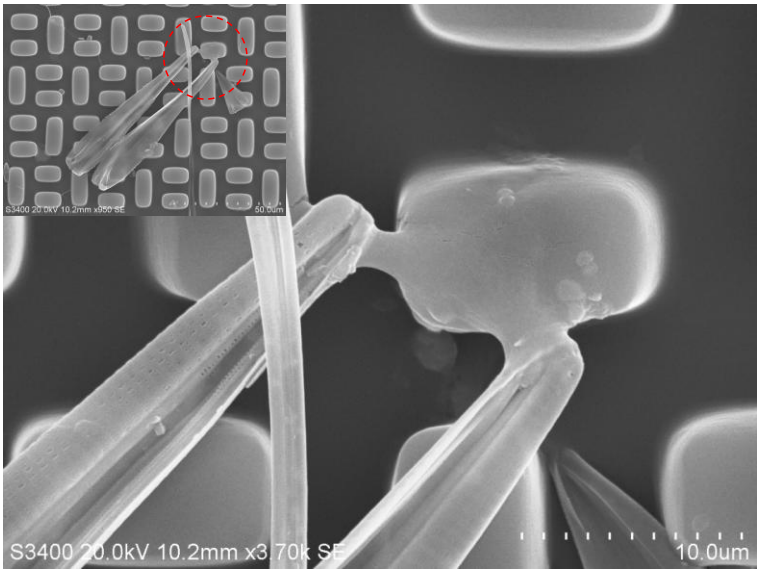

Figure 5-26: Scanning electron micrograph showing focal adhesion of Licomphora flabellata cells to a 12 x 6 µm PDMSe surface feature.

5.4.7 *Microbial aggregates and surface texture*

Much of the literature on the process of marine biofouling describes a succession model with individual bacteria and diatom cells as initial colonisers of exposed marine surfaces [42]. In this study, it was found that marine microbial aggregates were frequent present on the textured surfaces after 7 d. These aggregates consisted of bacterial cells, damaged and intact diatom frustules, bound together in by exopolymeric substances. Diatom species observed within such aggregates were representative of planktonic species, including small centric diatoms species such as *Thalassiosira* or *Minidiscus*. However, benthic cell forms such as *Navicula*, *Amphora*, or *Cocconeis* were also encountered within these aggregates, indicating that the attachment of such aggregates may have a role in the initial transport of the first colonising cells to a newly immersed surface. This is important as it represents a change in the view of how a microbial biofilm is formed. Rather than initial colonisation by individual cells, initial development of a biofilm may be accelerated by adhesion of microbial aggregates to a surface. Additionally, the presence of such aggregates may also significantly alter the

chemistry and hydrodynamic flow over a newly immersed surface, perhaps negating any anti-settlement effects of surface texture on colonising cells. An example of such a microbial aggregate is shown in Figure 5-27, in which both benthic and planktonic diatom species can be seen. The effects of such aggregates on the surface texture are also evident.

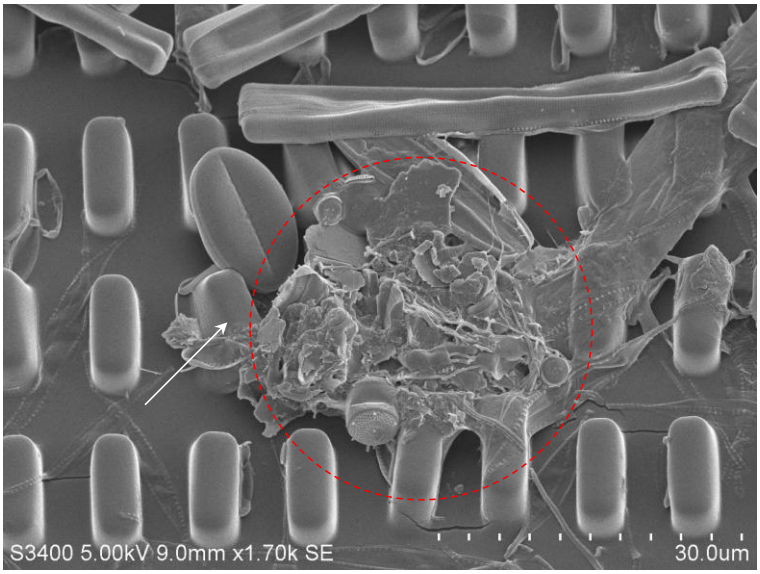

Figure 5-27: Scanning electron micrograph demonstrating microbial aggregates encountered on textured surfaces in the marine environment (circled). Distortion of PDMSe blocks of individual textures can also be observed (arrowed)

Small diatom species are the most common cell types found within aggregates and it can be speculated that diatom EPS plays a significant role in binding the aggregates together prior to contact with the surface. Aggregates also disrupted pattern fidelity on examined surfaces and topographic features were distorted in these areas. Shrinkage and distortion due to dehydration of the exopolymeric substances surrounding and within such aggregates during preparation for SEM may exaggerate the effect, but distortion was also observed during examination with a light microscope. While fabrication of surface texture using a material with a lower modulus of elasticity may prevent distortion of textures by settling cells, the fact that such surface features can be readily enveloped by microbial aggregates may have important consequences for the development of a non-toxic AF coating based on the anti-settlement properties of surface textures of similar dimensions. The capability of diatom frustules to distort a PDMSe surface feature is also illustrated by Figure 5-28, where the deflection of a 12 x 8 µm PDMSe block by some 30 ° from original alignment has occurred.

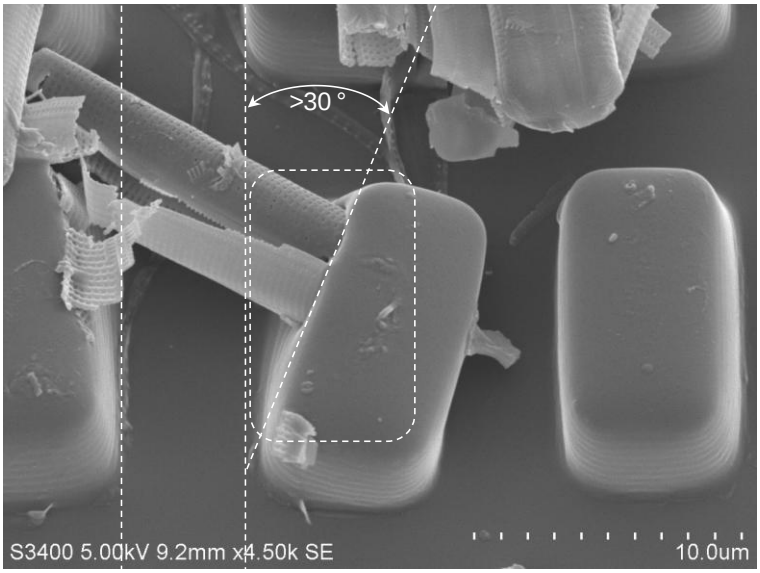

Figure 5-28: Scanning electron micrograph of the distortion of a PDMSe feature of 12 x 8 µm dimensions resulting from interaction with a diatom frustule. A deflection angle of >30 ° from the original location (dashed line) has occurred in the PDMSe microstructure. The diatom frustule is also no longer intact.

Another important consideration concerning microbial interaction with surface features relates to restriction of spreading EPS from initial cell attachment locations. Restriction of the ability of EPS to spread on surface by the presence of surface texture influences microbial adhesive strength and, at least among bacteria, can restrict the growth of a biofilm on the surface. This is regarded as the principle behind the use of surface textures such as Sharklet AF™ for reduction of microbial biofilms of bacterial species such as *Staphylococcus aureus* [10]. Since diatoms produce copious amounts of EPS [39], it is unlikely that surface texture of the dimensions examined in this study can prevent spreading of EPS on the surface. An example of this can be seen in Figure 5-29, where the adhesive plaque common to a number of diatom cells can be observed. The EPS can be seen to have spread between and over surface features.

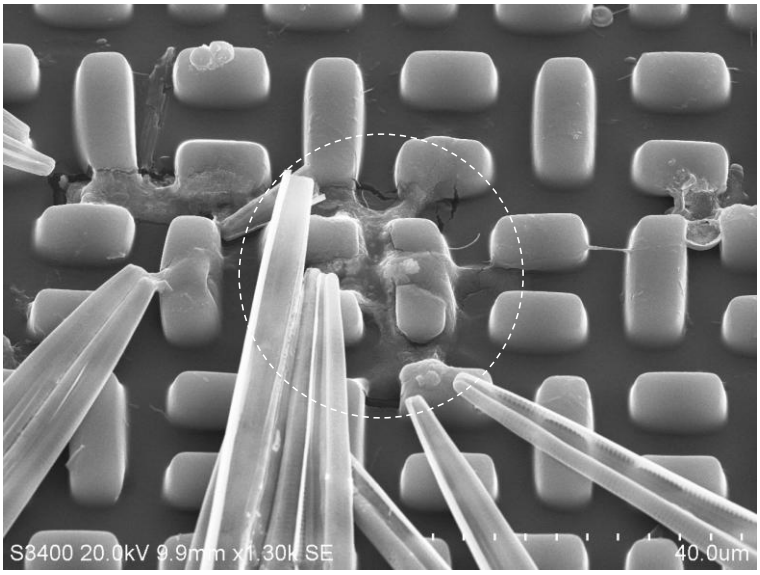

Figure 5-29: Scanning electron micrograph of an adhesive EPS plaque from a number of diatom cells (circled). The spread of EPS over the surface has not been restricted by the presence of surface features.

5.4.8 *Settlement of adnate diatom species on surfaces textures*

Adnate diatom species are described as attaching to a surface through one valve face, i.e. lying prostrate on the surface. This results in a large surface area for adhesion without the use of stalks or other attachment mechanisms. Individual diatom species generally categorised as adnate forms (major cell axis in direct contact with the substratum) were less abundant on the textured surfaces tested in this study. Both *Amphora* and *Cocconeis* species are generally regarded as adnate cell forms [43]. Cells exhibiting a high width to length ratio such as those of *Cocconeis* were less abundant on textured surfaces. This is likely due to the inability of such cells to form a complete adhesive bond with the surface. The optimum orientation of the cells and complete contact along the valve face was not possible. Therefore, such cells were unable to form a monolayer of connected cells as for a smooth surface. The exposed surfaces were thus able to select for larger diatom cell forms and if exposed over longer periods may eventually lead to the development of a significantly altered macro-fouling community compared to that of a smooth surface [44]. Figure 5-30 illustrates adhesion of *Cocconeis* sp on ED 4 where the inability of cells to gain maximum adhesive contact with the surfaces is observed. Cells of *Cocconeis* are unable to adhere on top of features in the texture, and yet are unable to settle completely between features. No data are available to examine the effects of hydrodynamic shear forces on adnate diatom cells forms from

textured surfaces but it can be speculated that the decreased surface area in contact with the surface will result in greater removal of cells.

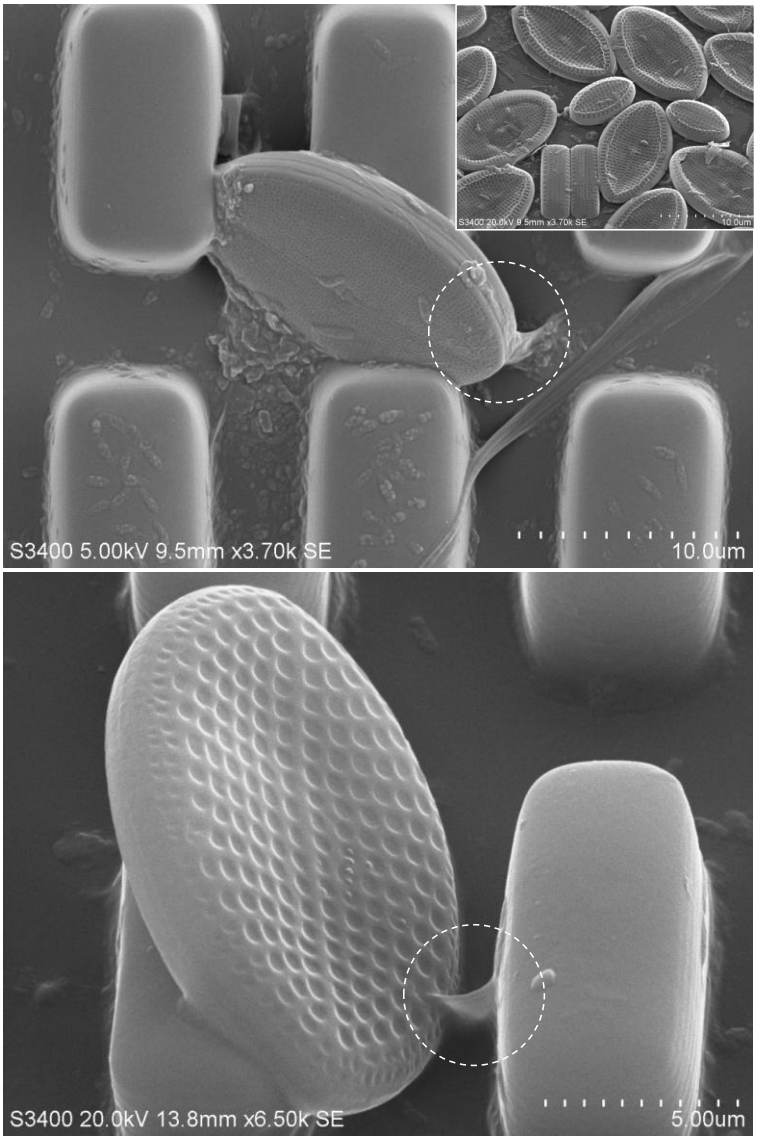

Figure 5-30: Scanning electron micrographs illustrating the positioning of adnate diatom species (Cocconeis) on the textured surfaces. Surface texture prevents cells from making complete adhesive contact with the surface as on an untextured surface (inset). Binding to the surface with EPS associated with the frustule is also visible (circled areas).

In contrast to diatoms such as *Cocconeis* sp., smaller motile diatom species with a width smaller than that of the spacing between topographic features were able to position between surface features. Such cells were generally found to align alongside surface features. An example of this is shown in Figure 5-31.

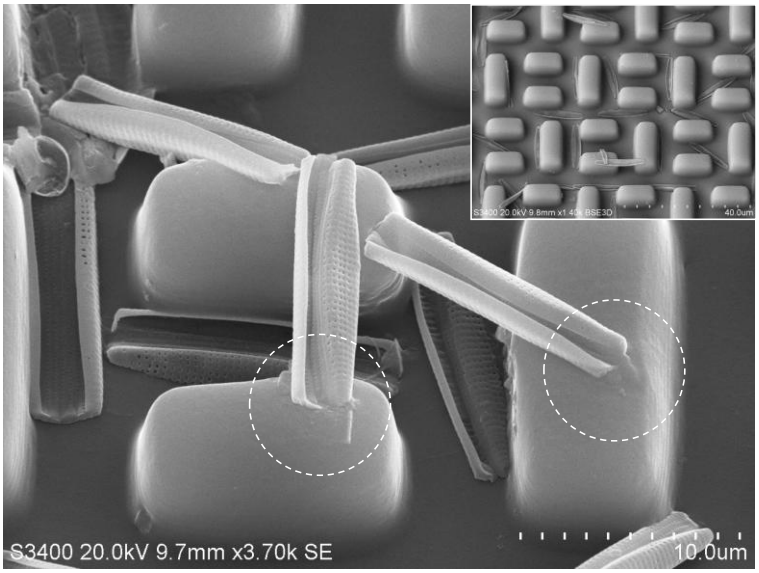

Figure 5-31: Scanning electron micrograph illustrating the adhesion of a small unidentified araphid diatom species to ED 2. Cells can be observed to settle and bind to PDMSe blocks (circled), however the majority of cells were found to align with surface features (inset).

5.4.9 *Biofouling development on textured PDMSe surfaces*

Continued immersion of textured surfaces for up to one month resulted in the development of a diverse microbial community on all surfaces. A substantial bacterial community developed within two weeks and had formed a monolayer of cells by termination of the study. Isolated bacterial cells were observed on textured surfaces after a 7-day exposure, however by 14 days bacterial colonisation of the surface had become extensive. An example of the settlement pattern of bacterial cells is shown in Figure 5-32, where the widespread distribution of cells on every surface is evident. However, in agreement with the results obtained by CFD modelling of shear forces over the surface, bacterial cell numbers appear reduced on edges of surface features.

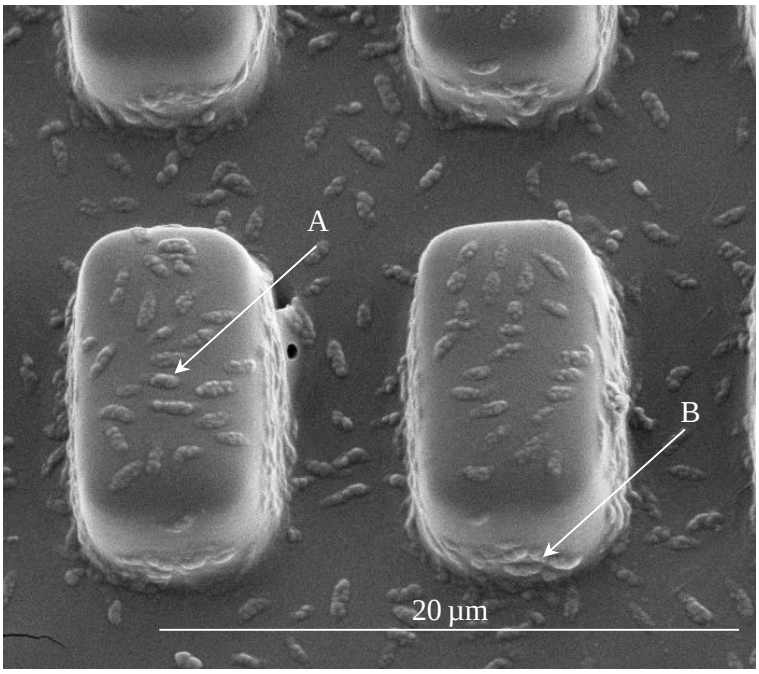

Figure 5-32: Scanning electron micrograph of bacterial attachment to the textured surfaces after 14 d. Cells are present on both horizontal (A) and vertical surfaces (B).

A number of recent reports on the influence of microtopographic structures on bacterial biofilm formation have been published [1, 45]. Hou and co-workers have examined the formation of *E. coli* biofilms on micro-structured PDMSe surfaces with comparable dimensions (10 µm feature heights) to those utilised in the present study [1]. These workers reported that *E. coli* cells preferentially attach and form biofilms in valleys between protruding features even when the dimension of the tops of square features are considerably larger than valleys.

Analysis of diatom settlement patterns on textured surfaces after 14 d demonstrated that colonisation by larger diatom species had occurred. The majority of diatoms identified on the surface after 14 d were chain-forming species of *Neosynedra*. *Cylindrotheca closterium* cells were still abundant on all surface textures but cells of *Licomophora* were reduced in abundance compared with a 7-day immersion period. Diatom species with frustules much greater in dimension than the produced surface features were positioned on top of surface textures. Comparison of abundance between smooth and textured surfaces indicated that recruitment of these species did not appear to be affected by surface texture. Highly silicified diatom species such as *Neosynedra* were sufficiently rigid to bridge surface features. Cells that bridged surface features were not significantly reduced in abundance on textured surfaces when compared with a smooth surface. The frustules of other less silicified species such as *Cylindrotheca closterium*

were observed to conform to surface features to a certain degree, although distortion of these cell types due artefacts produced by high vacuum necessary for SEM imaging may have some role in this.

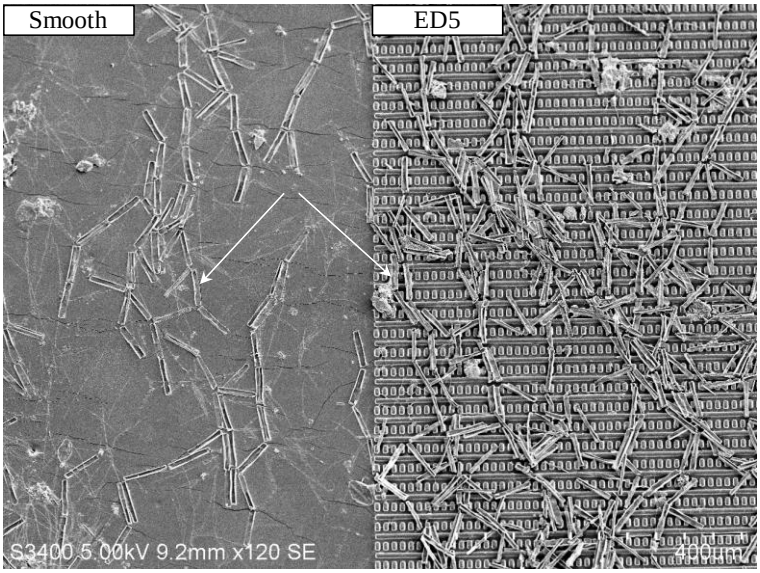

Figure 5-33: Scanning electron micrograph of diatom cells attached to both smooth and textured surfaces after 14 d. Chain of Neosynedra are now the dominant genus attached to the surface (arrowed).

After 14 days, diatoms could no longer be accurately counted using the described methods. Individual cells were now covered by larger diatom species and other algae. After 1 month exposure, the textured surfaces had in many cases > 90% surface coverage of biofouling. The extent of this surface coverage is shown in Figure 5-34. The experiment was terminated at this point.

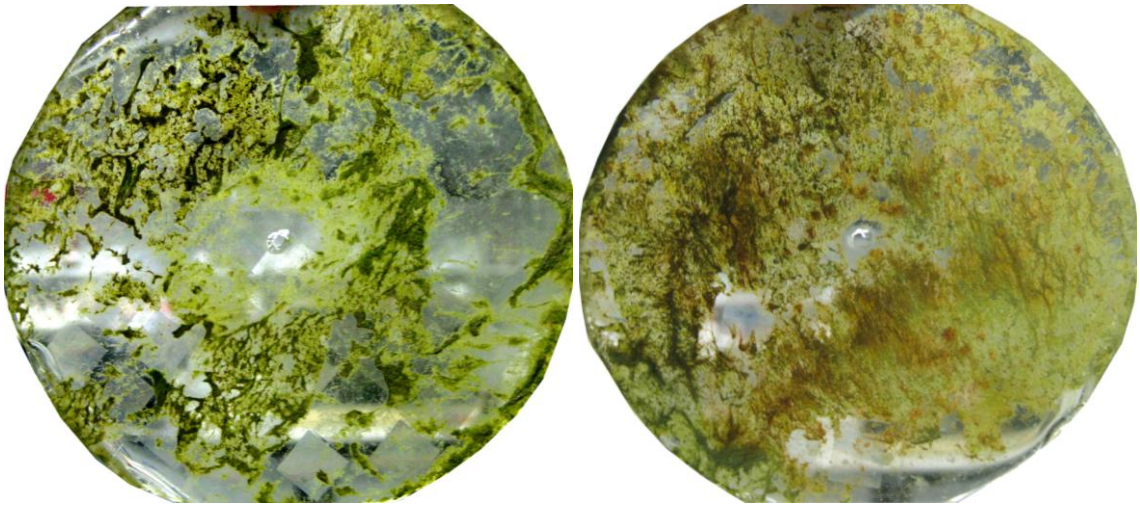

Figure 5-34: Digital images of biofouling of the complete textured wafer after 21 (left) and 30 days (right) exposure at Lough Hyne Marine Reserve (depth 1 m).

5.4.10 *Attachment point theory and diatom adhesion*

A concurrent and possibly complementary model to the ERI has been proposed widely known as attachment point theory. Attachment point theory is based on the premise that adhesion of a cell to a textured surface is increased when the number of attachment points on that surface available to a settling spore is maximised [15, 16]. The likelihood of permanent attachment of a cell is therefore dependant on the size of the settling spore or cell in relation to the scale of the topographic surface features. In contrast to the ERI, attachment point theory is based upon sinusoidal feature shapes of a defined wavelength while maintaining a constant aspect ratio. Features are not broken into individual patterns, but maintained as ridges and troughs over the lengths of the area under test. The settlement of a number of organisms including *Amphora* sp, *Ulva linza*, tubeworms, bryozoans and red algae spores have been shown to be influenced by patterns based on attachment point theory [15] in mainly laboratory based studies.

The number of potential focal adhesive sites are limited on the cell surface. This in turn will influence cell behaviour as cells will favour attachment to textures which allow the maximum contact between cell and surface and thus greater attachment strength. Textures that do not provide optimum attachment points will be avoided. A schematic of this theory is shown in Figure 5-35. Multiple local points of adhesion lead to a greater adhesive contact with the surface in question and thus lead to a stronger bond between the organisms and the surface. Fewer attachment points mean that the organism is easily removed by hydrodynamic shear forces. However, no allowance is made for

cellular orientation on the surface when feature sizes are restricted to a single topographic dimension, thus cells can adapt their position on the surface in order to take advantage of the position with the highest number of adhesive points.

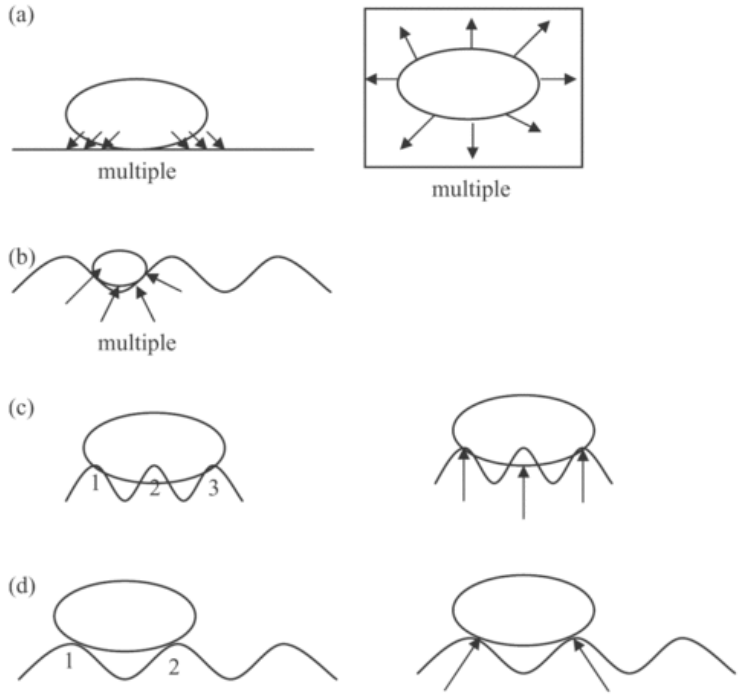

Figure 5-35: A schematic of attachment point theory as drawn in [15]*. (a) = cell settlement on a smooth surface (b) = cell settlement on a surface texture with much larger features than the cell, increasing settlement (c) = features much than the cell size again increasing settlement and (d) cell size in which the number of attachment points are reduced.*

The adhesion of a diatom surface increases with the effective area of contact between the cell and the surface. Increases in the number of attachment points would explain the increased attachment of small adnate cells types such as *A.coffeaeformis* in laboratory assays. Larger cells that are capable of bridging an increased number of surface features show preferential colonisation and growth on topographically textured surfaces. This model is supported by the data from the present study and is the first instance that influence of the number of available attachment points on diatom settlement under field conditions has been reported. However, data from this study has indicated that the attachment point theory is overly simplistic in relation to cell behaviour. As has been demonstarted in this study, cells are capable of changing orientation with respect to surface texture to take advantage of refuges within the surface. It is more probable that attachment point theory, in regard to the settlement of benthic diatoms, is more closely related to the position and orientation of the adhesive raphe structure on the surface of the cell, than overall orientation of the cell.

5.5 **Conclusions**

Application of surface texture as mechanism for reduction of settlement of marine algal spores has been widely regarded as an integral component of a non-toxic approach to AF. To date most tested surface textures have been examined in laboratory conditions against a limited number of biofouling species. In this study, a number of artificial textured surfaces have been successfully generated based on the dimensions of the common raphid biofouling diatom, *Amphora coffeaeformis*. These textures have been tested in both laboratory and field conditions where it has been demonstrated that the produced engineered topographic textures can effect settlement of diatoms in both situations. However, in the majority of cases, the presence of surface texture significantly increased settlement and retention of *Amphora coffeaeformis* in laboratory assays. One surface texture consisting of 12 µm x 6 µm and 6 µm x 3 µm features of 6 µm in height did reduce settlement compared to a smooth surface.

Subsequent field-testing of textured surfaces in the marine environment against a natural benthic diatoms community in the initial stages (1-7 d) of biofilm formation indicated that textured surfaces again influenced settlement. Small adnate diatoms of specific dimensions and shape were reduced on textured surfaces when compared to the smooth control surface. In addition, it has been demonstrated that benthic diatoms can attach to textured surfaces in a wide variety of orientations. These orientations are dependent on size and shape of the diatom cell in question. Frustule strength of particular species is also important, as highly silicified species appear capable of bridging features without adverse effects on unsupported areas of the frustule. How this affects attachment strength under conditions of high shear force relative to the surface is still unknown.

Investigation of the current models of cell attachment to structured surfaces in relation to the results from this study has revealed that many of the current theories relating to the prediction of cell settlement rate on topographically structured surfaces are not sufficient to explain the trends in adhesion of *Amphora coffeaeformis*.

5.6 **References**

1 S. Hou, H. Gu, C. Smith and D. Ren, *Langmuir*, 2011, **27**, 2686-2691.

2 R. G. Flemming, C. J. Murphy, G. A. Abrams, S. L. Goodman and P. F. Nealey, *Biomaterials*, 1999, **20**, 573-588.

3 A. Curtis and C. Wilkinson, *Biomaterials,* 1997, **18**, 1573-1583.

4 M. L. Carman, T. G. Estes, A. W. Feinberg, J. F. Schumacher, W. Wilkerson, L. H. Wilson, M. E. Callow, J. A. Callow and A. B. Brennan, *Biofouling*, 2006, **22**, 11-21.

5 J. F. Schumacher, M. L. Carman, T. G. Estes, A. W. Feinberg, L. H. Wilson, M. E. Callow, J. A. Callow, J. A. Finlay and A. B. Brennan, *Biofouling*, 2007, **23**, 55-62.

6 L. Hoipkemeier-Wilson, J. Schumacher, M. Carman, A. Gibson, A. Feinberg, M. Callow, J. Finlay, J. Callow and A. Brennan, *Biofouling*, 2004, **20**, 53-63.

7 A. Curtis, *IEEE Trans. Nanobiosci.*, 2004, **3**, 293-295.

8 E. Medilanski, K. Kaufmann, L. Y. Wick, O. Wanner and H. Harms, *Biofouling*, 2002, **18**, 193-203.

9 A. S. G. Curtis, B. Casey, J. O. Gallagher, D. Pasqui, M. A. Wood and C. D. W. Wilkinson, *Biophys. Chem.*, 2001, **94**, 275-283.

10 K. K. Chung, J. F. Schumacher, E. M. Sampson, R. A. Burne, P. J. Antonelli and A. B. Brennan, *Biointerphases*, 2007, **2**, 89-94.

11 J. F. Schumacher, C. J. Long, M. E. Callow, J. A. Finlay, J. A. Callow and A. B. Brennan, *Langmuir*, 2008, **24**, 4931-4937.

12 S. Petronis, K. Berntsson, J. Gold and P. Gatenholm, *J. Biomater. Sci. Polymer Edn.*, 2000, **11**, 1051-1072.

13 J. F. Schumacher, N. Aldred, M. E. Callow, J. A. Finlay, J. A. Callow, A. S. Clare and A. B. Brennan, *Biofouling*, 2007, **23**, 307-317.

14 A. J. Scardino, H. Zhang, D. J. Cookson, R. N. Lamb and R. d. Nys, *Biofouling*, 2009, **25**, 757-767.

15 A. J. Scardino, J. Guenther and R. de Nys, *Biofouling*, 2008, **24**, 45-53.

16 A. J. Scardino, E. Harvey and R. de Nys, *Biofouling*, 2006, **22**, 55-60.

17 E. Fadeeva, V. K. Truong, M. Stiesch, B. N. Chichkov, R. J. Crawford, J. Wang and E. P. Ivanova, *Langmuir*, 2011, **27**, 3012-3019.

18 B. Sarrat, C. Pécheyran, S. Bourrigaud and L. Billon, *Langmuir*, 2011, **27**, 3174-3179.

19 W. G. Koh, A. Revzin, A. Simonian, T. Reeves and M. Pishko, *Biomed. Microdevices*, 2003, **5**, 11-19.

20 N. Mitik-Dineva, J. Wang, R. C. Mocanasu, P. R. Stoddart, R. J. Crawford and E. P. Ivanova, *Biotechnol. J.*, 2008, **3**, 536-544.

21 N. Mitik-Dineva, J. Wang, V. K. Truong, P. Stoddart, F. Malherbe, R. J. Crawford and E. P. Ivanova, *Curr. Microbiol.*, 2009, **58**, 268-273.

22 K. Anselme, P. Davidson, A. M. Popa, M. Giazzon, M. Liley and L. Ploux, *Acta Biomaterialia*, 2010, **6**, 3824-3846.

23 A. R. Miller, R. L. Lowe and J. T. Rotenberry, *J. Ecol.*, 1987, **75**, 693-709.

24 P. J. Molino, E. Campbell and R. Wetherbee, *Biofouling*, 2009, **25**, 685-694.

25 R. R. Guillard and J. H. Ryther, *Can. J. Microbiol.*, 1962, **8**, 229-239.

26 R. Holland, T. M. Dugdale, R. Wetherbee, A. B. Brennan, J. A. Finlay, J. A. Callow and M. E. Callow, *Biofouling*, 2004, **20**, 323-329.

27 F. E. Round, R. M. Crawford and D. G. Mann, *The diatoms: biology & morphology of the genera*, Cambridge University Press, 1990.

28 X. M. Zhao, Y. Xia and G. M. Whitesides, *J. Mater. Chem.*, 1997, **7**, 1069-1074.

29 A. B. D. Cassie and S. Baxter, *Trans. Faraday Soc.*, 1944, **40**, 546-551.

30 J. Yang, J. Duan, D. Fornasiero and J. Ralston, *J. Phys. Chem. B*, 2003, **107**, 6139-6147.

31 K. Rasmussen and K. Østgaard, *Biofouling*, 2001, **17**, 103-115.

32 J. A. Finlay, M. E. Callow, L. K. Ista, G. P. Lopez and J. A. Callow, *Integr. Comp. Bio*, 2002, **42**, 1116-1122.

33 C. J. Long, J. F. Schumacher, P. A. C. Robinson, J. A. Finlay, M. E. Callow, J. A. Callow and A. B. Brennan, *Biofouling*, 2010, **26**, 411-419.

34 J. Bico, U. Thiele and D. Quéré, *Colloids Surf. Physicochem. Eng. Aspects*, 2002, **206**, 41-46.

35 J. Callow and M. Callow, in *Biological Adhesives*, ed. C. J. A. Smith A.M., Springer-Verlag, Berlin Heidelberg, 2006, p. 63-78.

36 M. E. Callow, J. A. Callow, J. D. Pickett-Heaps and R. Wetherbee, *J. Phycol.*, 1997, **33**, 938-947.

37 P. J. Molino and R. Wetherbee, *Biofouling*, 2008, **24**, 365-379.

38 C. Hamm, R. Merkel, O. Springer, P. Jurkojc, C. Maier, K. Prechtel and V. Smetacek, *Nature*, 2003, **421**, 841-843.

39 N. Staats, L. J. Stal and L. R. Mur, *J. Exp. Mar. Biol. Ecol.,* 2000, **249**, 13-27.

40 T. Alcoverro, E. Conte and L. Mazzella, *J. Phycol.,* 2000, **36**, 1087-1095.

41 G. Pletikapić, T. M. Radić, A. H. Zimmermann, V. Svetličić, M. Pfannkuchen, D. Marić, J. Godrijan and V. Žutić, *J. Mol. Recognit.,* 2011, **24**, 436-445.

42 L. D. Chambers, K. R. Stokes, F. C. Walsh and R. J. K. Wood, *Surf. Coat. Technol.,* 2006, **201**, 3642-3652.

43 C. Totti, M. Poulin, T. Romagnoli, C. Perrone, C. Pennesi and M. De Stefano, *Polar Biol.,* 2009, **32**, 1681-1691.

44 A. Terlizzi, E. Conte, V. Zupo and L. Mazzella, *Biofouling,* 2000, **15**, 327-342.

45 A. Almaguer-Flores, R. Olivares-Navarrete, M. Wieland, L. Ximénez-Fyvie, Z. Schwartz and B. Boyan, *Clin. Oral Implants Res.*, 2012, **3**, 301-307.

6 Conclusion

Prevention of biofouling and the development of novel AF mechanisms are of prime importance to many industries. However, in order to develop effective novel AF materials, a fundamental understanding of the interaction between microorganisms and the surface on which they settle and adhere is required. At present, many of the factors influencing biological adhesion at interfaces are not yet well understood. It has been the aim of this thesis to investigate a single fundamental parameter affecting the behaviour of biofouling organisms on a surface – that of surface texture and topography.

To pursue this aim, this thesis has examined the influence of surface texture on biofouling from a number of perspectives. These include investigation of biofouling on synthetic surfaces in challenging environmental conditions, biomimetic approaches, aimed at understanding the influence of surface topographies on fouling of marine organisms and the influence of engineered surface texture on the adhesion of raphid biofouling diatoms.

Chapter 2 has examined the biofouling process on surfaces in both marine and estuarine environments. To do this, environmental sensors and a variety of material types and AF coatings were deployed in the natural environment. These field trials were also conducted in three locations at two environmentally important sites so that data produced would prove of use in future environmental sensing deployments. The results of these field studies have indicated that surface texture does indeed have profound effects on both initial recruitment and species composition of biofouling in real-world situations. These studies have informed future environmental sensing programmes in both locations, and AF technologies utilised in future will be adapted based on the results of this research. The magnitude of both spatial and temporal variability in biofouling has also been demonstrated. This research has directly contributed to recommendations regarding materials and AF.

Chapters 3 and 4 have examined biomimetics as a means of producing novel surface textures for biofouling prevention. To do this the role of surface texture from sharkskin and the carapace of two common crustaceans in epibiosis prevention have been examined. These chapters have resulted in complete characterisation of the surface texture from a number of marine organisms in detail for the first time. Additionally, synthetic replicas of the surface texture of these organisms have been produced and tested for the first time against benthic diatoms. The overall objective of this research has been to evaluate the potential of incorporating natural mechanisms of epibiosis

prevention based on surface texture into future synthetic non-toxic AF materials. Previously reports had indicated the surface texture of certain crustacean species possess AF ability mediated by the presence of specific surface textures. However, the findings of this work have demonstrated that any effect of physical surface texture is weak at best against microfouling organisms. Nonetheless, anti-settlement activity of the natural carapace structure of *C. pagurus* was demonstrated for the first time by mapping epiphytic diatom abundance and distribution on this surface. Areas of low diatom abundance on the carapace have been related to chemical differences in the carapace structure rather than the surface texture. The area of protrusion of a highly calcified endocuticular layer through the epicuticle of *C. pagurus* is correlated with reduce diatom abundance, perhaps indicating a previously unidentified epibiosis prevention mechanism of the carapace of this species.

AF mechanisms of sharkskin due to surface texture have also been investigated in this work. While physical mechanisms of epibiosis prevention due to the presence of dermal denticles have not been disproven, the effects have been demonstrated to be minimal at best. It is suggested that chemical and mucilage secretions have a greater role in prevention of epibiosis of sharkskin, although it should be noted that no evidence to disprove the suggestion that dermal denticles reduce parasitic colonisation has been found.

In chapter 5, a series of engineered textured elastomer surfaces have been tested in both laboratory and field studies against marine biofouling diatom species. Although the majority of produced surface textures increased diatom growth and retention when compared to a smooth control, one produced surface texture had some anti-settlement activity against the benthic diatom *A. coffeaeformis* in laboratory studies. The results of field trials of these textured surfaces were inconclusive with regard to overall diatom settlement. This indicated that caution should be exercised when transposing the positive results of single species assays from laboratory studies into AF surfaces for exposure to natural biofilms, where the effects of microbial aggregate adhesion can negate the effects of engineered surface textures.

Nonetheless, these studies have provided informative data regarding initial diatom adhesion to such surfaces for the first time. Results have demonstrated that surface texture must be carefully designed and fabricated based on target diatom species, however, optimisation of surface texture for anti-settlement against one biofouling

diatom species may result in increased recruitment of other species to any surface. It is indicated that this can be related to differences in adhesive strategies utilised by benthic diatoms. Those species that utilise adhesive stalks or pads exhibit focal adhesion to surface features, while diatom species utilising an adnate adhesion strategy may be highly influenced by the presence of surface texture of specific dimensions. With these results in mind, it appears unlikely that micro-textured surfaces can be used in isolation as a broad-spectrum AF mechanism against benthic diatoms. However, this approach still has potential when combined with other AF strategies. In particular, designed surface topography targeted to reduce the adhesive strength of diatom species with morphology typical of species such as *Cocconeis* has potential in AF applications. As an example, optical windows from sensors such as those utilised in current turbidity sensors may benefit from the results of this study where application of surface texture to reduce diatom biofouling is feasible when combined with mechanical wipers.

To conclude, this work has demonstrated the importance of control of surface texture when designing and producing materials for optimum AF performance. All real materials will exhibit surface texture to some degree, and knowledge of how to control this is one of the keys to developing effective, durable AF materials, this work has contributed significantly to that knowledge.